THE UNIVERSITY OF HULL

# The Role of Soft Tissues and Minor Osseous Structures in Cranial Biomechanics

Being a Thesis submitted for the Degree of

Doctor of Philosophy (PhD)

In the University of Hull

by

Víctor Sellés de Lucas, MSc (Hons)

School of Engineering and Computer Science

University of Hull

November 2019

## Abstract

Finite element analysis is now widely recognised as an invaluable technique to investigate and understand cranial biomechanics since it can incorporate the complexity of a skull's geometry, its construction, different materials and complex loadings. However, while the biofidelity of some aspects of these models is increasing, most still only consider the larger bony structures of the skull. This study examines the role of soft tissues and some smaller bony parts, to determine whether they should also be incorporated in such studies of cranial biomechanics. The structures that have been investigated include: the dura mater, the falx cerebri and the tentorium cerebelli, the periodontal ligament, the nasal turbinates and the osseous nasal septum, the postorbital bars and septa and the bulk tissues that surround the cranial bones. They are considered both in terms of their functional role and as part of the general functioning of the FE model that includes them. For this purpose, two FE models were used: a model of a *Felis silvestris catus*, which was created specifically for this project, and an adaptation of a previous head model of *Homo sapiens*.

The results reveal that in *Felis silvestris catus*, the osseous tentorium does play a minor role in reducing stress in the parietal and temporal bones during feeding activities regarding of the biting regime. The causes of ossification and its possible mechanical role in several mammalian lineages, however, remain currently unclear. Moreover, inclusion of the nasal turbinates and the osseous part of the nasal septum is advisable in future FE models, as they impact the pattern of stress in the cranium, but the presence of generic bulk soft tissues in an FE model does not seem to have a meaningful effect on the results. On the other hand, modelling of the periodontal ligament has a localised effect in the alveolar region, but does not alter the general pattern of stress in the cranium.

In the *Homo sapiens* model, the postorbital bars and the postorbital septa not only help reduce strain in various areas of the cranium, but also shelter the contents of the orbit and avoid distortion of the eye. The postorbital septa also reduce strain in the postorbital bars and minimize asymmetrical deformation between the working and balancing sides in unilateral molar bites.

Altogether, this thesis offers a body of work which future researchers may find useful when investigating cranial biomechanics, to avoid oversimplification or incorporation of unnecessary complexities.

## Acknowledgments

**Table of Contents**

## List of Figures

XIII

## List of Tables

# Glossary

| | |
|---|---|
| cm | Centimetre |
| CT | Computed tomography |
| DTI | Diffusion tensor imaging |
| $E$ | Young's modulus |
| FE | Finite element |
| FEA | Finite element analysis |
| g | gram |
| GPa | Gigapascal |
| Kg | Kilogram |
| mm | Millimetre |
| μm | Micrometre |
| MDA | Multibody dynamics analysis |
| MPa | Megapascal = 1 N/mm$^2$ |
| MRA | Magnetic resonance angiography |
| MRI | Magnetic resonance imaging |
| N | Newton |
| Pa | Pascal = 1 N/m$^2$ |
| PCSA | Physiological cross-sectional area |
| PDL | Periodontal ligament |
| SMAS | Superficial musculoaponeurotic system |
| TMJ | Temporo-mandibular joint |
| ν | Poisson's ratio |
| 2D | Two-dimensional |
| 3D | Three-dimensional |

# Chapter 1. Introduction

By its own definition, a model is not a literal representation of reality, but a simplification, and digital models are no exception. In particular, digital models allow the examination of conditions or morphological changes not found in reality, allow permanent repeatability of the experiments and, in the case of biological specimens, may also help circumvent ethical issues, amongst many other advantages. Furthermore, far from being a disadvantage, simplification helps scientists work with a limited number of variables and study elements in isolation. Thus, because biological systems are frequently extremely complex, models provide a suitable way to study them in a simplified manner and in a controlled environment (Anderson *et al.*, 2012).

Most finite element models of the vertebrate head to study functional morphology have tended to focus on predicting bone stress and strain when subjected to masticatory forces. The amount of detail and structures included, however, varies depending on the study. For example, some authors have included the periodontal ligament of the teeth (Wood *et al.*, 2011; Gröning *et al.*, 2011), the postorbital fascia (Curtis *et al.*, 2011), the internal trabecula of bone (Dumont *et al.*, 2011, except for the occipital region; Sellés de Lucas *et al*., 2018), the cranial sutures (Moazen *et al.*, 2008; Wang *et al.*, 2012; Bright, 2012; Curtis *et al.*, 2013), the keratin of the beaks of avian species (Soons *et al.*, 2012) and so forth.

Although studied before, biomechanics did not emerge as a truly distinct discipline until the mid-1960s – shortly after the appearance of the first transistor-based computers and shortly before the development of the finite element method (Zienkiewicz, 1971). With the advent of personal computers, the increase in computer power and the decrease in the cost of the components, a similar revolution took place in the 1970s. Many finite element models have since then been produced to solve complex biomechanics problems in Medicine and more recently Life Sciences, for example in the fields of Biomedical Sciences, Comparative Anatomy and Palaeontology (Rayfield, 2007; Cunningham *et al.*, 2014). Concurrently, during the last decades there has been an increasing trend to improve the level of detail of digital models, both in terms of pure number of elements and precision in the shape of the structures included.

However, it is important to note that, "while models that attempt to model all the complexity in a system are impractical, models that neglect a crucial variable will give erroneous results" (Bright, 2014). Consequently, the main focus of the present work is to analyse various cranial elements (such as the dura mater, the falx cerebri and the tentorium cerebelli, the periodontal ligament, the nasal turbinates and the osseous nasal septum, the postorbital ligaments, bars and septa, the eyes and the bulk tissues that surround the cranial bones) and methodologies (inclusion of the neck musculature, muscle wrapping and asymmetrically scaled muscle forces based on electromyographic data) that have been typically neglected in FE studies or still remain insufficiently studied. This thesis deals with these issues as part of a larger collective project which focused on the biomechanical role of cranial soft tissues in both reptiles and mammals.

The present study used two 3-dimensional mammalian finite element models, one developed from the microCT scan of a common household cat (i.e. *Felis silvestris catus* head) and the other adapted from the digital anatomical human head model (MIDA) of Iacono *et al.* (2015; FDA, Center for Devices and Radiological Health, IT'IS Foundation) using advanced computer modelling techniques. *Felis silvestris catus* was chosen because of the completely ossified condition of its tentorium cerebelli, which made this species ideal to test the hypothesis (in Chapter 5) that ossification may help decrease stress in the skull dome during biting. The *Homo sapiens* model was selected specifically to examine the role of the postorbital septa and its relationships with the postorbital bars (in Chapter 8). Both models, however, included various other structures and served multiple research purposes.

Therefore, the aims of the project were twofold. In the first place, to determinate what function (if any) each of the structures listed above play from a biomechanical and a biological point of view. In the second place, to test how these parts interact with the remaining components of the cranial system in the finite element model in order to investigate whether (and how) they alter the biomechanics of the skulls considered. The conclusions reached should potentially help future researchers to decide the level of detail required in their finite element models and what specific structures to include in order to test a given hypothesis, either by avoiding oversimplification or striving for impractical and unnecessary complexity.

## 1.1. Chapter organization

The thesis has been organized into the following chapter structure:

*Chapter 2* comprises a review of the current literature of the topics discussed throughout this work, including information about the mammalian cranium and masticatory muscles, the scalp and the meninges, focusing particularly in two of the four dural folds: the falx cerebri and the tentorium cerebelli. It also discusses the different conditions of the postorbital bars and postorbital septa and their evolutionary significance and possible biomechanical role. Current techniques of digitalization and *in silico* model creation and analysis are the focus of the last part of the chapter, which concludes with a retrospective look at some relevant head FE models from the last three decades that consider soft tissues and other minor structures.

*Chapter 3* gathers together, for the first time, all available literature, complemented with additional information gathered from new specimens (from the Grant Museum of Zoology, UCL, London), to examine the functional role, if any, provided by ossification of the falx cerebri and/or tentorium cerebelli of certain species of mammals, together with a review of the possible origin of this condition. Under the light of this new corpus of information, this chapter concludes by evaluating and dismissing some conflicting hypotheses that have been proposed in the past.

*Chapter 4* presents the process of creation of the *Felis silvestris catus* multi-purpose finite element model. It also covers the generation of a muscle wrapping protocol and the modelling of the neck muscles.

*Chapter 5* examines the role of the ossification of the falx cerebri and the tentorium cerebelli in the *Felis silvestris catus* model by testing the hypothesis that the osseous structures help to support the loads arising during feeding, a suggestion that has never been tested quantitatively before.

*Chapter 6* assesses the role of some other "minor" structures present in the mammalian head during biting, such as the periodontal ligament, the nasal turbinates and the nasal septum. These structures are frequently neglected from FE analyses and therefore the aim of the chapter is to evaluate if their omission affects the results of these studies in a significant or meaningful manner.

***Chapter 7*** describes the process of modification and conversion of an existing 3D visualization of a human head into a finite element model, as well as comparing the effects of considering scaled and unscaled masticatory forces in FE analyses. The importance of including bulk soft tissues (such as skin and muscles) in FE biting analyses is then investigated.

***Chapters 8*** follows the previous chapter by using the human head FE model to test the role of the postorbital bars, the postorbital ligaments and the postorbital septa during a unilateral molar biting regime, and to test the effects that these structures play in the strain patterns of the skull and deformation of the ocular globes.

***Chapter 9*** brings together the results and discussions of the previous chapters, to put them into perspective and offering further insights, while at the same time highlighting potential limitations of the current research.

***Chapter 10*** concludes with some final remarks in relation to the overall aims of the project and points to possible new directions for further research.

# Chapter 2. Literature Review

## 2.1. Introduction

The mammalian head is a highly complex system that supports a wide array of important functions, some of which are: to encase and protect the brain, to serve as part of the feeding system, including mastication and prey capture, and to house various sensory organs (Santana and Lofgren, 2013). To understand the functioning of this biological system, two concepts, modularity and integration, are particularly important: the head is composed of several independent units or modules, and these combine or "integrate" with one another at different levels. From this derives the fact that an alteration in either the form or the function of one of the modules of the head inevitably affects the form and/or the function of other modules (Lieberman, 2011). This leads to important implications in the fields of functional morphology and evolution, including the question of how morphological variation (i.e. shape) impacts function. When undertaking biomechanical studies to investigate this issue, the craniofacial vertebrate skeleton has usually been the structure preferred by researchers. Until recently, most research in cranial evolution that used biomechanical models has focused on the skull itself, but of course there is not only bone in the head. Many other different tissues interplay in the system, including muscle, brain, cartilage, tendon, fat, ligament, enamel, dentine, cementum and others (Lieberman, 2011).

This chapter first establishes some general characteristics of the mammalian head (with a special focus on humans) before detailing some specific structures of the head that are the subject of study in subsequent sections of this work, such as the postorbital bar and septum, the falx cerebri and the tentorium cerebelli. The chapter closes with a description of previous *in silico* models and the current methods and techniques involved in the research.

## 2.2. The mammalian skull

The class Mammalia arose from Synapsida at the end of the Triassic period (Benton, 2005), and today they comprise more than 150 families and over 6,000 extant species (Burgin *et al.*, 2018). Concerning head morphology, an important characteristic of

mammals is that, contrary to most other living vertebrates, they have akinetic skulls (Herring *et al.*, 2001; Vaughan *et al.*, 2015), with the exception of hares, which have an intracranial joint (Bramble, 1989). Moreover, their teeth have reached a high level of specialization, with most mammals having a heterodont dentition, meaning that a single species possesses more than one type of tooth morphology (Vaughan *et al.*, 2015).

In therian mammals (placental and marsupials) many dermal bones are lost from their earlier synapsid ancestors, including the prefrontal, postorbital, postfrontal, quadratojugal, and supratemporal (Kardong, 2012). Also, in certain species of mammals, individual bones become fused, leading to the formation of compound bones (occipital, temporal, and sphenoid; Rommel *et al.*, 2015). The synapsid interparietal, for example, becomes fused with the occipital in therians. Monotremes, on the other hand, retain many synapsid characteristics, such as unfused occipitals, and the bones prefrontal, postfrontal and pleurosphenoid (Kardong, 2012). In order to establish which bones are homologous among species, researchers sometimes use a generalized schematic skull (such as the one displayed in Figure 2.1).
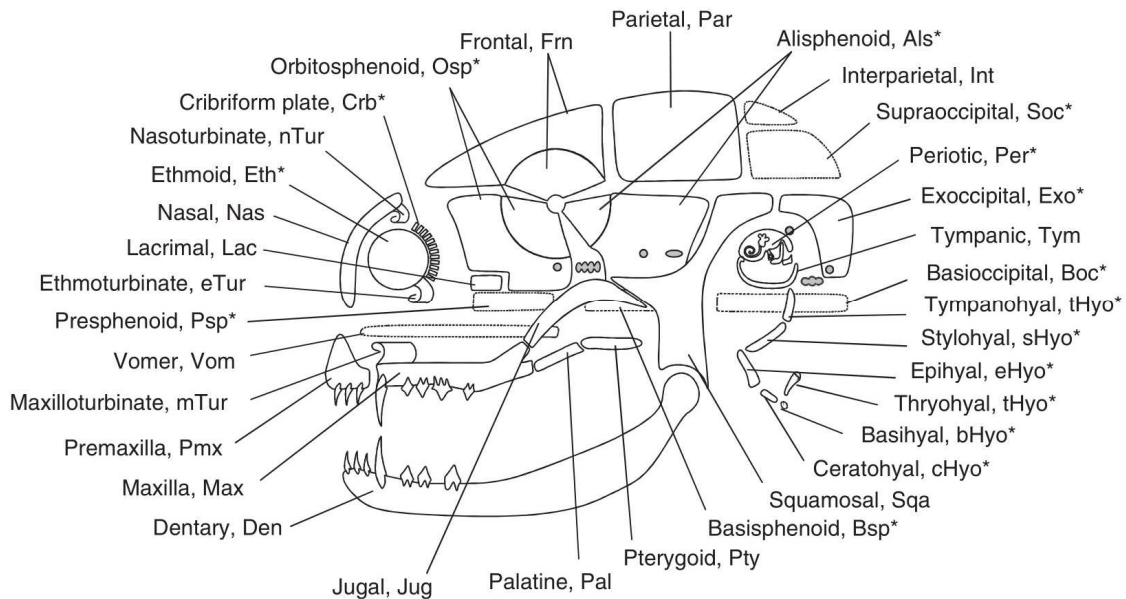


**Figure 2.1. Schematic view of the mammalian skull, showing the relative position of bones, thus offering a framework for mammalian comparative anatomy (Rommel *et al*., 2015).**

The temporal bone is of particular relevance to the current project, and is formed from various individual elements, which may include the squamosal, the periotic, the tympanic and the middle ear ossicles, becoming a single unit in many mammals (Rommel *et al.*, 2015). The single occipital of therian mammals is also formed by the fusion of various independent bones (basioccipital, exoccipitals, supraoccipital, and interparietal). The bone has a ring shape around the foramen magnum, an oval or circular opening that serves as a passage for the spinal cord and can include a nuchal crest on the back of the bone where neck muscles and ligaments attach, as is the case for common cats (*Felis silvestris catus*). Moreover, in contrast to other tetrapods, in most mammals the ethmoid portion of the nasal capsule becomes ossified to form the turbinates. This structure can be subdivided into three areas or regions (nasoturbinates, maxilloturbinates and ethmoturbinates), each one connected to the corresponding bone (Kardong, 2012).

### 2.2.1. Anatomy of the mastication muscles

The masticatory apparatus is composed of various anatomically independent but interconnected parts: the teeth and the bony elements that support them, the mandibular joints, various accessory structures (such as the tongue, the salivary glands, etc.) and the mastication muscles (Hemae, 1967). In mammals, these muscles are particularly well developed. They can be classified into a single jaw-opening group (the digastric), and three different jaw-closing groups: the masseter, the temporalis and the pterygoid (Turnbull, 1970). The temporalis muscles typically insert into the coronoid process of the mandible (i.e. dentary bone), the masseter muscles attach to the lateral face of the coronoid fossa, and the pterygoid muscles attach to the medial side (Vaughan *et al.*, 2015; Figure 2.2).
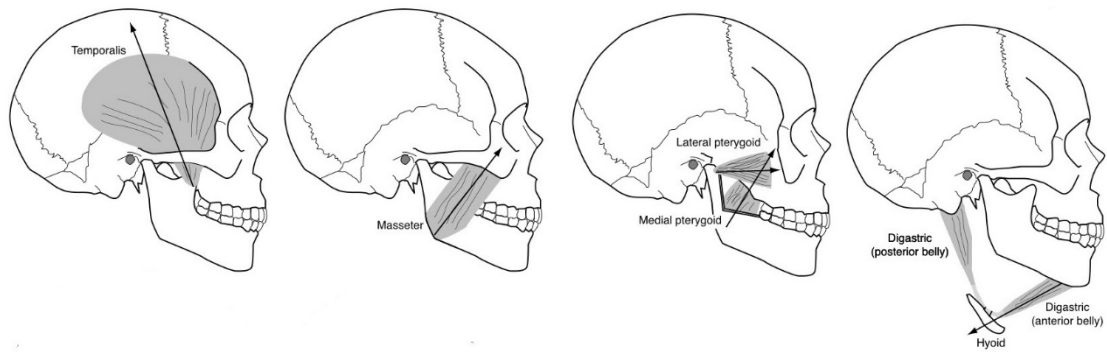
**Figure 2.2. The jaw-opening and jaw-closing muscular groups in humans. After Lieberman, 2011.**

According to the relative weight of each muscular assemblage, a functional classification can be established between those species with a more developed temporalis usually recognized as generalized feeders or specialized carnivores, while those with a more developed masseter and pterygoid are typically omnivores or herbivores. This characteristic is also linked with the mobility and position of the temporo-mandibular joint (TMJ), the union of the jaw with the cranium (Herring, 2007). In carnivores, the TMJ operates in a hinge-like way, while, in herbivores, it may perform wide lateral movements, with the TMJ of omnivores usually having intermediate characteristics (Bermejo *et al*., 1993).

### 2.2.2. The particularities of the human head

The human head shares many similarities to that of other mammals, but even when comparing it to those of our closest living relatives, the chimpanzee (either *Pan troglodytes*, the common chimpanzee, or *Pan paniscus*, also known as pygmy chimpanzee or bonobo), many distinguishing features become self-evident: for example, smaller teeth and canines, a brain more than five times larger than expected for the body size (based on a revised equation by Martin (1981) of the encephalization quotient formula), a chin, and a projecting nose with downward-oriented nostrils. Humans also have a neck attached at the centre of the cranium, not at the back, and a distinct articulation of the elements of the pharynx (Lieberman, 2011). However, the most relevant differences in the human head are the facial retraction and a globular-shaped neurocranium (an almost spherical braincase). The developmental changes that produced

8

this particular shape derived from shifts in cranial base angle, facial length, and cranial fossae dimensions, and probably also from an increase in temporal and frontal lobe size (Lieberman *et al.*, 2002).

The masticatory system is larger in the great apes than in humans, with larger muscles and attachment areas. In some cases (for example, male gorillas and orangutans, sometimes also in male chimpanzees) a sagittal crest serves as the origin for the temporalis muscle (Aiello and Dean, 1990). This robustness in the feeding musculature of other great apes has sometimes led to the assumption that the cranium and mandible of *Homo sapiens* are less well adapted than other hominids to generate or withstand high forces. Nonetheless, it has been demonstrated that the human head can produce similar bite forces to other hominids of the same size by applying less muscular force, and that the stresses are apparently better distributed in the mandible, with lower peak stresses, when adjusted to the same surface area and bite force of other taxa, such as *Pan troglodytes* or *Gorilla gorilla* (Wroe *et al*., 2010). These results therefore suggest that the human mandible is actually better adapted to resist stresses than the mandibles of other apes (Figure 2.3).
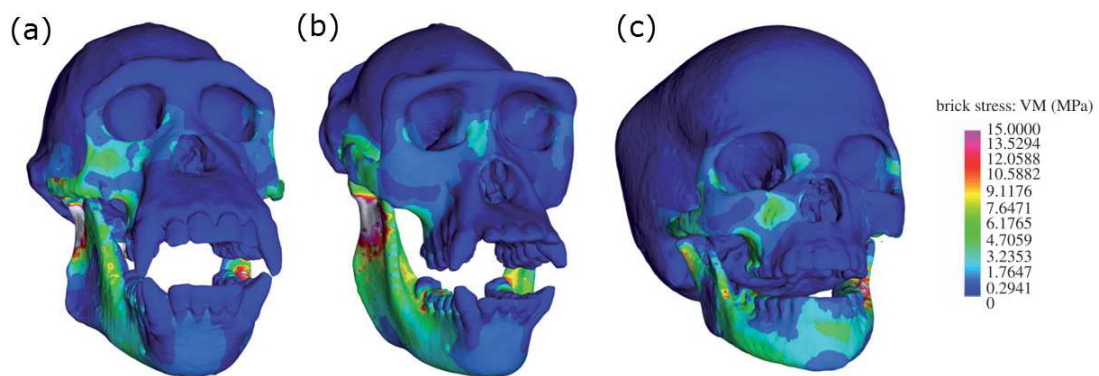


**Figure 2.3. von Mises stress distributions in FE models scaled to the same bite force and surface area after a unilateral bite at the second molar. (a)** *Pan troglodytes***; (b)** *Gorilla gorilla***; (c)** *Homo sapiens* **(adapted from Wroe *et al*., 2010).**

## 2.3. The postorbital bar and ligament

Postorbital bars are osseous arches that surround the external lateral part of the orbit and are usually generated by the fusion of the dorsal process of the frontal bone and a ventral process of the zygomatic bone (with the exception of equines, where it is the squamosal bone that provides the ventral process). Postorbital bars are present in different groups, as they have evolved multiple times either in whole mammalian orders or as occurrences in individual taxa (Heesy, 2005).

The postorbital process is the most probable intermediate condition before postorbital bars are developed. This structure is completed with a ligament, which in fact is the thickened most anterior part of the temporal fascia, with which if forms a continuum (Heesy, 2005). The ligament spans from the frontal process to the zygomatic bone and then performs a medial turn to form a dividing structure between the orbit and the temporal fossa (Herring *et al.*, 2011).

Most felid species possess postorbital processes, but in some cases these join the jugal process to create a fused postorbital bar. This seems to be a characteristic of small felids (Martin, 1980), and Salles (1992) identified two different states for this trait. The first was a 'tendency' to encircle the orbit, a condition shared by *Prionailurus viverrina* (fishing cat), *P. bengalensis* (leopard cat), *P. rubiginosa* (rusty-spotted cat), *Profelis badia* (bay cat), and *Otocolobus manul* (Pallas's cat). The second was the completely fused postorbital processes in the shape of a postorbital bar. This was only identified by Salles in *Pardofelis marmorata* (marbled cat; Figure 2.4, left) and *Prionailurus planiceps* (flat-headed cat). Additionally, *Felis silvestris catus* may also exhibit closed postorbital processes, which can, on occasion, develop into full postorbital bars. There is an example of this in the literature in Heesy *et al*. (2006), where two of the cats used for their experiment had "postorbital processes and short postorbital ligaments, and one had bilaterally complete postorbital bars, as verified by radiographs."

**Figure 2.4. Two extreme and contrasting cases of the postorbital bar/process found among Felidae. Left:** *Pardofelis marmorata* **(AMNH 102844); Right:** *Neofelis nebulosa* **(clouded leopard) (AMNH 35808). Lateral views (adapted from Salles, 1992).**

The mechanical role of the postorbital bar has been controversial for a long time. The excellent overview provided by Cox (2008) (with some extra information from Ravosa *et al.*, 2000b and Heesy, 2005) is used here to summarize the various hypotheses:

**Hypothesis 1:** The postorbital bar serves as a way to reroute pressure exerted by the mandibular articulation, or to divert pressure over the molars as a consequence of the action of the temporalis muscle, depending on the species.

**Hypothesis 2:** The postorbital bar serves as a skull reinforcement and a necessary requirement for the development of horns.

**Hypothesis 3:** The postorbital bar serves as a structure to protect the eye laterally from injury during locomotion.

**Hypothesis 4:** The postorbital bar serves as a system to avoid distortion in the orbital margin after contraction of muscles during mastication in mammal species with convergent eye orbits.[1] With intermediate degrees of orbital convergence, this

---

[1] Here, convergence means reorientation of the lines of sight of the eyes from lateral to frontal, as may have happened in primate evolution to facilitate nocturnal predation (see Figure 2.7, a).

reorientation in the orbit position in relationship to the temporal fascia goes hand-in-hand with the substitution of postorbital ligaments with postorbital processes, and a more extreme condition would lead to complete ligament ossification and therefore to the creation of a postorbital bar. In that manner, the animal can chew while foraging or hunting without having its vision acuity reduced. The visual predation hypothesis was originally proposed by Cartmill (1970; Figure 2.5).
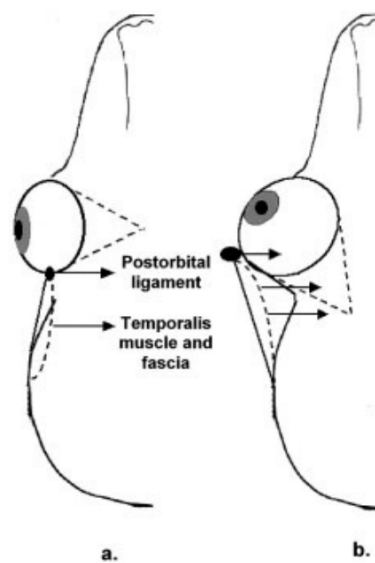


**Figure 2.5. Schematic representation of the visual predation hypothesis. With an increase in orbital convergence, the postorbital ligament would be moved into an anterior more lateral position (images a and b). As a consequence, the ligament could be deformed when the temporalis contracts. Images from Heesy (2005).**

**Hypothesis 5:** The postorbital bar serves as a structure to resist torsion in species with large masseter and pterygoid muscles. With postcanine unilateral biting, which is commonplace in mammals, the loads in the chewing side are higher at the teeth, but lower in the area surrounding the jaw joint and vice versa. Therefore, the balancing side strain is higher at the jaw joint and thus generates a 45 degrees torsion loading relative to the long axis of the skull (i.e. rostro-caudally). The postorbital bars counter axial compression on the chewing side and axial tension on the balancing side. It was proposed by Greaves (1985) and it is sometimes referred as the facial torsion model (Figure 2.6).
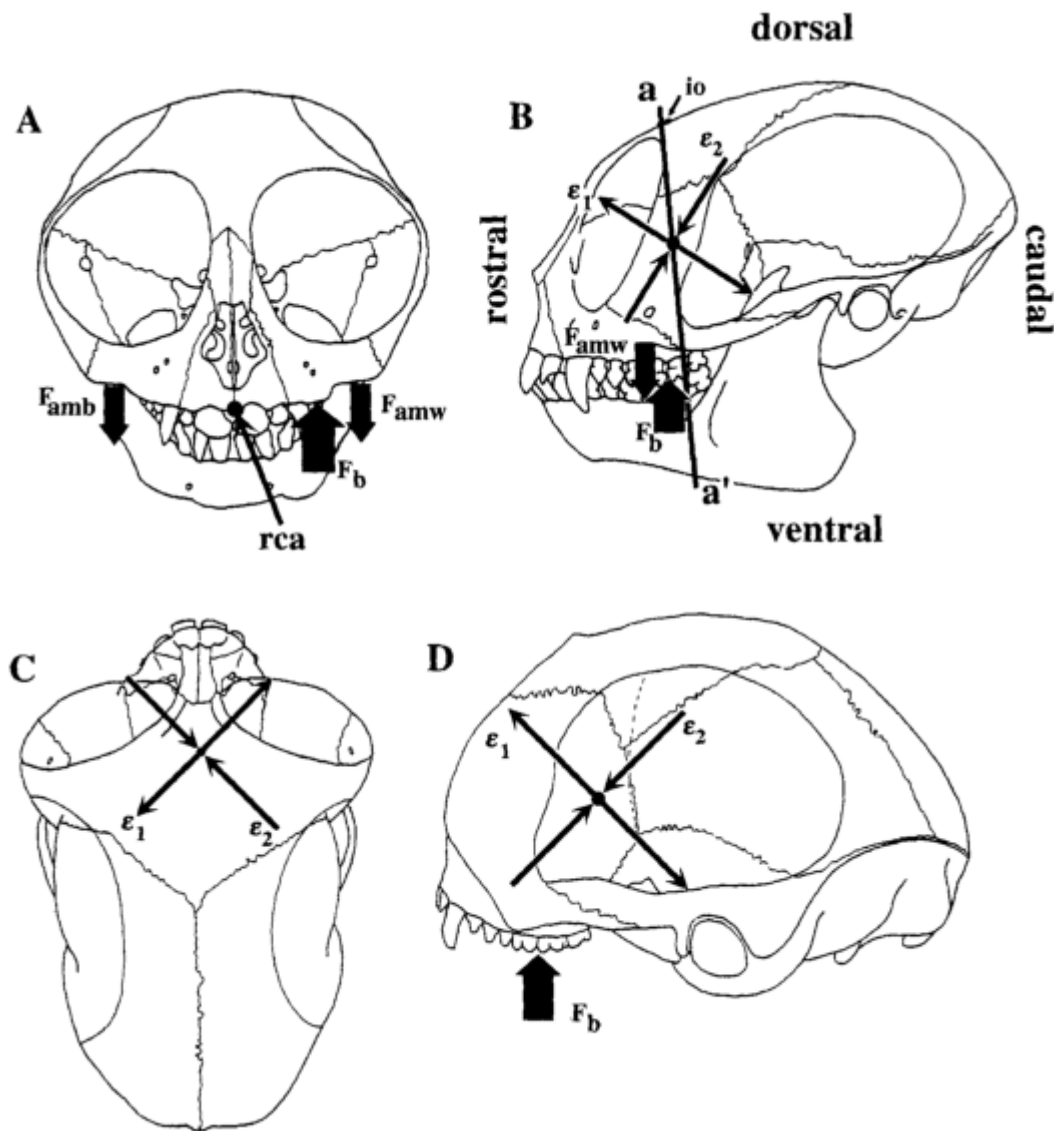
**Figure 2.6. Diagram summarizing Greaves' facial torsion model. (A) Hypothetical forces that act on the rostral area of the skull during unilateral biting. (B) Patterns of strain predicted in the surface of the postorbital bar. (C) Patterns of strain predicted in the interorbital region. (D) Patterns of stress predicted in the medial surface of the postorbital septum (from Ross and Hylander, 1996).**

Today, a general consensus supports the visual predation hypothesis. Jašarević *et al.* (2010) performed histological analyses on the postorbital ligament of rabbits and found out that this structure could only resist moderate-to-low stresses in multidirectional loads. They determined that high loads (as a consequence of a tougher diet) in the soft tissues of the lateral orbit wall would more likely cause a degradation of the ligament tissue rather than the development of an osseous postorbital bar, leading to the conclusion

that there was insufficient evidence to support the view that bars were a consequence of high mastication loads.

Additionally, studies performed by Noble *et al.* (2000) and Ravosa *et al.* (2000a; 2000b) demonstrated that the postorbital bar was overbuilt to resist torsion during feeding and thus the amount of bone that composed the structure could be greatly reduced without causing structural failure, dismissing the facial torsion model. The studies concluded that the development of this structure seemed more related with orbital convergence (felids, for example, have extremely convergent orbits when compared with other Carnivora, with a divergence of only 5°, instead of 15-30° (Cox, 2008)) as well as orbital frontation (the degree of verticality of the margins of the orbit; see Figure 2.7b). Two further factors were the allometry between orbit size and body size, and encephalization. For example, smaller cats are more frontated than larger felids, and there is indeed a link between relative brain size and orbital frontation, because frontal lobes tend to displace the superior part of the margins of the orbit and the orbital apertures become more vertical (Ravosa *et al.*, 2000b). However, later work by Finarelli and Goswami (2009) found that this correlation is only applicable to felids and canids, after testing the hypothesis in 68 different extant and extinct species, and concluded that it cannot be extrapolated universally to all Carnivora.
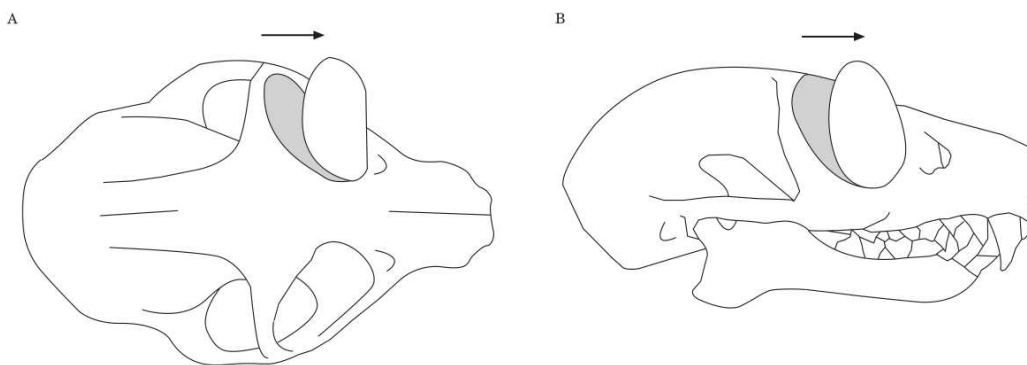


**Figure 2.7. Schematic examples for orbital convergence (extent to which the orbital margins face forward (a)) and orbital frontation (the degree of verticality of the margins (b)). Convergence angle provides better stereoscopic vision and depth perception (Finarelli and Goswami, 2009). Image adapted from Ravosa *et al.*, 2000b).**

Heesy (2005) collected morphometric data from over a thousand specimens of 324 taxa from various orders of extant mammals to test if the occurrence of a postorbital bar is related with orbit orientation, and his results seem to corroborate the visual predation hypothesis. His study identified a correlation between the angles of the orbital and the temporal fossa planes where, the greater the deviation of the second from the first, the larger the size of the postorbital processes and, consequently, the shorter the postorbital ligament. He also proved that orbit frontation, as well as orbit convergence and orbit verticality, all play a role, in decreasing level of importance, to define this orbitotemporal angle, but the specific importance of these three different types of orientation differs from one taxa to another. He concluded that the role of the postorbital bar is to stiffen the lateral orbit to avoid deformation which can alter normal oculomotor function.

In a later study Heesy *et al.*, (2007) used ocular kinematic methods in one *Otolemur* (a galago) and three *Felis* specimens to confirm that contraction of the anterior temporalis and the medial pterygoid affect the position of the eyes during feeding, possibly causing visual problems and diplopia (double vision). They determined that the difference between the presence of large postorbital processes and fully developed postorbital bars was negligible (in the sense that they both accomplish the same purpose of avoiding gross deformation of the orbital margin and provide a supporting structure for the extraocular muscle system), but also that, by themselves, they were not enough to maintain normal oculomotor function, and suggested various mechanisms and neural reflexes that could also serve to correct the minor displacements created by muscle contraction.

Herring *et al.* (2011) tested the role of the postorbital ligament *in vivo* in Hanford miniature swine (*Sus scrofa*). They demonstrated that the ligament stretched (average strain values of typically 1%, with a maximum of ~3%) during mastication. This stretching was not a consequence of jaw movement, but of the stimulation of either the masseter or the temporalis which contributed equally (~0.5%) to the final maximum elongation. However, it was also noted that the masseter did it in a more direct manner and showed higher tensile stresses after stimulation, probably as a result of the tension in the temporal fascia. Curiously, they also concluded that, given the orbit and the postorbital ligament configuration, pigs would be very likely to have their vision affected

when feeding, and perhaps this was corrected by minor oculomotor adjustments, but this idea was not proven.

Parisi (2010) performed analyses on a *Eulemur fulvus* cranium, a protosimian primate with fully closed postorbital bars, and which, in some respects, resemble early primates from the Eocene period. The results showed that the model with postorbital bars exhibited reduced strain values on the orbital walls, but led to high values on the zygomatic arches. Parisi's conclusion was that the bars help to reduce stress on the orbital walls via transmission to the zygomatic arches, which are more able to withstand stresses given its thicker configuration. In a similar manner, Curtis *et al.* (2007) tested the role of the postorbital ligament over a *Felis catus* cranium by producing models with and without the structure and performing FE analyses. He found out that peak stresses in the orbital margin and the zygomatic arch were reduced by the presence of the ligament, but nonetheless remained high.

## 2.4. The postorbital septum

In humans, the postorbital bar is accompanied by a postorbital septum, an osseous plate formed by the contact of the zygomatic and the alisphenoid bones that isolates the orbit from the temporal fossa. The postorbital septum is a structure unique to anthropoids and the genus *Tarsius*, in which it is present in a less state of completion (Cartmill, 1980). As with the postorbital bar, the postorbital septum has received different functional explanations, and there are various hypotheses proposing that it plays a role as a strain moderating structure during feeding activities, the most relevant of which were summarized by Ross and Hylander (1996):

**The facial-torsion hypothesis:** This is part of the facial torsion model proposed by Greaves (1985) and summarized above (as hypothesis 5) when discussing the role of the postorbital bar. Both the bars, the septa and the supraorbital torus are considered to be structures adapted to counteract the twisting of the skull. In the case of the septum of anthropoids, this would be a consequence of the closeness of the orbits to the midline.

**The transverse-bending hypothesis:** This hypothesis was proposed by Cartmill (1980), and suggests that the postorbital septum acts as a support for the postorbital bar

by resisting the temporal fascia which tenses as a consequence of the action of the temporalis muscle when it pulls posteriorly.

**The tension hypothesis***:* Initially proposed by Rosenberger (1986), this was reformulated by Ross and Hylander (1996). It suggests that the postorbital bar will be subjected to tension due to the contraction of the masseter, pulling it from the frontal bone. This is counteracted by the postorbital septum, as it connects the postorbital bar to the lateral wall of the skull and gives it mechanical support.

## 2.5. Scalp and meninges

### 2.5.1. Scalp

The word "scalp" is a term used to refer collectively to all soft-tissue covering the cranium. It is composed of five different layers: skin, connective tissue, galea aponeurotica, loose areolar tissue and pericranium (Figure 2.8).

Skin is composed of three layers: epidermis, dermis and hypodermis. The thickness of each depends on age, body region and/or hydration. It is because of the latter two (the thick dermis and the subcutaneous fat) that skin has its toughness and elasticity (Cua *et al.*, 1990; Pailler-Mattei *et al.*, 2008). Among the many functions that skin performs, one of them is the protection against mechanical trauma (Edwards and Marks, 1995; but see Huempfner-Hierl, *et al.*, 2015).

The galea aponeurotica, or epicranial aponeurosis, is located over the periosteum to which it attaches via a loose aureolar tissue, and covers the upper part of the cranium as a helmet-like structure. It is attached posteriorly to the highest nuchal line and the external occipital protuberance (Feneis and Dauber, 2000).

The periosteum is a connective tissue which covers the surface of nearly every bone of the human body (exceptions are the intra-articular surfaces and the sesamoid bones), and is anchored to them through Sharpey's fibres. It is composed of two different layers. The outer one is fibrous in nature and can be subsequently divided into two different parts: a superficial, inelastic portion, and a deep highly collagenous fibroelastic layer. The inner layer of the periosteum (also called cambium) is composed of mesenchymal stem cells, osteoblasts, nerves and capillaries. It is clearly visible in foetuses, but becomes thinner with age, and is almost indistinguishable from the outer

layer in adults (Dwek, 2010; Malizos and Papatheodorou, 2005). The periosteum of the head is also called pericranium.
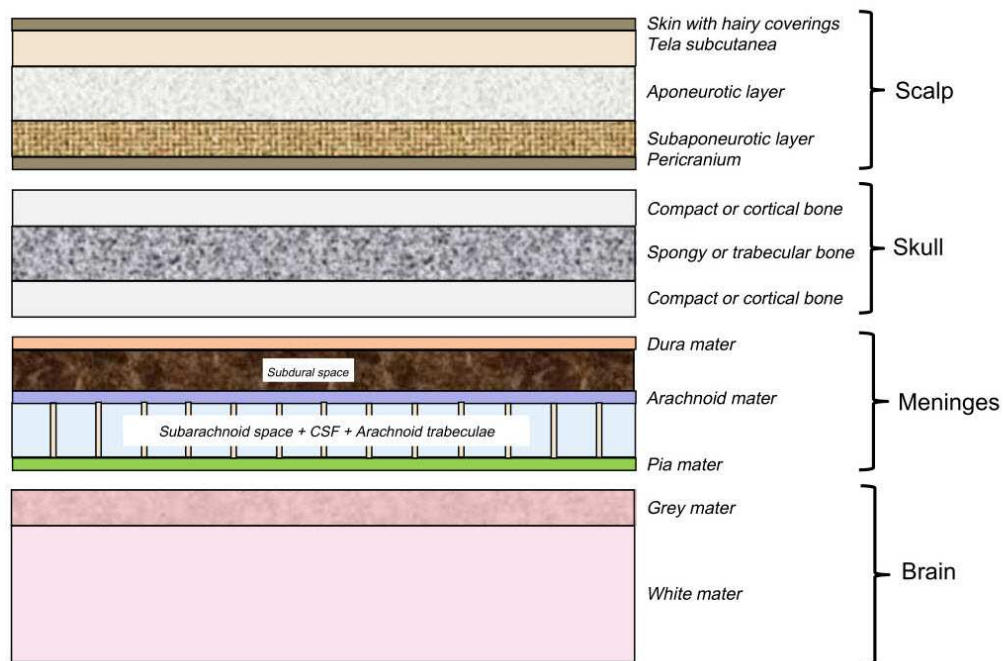


**Figure 2.8. Simplified representation of the human head layers of the scalp, skull, meninges and brain (after Yan and Pangestu, 2011).**

### *2.5.2. The dura mater and dural folds*

The membranes of the brain are collectively called the meninges, and consist of the dura mater, the arachnoid mater and the pia mater. Together, the arachnoid and pia are known as leptomeninges. The arachnoid is in direct contact with the dura, but it is separated from the pia through the subarachnoid space, which is filled with the cerebrospinal fluid (CSF). Despite this fact, arachnoid and pia are still connected via filaments named arachnoid trabeculae (Adeeb *et al.*, 2013).

The dura mater is composed of two layers, an outer endosteal layer (the periosteum covering) and an inner meningeal layer, which is the proper dura. This layer is a dense and fibrous membrane which covers the brain and the spinal cord, and extends inwards into four septa, dividing the cranial cavity: the falx cerebri, the tentorium cerebelli, the falx cerebelli, and the diaphragma sellae (Snell, 2010). The current research focuses only on the first two of these structures.

The falx cerebri is a sickle-shaped projection of dura mater which extends longitudinally in the fissure between cerebral hemispheres, forming an incomplete partition. It extends anteriorly in humans, from the crista galli, where it is thinner, to the internal occipital protuberance, where it blends with the surface of the tentorium cerebelli (Butler *et al.*, 1999). The tentorium is a crescent-shaped fold covering the surface of the cerebellum and supporting the cerebral lobes. Its most recognizable structure is the tentorial notch, an anterior opening which acts as a passage for the midbrain (Snell, 2010). Therefore, the falx cerebri separates both cerebral hemispheres, and the tentorium cerebelli separates those hemispheres from the cerebellum (Figure 2.9).

As with virtually all other soft tissues in the vertebrate body, dura mater is an anisotropic material. However, in large areas it effectively behaves isotropically, with its collagen fibres having no consistent pattern, except in the temporal region, where 80% of them share the same orientation (Hamann *et al.*, 1998).
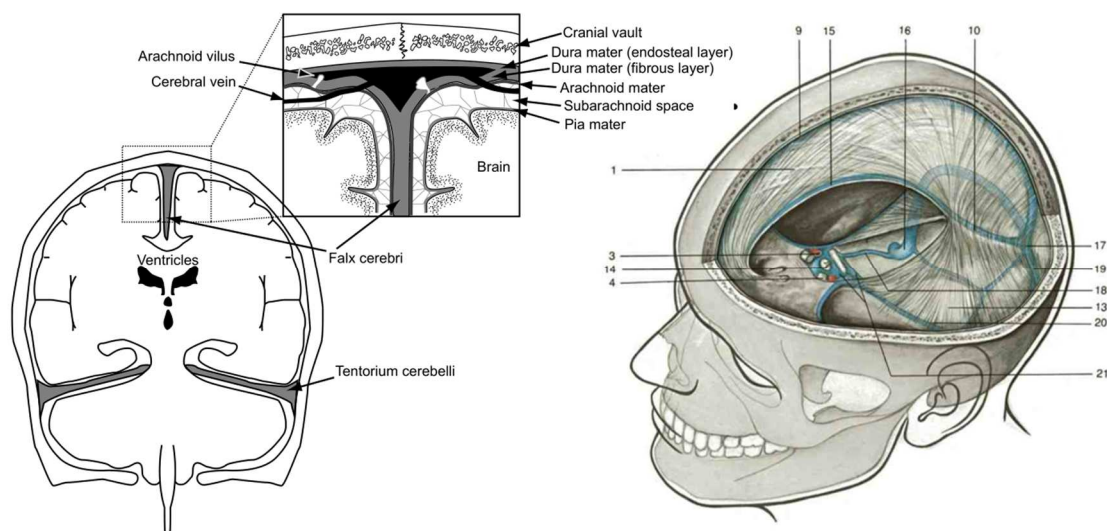


**Figure 2.9. Left: Coronal section through the plane of the foramen magnum showing the meningeal layers (after Lieberman, 2011). Right: Left lateral view of the human head with falx cerebri (1) and tentorium cerebelli (13) (after Rohen *et al.*, 2006).**

### 2.5.3. Function

Several authors (*e.g.* Bull, 1969; and see references in Jeffery, 2002) have concluded that the most probable function for the tentorium is to withstand the weight of the cerebrum.

Apparently, both membranes support the brain to some degree, and also restrict its displacement when subjected to acceleration and deceleration, preventing it from rotating inside the skull (Kumaresan and Radhakrishnan, 1996; Snell, 2010). An experiment carried out by Sabet *et al.* (2008) highlighted the importance of the falx, as the fissure isolates both hemispheres over the corpus callosum. When subjected to normal forces, the falx acts as a lateral constraint; however, the structure seems less effective in rotational impacts, as they subject the brain to a combination of shear forces which cause it to move around the tip of the falx in the region of the corpus callosum (Bradshaw, 2001). The presence of cerebral partitions also affects the spatial distribution of intracranial pressure (Kumaresan and Radhakrishnan, 1996).

The dural folds may also have played a role in human evolution. In their influential paper, Moss and Young (1960) suggested that soft tissues of the head define, to a large extent, the morphology of bone. For the neurocranium in particular, the dura would play a crucial part, defining growth vectors which direct the size and shape of the braincase during brain development. This may be supported by the creation of a *Bauraum* of *Homo neardenthalensis* (Witzel, 2011). In this study, external forces are applied to a homogeneous and undefined FE model (with six prior assumptions), and low stress areas are removed iteratively until the shape of the *Bauraum* resembles that of the specimen. This may demonstrate that applying lateral acceleration forces to the brain leads to tensile stresses along the periphery of the falx cerebri, and results in compression of the calvarium, which is described by Witzel as "rather like the situation found in a bridge".

It has also been suggested that the falx and tentorium not only act as constraints during cranial development, but exert tension that may also have constrained the shape of the neurocranium and brain development during evolution of the genus *Homo*. Following Moss and Young (1960), it is hypothesized that with progressive brain enlargement, the falx was unable to grow at the same rate, and as a consequence it acted as a longitudinal tensor, causing a parietal midsagittal shortening (Bruner *et al.*, 2004). Interestingly, in humans, the tentorium's midline ridge is more orientated in its posterior area towards the foramen magnum than in non-human primates and other mammals, perhaps as a response to the increased load of the cerebrum, in part due to the upright posture, and therefore altering the general load distribution of the skull (Bull, 1969), but this hypothesis still needs to be proven (Jeffery *et al*., 2002).

### 2.5.4. Comparative anatomy and ossification of the dural folds

The tentorium cerebelli is present in mammals and birds, but absent in reptiles, amphibians and fishes (Klintworth, 1968). These findings suggest that this structure evolved late in evolution, first as independent symmetrical folds of dura mater (stage A), and then gradually merging behind the brainstem, thus forming the classic crescent shape (stages B and C) (Klintworth, 1968; Figure 2.10). In humans, the tentorium is more developed than in other species, perhaps due to its role in supporting their cerebral hemispheres, which are heavier (Bull, 1969).
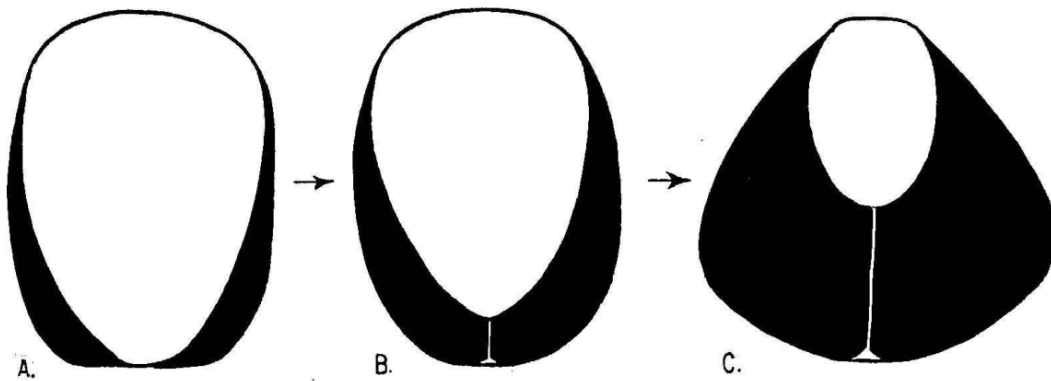


**Figure 2.10. Schematic diagram with the proposed stages of tentorium evolution (Klintworth, 1968).**

Ossification of the falx cerebri exists in some pinnipeds, ursidae, sirenians and cetaceans (Nojima, 1988; Colbert *et al*. 2005). It is also present in Monotremata. An analysis of the endocast of a modern platypus (*Ornithorhynchus anatinus*) revealed a prominent ossified falx cerebri, a feature which was also present in the Miocene fossilized platypus *Obdurodon dicksoni* (Macrini *et al.*, 2006a). Vincelestes, a fossil of an Early Cretaceous nonmammalian cynodont, also has an ossified falx cerebri (Macrini *et al*., 2007 and Macrini, 2006b).

An ossified tentorium was identified in a larger number of groups by Nojima (1988): carnivorans, odontocetes (Colbert *et al*., 2005), equids (Solano and Brawer, 2004) and pholidotes (Macrini *et al*., 2007), but in some of these groups, complete ossification is still rare. It has also been reported in some primates (Saban, 1975; Nojima, 1990a; Horovitz and McPhee, 1999; Kay *et al.*, 2008). Vincelestes also possesses an ossified tentorium (Macrini *et al*., 2007).

Curiously enough, there does not seem to be any direct correlation between the bony falx and the corresponding bony tentorium, despite the fact that they are almost identical histologically (Nojima, 1990a). Platypuses have only the former, whereas canids and felids, for example, only have the latter. Bony falx and tentorium are both present in Vincelestes, as they are in cetaceans, and many other mammal species lack ossification in both structures.

Matters become even more complex when the origin of ossification is considered, because the process can occur prenatally or postnatally depending on the species. For example, new-born specimens of *Felis silvestris catus* (common household cats) present an almost completely ossified tentorium cerebelli, while in *Stenella attenuata* (spotted dolphins) dural folds become gradually ossified during their lives. This led to Nojima (1988; 1990b) to differentiate between the carnivore type and the dolphin type. Marsupialia, Perissodactyla, Sirenia, Carnivora and some Cetacea (the families Physeteridae and Ziphiidae) would then belong to the carnivore type, meaning that their falx and/or tentorium would ossify during fetal ontogenetic stages. On the other hand, Primates and other Cetaceans (specifically, several genus of Delphinidae and Phocoenidae; Figure 2.11) would belong to the less common dolphin type.
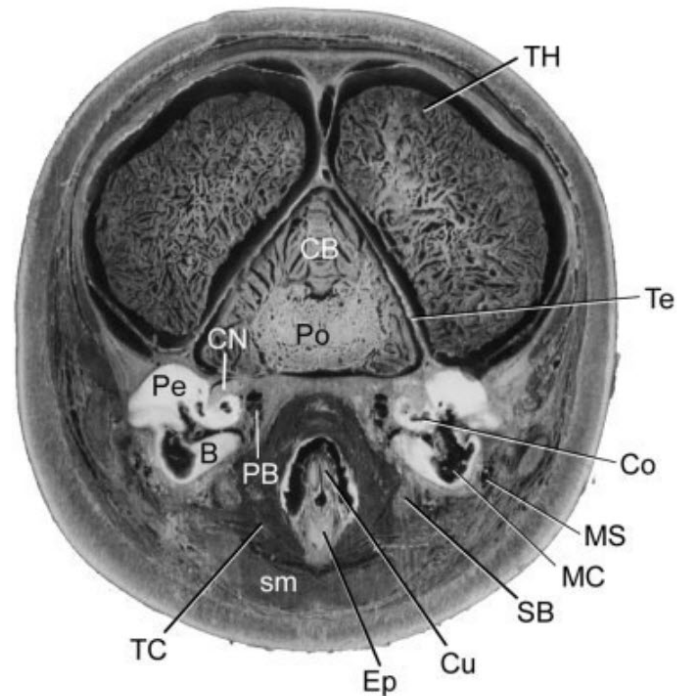
**Figure 2.11. Transverse section in frontal view in a perinatal specimen of spotted dolphin (*Stenella attenuata*) showing the tentorium cerebelli (Te). After Rauschmann *et al.*, 2006.**

A detailed account of ossification of dural folds in Mammalia is presented in the following chapter.

### 2.5.5. Anatomy of the tentorium cerebelli

The tentorium cerebelli has a fixed margin and a free margin. The fixed margin is the outer region that is connected to the bone, specifically to the posterior clinoid processes of the sphenoid anteriorly, to the superior border of the petrous part of the temporal in the middle part, and to the transverse sinus grooves of the occipital in the posterior part in humans. The free margin is the internal edge of the tentorium; it is in the shape of a U that forms the tentorial notch, also known as incisura tentoria, and offers a passage for the midbrain (Adeeb *et al*., 2012; Rai *et al*., 2018).

As discussed above, depending on the species, the tentorium can appear as a completely non-ossified structure, but it can also be partially ossified or (much more

rarely) completely ossified, as it is the case in Felids (Klintworth, 1968; Nojima, 1990a). When ossification is partial, a reflection of dura mater encloses the bone and extends beyond it as the soft tentorium. The ossification frequently manifests in the shape of a tentorial process (*processus tentoricus*, Figure 2.12), a rostro-medial projection at the dorsal part of the caudal border of the parietal bone in the shape of a leaf (Evans and De Lahunta, 2012). In some species, particularly in Carnivorans and Equids, the tentorial process, together with the occipital process, form the osseous tentorium cerebelli (König and Liebich, 2005). The occipital process or internal occipital protuberance is the area where the four fossae of the cruciform eminence intersects. The horizontal arm of the cross, where the two superior cerebral fossae are separated from the two inferior cerebellar fossae, is formed by a groove that accommodate the transverse sinuses, which drain blood from the back of the head.
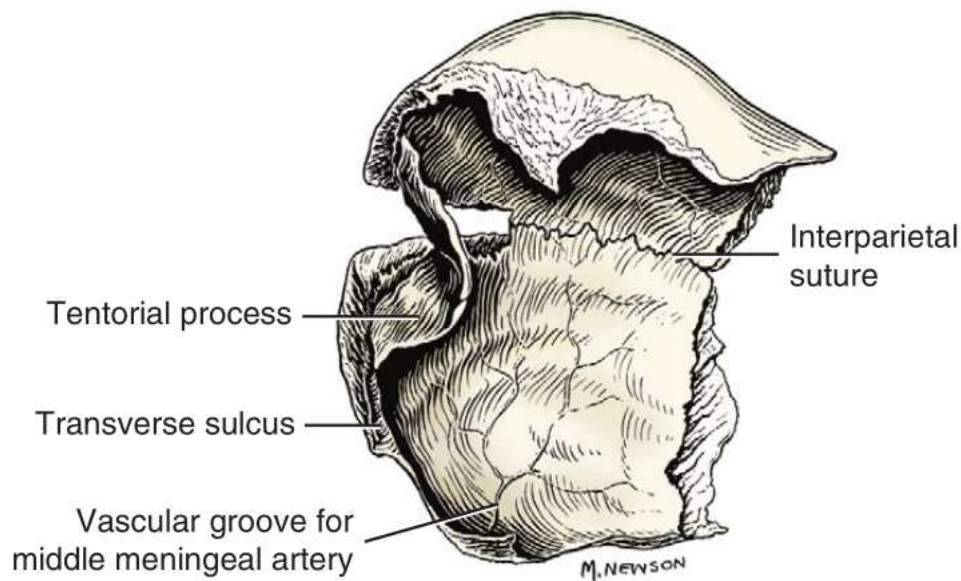


**Figure 2.12. Ventral aspect of the parietal bone of the dog, showing the location of the tentorial process. After Evans and De Lahunta (2012).**

Nojima (1990c) described two different types of ossified tentoria (A and B), both subdivided further into two subtypes (I and II). Type A indicates a species in which the tentorial process reaches the base of the skull, while Type B corresponds to species where it does not. In the subtype A-I, the tentorial process projects from the occipital border of the parietal bone. In the subtype A-II it projects from the squamous border of the parietal

bone. In the subtype B-I, the tentorial process is present, and in the subtype B-II it is absent (see Table 2.1).

| BT types | Illustrations of BT (superior surface)[a] | BT as a whole . . . | *Proc. tent.* projects from . . . | Family names | BF |
|---|---|---|---|---|---|
| A Type I | | crosses on the petrosa and articulates with the alisphenoid (left side) or crosses beyond petrosa and fuses with the anterior portion of the middle cranial fossa (right side). | the (whole) occipital border of the parietal bone. | Felidae (probably all spp.) | (−) all spp. |
| | | | | Viverridae[b] | (−) |
| | | | | Hyaenidae[b] | (−) |
| A Type II | | crosses beyond the petrosa and forms the lateral floor of the middle cranial fossa (★) (left side) or terminates on the base of the petrosa (right side). | posterior one-third or two-thirds of the squamous border of the parietal bone. | Procyonidae[b] | (−) |
| | | | | Ursidae (probably all spp.) | (+) only *Ursus* |
| | | | | Otariidae (all spp.) | (+) all spp. |
| | | | | Odobenidae | (+) |
| | | | | Phocidae (harp, ribbon seals) | (+) all spp. |
| | | | | Mustelidae (probably all spp.) | (−) all spp. |
| B Type I | | does not reach the base of the skull. The BT and BF are composed of the occipital element (left side) only or plus the fontanel element (right side). | (The *proc. tent.* is absent.) | Phocidae (gray, common, ringed, leopard, hooded seals) | (+) all spp. |
| B Type II | | does not reach the base of the skull. | the occipital border of the parietal bone. | Canidae (all spp.) | (−) all spp. |
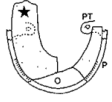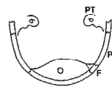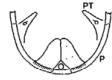
[a] Dotted portions are the *proc. tent.* (parietal elements) which project from the lined portions of the parietal bones (P). PT: petrosa, O: occipital element, F: fontanel element.

[b] These families are classified into A type; however, the BT elements have not been examined.

**Table 2.1. Comparison of the osseous tentorium types of Carnivorans. Nojima, 1990c.**

### 2.5.6. Tentorial index

Klintworth (1968) proposed the tentorial index formula, which was intended to serve as an indication of variability in the shape of the tentorium and, in particular, of the variation of the length of the straight sinus relative to the notch length. The formula is obviously only applicable in mammal species in which a straight sinus is present:

$$TI_i = \frac{PTL_i \times 100}{LN_i}$$

where $TI_i$ is the tentorial index, $PTL_i$ corresponds to the posterior tentorial length (the distance between the tip of the tentorial notch and the most anterior point of the confluence of sinuses or torcula), and $LN_i$ is the notch length (the distance between the posterior end of the dorsum sellae and the tip of the tentorial notch) of a given species *i* (Figure 2.13). Table 2.2 presents the tentorial indices of various mammalian species, as calculated by Klintworth (1968).
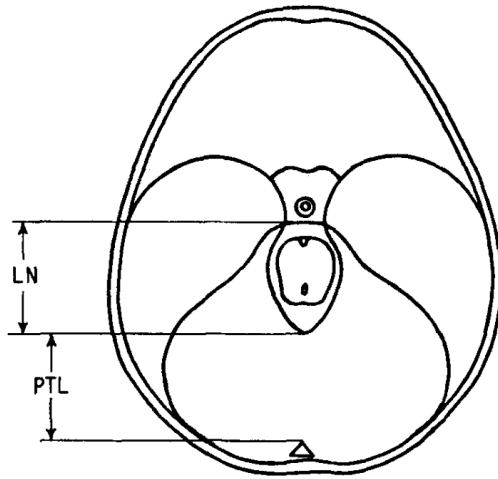
**Figure 2.13. Diagram summarizing the measurements for the tentorial index formula. (From Klintworth, 1968).**

| Order | Species | Tentorial index |
|---|---|---|
| Primates | Hussar monkey (*Erythrocebus patas*) | 87 |
| | Human (*Homo sapiens*) | 52-131 (76) |
| | Rhesus monkey (*Macaca mulatta*) | 115 |
| | Squirrel monkey (*Saimiri sciurea*) | 122 |
| | Vervet monkey (*Cercopithecus aethiops*) | 68-143 (95) |
| | Western baboon (*Chaeropithecus papio*) | 100 |
| | Angwanatibo (*Arctocebus calabarensis*) | 14 |
| Carnivora | Domestic cat (*Felis catus*) | 50 |
| | Domestic dog (*Canis familiaris*) | 61 |
| | Mink (*Mustela vison*) | 50 |
| Artiodactyla | Domestic goat (*Capra hircus*) | 11 |
| | Domestic swine (*Sus scrofa*) | 17 |
| | Sheep (*Ovis aries*) | 17 |
| | White-tailed deer (*Odocoileus virginianus*) | 13 |
| Chiroptera | Evening bat (*Nycticeius humeralis*) | 0 |
| Cetacea | Pacific bottle nose dolphin (*Tursiops gilli*) | 63 |
| | Pacific common dolphin (*Delphinys bairdi*) | 66 |
| Rodentia | Guinea pig (*Cavia porcellus*) | 0 |
| | Gerbil (*Gerbillus paeba*) | 0 |
| | Golden hamster (*Mesocricetus auratus*) | 0 |
| | House mouse (*Mus musculus*) | 0 |
| | White rat (*Rattus norvegicus albinus*) | 0 |
| Lagomorpha | Rabbit (*Oryctolagus cuniculus*) | 7 |
| Marsupialia | Opossum (*Didelphus virginiana*) | 0 |
| | Wallaby (*Marcopus brownii*) | 19 |

**Table 2.2. Tentorial indices of various mammalian species. Data for human (*Homo sapiens*) and vervet monkey (*Cercopithecus aethiops*) are mean values of samples of 48 and 47 specimens. The other indices are based on single observations (after Klintworth, 1968).**

### 2.5.7. Ossification in humans

The composition of the dura mater varies with age, with the proportion of calcium, phosphorus and magnesium increasing progressively with aging, while sulphur, iron and zinc remain constant (Tohno *et al*., 2000). There is considerable confusion in the literature when discussing the mineralization of the dural folds and when it is merely calcification and when is proper ossification, which is the generation of true, complete bone tissue. To provide a consistent terminology, the term "ossification" will be used here and throughout this work, as it is more commonly employed in the literature, not only for referring to the consistent mineralization of dural structures in many mammalian orders (Klintworth, 1968; Nojima, 1990a, 1990b and 1990c), but also in several studies concerning humans which present mineralization in their dural folds either spontaneously or as a consequence of a clinical condition (Tsitouridis *et al.*, 2006; Debnath *et al.*, 2009; Tubbs *et al.*, 2012; although there are exceptions, such as Zandian *et al.*, 2014). The distinction between calcification and ossification and its implications will be discussed in greater detail in Section 3.4.1.

Ossification of the falx cerebri (Figure 2.14), either partial or complete is relatively rare in humans, but there are several examples in the literature (Batnitzky *et al.*, 1974; Tsitouridis *et al.*, 2006; Rangoji *et al.*, 2007; Debnath *et al.*, 2009; Zandian *et al.*, 2014). Percentages of ossification in the general population vary depending on the study. Sands *et al.* (1987) identified 0.4% of cases in a sample of 3,000 MRI scans. Other research provide much higher occurrences of this condition: for example, after studying 1,162 patients, Tanaka and Takeuchi (1974) found 10% cases of ossification of the falx cerebri. In fact, Saldino (1974) points out that authors have reported extreme values, as low as 1% and as high as 15%. Two different types of falx ossification can be differentiated. In Type A, ossification starts at the interior surface of the calvarium and closely follows it, while in Type B, it does not have any continuity with this structure (Tsitouridis *et al*., 2006).
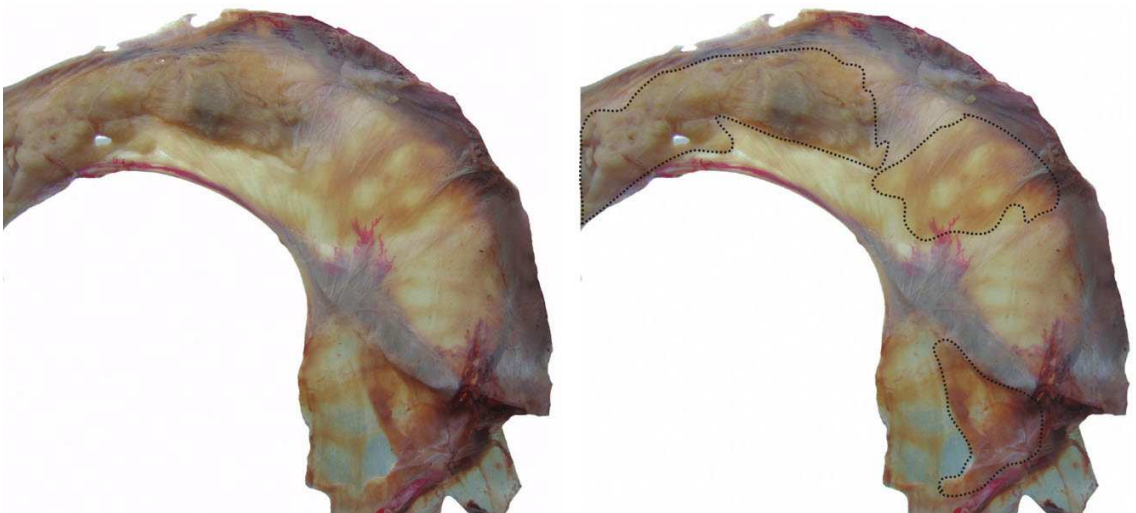
**Figure 2.14. Partial ossification of the falx cerebri in two human specimens. Above, Rangoji *et al*., 2007; below, Zandian *et al*., 2014. Dotted lines indicate areas of ossification.**

In individuals with partial ossification, the condition usually manifests in the form of small bony islands in the frontal portion of the falx near its attachment to the crista galli (in 27 out of 40 cases studied by Tsitouridis *et al*., 2006), followed by the middle area, and then the posterior part. Complete ossification is much rarer, with perhaps only one case reported in the literature, that of a 74 year-old male (Tubbs *et al*., 2006). On the

other hand, ossification of the tentorium cerebelli (Figure 2.15) is extremely rare in humans (Tanaka and Takeuchi, 1974), and according to Tubbs *et al.* (2012) only a handful of cases have been reported.



**Figure 2.15. CT scans showing ossification of tentorium cerebelli in a human specimen. Tubbs *et al.*, 2012.**

## 2.6. Techniques for 3D cranial digitalization, modelling and analysis

This section discusses the main techniques and methods used in the analyses of this thesis. It starts with an introduction to biomechanics, followed by a brief description of two imaging techniques able to produce digital models of specimens (CT and MRI scanning) and a detailed explanation of the process of creation of a finite element (FE) model and its subsequent analysis. The section concludes with a retrospective of FE models of the human head of the past decades, focusing in particular on those that include soft tissues.

### 2.6.1. Vertebrate Biomechanics and digital biomechanical models

Biomechanics is a term that describes the multidisciplinary science which uses the principles of mechanics to study the shape and function of living organisms. It can be used to study both the internal and external forces that act on a specimen's body (Hall, 2014). The most traditional biomechanical method involves a theoretical approach to

produce a hypothesis that is later tested via experimental techniques that offer information about forces in the biological structure of interest, such as the use of strain gauges or force transducers (Richmond *et al.*, 2005). A more recent approach is the generation of a digital model in which it is possible to test how a complex structure reacts to applied forces in ways that sometimes are not possible to perform with *in vivo* specimens; for example, to digitally alter a biological structure to test its functional implications or to simulate activities such as biting in extinct specimens (Bright, 2014).

In the last two decades, FEA has rapidly become one of the most important techniques in the field of vertebrate biomechanics. In the case of cranial biomechanics it seems that, although the skulls (as complex systems that perform multiple competing functions) are optimized for more than one activity, feeding behaviour strongly defines the craniofacial form in mammals (Dumont *et al.*, 2005) and this is perhaps one of the reasons why analyses of biting and feeding are by far the most frequent ones performed with skull models.

### 2.6.2. Digitalization techniques: CT and MRI

Computed tomography (CT) and magnetic resonance imaging (MRI) are two imaging methods used for medical and non-medical applications (Figure 2.16). In the fields of Palaeontology, Biology and Biomedicine these two non-invasive techniques can be employed to provide a digital 3D reconstruction of the internal anatomy of a given specimen in order to perform FE analyses, although each works in a different manner (Ziegler *et al.*, 2011; Cunningham *et al.*, 2014).

From the measurement of the attenuation of X-rays, CT can create a series of stacked images of cross-sections of the specimen (Herman, 2009). The basis for the technique is that some tissues, for example, bone, absorb X-rays more effectively than others (Smith and Webb, 2011). More recently, micro-CT scanning has allowed a significant increase in resolution, down to a few microns or less (Cunningham *et al.*, 2014), revealing much more detailed information.

MRI uses magnetic fields to generate the images instead of X-rays, and operates in the radio-frequency range, and therefore does not employ ionizing radiation (Landini *et al.*, 2005). In CT, the contrast is achieved by the X-rays traversing through tissues with

different densities and consequently being absorbed and weakened to various degrees, while in MRI the contrast is obtained by detecting changes in the spin directions of the hydrogen nuclei in the tissues analysed. The image can be further enhanced by variations in the pulse sequences related to the longitudinal and transverse relaxation times (T1 and T2 respectively) (Kalra, 2018).

The images obtained with CT and MRI can then be used to reconstruct a digital three-dimensional version of the specimen, but each technique has its own advantages. Most significantly, MRI provides better soft-tissue contrast than CT, as illustrated in Figure 2.16, but is more expensive and generates images of lower resolution (Smith and Webb, 2011; Cunningham *et al.*, 2014).
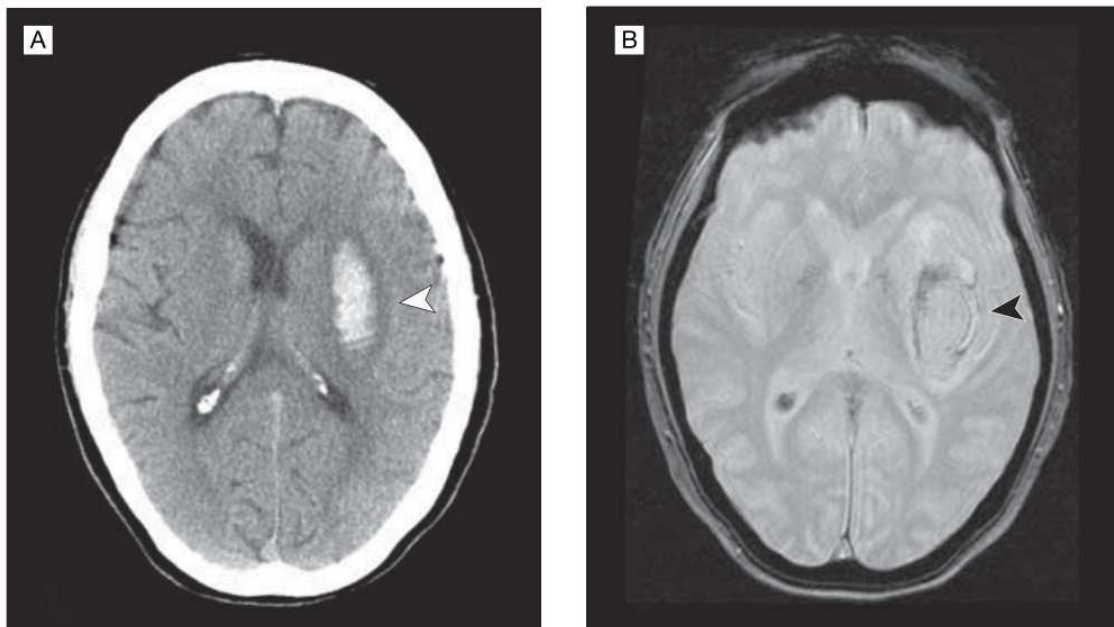


**Figure 2.16. Acute intraparenchymal hematoma visualized with Computed Tomography technology (left) and Magnetic Resonance Imaging (right). Kidwell *et al.*, 2004.**

### 2.6.3. Finite Element Analysis

Finite element analysis (FEA) is a technique for reconstructing stress, strain and deformation. It redefines the structure of interest by a (finite) number of discrete elements with properties that spatially represent the physical problem (Rayfield, 2007). In 3D, these elements are normally tetrahedral or hexahedral in shape, and are connected

together to create a three-dimensional mesh. FEA has been used in engineering and (for example) medical implant design (Fagan and Lee, 1986) for many years, but it has only relatively recently been used to study biological systems, in particular, in the field of functional morphology (Kupczik, 2008).

The FE modelling process can be summarized in four main steps: pre-processing, solution, post-processing and validation (Figure 2.17).
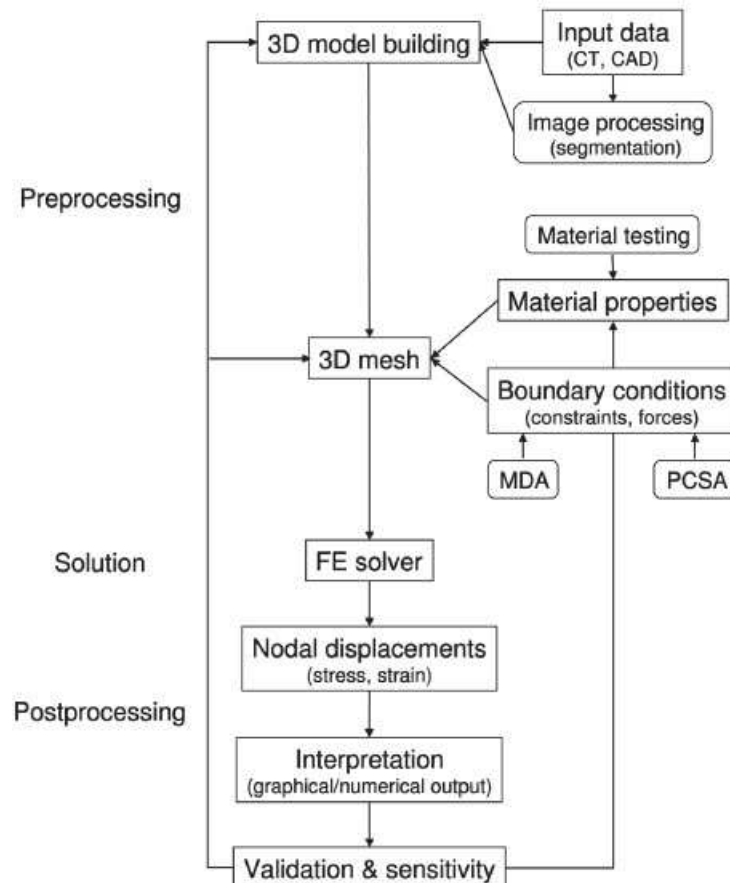


**Figure 2.17. Flow chart of the different steps involved in finite element analysis (from Kupczik, 2008).**

2.6.3.1. Pre-processing

**Scan:** Most recent FEA models are three-dimensional, with structures needing to be scanned and reconstructed as a virtual model for analysis. Although a variety of methods exist, the most widely used are CT or MRI scans (see previous section).

**Segmentation:** In this stage the structures of interest in the scans are separated from one another. Different tissues (brain, muscles, bone, etc.) normally have different contrast thresholds and thus they can be segmented (separated) by using one of the multiple algorithms available. However, further manual refinement is still necessary in most cases, requiring either painting or masking to further define the structures of interest. This is normally required due to the quality and definition of the scans, or the presence of artifacts (motion, rings) or other factors. Segmentation then becomes a rather laborious and time-consuming semi-automatic process that may include several intensity-based methods, such as thresholding, region growing, clustering etc. (Kalra, 2018; Figure 2.18).
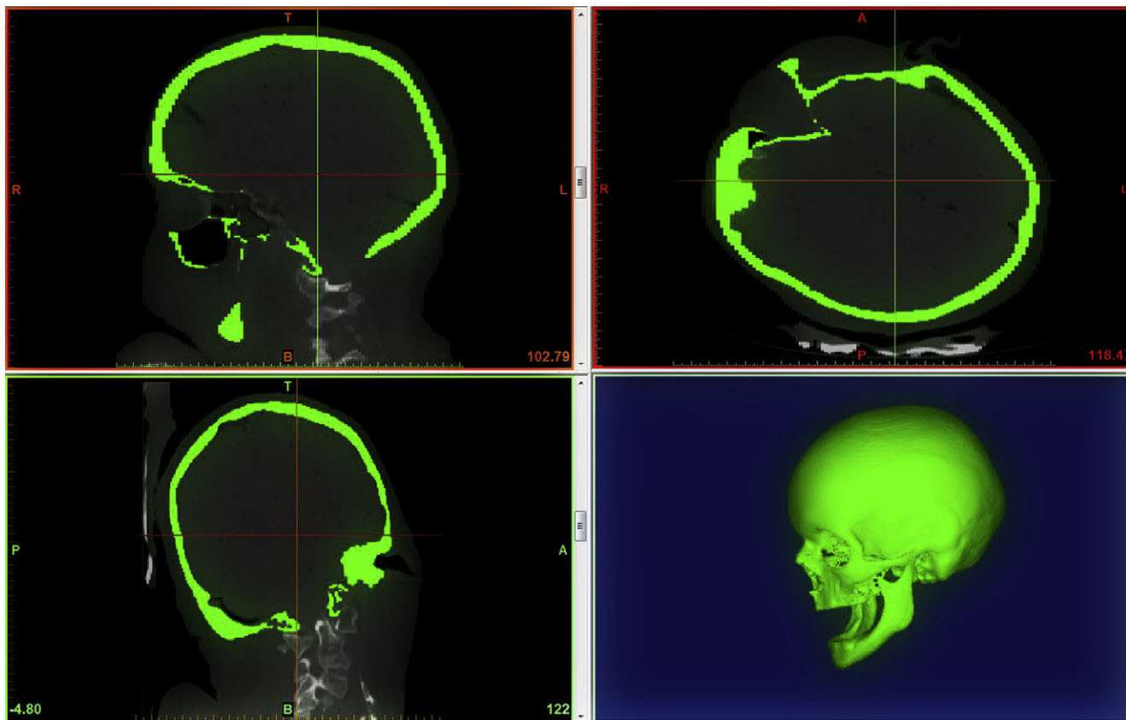


**Figure 2.18. An example of the segmentation process using the bone material of a human cranium from CT scans (Kalra, 2018).**

**Mesh creation:** Following segmentation, the areas of interest are extracted from the digitalised images and assigned to discrete labels (Kupczik, 2008). The different regions of the physical structure are then divided into the finite elements, normally by a meshing algorithm in the image processing software, with options to control their number and distribution.

**Assign material properties and recreate loading conditions:** The next step is to define the material properties of the elements which describe the mechanical behaviour of the tissue. For an isotropic material, these are defined by Young's modulus of elasticity and Poisson's ratio (Kupczik, 2008). In reality, bone properties, as many other tissues in the head, vary with orientation (a condition known as anisotropy) and location, complicating the process. However, it is impractical to determine all the material constants required to fully define anisotropic properties of biological materials. In practice, therefore, most FE analyses of biological materials assume isotropy and homogeneity, which, fortunately, has been demonstrated to produce reliable results, especially for comparative studies (Rayfield, 2011).

Boundary conditions, that is where the object being studied interacts with other bodies, must also be defined. Most importantly these must collectively ensure that the model is sufficiently constrained to avoid free body motion. This can be achieved by applying single node constraints (Cox *et al.*, 2012) or frameworks of rigid links (Degrange *et al.*, 2010) if wanting to represent a more complex or distributed contact. This step is very important, because constraint application at the wrong places will generate erroneous results, and possibly stress and strain concentrations (Rayfield, 2011). After that, the loading conditions must be recreated. Again their correct application is critical, if accurate results are to be produced.

2.6.3.2. Solution and Post-processing

The FE solver calculates the nodal displacements from which the stresses and strains are calculated. The post-processing involves the numerical or graphical presentation of the solution, generally using contour plots which present the location and variation of a given parameter.

2.6.3.3. Validation

The process of validation involves the assessment of the accuracy and validity of the results. This is done by comparing those results against theoretical and, ideally, experimental data. According to Richmond *et al.* (2005): "Accuracy is defined here as the closeness of the model's results to the real biological situation. Precision is defined

here as the closeness of the model's results to the exact solution of that biomechanical model".

Accuracy can only be evaluated with empirical data, but the precision of a model can be assessed through convergence tests. Complex FE models demand extremely high computational requirements, and this has led researchers to develop strategies to simplify their models by different means: using a two-dimensional approximation, modelling half of the model in symmetrical structures, or reducing the size of the mesh by reducing the number of its constituent elements (Richmond *et al*., 2005). All models imply some degree of simplification when trying to reflect reality, but over-simplification can lead to inaccuracies and misinterpretations. By performing a process known as mesh convergence testing it is possible to confirm that a given model has a sufficient number of elements to ensure mathematical convergence to the current representation (Bright and Rayfield, 2011). However, with experience and the continuous increase in computational power, this step has become less and less necessary, with users now able to create models with several million elements that can still be solved reasonably quickly. In parallel with this, sensitivity analyses are then used to test the effects of any approximations or simplifications in size, structure, boundary conditions or material properties, for example (Kupczik, 2008).

### 2.6.4. Soft-tissue modelling in previous FE models

With the exception of human models, to which more attention has generally been devoted, most cranial FE analyses have been focussed on the bone. However, there are a few exceptions: for example, keratin in the beak of birds (Soons *et al.*, 2012) or cartilage in fishes or reptiles (Wroe *et al*., 2008; Jones *et al.,* 2017). Sometimes, 3D models of primates have also been used as testing specimens, perhaps in substitution of human models (Curtis *et al*. (2011) for the temporal fascia; Wood *et al*. (2011) for the periodontal ligament). In most of these examples the tissues were modelled by using linear elastic, isotropic material properties. Also, the increase in computational power over the last decades has driven some researchers to include nonlinearity in FE models with more ease. For example, and limiting the list merely to cranial structures, some researchers have created nonlinear models of the eyes (Stitzel *et al.*, 2002; Schutte *et al.*, 2006; Girard *et al.*, 2011), the dura mater (Yue *et al.*, 2008; Li *et al.* 2017; MacManus *et al.*, 2017), the

periodontal ligament (Toms and Eberhardt, 2003; Wood *et al.*, 2011) and the brain (e.g. the six models reviewed by Miller *et al.* (2017), which follow either viscoelastic or hyperelastic approaches, but there are many others). However, it should be noted that most of these models are either concerned with single-organ structures (as is the case of the several nonlinear models of the eyes) where strains are studied locally, or deal with the effects of impact trauma (which is the case of the modeling of the brain to assess injuries), where strain rates are much higher than in the biting FE models used for most functional morphology studies, and therefore the modeling of nonlinearity has a greater impact in the results.

During the last few decades, a great deal of effort has also focused in the development of FE human head models for testing of impact and trauma, which use soft tissues in their analysis of overall dynamic effects. One of the very first attempts which involved experimental validation with cadaveric heads, was the one developed by Ward and Thompson (1975). The brain, together with the dural folds (falx cerebri, tentorium cerebelli), were included in this early model. Later, the Wayne State University Brain Injury Model (WSUBIM; Ruan *et al.*, 1992; improved in Ruan *et al.*, 1993) marked a new milestone in research of human head FE models. The original WSUBIM model consisted of 6080 nodes and had a three-layered skull, membranes and scalp, but was improved several times during the following decade, reaching a high level of detail, which included many facial features (Ming, 2013). With the new millennium, the increase in computing power and the technology cost reductions have allowed the scientific community to create ever more accurate and detailed models, opening multiple research possibilities. As a recent example, Mao *et al.* (2013) developed a human head model which was used to test thirty-five different impact-case scenarios. The model had 270,552 elements, which differentiated between dura, pia and arachnoid matter, and included bridging veins, facial tissue and scalp, amongst others.

Some of these models, together with their principal characteristics, are summarised in Table 2.3. The table is by no means exhaustive, but offers a good overview of the most relevant FE head models created for research purposes during the last two decades. For full reviews of FE models related with impact research, see Deck and Willinger (2009), Yang *et al.* (2011), Ming (2013) and Madhukar and Ostoja-Starzewski (2019).

There are other human head models not related to the study of trauma that also include detailed soft tissues. For example, Barbarino *et al.* (2009) produced a model of the human face for aging simulations, amongst other possible applications. The epidermis and dermis were modelled as a 2 mm layer of constant thickness, and the SMAS[2] was added as a contiguous layer 3 mm thick. Deep fat and mucosa were also taken into account. The reconstruction was limited to the facial "mimic" muscles and the masseter; other muscles involved in mastication, such as the temporalis or the pterygoid were not included in the model. An improved FE model to assess facial soft tissue interactions was developed by Weickenmeier (2015).

The multimodal imaging-based detailed anatomical model (MIDA) of Iacono *et al.* (2015; Figure 2.19) goes further and reproduces 153 hard and soft tissue structures of the human head and the neck down to the level of the fifth cervical vertebra, being currently one of the most detailed virtual reconstruction of its kind. It is this geometry that is used as the basis for the FE model developed in Chapter 7 and Chapter 8. The data (belonging to a 29 year-old female volunteer) was acquired using various modalities. T1- and T2-weighted structural MRI with an isotropic resolution (identical in all dimensions) of 500 μm were used to obtain different contrast information. An additional heavily T2-weighted MRI was necessary to achieve additional detail level in the eye, the ear, and other structures. Two magnetic resonance angiogram (MRA) datasets were used to offer a better visualization of the vasculature. Finally, diffusion tensor imaging (DTI) was used to obtain data on fibre orientation and anisotropy.

---

[2] The superficial musculoaponeurotic system (SMAS) is a continuous non-uniform fibrous layer which connects the facial muscles with the dermis. It is a term commonly used in aesthetic surgery, but remains contentious, as no clear anatomic definition exist and some authors even doubt of its existence (Broughton and Fyfe, 2013; Ghassemi *et al.*, 2003).
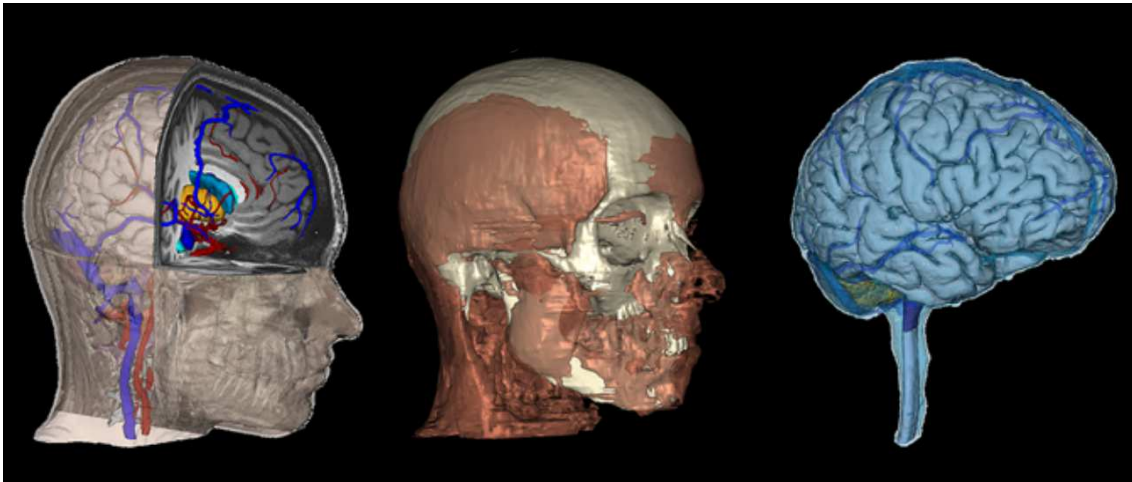
**Figure 2.19. Different 3D surfaces showing various structures created for the MIDA anatomical model. From left to right: complete MIDA model, muscles, dura mater and brain structures (adapted from Iacono *et al.*, 2015).**

A recent study by Cotton *et al.* (2016) proposed a novel approach for generating finite element head models, in which pre-segmented image data is modified and meshed in order to create FE head models that are adapted to the available computational resources and prepared to solve specific problems. This flexibility allows the level of detail of the final mesh to be defined and the incorporation of new structures or merging of previous ones.

| Reference | Name | Data | Purpose | Mesh type | Falx | Tentorium | Brain | Muscles | Skin/scalp | Eyes |
|---|---|---|---|---|---|---|---|---|---|---|
| Kang *et al.*, 1997 | ULP | Based on a single male | Impact | Generic | ✓ | ✓ | ✓ | | ✓ | |
| Hartmann and Kruggel, 1999 | | MRI | Impact | Subject specific | | | ✓ | | ✓ | |
| Kleiven and Holst, 2002 | | CT, MR and sliced photos | Impact | Generic | ✓ | ✓ | ✓ | | ✓ | |
| Horgan and Gilchrist, 2003 | | CT scans | Impact | Generic | ✓ | ✓ | ✓ | | ✓ | |
| Takhounts *et al.*, 2003 | SIMon | CT scans | Impact | 50th per. male | ✓ | ✓ | ✓ | | | |
| Kimpara *et al.*, 2006 | | Previous model and anat.ref. | | 50th per. male | ✓ | ✓ | ✓ | | ✓ | |
| Iwamoto *et al.*, 2007 | THUMS | ? | Impact | 50th per. male | ✓ | ✓ | ✓ | | ✓ | |
| Barbarino *et al.*, 2009 | | MRI | Aging | Subject specific | | | | ✓ | ✓ | |
| Brichtová *et al.*, 2009 | | CT scans | Impact | Subject specific | | | ✓ | | | |
| Chen and Ostoja-Starzewski, 2010 | | T1- and T2-weighted MRI | Impact | Subject specific | | | ✓ | | | |
| Huang *et al.*, 2011 | | CT scans | Impact | Subject specific | | | ✓ | | ✓ | ✓ |
| Truong *et al.*, 2012 | | MRI | tDCS | Subject specific | | | ✓ | | ✓ | |
| Hoursan *et al.*, 2013 | | CT and MRI | Impact | Subject specific | | | ✓ | | | |
| Mao *et al.*, 2013 | WSUHIM | CT and MRI, literature | | | ✓ | ✓ | ✓ | | ✓ | |

| | | | | | | | | | | |
|---|---|---|---|---|---|---|---|---|---|---|
| Hannula *et al.*, 2014 | | CT, MRI and cryo-sections | Biolectric Applic. | Subject specific | | | ✓ | ✓ | ✓ | ✓ |
| Sarvghad-Moghaddam *et al.*, 2014 | | Previous model | Impact | Generic | ✓ | ✓ | ✓ | | ✓ | |
| Huempfner-Hierl *et al.*, 2015 | | CT scans | Impact | Subject specific | | | | ✓ | ✓ | |
| Iacono *et al.*, 2015 | MIDA | MRI, MRA, and DTI | Multi-purpose | Subject specific | | ✓ | ✓ | ✓ | ✓ | ✓ |
| Tse *et al.*, 2015 | | CT and MRI | Vibration | Generic | | | ✓ | | | |
| Weickenmeier, 2015 | | MRI | Facial soft tissue interactions | Subject specific | | | | ✓ | ✓ | |
| Cotton *et al.*, 2016 | NRL-Simpleware | T1 weighted MRI | Multi-purpose | Subject specific | ✓ | ✓ | ✓ | ✓ | ✓ | ✓ |
| Fernandes *et al.*, 2018 | YEAHM | CT and T2-weighted MRI | Impact | Subject specific | | | ✓ | | | |
| Cai *et al.*, 2018 | | CT | Impact | Subject specific | ✓ | ✓ | ✓ | | ✓ | |

**Table 2.3. Some of the human head FE models created during the last decades which possess structures other than bone.**

**2.7. Conclusions**

The vertebrate head is an extremely complex biological system which performs multiple (and sometimes competing) functions, composed of many biological structures and modules that interact with one another. In the field of biomechanics, the finite element analysis technique can be used to create functional models of heads to be used for *in silico* experiments with the aim to test scientific hypotheses. However, the creation of these FE models must deal with the issue of complexity in such a way that simplification does not come at the cost of accuracy.

So far, most FE studies have focused on the cranium itself, but many other different tissues and internal structures interact in the head system, the mechanical function of some of which is still poorly understood. For example, the falx cerebri and the tentorium cerebelli have been routinely included in human models for studies of trauma, but never assessed in a mastication study, and the cause for ossification of these dural folds in various mammalian lineages is currently unknown. Moreover, FE analyses can be used to replicate conditions not found *in vivo*; for example, the postorbital bars, the postorbital septa and the postorbital ligaments can be altered digitally to assess their mechanical role over a single geometry.

These and other understudied biological structures of the mammalian head are the main focus of the study in this thesis. The following chapter includes a thorough review of the dural ossification literature, together with new findings and a discussion of two hypotheses for the ossification that have been proposed in the past.

# Chapter 3. A study of dural ossification in Mammalia

Partial or total ossification of the intracranial dural folds, affecting either the falx cerebri or the tentorium cerebelli, have been identified in several species of mammals, but the functional significance of this condition has never been fully explained. Moreover, the last systematic study of dural ossification in mammals was undertaken almost three decades ago. In an attempt to fill this gap, this chapter provides a comprehensive review of the body of literature surrounding dural ossification, complements it with further personal observations of the cranium of various groups missing from these earlier studies, and presents a full list of mammalian species detailing the condition of their falx and tentorium. With this comprehensive data, two earlier hypotheses are presented, discussed and, for the moment, disregarded.

## 3.1. Introduction

A wide range of authors have previously described the anatomy of the falx or tentorium in their studies for different animal species, either extant or extinct (for example, Poggesi *et al*., 1982; Polly, 1993; Macrini *et al*., 2007; Feijó and Cordeiro-Estrela, 2016; and many others), but the number of works which have dealt specifically with comparative anatomy and ossification are very scarce. Klintworth (1968) studied the presence, shape and degree of ossification of the tentorium in 44 species across different classes. Decades later, Nojima investigated the falx and tentorium in a further set of 172 species pertaining to 52 different families of mammals, including 48 species of Carnivorans (1990c), 40 species of Cetaceans (Nojima, 1990b) and 42 species of Primates (Nojima, 1990a).

The present study adds personal observations of another 40 extant specimens from various orders and families. Some have been already covered by Klintworth, Nojima or other authors; but many don't appear to have been described elsewhere. Table 3. includes a list of these additional specimens.

The aim of this work is twofold. Firstly, to provide a more comprehensive study of the osseous tentorium in Mammalia by gathering and updating all previous research and adding to it, especially to include underrepresented groups and fossil specimens, in an attempt to understand the resulting "big picture". In this sense, this chapter is intended

to serve as a literature review of dural ossification research as well as drawing together this large body of information for the first time. Taking into account both bibliographic references and personal observations, a total of over 250 different extant species are considered (with the condition of the dural folds summarised Appendix 1. Dural folds condition in extant species), and many other extinct ones. The second goal of this research is to test the evidence currently available against two explanations of ossification that have been offered in the past. These are summarized below:

**Ossification due to diet:** This suggests that postnatal dural fold ossification (so-called dolphin-type) could be related to a high dietary intake of food rich in calcium, phosphorus and vitamin D, and was originally proposed by Nojima (1988) after observing that ossification in spotted dolphins (*Stenella attenuata*) was a slow phenomenon that took place during the course of aging. However, he later dismissed this hypothesis after finding progressive postnatal tentorial ossification in spider monkeys (of the species *Ateles geoffroyi* and *Ateles paniscus*) which had been bred in a zoo with a diet that was not particularly high in vitamin D (Nojima, 1990a).

**Ossification due to behavioural causes**: Locomotion, concussion, biting and feeding – all these regular activities have been suggested to play a role in dural ossification in the past. They were summarized by Nojima (1990c), although the author did not provide the original source for them or perhaps they were never methodically tested before. In any case, Nojima refuted these arguments on the basis of the absence of ossification in most herbivores and rodents. The author concluded that "the former also appear to suffer considerable concussion during their habitual actions, for instance, bulls fighting during the rut. The latter gnaw hard materials using their incisors." (Nojima 1990c). The hypothesis that falx and tentorial ossification could play a role in Carnivoran biting combined with neck movements, has been tested systematically by performing an FE analysis on a 3D model of a *Felis silvestris catus* skull, which has an osseous tentorium, (Chapter 5 and Sellés de Lucas *et al.*, 2018). Briefly, that study found that an ossified tentorium slight decreases stress in the posterior part of the skull.

| Order | Family | Species | Common name | Sp. number |
|---|---|---|---|---|
| Dasyuromorphia | Thylacinidae | *Thylacinus cynocephalus* | Tasmanian tiger | Z90 |
| Dasyuromorphia | Dasyuridae | *Antechinus flavipes* | Yellow-footed Antechinus | Z98b |

| | | | | |
|---|---|---|---|---|
| Peramelemorphia | Peramelidae | *Perameles nasuta* | Long-nosed bandicoot | Z1684 |
| Peramelemorphia | Peramelidae | *Isoodon sp* | Short-nosed bandicoot | Z1751 |
| Diprotodontia | Phascolarctidae | *Phascolarctos cinereus* | Koala | Z699 |
| Diprotodontia | Vombatidae | *Vombatus ursinus* | Common wombat | Z68 |
| Diprotodontia | Phalangeridae | *Trichosurus vulpecula* | Silver-grey brushtail possum | Z100 |
| Diprotodontia | Macropodidae | *Macropus giganteus* | Eastern grey kangaroo | Z1681 |
| Diprotodontia | Macropodidae | *Macropus fuliginosus* | Western Grey kangaroo | Z1210 |
| Diprotodontia | Pseudocheiridae | *Pseudocheirus sp* | Ring-tailed possum | Z74 |
| Diprotodontia | Petauridae | *Dactylopsila trivirgata* | Striped possum | Z72 |
| Pilosa | Megalonychidae | *Choloepus didactylus* | Two-toed sloth | Z130a |
| Pilosa | Myrmecophagidae | *Myrmecophaga tridactyla* | Giant anteater | Z1554 |
| Cingulata | Dasypodidae | *Dasypus novemcinctus* | Nine banded armadillo | Z134 |
| Insectivora | Tenrecidae | *Tenrec ecaudatus* | Tenrec | Z3064 |
| Insectivora | Tenrecidae | *Setifer setosus* | Large Madagascar hedgehog | Z610 |
| Insectivora | Erinaceidae | *Echinosorex gymnura* | Moonrat | Z606 |
| Insectivora | Talpidae | *Talpa europaea* | European mole | Z600a |
| Primates | Galagidae | *Galago sp* | Galago | Z2361 |
| Primates | Cheirogaleidae | *Cheirogaleus sp* | Dwarf lemur | Z411 |
| Primates | Indriidae | *Propithecus sp* | Sifaka | Z405 |
| Primates | Cebidae | *Cebus sp* | Capuchin monkey | Z910 |
| Primates | Cebidae | *Aotus trivirgatus* | Three-striped night monkey | Z414 |
| Carnivora | Herpestidae | *Herpestes sp* | Mongoose | Z366 |
| Carnivora | Mephitidae | *Conepatus chinga* | Molina's hog-nosed skunk | Z376 |
| Carnivora | Mephitidae | *Mephitis mephitis* | Striped skunk | Z375 |
| Carnivora | Mephitidae | *Mephitis macroura* | Hooded skunk | Z375 |
| Perissodactyla | Tapiridae | *Tapirus indicus* | Malayan tapir | Z163 |
| Hyracoidea | Procaviidae | *Procavia capensis* | Rock hyrax | Z1743 |
| Tubulidentata | Orycteropodidae | *Orycteropus afer* | Aardvark | Z781 |
| Artiodactyla | Suidae | *Babyrousa babyrussa* | Buru babirusa | Z111 |
| Artiodactyla | Giraffidae | *Giraffa camelopardalis* | Giraffe | Z116 |
| Artiodactyla | Cervidae | *Odocoileus virginianus* | White-tailed deer | Z224 |

| | | | | |
|---|---|---|---|---|
| Artiodactyla | Bovidae | *Madoqua phillipsi* | Dik-dik | Z2251 |
| Pholidota | Manis | *Manis sp* | Pangolin | Z556 |
| Rodentia | Dipodidae | *Dipus sp* | Jerboa | Z209 |
| Rodentia | Hystricidae | *Hystrix indica* | Indian porcupine | Z1219b |
| Rodentia | Caviidae | *Hydrochoerus hydrochaeris* | Capybara | Z188 |
| Rodentia | Dasyproctidae | *Dasyprocta sp* | Agouti | Z3044 |
| Macroscelidea | Macroscelididae | *Rhynchocyon cirnei* | Checkered elephant shrew | Z609 |

**Table 3.1. List of species examined in the current study, all kindly made available by the Grant Museum of Zoology, UCL. The identification numbers are those used by the Museum.**

## 3.2. Materials and Methods

All available information about the ossification condition of the dural folds in mammalian species, both extant and in the fossil record, was collected. The information was assembled into a spreadsheet to provide a general view of the presence or absence of ossified dural structures, either the tentorium cerebelli, the falx cerebri, or both. Additionally, 40 articulated skulls from different species of mammals were analysed and photographed, in an attempt to provide information for those groups that were not represented in previous academic works or to corroborate their findings. The structures of interest were observed through the foramen magnum using an endoscope provided with LED lights and a camera. All photographs were taken with the aforementioned endoscope or, when the shape and size of the foramen magnum allowed it, with a handheld camera. Photographs were taken with the skulls positioned in ventral view, sometimes turning the specimen left or right to offer a better view of the attachment areas. The sex and age of the specimens were unknown in most cases, and were considered to be adults unless stated otherwise. This is a limitation of the study, because in some groups ossification develops with age (Nojima, 1988). To differentiate between the dolphin-type and the carnivore-type dural folds (see Chapter 2) it would be necessary to have access to full ontogenetic sequences for each species, but unfortunately material available for study in most museum collections does not allow for such a study.

It should be noted that in some cases it was difficult to decide whether some smaller osseous growths at the rear of the cranium were actually osseous tentoria cerebelli or just ridges on which a soft tentorium might attach. Klintworth (1968) pointed out that, in some rodents, the soft tentorium is attached to a narrow bony ridge with a variable breadth. Similarly, in humans and some primates, the soft tentorium also attaches to the small ridges of the occipital bone, on both sides of the transverse sinuses. Because of the difficulty in determining whether some ridges were sufficiently developed in a particular species to consider the tentorium cerebelli as partially ossified, a conservative view was taken in identifying ossification in the skulls, and if there was any doubt, it was recorded. Falx ossification is much more infrequent and, excepting one or two dubious cases, it was not observed in any of the specimens of the Grant Museum.

## 3.3. Dural ossification in Mammalia

What follows is an extensive analysis of falx and tentorium ossification in mammals. The study is arranged by orders where possible, but they are grouped together or subdivided when it helps to organise the descriptions in a more useful manner. Some groups have not been included if there is insufficient information, and the amount of space devoted to the remaining ones varies greatly depending on the data available. For example, Carnivora, Cetacea and Primates have deserved more attention in the bibliography and therefore this has an impact on the amount of data compiled.

### 3.3.1. Monotremata

Monotremes comprise two extant clades, Ornithorhynchidae and Tachyglossidae, the first comprising the platypus (*Ornithorhynchus anatinus*), the second a small number of echidna species. According to molecular clocks, echidnas diverged from platypus between 18 and 80 million years ago, but fossil evidence suggest that both groups were distinct during the Early Cretaceous period (Rowe *et al.*, 2007). There is no evidence of the presence of an osseous tentorium, but ossification of the falx cerebri in the extant platypus has been observed by various authors (Owen 1866; Nojima, 1990a; Macrini *et al*., 2006a; Figure 3.1, left) and, although no developmental information is available, the bony structure was already present in a juvenile specimen examined by Macrini *et al.*

47

(2006a). *Obdurodon dicksoni*, a fossil platypus from the Miocene period, also has a well-developed ossified falx cerebri (Macrini *et al.*, 2006a; Figure 3.1 right).
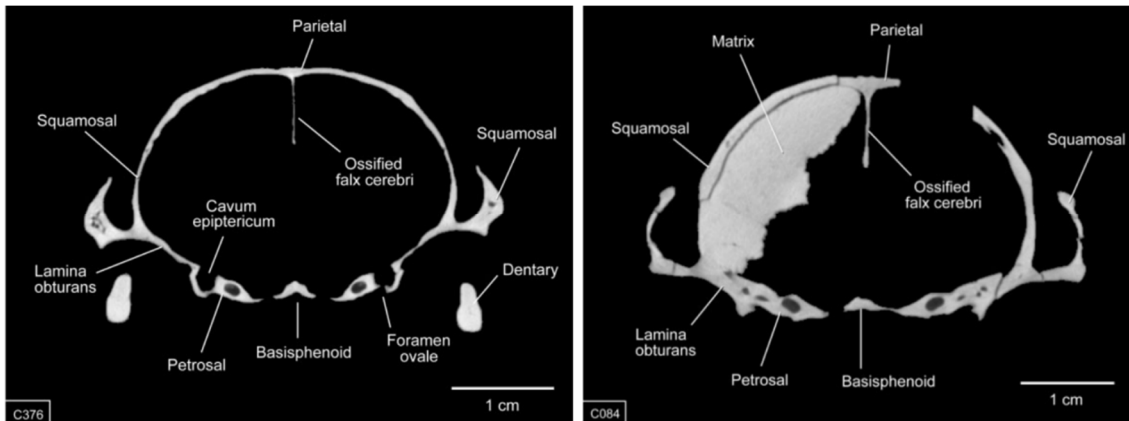


**Figure 3.1. CT scans in coronal view for *Ornithorhynchus anatinus* (left) and *Obdurodon dicksoni* (right) where an ossified falx cerebri is clearly visible (after Macrini *et al.*, 2006).**

In contrast to platypuses, echidnas do not exhibit any falx (or tentorial) ossification. The two families are very different in their respective ecologies and morphologies, with Echidnas being terrestrial while *Ornithorhynchus anatinus* is aquatic. It is also believed that *Obdurodon* was aquatic as well, as the specimen was found on an aquatic deposit (Macrini *et al.*, 2006a; but this assumption fails to acknowledge the biased nature of the fossil record, see Camens (2010) for further discussion). The Short-beaked echidna (*Tachyglossus aculeatus*) is an ant- and termite-eating specialist while the Long-beaked echidnas consume mostly earthworms, but all echidna species will, on occasion, prey on other small invertebrates such as beetles, moths and insect larvae (Abensperg-Traun and De Boer, 1992). Platypuses consume invertebrates, including snails, crustaceans, crayfish, etc. (Holz, 2014).

| Family | Species | Fossil | Ossif. falx | Reference |
|--------|---------|--------|-------------|-----------|
| Tachyglossidae | *Tachyglossus aculeatus* | ✗ | ✗ | Grant, 1834 |
| Tachyglossidae | *Zaglossus bartoni* | ✗ | ✗ | Grant, 1834 |
| Tachyglossidae | *Zaglossus bruijni* | ✗ | ✗ | Grant, 1834 |
| Ornithorhynchidae | *Ornithorhynchus anatinus* | ✗ | ✓ | Nojima, 1990a [after Owen 1866]; Macrini, 2006a |
| Ornithorhynchidae | *Obdurodon dicksoni* | ✓ | ✓ | Macrini *et al.*, 2006a |

**Table 3.2. Species from the order Monotremata where the condition of the falx is currently known.**

### *3.3.2. Marsupialia*

The marsupials (infraclass Marsupialia) include seven orders of mammals that, today, mostly inhabit Australasia and South America (May-Collado *et al.*, 2015); from these, no data could be gathered for Notoryctemorphia, Microbiotheria or Paucituberculata, and data for a single species of Didelphimorphia was obtained from Klintworth (1968). The information retrieved for the remaining orders (Dasyuromorphia, Peramelemorphia and Diprodontia) is based on examination of a single specimen for any given species and must be treated with care. Also, it is unknown if the tentorial ossification identified in some of the specimens below was produced as part of a prenatal or a postnatal process or even as part of a clinical condition.

3.3.2.1. Didelphimorphia, Paucituberculata and Microbiotheria

Didelphimorphia (opossums and mouse opossums), Paucituberculata (shrew-opossums), and Microbiotheria (which is represented by a single extant species: *Dromiciops gliroides*, the "monito del monte") are three orders of marsupials identified in Nearctic and Neotropical areas (Palma and Spotorno, 1999). Unfortunately, barely any information could be gathered for these groups, either by references or personal observation. The only exception to this is a mention in Klintworth (1968), where he described the (unossified) tentorium of the Virginia opossum (*Didelphis virginiana*) as a series of bilateral symmetrical folds, in the same manner as members of the order Rodentia, and he noticed the absence of a straight sinus (Figure 3.2). Concerning diet, this species is omnivorous

and highly opportunistic, including mainly insects and carrion, but also plant materials such as fruits and grains (McManus, 1974).
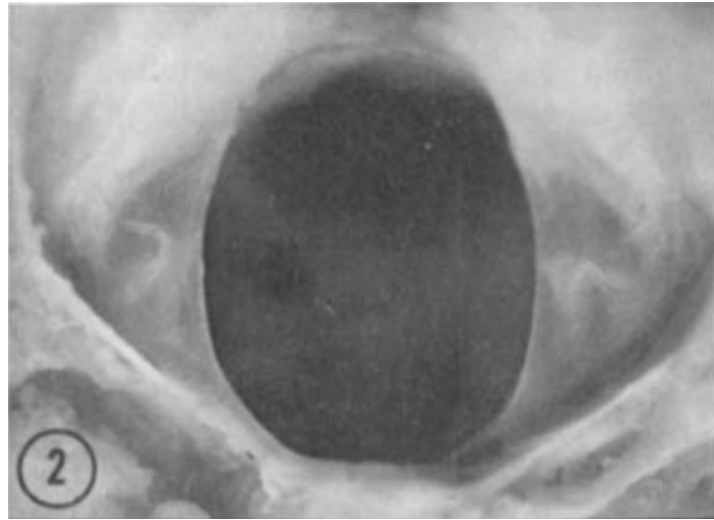


**Figure 3.2. A soft tentorium cerebelli from Didelphis virginiana. From Klintworth (1968).**

### 3.3.2.2. Dasyuromorphia

The marsupial order Dasyuromorphia comprises three different families: Thylacinidae, Myrmecobiidae and Dasyuridae. Recent phylogenetic analyses (Westerman *et al.*, 2016) place Thylacinidae as a sister taxa of Myrmecobiidae and Dasyuridae. An examination of a male skull of an adult Tasmanian tiger (*Thylacinus cynocephalus*, Grant Museum, specimen Z90, Figure 3.3) revealed extensive ossification of the tentorium cerebelli, with a well-developed tentorial process. However, a member of the Dasyuridae, a Yellow-footed Antechinus (*Antechinus flavipes*, Grant Museum, specimen Z98b) also examined, did not exhibit ossification. No Myrmecobiidae specimens were available. Although now extinct, it is believed that thylacines were exclusively carnivores and are commonly studied as an example of evolutionary convergence with the wolf (Figueirido and Janis, 2011; but see the paper for a comparison between the thylacine, the wolf and the tiger).

**Figure 3.3. The ossified tentorium cerebelli of a Tasmanian tiger (*Thylacinus cynocephalus*, Grant Museum, specimen Z90).**


3.3.2.3. Peramelemorphia

An individual from the genus *Perameles* (*Perameles nasuta* or long-nosed bandicoot; specimen Z1684) and another from the genus *Isoodon* (short-nosed bandicoot, specimen Z1751) were examined (Figure 3.4). Both Perameles and Isoodon possess slightly developed osseous tentorial processes. They are grouped as part of a single subfamily (Peramelinae) which is part of the family Peramelidae (Meredith *et al*., 2008). Bandicoots exhibit a wide range of locomotor gaits and, as omnivores, commonly dig with their forelimbs to get access to fungi and invertebrates that, together with plants, constitute the basis of their diet (Warburton and Travouillon, 2016).

**Figure 3.4. Left:** *Perameles nasuta* **(long-nosed bandicoot; specimen Z1684). Right:** *Isoodon* **sp., (short-nosed bandicoot; specimen Z1751).**

3.3.2.4. Diprotodontia

With over 125 extant species, Diprotodontia is the largest marsupial order. Although they are mostly herbivores, some species are also insectivores, nectarivores or folivores. Concerning locomotion, they also exhibit a wide range of specializations, such as bipedal locomotion, gliding, fossoriality or arboreality (Meredith, 2009). Despite being such a diverse group, most Diprotodontia seem to possess an ossified tentorium. In Macropodidae, this structure was already identified by Klintworth (1968) in a Wallaby specimen (*Macropus brownii*) and by Nojima (1988), who also found ossification in *Dendrolagus*, the other Macropodidae genus. This was confirmed in an examination of two further species of *Macropus*, *Macropus giganteus* (Eastern grey kangaroo; specimen Z1681) and *Macropus fuliginosus* (Western Grey kangaroo; specimen Z1210). However, the morphology varies between both species in the shape and length of the tentorial process (Figure 3.5). In *Macropus giganteus* the structure exhibits a characteristic lanceolated shape with lateral blades, while the ossified structure in *Macropus fuliginosus* is shorter, wider and rounder.

**Figure 3.5 Left:** *Macropus giganteus* **(Eastern grey kangaroo; specimen Z1681).** **Right:** *Macropus fuliginosus* **(Western Grey kangaroo; specimen Z1210).**

No data could be gathered for Potoroidae, Burramyidae, Tarsipedidae and Acrobatidae families but, for the rest of the groups studied, the ossified tentorium is less developed, and in some cases its existence is uncertain. The groups observed were Pseudocheiridae (Ring-tailed possum; specimen Z74, Figure 3.6, left), Petauridae (*Dactylopsila trivirgata*, Striped possum; specimen Z72) and Phascolarctidae (*Phascolarctos cinereus*, koala; specimen Z699). In Phalangeridae (*Trichosurus vulpecula*, Silver-grey Brushtail possum; specimen Z100, Figure 3.6, right), the presence of an osseous tentorium is also questionable.



**Figure 3.6. Left:** *Pseudocheirus* **sp., Ring-tailed possum; specimen Z74. Right:** *Trichosurus vulpecula***, Silver-grey Brushtail possum; specimen Z100.**

### *3.3.3. Placentals*

Mammalia is divided into two extant subclasses based primarily on the reproduction method: Prototheria (monotremes) and Theria, which include marsupial (metatherians) and placental (eutherians) mammals. The great majority of extant mammals belong to the eutherians (Feldhamer *et al.*, 2015), but the amount of information available for dural ossification varies between the different groups. Data is currently missing for the orders Scandentia and Dermoptera. From Hyracoidea, a female *Procavia capensis* (Rock Hirax, specimen number Z1743) was examined and no trace of tentorial ossification was found. From Lagomorpha, Klintworth (1968) studied seven specimens of rabbits (*Oryctolagus cuniculus*) and did not report ossification. From Chiroptera, a single fresh specimen of *Rousettus aegyptiacus* (Egyptian fruit bat, from the Pteropodidae family) was examined, and again no ossification was found either. Negative results were also obtained for members of the now defunct order Insectivora. This includes hedgehogs and tenrecs of the family Tenrecidae (*Tenrec ecaudatus*, specimen number Z3064, and *Setifer setosus*, specimen number Z610), a moonrat, from the family Erinaceidae (*Echinosorex gymnura*, specimen number Z606), and a European mole, from the family Talpidae (*Talpa europaea*, specimen number Z600a).

The remaining placental groups are discussed in detail below.

### 3.3.3.1. Xenarthra

The superorder Xenarthra is one of the four main clades of placentals, enclosing 31 extant species of armadillos, anteaters and sloths (Delsuc *et al.*, 2001; Tambusso and Fariña, 2015a). Many of these species are myrmecophagous and therefore show feeding adaptations for the consumption of ants and termites. In the cranium, this manifests in the reduction or complete absence of dentition (loss of incisors and canines) and in the length of the snout. Moreover, there are over 200 extinct genera described, which include giant armadillos and the giant sloth (Feldhamer *et al.*, 2015).

The order Pilosa, which comprises anteaters and sloths, do not seem to exhibit tentorial ossification. This was confirmed in the family *Megalonychidae*, in a specimen of Two-toed sloth (*Choloepus didactylus*, Z130a, Figure 3.7; left) and in the family

*Myrmecophagidae*, in a specimen of Giant Anteater (*Myrmecophaga tridactyla*, z1554, Figure 3.7; right).



**Figure 3.7. Left:** *Choloepus didactylus***, Two-toed sloth; specimen Z130a. Right:** *Myrmecophaga tridactyla***, Giant Anteater; specimen z1554.**

The order Cingulata comprises the clades Dasypodoidea (living and extinct armadillos) and Glyptodontoidea (glyptodonts and pampatheres) (Tambusso and Fariña, 2015a). An osseous tentorium cerebelli is absent in glyptodonts, but is present in living species of armadillos (Tambusso and Fariña, 2015b) and in the extinct *Pampatherium humboldtii*. In an endocast fossil of *Pampatherium* from the Late Pleistocene, the tentorium "spans across all the width of the cerebellum and obliterates the transverse sulcus" (Tambusso and Fariña, 2015a, Figure 3.8).
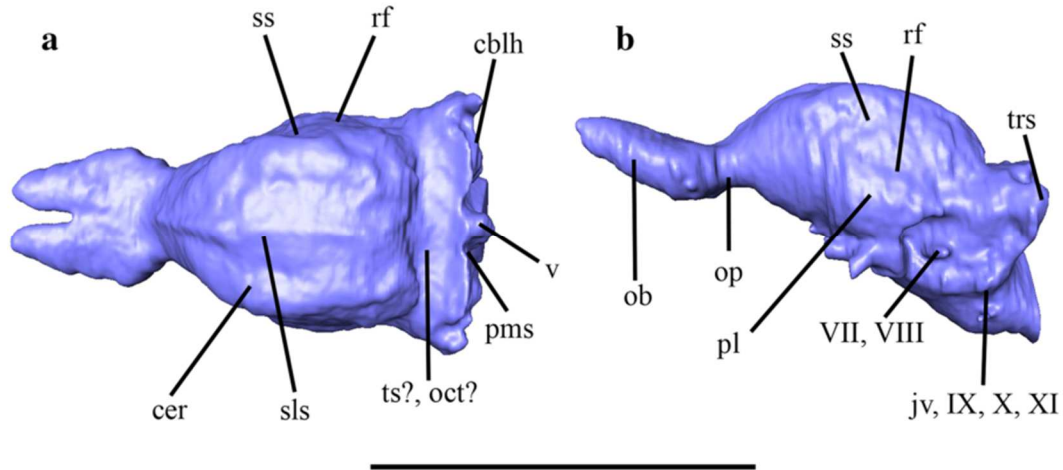
**Figure 3.8. Digital endocast of a fossil specimen of *Pampatherium humboldtii* in dorsal (left) and lateral (right) views. "..oct?.." indicates the location of a possible osseous tentorium cerebelli. Scale bar 10cm. After Tambusso and Fariña (2015a).**

In *Dasypodidae*, the shape of the ossified tentorium varies even between very closely related species, as in the case of *Dasypus kappleri*, *Dasypus pastasae* and *Dasypus beniensis* which, for a long time, have been considered subspecies of a strongly polytypic species. While in *Dasypus kappleri* and *Dasypus pastasae* the tentorial process of the parietals exhibits a rectangular shape (Figure 3.9; left), in *Dasypus beniensis* it adopts a less developed but very distinct pentagonal shape (Figure 3.9; right) (Feijó and Cordeiro-Estrela, 2016). Observations also confirmed the rectangular shape of the tentorial process in a specimen of the Nine banded armadillo (*Dasypus novemcinctus*, Z134).
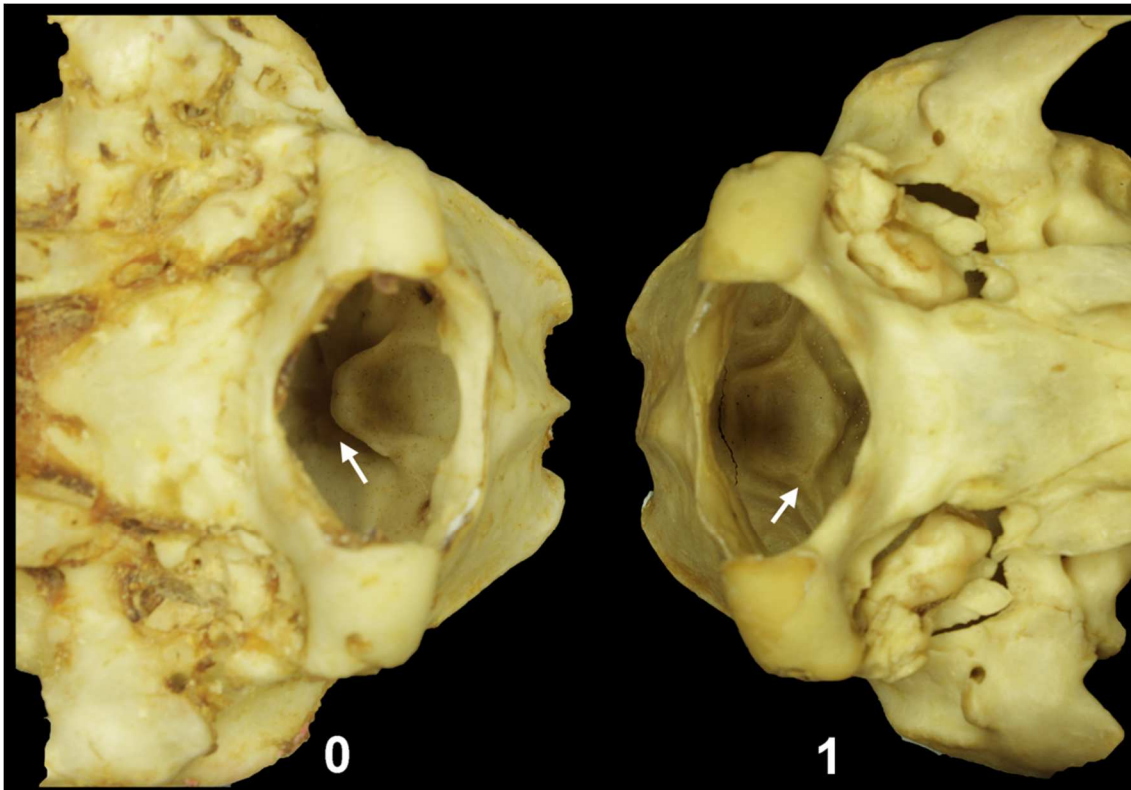
**Figure 3.9. Variation in the shape of the tentorial process in two closely related species of *Dasypus*. Left: *Dasypus kappleri*, rectangular shape; Right: *Dasypus beniensis*, pentagonal shape. After Feijó and Cordeiro-Estrela (2016).**

| Family | Species | Fossil | Ossif. tent. | Reference |
|---|---|---|---|---|
| Megalonychidae | *Choloepus didactylus* | ✗ | ✗ | Grant Museum (specimen Z130a) |
| Dasypodidae | *Dasypus kappleri* | ✗ | ✓ | Feijó and Cordeiro-Estrela (2016) |
| Dasypodidae | *Dasypus pastasae* | ✗ | ✓ | Feijó and Cordeiro-Estrela (2016) |
| Dasypodidae | *Dasypus beniensis* | ✗ | ✓ | Feijó and Cordeiro-Estrela (2016) |
| Dasypodidae | *Dasypus novemcinctus* | ✗ | ✓ | Grant Museum (specimen Z134) |
| Myrmecophagidae | *Myrmecophaga tridactyla* | ✗ | ✗ | Grant Museum (specimen Z1554) |
| Glyptodontinae | *Pseudoplohophorus absolutus* | ✓ | ✗ | Tambusso and Fariña (2015b) |
| Pampatheriidae | *Pampatherium humboldtii* | ✓ | ✓ | Tambusso and Fariña (2015a) |

**Table 3.3. Species from the superorder Xenarthra where the condition of the ossification of the tentorium is currently known.**

3.3.3.2. Primates

There is perhaps no other animal order where the identification of a bony tentorium cerebelli is as elusive as in Primates, where ossification varies greatly across families and

where there are even conflicting descriptions among researchers (see below). Primates radiated in the Paleocene and Eocene, having extended to all continents by the mid-Tertiary with the exception of Australia. Because of these radiations, two different suborders can be identified today, Strepsirhini and Haplorhini. Together, they can be subdivided into 14 families that comprise about 450 extant species (Feldhamer *et al*., 2015). Tentorial ossification in this group may be traced back to their earlier ancestors, the Plesiadapiformes, with Kay *et al*. (1992) describing a cranial fossil specimen of *Ignacius graybullianus* with a distinct osseous tentorium cerebelli.

### 3.3.3.2.1. Strepsirhini

Strepsirhini is composed of seven living families (Lorisidae, Galagidae, Lemuridae, Lepilemuridae, Indriidae, Daubentoniidae and Cheirogaleidae; the last five form the superfamily Lemuroidea) and three extinct ones (Megaladapidae, Archaeolemuridae, and Palaeopropithecidae) (Feldhamer *et al*., 2015). According to Horovitz and McPhee (1999), Lemuroidea have a characteristic T-shaped tentorial ossification in front of the petrosal apex very distinct from any ossification found in Platyrrhini. This structure was identified in the Lemur aye-aye (*Daubentonia madagascariensis*) by Saban (1975), (Figure 3.10). However, Nojima (1990) also studied specimens from the families Lemuridae (*Lemur catta* and *Eulemur mongoz*) and Lorisidae (*Loris tardigradus, Nycticebus Coucang* and *Galago senegalensis*) and found that they did not present an osseous tentorium. It is unknown if the specimens analyzed by Nojima lacked any trace of ossification or the author disregarded the T-shaped bony structured identified by Horovitz and McPhee due to the absence of extensive ossification.
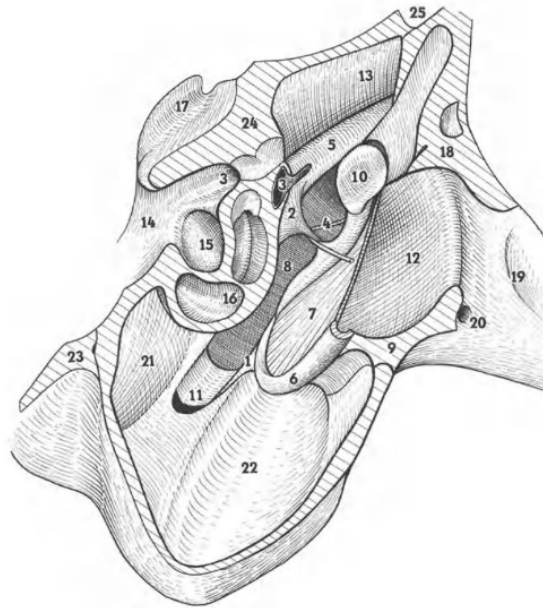
**Figure 3.10. Anterior portion of a cross-section of the right temporal bone of *Daubentonia madagascariensis*. The osseous tentorium cerebelli is indicated by the number 17 (Saban, 1975).**

The current work contributes to the study of Strepsirhini by analysing specimens from the families Indriidae (*Propithecus sp.*, specimen number Z405), Galagidae (*Galago sp.*, specimen number Z2361) and Cheirogaleidae (*Cheirogaleus sp.*, Z411) and confirms the absence of a bony tentorium with its corresponding tentorial process. No specimens from the family Lepilemuridae could be studied. Nonetheless, in *Cheirogaleus*, and particularly in *Propithecus* (Figure 3.11 left and right, respectively) the presence of a well-developed internal sagittal crest (*crista sagittalis interna*) was identified. This crest serves as the attachment of the falx cerebri and it is a common occurrence in other species, for example in dogs (Evans and De Lahunta, 2013), but in the case of *Propithecus* is so extensive that it could perhaps be regarded as a partial ossification of the falx cerebri. Because no other specimens were available for study, it is not known if this is characteristic of the species observed or part of a clinical condition.
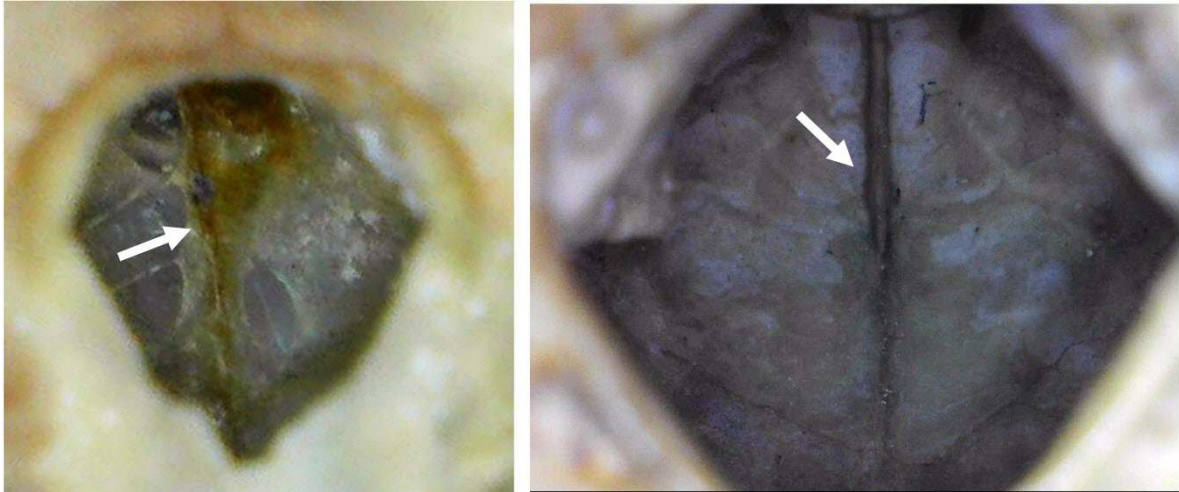
**Figure 3.11. Two specimens from the superfamily Lemuroidea with an extensive internal sagittal crest (*crista sagittalis interna*). Left: *Cheirogaleus* sp., Z411. Right: *Propithecus* sp., Z405.**

3.3.3.2.2. Haplorhini

Haplorhini are composed of seven living families (Tarsiidae, Cebidae, Pitheciidae, Atelidae, Cercopithecidae, Hylobatidae, and Hominidae) and four extinct ones (Omomyidae, Parapithecidae, Oreopithecidae, and Pliopithecidae) (Feldhamer *et al.*, 2015). Two sister taxon can be identified: Platyrrhini (or New World Monkeys) and Catarrhini (Old World Monkeys).

While there is no tentorial ossification in *Tarsius* or catarrhines (Nojima, 1990a; Kay *et al.*, 2008; Figure 3.12), its existance in most extant Platyrrhini seems to be disputed. According to Horovitz and McPhee (1999), in these species the osseous tentorium "extends behind the subarcuate fossa as well as above and in front of it." However, the degree of tentorial ossification varies across families. In Pitheciidae and atelines it is more extensive while in callitrichines it is reduced to the area of the tentorium that is attached to the petrosal apex (Horovitz and McPhee, 1999; Kay *et al.*, 2008). Horovitz and McPhee (1999) also reported that ossification in *Saimiri* varies among specimens: in some occurrences it is similar to callitrichines, but in others no tentorial ossification was found. Its presence in the atelines *Ateles geoffroyi* and *Ateles paniscus* (black-handed spider monkeys and black spider monkeys, respectively) was also confirmed by Nojima (1990a), who described variations in the extension of the ossification across specimens that, in any case, never reached the inner surface of the

occipital bone (Figure 3.13 and Figure 3.14). Surprisingly, however, Nojima did not report ossification in any other members of Platyrrhini.
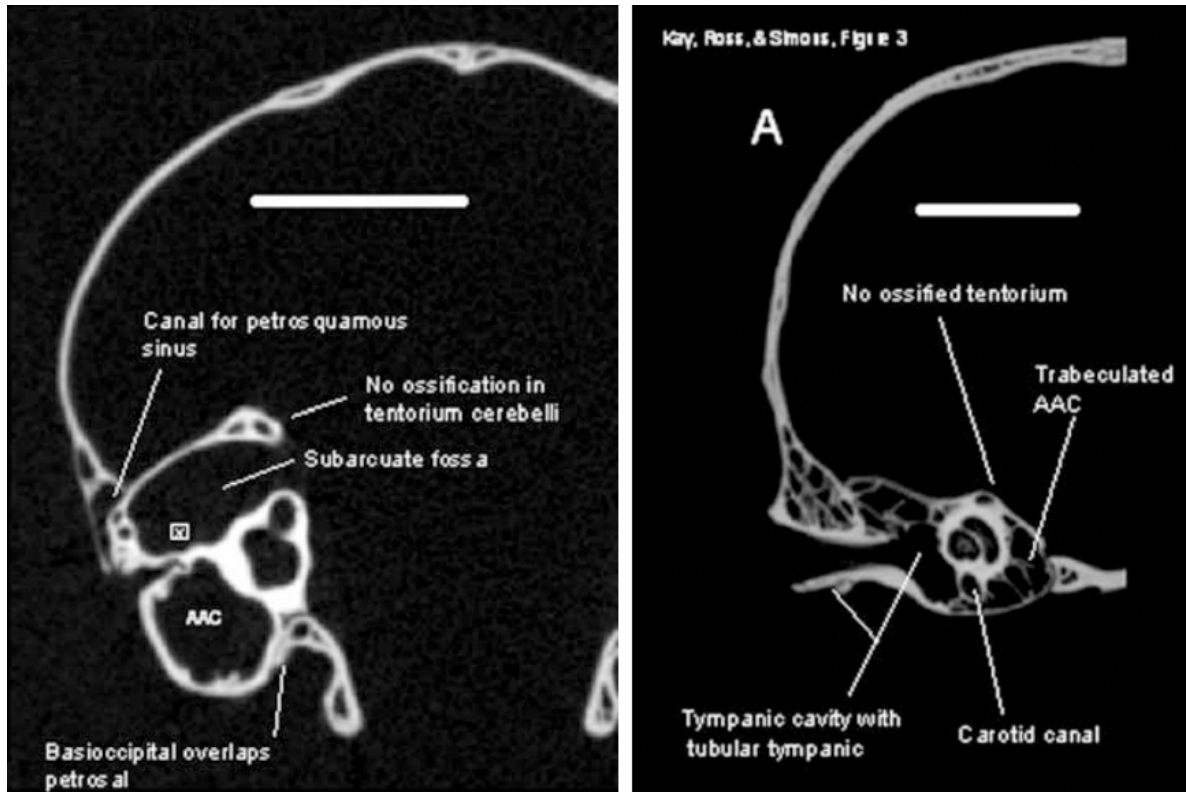


**Figure 3.12. CT- scan cross sections illustrating the absence of an osseous tentorium cerebelli in two species of Haplorhini. Left: *Tarsius bancanus* (currently assigned to the genus Cephalopachus; see Groves and Shekelle, 2010); Right: *Miopithecus talapoin*, an extant cercopithecoid catarrhine. After Kay *et al.*, 2008.**
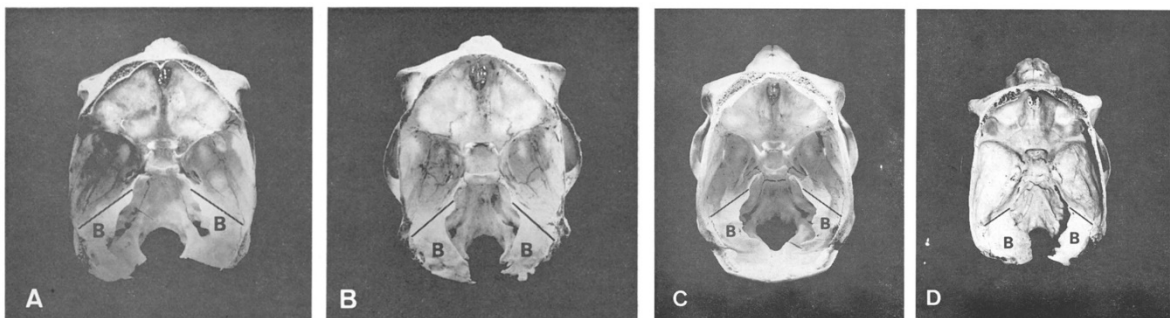


**Figure 3.13. Two specimens of *Ateles geoffroyi* (A and B) and two of *Ateles paniscus* (C y D) showing different degrees of tentorial ossification. The black line indicates the boundary area between the osseous tentorium and the petrosa. After Nojima (1990a).**
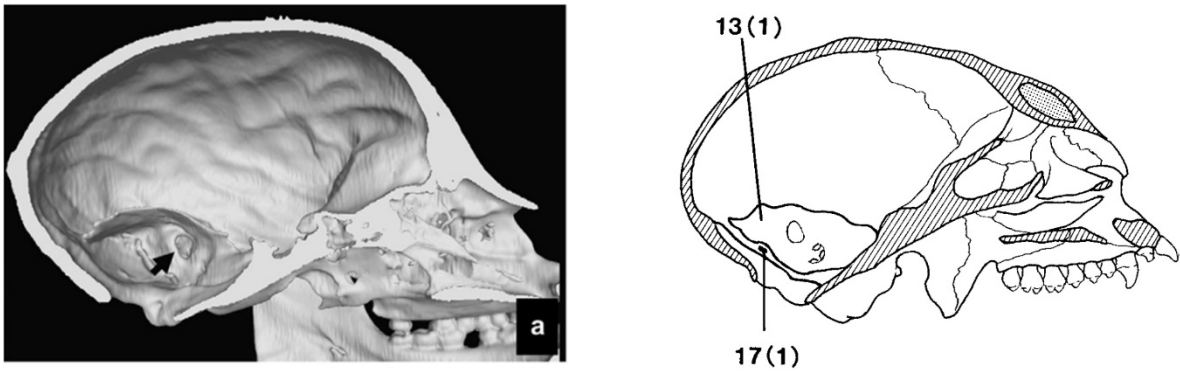
**Figure 3.14. Left: midline bisection of a digital model of *Ateles geoffroyi* showing the tentorium cerebelli (Jeffery *et al*. 2008). Right: Medial view of sagittal section of *Callicebus moloch*. The osseous tentorium cerebelli is indicated by the number 13 (Horovitz and McPhee, 1999).**

The discrepancies in the assessment of the presence or absence of tentorial ossification in the two studies by Horovitz and McPhee (1999) and Nojima (1990) are surprising. They occur in all members of Callitrichidae that were observed and most of the Cebidae; where Horovitz and McPhee (1999) identify the existence of ossification, Nojima (1990) does not, concluding that "the existence of a clear BT (bony tentorium) appears to be peculiar to spider monkeys among primates". To try to shed some light on the issue, two specimens of Cebidae from the Grant Museum (*Cebus sp*, specimen number Z910, and *Aotus trivirgatus*, specimen number Z414) were observed. An extensive ossification of the tentorium was found in the former specimen, but only partial ossification in the latter (Figure 3.15; left and middle, respectively). Ossification in *Aotus trivirgatus* was also seen by CT-scans in another specimen (Kay *et al*., 2008; Figure 3.15; right). Given that ossification in spider monkeys (*Ateles geoffroyi* and *Ateles paniscus*) occurs during the course of aging (Nojima, 1990a), it could be that the discrepancies are due to a varying degree of ossification in the tentorium of individuals of the same species, either from this or from other causes. However, a more extensive and systematic study would be necessary to solve the issue.
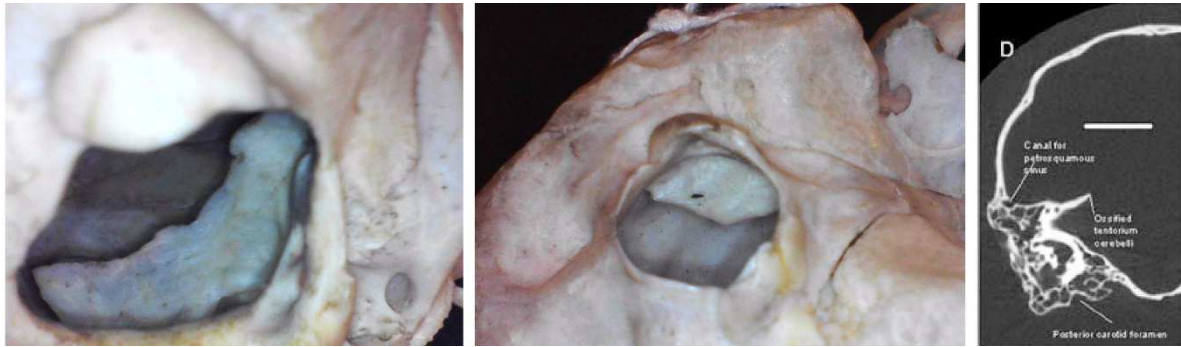
**Figure 3.15. Left:** *Cebus* **sp, specimen number Z910; Middle:** *Aotus trivirgatus* **(Three-striped night monkey, specimen number Z414). Right: CT-scans showing ossification of the tentorium cerebelli in** *Aotus trivirgatus* **(Kay** *et al.***, 2008).**

Tentorial ossification is also present in older specimens, such as extinct Platyrrhini from Early Miocene to Recent. As described by Kay *et al.* (2008), in these fossils tentorial ossification "begins proximally along the petrosal and encases the superior petrosal venous sinus, if present. It extends medially, although never forming a complete sheet of bone as occurs in some carnivorans." Ossification is present in *Dolichocebus*, *Tremacebus*, *Parapithecus grangeri* (Figure 3.16; left) *Proteopithecus slyviae* and *Catopithecus browni* (Figure 3.16; right), and in *Paralouatta varonai* and *Cebupithecia* from the family Pitheciidae (Horovitz and McPhee, 1999). It is absent in *Aegyptopithecus zeuxis* and *Omomys* (Kay *et al.*, 2008).
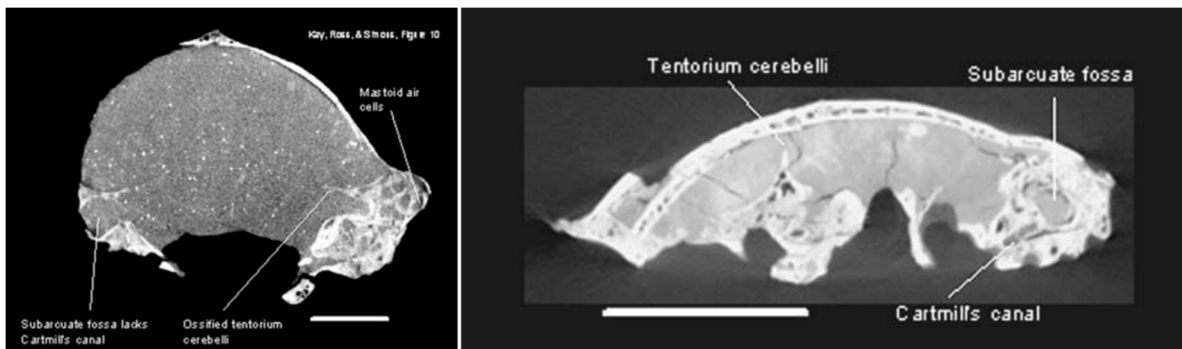


**Figure 3.16. Left: Coronal CT slice from a fossil specimen of** *Parapithecus grangeri* **(from the early Oligocene, Egypt); Right: Fossil specimen of** *Catopithecus browni* **from late Eocene, Egypt, showing ossification of the tentorium cerebelli. After Kay** *et al.***, 2008.**

3.3.3.3. <u>Carnivora</u>

Carnivora is comprised of 16 families and around 300 species. Obviously, the majority are carnivorous (although not all; bears, for example, are omnivore), but their feeding habits vary enormously. The order is divided in the two suborders Feliformia and Caniformia. The former includes seven families: Felidae, Herpestidae, Hyaenidae, Viverridae, Eupleridae, Nandiniidae and Prionodontidae. The latter comprises Canidae, Ursidae, Mustelidae, Procyonidae, Mephitidae, Ailuridae, Odobenidae, Otariidae and Phocidae; the last three are aquatic and referred collectively as "pinnipeds" (Feldhamer *et al.*, 2015).

In Carnivora, the osseous tentorium is present in almost all species studied, and the osseous falx appears in all pinnipeds and in the genus *Ursus*. The majority of the systematic work describing and classifying these structures in carnivorans was performed by Nojima (1990c), who observed 48 different species and created four different typologies based on the degree of ossification of the tentorium (which were briefly discussed in Chapter 2). Nojima discovered that in most families the osseous part of the structure reached or crossed the petrosa, but the ossification was even more extensive in Felidae, Viverridae and Hyaenidae where, in addition, the tentorial process projected from the whole occipital border of the parietal bone. In contrast, he also noted that in some Phocidae and all Canidae the osseous tentorium did not reach the base of the cranium and, in the case of Phocidae, the tentorial process was also missing.

The only exception seems to be the family Mephitidae, which does not exhibit any degree of ossification whatsoever in the tentorium cerebelli. This peculiarity was first identified by Nojima (1990c) in the Striped Skunk (*Mephitis mephitis*) and then confirmed by Bryant *et al.* (1993) and by the recent examination of two further specimens from the Grant Museum (Z376 and Z375; Figure 3.17). There is also no trace of an osseous tentorium cerebelli in the *Conepatus* fossil specimen described by González-Guarda (2009). For a full list of members of the family Mephitidae described in the literature, see Table 3.4.

Among aquatic Carnivora, ossification of the falx cerebri is commonplace. It can be found in all pinnipeds: Otariidae, Odobenidae and Phocidae (Nojima, 1990c). In terrestrial Carnivora, the ossification of the falx is only present in the family Ursidae, but not in all species. It is absent in the Sloth bear (*Melursus ursinus*) and in the Asian black bear (*Ursus thibetanus*) (Nojima, 1988; Nojima, 1990c). When it is present, the osseous

falx is partial, and formed not by strict ossification of the falx cerebri but by two osseous plates that protrude from the most anterior part of the tentorial process (Nojima, 1990c).

| Genus | Species | Common name | nº | Reference |
|---|---|---|---|---|
| Conepatus | Unidentified fossil | | 1 | González-Guarda, 2009 |
| Conepatus | *Conepatus chinga* | Molina's Hog-nosed Skunk | 6+1 | Bryant *et al.*, 1993; sp. Z376 |
| Conepatus | *Conepatus humboldtii* | Humboldt's hog-nosed skunk | 6 | Bryant *et al.*, 1993 |
| Conepatus | *Conepatus mesoleucus/leuconotus* | Western hog-nosed skunk | 8 | Bryant *et al.*, 1993 |
| Mephitis | *Mephitis mephitis* | Striped skunk | 1+7+1 | Nojima, 1990c; Bryant *et al.*, 1993; sp. Z375 |
| Mephitis | *Mephitis macroura* | Hooded skunk | 3+1 | Bryant *et al.*, 1993; sp. Z375 |
| Mydaus | *Mydaus javanensis* | Sunda stink badger | 14 | Bryant *et al.*, 1993 |
| Mydaus | *Mydaus marchei* | Palawan stink badger | 7 | Bryant *et al.*, 1993 |
| Spilogale | *Spilogale putorius* | Eastern spotted skunk | 13 | Bryant *et al.*, 1993 |

**Table 3.4. List of species of the family Mephitidae that do not exhibit any trace of tentorial ossification (nº refers to the total number of specimens observed for the given species; specimen Z375 of the Grant Museum was labelled as either an individual from *Mephitis mephitis* or from *Mephitis macroura*).**



**Figure 3.17. Two species of the family Mephitidae showing absence of an osseous ossification. Left: Molina's Hog-nosed Skunk (*Conepatus chinga*; specimen number Z376); Right: Striped skunk (*Mephitis mephitis*) or Hooded skunk (*Mephitis macroura*), specimen number Z375.**

Tentorial ossification has also been recorded in all species of Ursidae that have been studied (Nojima 1990c; Dong, 2008; Figure 3.18), including two fossil specimens from Ailuropoda. Referring to that figure, it appears that there is a steeper inclination of the tentorium cerebelli in the giant pandas (a, and especially b and c), but it is much less inclined in the polar bear specimen (Figure 3.18, d) (Dong, 2008).

Table 3.5 summarises the presence or absence of ossified dural folds in all Ursidae species studied.
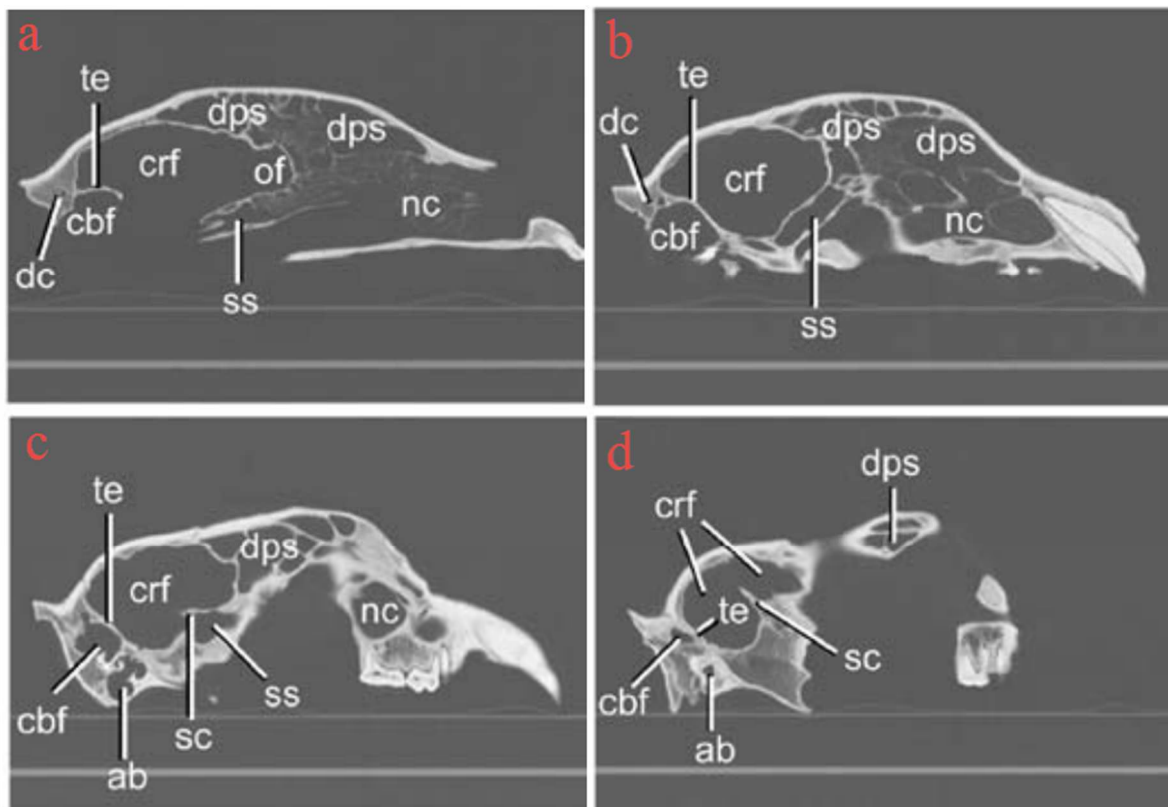


**Figure 3.18. Sagittal CT-slices of four species of Ursidae, showing the tentorium cerebelli (te); a: *Ailuropoda microta*; b: *Ailuropoda baconi*; c: *Ailuropoda melanoleuca*; d: *Ursus maritimus*. After Dong (2008).**

| Genus | Species | Fossil | Ossif. Fax | Ossif. Tent. | References |
|---|---|---|---|---|---|
| *Thalarctos* | *Thalarctos maritimus* | ✗ | ✓ | ✓ | Nojima, 1988; Nojima, 1990c; Dong, 2008 |
| *Ursus* | *Ursus arctos* | ✗ | ✓ | ✓ | Nojima, 1988; Nojima, 1990c |
| *Ursus* | *Ursus arctos middendorffi* | ✗ | ✓ | ✓ | Nojima, 1988; Nojima, 1990c |
| *Melursus* | *Melursus ursinus* | ✗ | ✗ | ✓ | Nojima, 1988; Nojima, 1990c |
| *Ursus* | *Ursus thibetanus* | ✗ | ✗ | ✓ | Nojima, 1988; Nojima, 1990c |
| *Ailuropoda* | *Ailuropoda melanoleuca* | ✗ | ? | ✓ | Dong, 2008 |
| *Ailuropoda* | *Ailuropoda microta* | ✓ | ? | ✓ | Dong, 2008 |
| *Ailuropoda* | *Ailuropoda baconi* | ✓ | ? | ✓ | Dong, 2008 |

**Table 3.5. List of species of Ursidae observed in previous studies and the status of ossification of their falx cerebri and tentorium cerebelli.**

In Mustelidae, an osseous tentorium has been observed in 30 different species (Nojima, 1988; Nojima, 1990c; Bryant, 1991; Bryant *et al.*, 1993; He *et al.*, 2002). In this family, ossification tends to be moderate in the medial portion and weak in the laterals (Bryant *et al.*, 1993). It has also been found in the fossil record, in *Howellictis valentini* (de Bonis *et al.*, 2009; Figure 3.19, right).
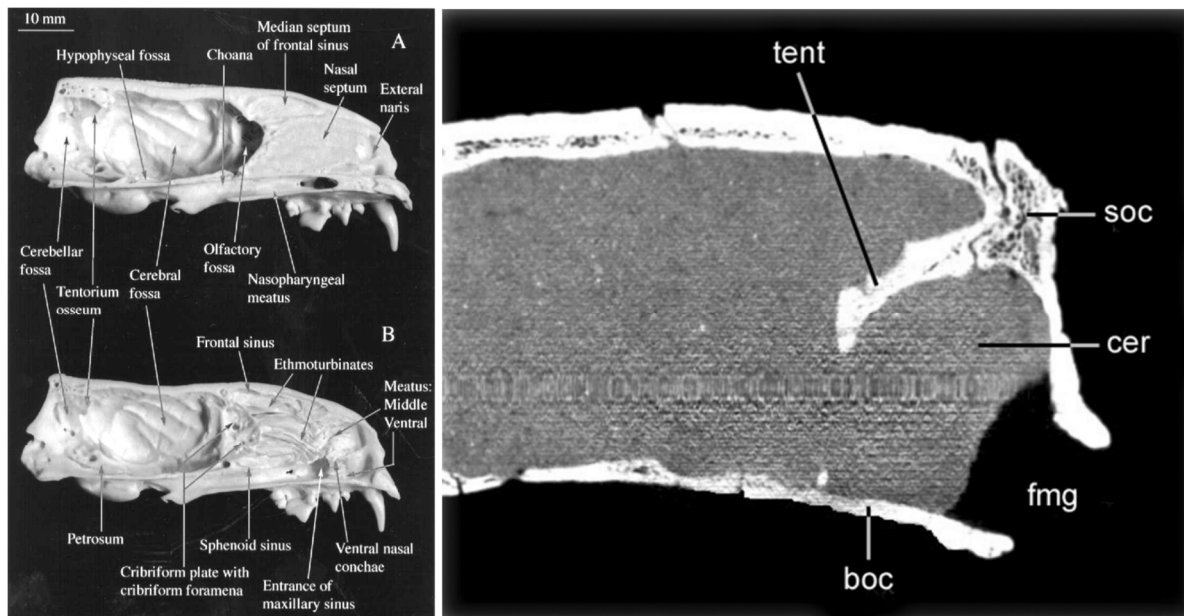


**Figure 3.19. Tentorial ossification in Mustelidae. Left: Midsagittal view of the cranium of a ferret (*Mustela putorius furo*) (He *et al.*, 2002); Right: CT-scan, longitudinal section of the fossil *Howellictis valentini* (de Bonis *et al.*, 2009).**

In Feliformia, the osseous tentorium cerebelli appears to be more developed than in Caniformia, in many cases with a clearly-shaped tentorial process and ossified tentorial wings (Figure 3.20, left). This has been confirmed in several species from the Felidae, Hyaenidae and Viverridae families (Nojima, 1990c). Concerning Herpestidae, a mongoose specimen from the Grant Museum was studied (*Herpestes sp*; specimen number Z366; Figure 3.20, right), identifying a well-developed osseous tentorium, with an asymmetric medial portion, which may be a consequence of a possible breakage.
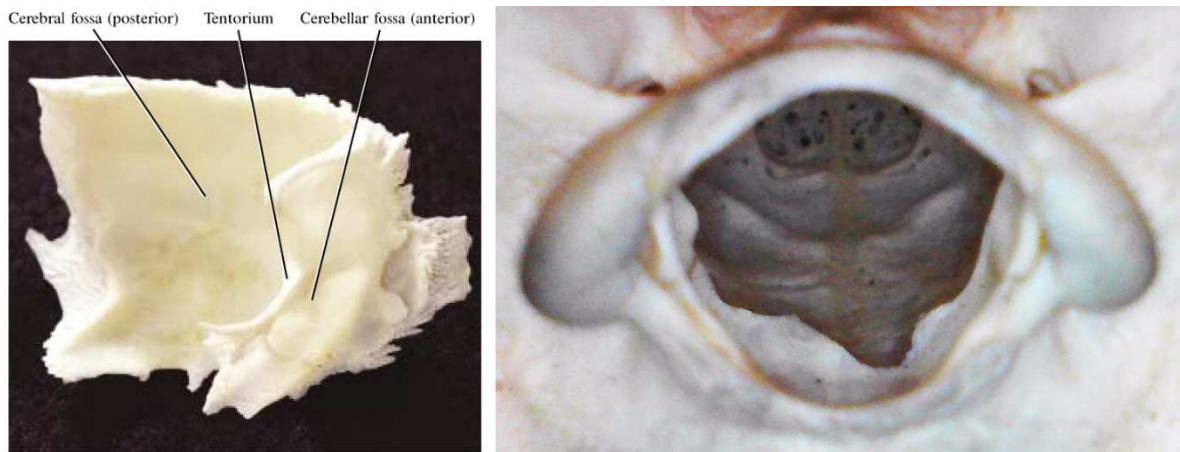


**Figure 3.20. Left: Medial view of a parietal bone in *Felis silvestris catus*, showing a completely ossified tentorium cerebelli (Sebastiani and Fishbeck, 2005); Right: *Herpestes* sp (specimen number Z366).**

In the suborder Feliformia, the tentorium cerebelli has also been found in the fossil record of members of the families Nimravidae and Barbourofelidae, which are catlike carnivorans from the late Eocene to the late Miocene with very similar morphology to felids and sometimes referred as false sabre-toothed cats. In *Barbourofelis*, the osseous tentorium cerebelli extends ventrally until reaching the anterior end of the petrosa (corresponding to the type A-II in Nojima's classification) while in the nimravids *Dinictis* and *Hoplophoneus* the ossification is more reduced, as it is in extant Canidae (Bryant, 1991).

3.3.3.4. Sirenia

Sirenia are aquatic and strictly herbivorous. Today, there are only two extant families: Dugongidae, with a single living species, the Dugong (*Dugong dugon*), and Trichechidae,

with three living species of manatees. Two extinct families that are well-represented in the fossil record, Prorastomidae and Protosirenidae (Feldhamer *et al.*, 2015) must also be noted. The prorastomids were amphibious quadrupeds, while protosirens had "complete hindlimbs but a weak sacroiliac joint that probably precluded quadrupedal locomotion on land" (Domning *et al.*, 2010).

In his description of sirenian fossil specimens, Domning *et al.* (2010) identifies both an ossified falx and an ossified tentorium in two species of Dugongidae, but he also notes the absence of ossification in two species of Protosirenidae, describing the endocranial surface as smooth and only referring to "faintly marked" dural folds in one of the *Protosiren smithae* specimens (see Table 3.6 below). A description of two specimens of *Dioplotherium allisoni* (Dugongidae) informs us of different degrees of ossification among individuals of the same species: in one of the fossils described, the osseous tentorium is underdeveloped and the osseous falx disappears halfway to the frontoparietal suture; in the other, the falx reaches the suture and the tentorium is missing in the area lateral to the internal protuberance (de Toledo and Domning, 1989).

In extant species, Nojima (1988) found falx cerebri ossification both in Dugong and at least in one species of Trichechidae (*Trichetus manatus*). In these two cases, no tentorial ossification was recorded.

| Family | Species | Fossil | Oss. falx | Oss. Tent | References |
|---|---|---|---|---|---|
| Dugongidae | *Eotheroides aegyptiacum* | ✓ | ✓ | ✓ | Domning *et al.*, 2010 |
| Dugongidae | *Eosiren imenti* | ✓ | ✓ | ✓ | Domning *et al.*, 2010 |
| Dugongidae | *Dioplotherium allisoni* | ✓ | ✓ | ✓ | de Toledo and Domning, 1989 |
| Dugongidae | *Dugong dugon* | ✗ | ✓ | ✗ | Nojima, 1988 |
| Trichechidae | *Trichetus manatus* | ✗ | ✓ | ✗ | Nojima, 1988 |
| Protosirenidae | *Protosiren fraasi* | ✓ | ✗ | ✗ | Domning *et al.*, 2010 |
| Protosirenidae | *Protosiren smithae* | ✓ | ✗ | ✗ | Domning *et al.*, 2010 |

**Table 3.6. List of species of the order Sirenia observed in previous studies and the status of ossification of their falx cerebri and tentorium cerebelli.**

3.3.3.5. Perissodactyla and Artiodactyla

The Perissodactyla is a very diverse order, both in terms of locomotion and morphologies. It is composed of three families (Equidae, Tapiridae and Rhinocerotidae), but all its

species have in common is that they are medium to large terrestrial herbivores (Feldhamer *et al*., 2015). In Equidae, an ossified tentorium cerebelli has been identified in four species: *Equus caballus* (Nojima, 1988; Solano and Brawer, 2004; Figure 3.21), *Equus burchelli*, *Equus zebra* and *Equus hemionus* (Nojima, 1988). A single specimen of *Tapirus indicus* (family Tapiridae) was also observed; (specimen number Z163), where only a slight lateral ossification of the tentorium was found.
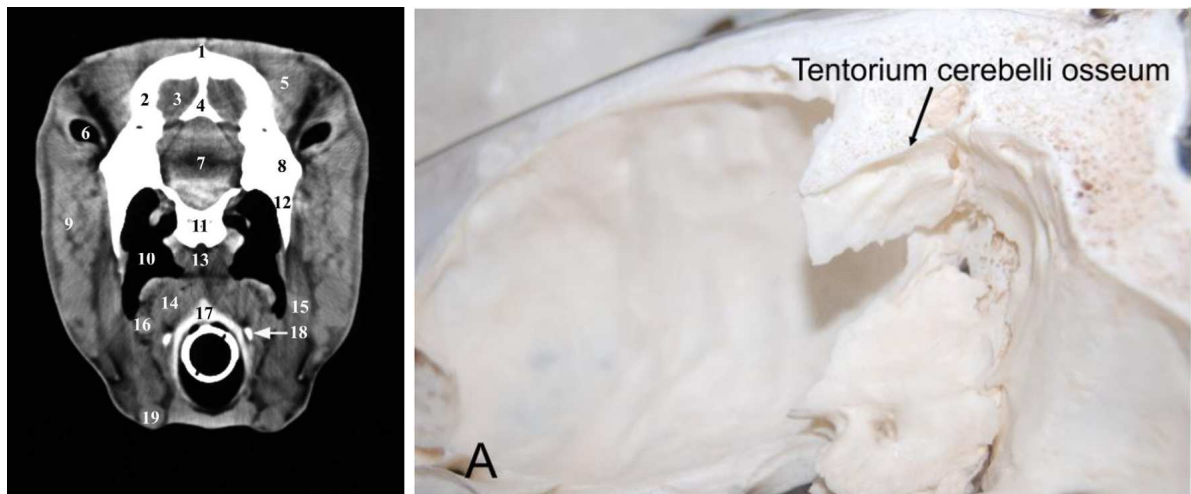


**Figure 3.21. Left: Transverse section of a CT scan of an *Equus caballus* head (horse). The osseous tentorium is indicated by number 4 (Solano and Brawer, 2004). Right: Tentorium cerebelli of an *Equus caballus* (Schmidt, 2015).**

While perissodactyls consume fibrous vegetation, artiodactyls, which are very different in terms of shape, are more selective. This order is composed of 10 terrestrial families, not counting Cetacea, an infraorder of the order Artiodactyla and a sister group to the family Hippopotamidae (Feldhamer *et al*., 2015). For the purposes of this work, Cetacea is described in detail first, before proceeding to the remaining terrestrial families of Artiodactyla.

### 3.3.3.6. Cetacea

The infraorder Cetacea is composed of one extinct suborder (Archaeoceti, which survived until the Late Eocene) and two extant suborders: Odontoceti (toothed whales, dolphins and porpoises, comprising 75 living species from 10 families) and Mysticeti (Baleen whales, comprising 14 living species from four families) (Ridway *et al.*, 2017). There is

some evidence of dural ossification in Archaeoceti. In the Protocetidae *Carolinacetus gingerichi*, from the Late Middle Eocene, an underdeveloped ossified tentorium projects from the occipital (Geisler *et al.*, 2005). In extant Cetacea, however, dural ossification is limited to the Odontoceti.

In this suborder, ossification of both the falx cerebri and the tentorium cerebelli occurs in Ziphiidae, Monodontidae, Delphinidae and Phocoenidae families. In the sperm-whale (*Physeter macrocephalus* or *Physeter catodon*) only the falx cerebri is ossified, a condition that does not affect other members of the Physeteridae from the genus Kogia (Nojima, 1990b). These structures are observed in the fossil record as well, in an extinct member of the delphinids (in Globicephaline remains of which the species is unknown, Boessenecker *et al.*, 2013), and phocoenids (*Haborophocoena toyoshimai*, Ichishima and Kimura, 2005; Ichishima and Kimura, 2013; Figure 3.22, left). In the latter, the osseous tentorium consists of a small portion in the area where it joins with the osseous falx.
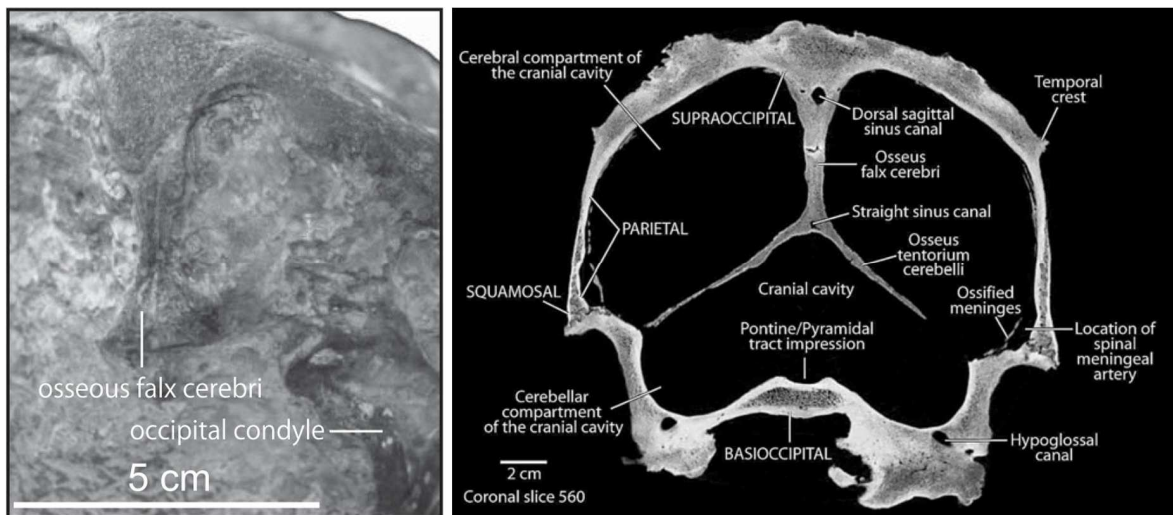


**Figure 3.22. Left: Osseous falx cerebri in a fossil specimen of *Haborophocoena toyoshimai* in posterior view (Ichishima and Kimura, 2013). Right: CT coronal slice of a *Tursiops truncatus* (Colbert *et al.*, 2005).**

Other families from the order Cetacea did not show signs of ossification. This was the case for Balaenidae, Balaeonopteridae, *Eschrichtiidae* and Platanistidae (Nojima, 1990b). It is important to note that Nojima only examined one specimen of narwhal (*Monodon monoceros*) and did not observe the structures directly, but inferred their

presence from the roughness of the internal occipital protuberance. There does not appear to be any information about Neobalaenidae meninges in the literature.

3.3.3.7. <u>Artiodactyla</u>

With the exception of Cetacea, dural ossification in Artiodactyla has yet to receive proper attention by researchers. As a result, four specimens from the Grant Museum were studied, belonging to different families: *Babyrousa babyrussa* (Suidae, specimen Z111), *Giraffa camelopardalis* (Giraffidae, specimen Z116), *Odocoileus virginianus* (Cervidae, specimen Z224) and *Madoqua phillipsi* (Bovidae, specimen Z2251). No signs of falx or tentorial ossification were observed, although it should be noted that specimen Z116 was a juvenile and the posterior part of the cranium of specimen Z2251 was broken and partially missing. In this last case, evidence of an ossified tentorium cerebelli was provided by Poggesi *et al.* (1982, Figure 3.23) who described in detail a male *Madoqua* embryo in an advanced stage of development. A full excerpt has been included here, given the amount of detail provided and the general lack of information in literature about tentorial prenatal ossification:

"[…] the front part of the lamina parietalis has been resorbed, so that there is no longer a commissura orbito-parietalis. However, soon afterwards, a strong ossified tentorium grows out from the dorsal region of the periotic into the ligamentous tissue which has taken the place of the lamina parietalis. This tentorium is triangular in shape and joins the posterior margin of the orbitosphenoid, while a branch of it, which is also ossified, joins the dorsum sellae (which is very large both in juveniles and adults). This tentorium ossifies quite early and a further bony lamella growing in a dorsal direction from the point where the apex of the temporal joins the basisphenoid (and thus topographically corresponding with the pita antotica vera) joins, with its tip, the lower surface of the ossified tentorium described above." (Poggesi *et al.*, 1982)

According to Nojima (1988), therefore, the osseous tentorium of *Madoqua phillipsi* would be assigned to the Carnivore type.
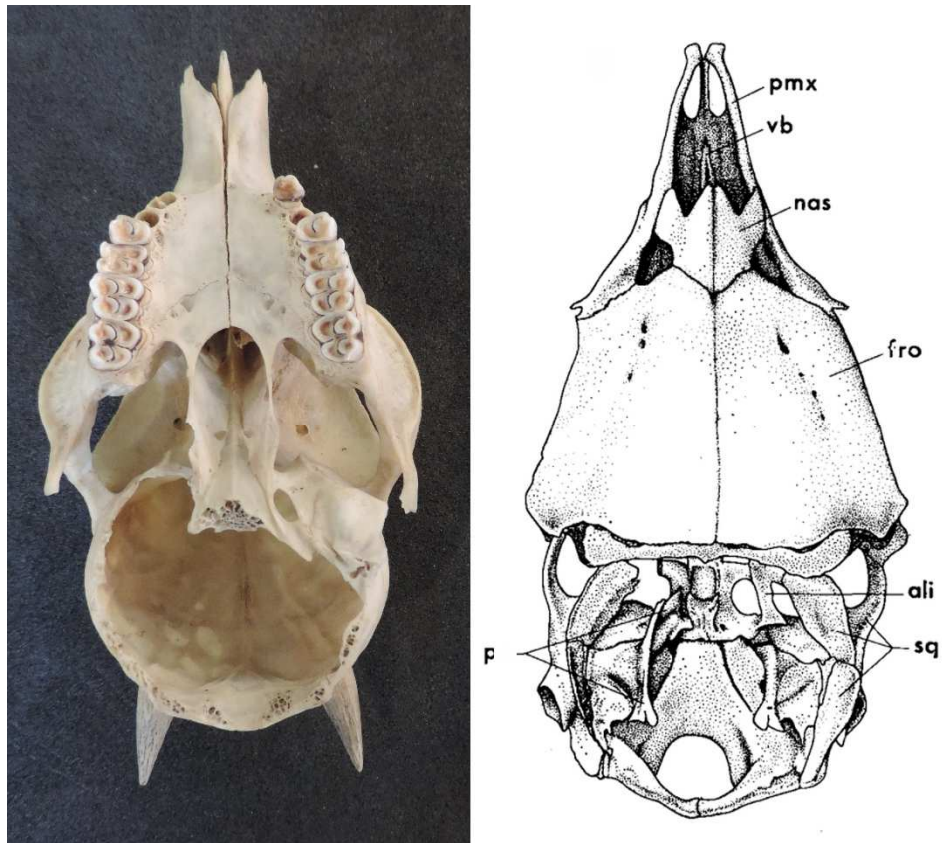
**Figure 3.23. Crania of *Madoqua phillipsi*. Left: specimen from the Grant Museum (Z2251) in ventral view; Right: Drawing of the inside view of an adult female Madoqua cranium in dorsal view, showing ossification of the tentorium cerebelli (the left branch of the alisphenoid and the anterior part of the right tentorium has been removed; Poggesi *et al.*, 1982).**

There is also evidence of an osseous tentorium cerebelli in specimens of *Camelus dromedarius* (Al-Sagair *et al.*, 2002; El Allali *et al.*, 2017), where the structure is described as being composed of a lateral tentorial process formed by the parietal and temporal bones and "a sharp crest extending ventrally to the basal part of the cranium cavity" (El Allali *et al.*, 2017). Moreover, an osseous tentorium has also been identified in fossilized remains of Merycoidodontoidea, sometimes referred to as oreodonts (Macrini, 2009). Apart from this, no references to the remaining Arctiodactyla families have been found in the literature. Of particular interest would be to assess the dural condition in Hippopotamidae, given its sister relationship with Cetacea.

3.3.3.8. Tubulidentata and Pholidota

As was the case with superorder Xenarthra, both orders Pholidota and Tubulidentata are mainly myrmecophagous – which explains why they share some convergent morphologies – although these groups are not close phylogenetically. On one side, Pholidota is composed of eight species of pangolins (Feldhamer *et al*., 2015). Of these, seven have been studied by Gaudin and Wible (1999), identifying a well-developed ossified tentorium that extends to the roof of the cranial cavity. On the other hand, Tubulidentata is currently composed of one Family (Orycteropodidae) with one species, *Orycteropus afer*, known as the aardvark (Feldhamer *et al*., 2015). According to Shoshani and McKenna (1998), this species possesses an ossified tentorium that is very similar to the one in members of Pholidota.

Additionally, two crania of an unidentified *Manis* species were observed in the Grant Museum (specimen number Z556, which was composed of two skulls). One of them (Figure 3.24, left) had a well-developed osseous tentorium, U-shaped and with complete tentorial wings. In the second, the structure was broken and missing, but part of a possible osseous tentorium still remained inside the cranial cavity (Figure 3.24, right).

Fossil specimens of pholidotans Palaeanodon (Emry, 1970) and Patriomanis (Gaudin and Wible, 1999) also have an osseous tentorium, although, in this case, the structure presents a lesser degree of ossification than in other individuals of *Manis* and is only developed "inferiorly on petrosal" (Gaudin and Wible, 1999).



**Figure 3.24. Two craniums of *Manis* sp. (specimen number Z556). Left: The osseous tentorium is complete and U-shaped. Right: The osseous tentorium is broken and missing, but part of it can still be observed in the endocraneal cavity.**

3.3.3.9. Rodentia

With the highest number of species (close to 2,300), Rodentia is by far the largest mammalian order (Feldhamer *et al.*, 2015). There are currently 36 extant families of Rodentia but, concerning dural ossification, only a very small number have received attention by researchers. Klintworth (1968) described the unossified tentorium of rodents such as *Cavia porcellus*, *Mus musculus* or *Rattus norvegicus* as two bilaterally-symmetrical folds or dural partitions, thus confirming that in these species the structure was under-developed. Therefore, dural ossification in Rodentia seemed unlikely and, in fact, Nojima (1990c) assumed that all rodents lacked an ossified tentorium. However, the existence of an osseous tentorium in three species of Heteromyidae (*Dipodomys*, *Microdipodops* and *Perognathus*, the latter with a lesser degree of development) had already been observed by Nikolai (1983). Sometimes referred as "kangaroo rats", Heteromyidae are bipedal, saltatorial rodents. About them, Nikolai described "well-formed bony partitions [that] project medially from the otic capsules into the space between the cerebral and cerebellar lobes of the brain. […] These partitions, which tend to compartmentalize the brain within the cranium, appear to be true tentorial ossifications."

In order to confirm dural ossification in Rodentia, four specimens from different families were observed. Although heteromyids were not available at the Grant Museum, a specimen of Dipodidae (*Dipus sp*, Z209) was studied, a family which shares with heteromyids the saltatorial method of locomotion. Specimens of the families Hystricidae (*Hystrix indica*, Z1219b), Caviidae (*Hydrochoerus hydrochaeris*, Z188) and Dasyproctidae (*Dasyprocta sp*, Z3044) were also studied. Observations (Figure 3.25) confirm the presence of endocranial partitions in the four specimens, but they were much less developed in specimen Z188. Whether these osseous partitions can be regarded as true tentorial ossification may require further investigation.
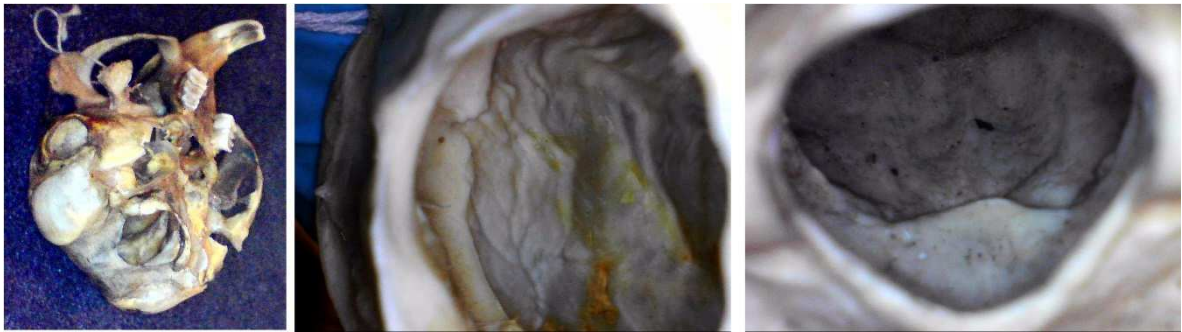
**Figure 3.25. Internal osseous partitions in the skulls of three rodent species. Left:** *Dipus* **sp, Z209; Middle:** *Hystrix indica*, **Z1219b, detail of a possible left tentorial wing; Right:** *Dasyprocta* **sp, Z3044.**

### *3.3.4. Dural fold ossification in the fossil record*

As happens with all osseous materials, in certain circumstances ossification of the dural folds is preserved in the fossil record. The commonplace use of computer tomography and digitalization in paleontology during the last two decades has allowed researchers to analyse the endocranium of fossil skulls with unprecedented detail. Because of this, today there is a significant number of testimonies of an osseous falx or tentorium in mammals and pre-mammals. Some of them – in particular, those more closely related with extant species – have been already discussed in the preceding sections, but there are many others, and this chapter would not be complete without summarizing some of the most relevant ones.

The earliest evidence of osseous tentoria can be traced back to basal mammaliaforms, during the Mesozoic Era, in specimens of *Sinoconodon*, *Triconodon mordax* and *Morganucodon* (Kermack, 1981). However, it should be noted that the existence of an osseous tentorium in *Morganucodon* is questioned, and has been disputed (Jaworowska, 1996; Jaworowska *et al.*, 2004). Both an osseous falx and a diamond-shaped osseous tentorium have also been found in a specimen of *Vincelestes neuquenianus*, a Cretaceous theriiform mammal from Argentina (Macrini *et al.*, 2007; Figure 3.26).
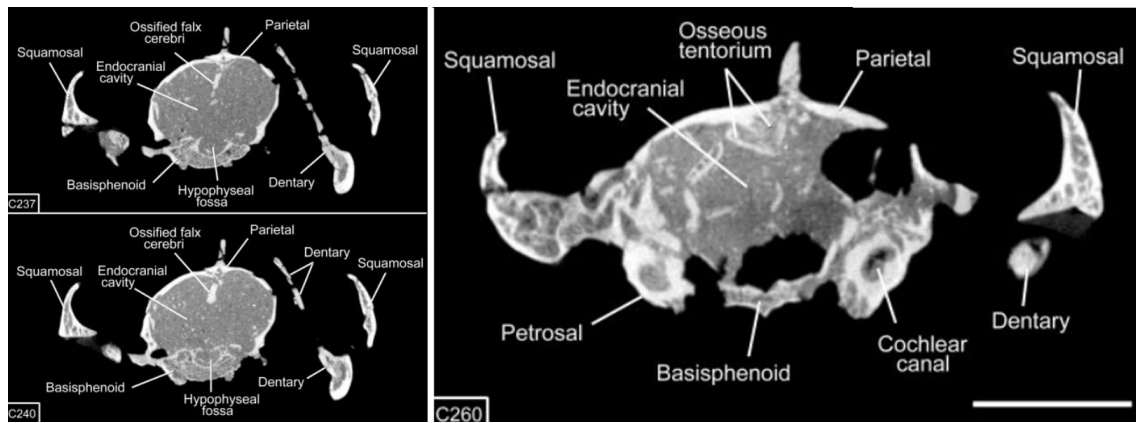
**Figure 3.26. CT- scans showing the presence of an osseous falx cerebri (left) and a fragmented osseous tentorium cerebelli (right) in a fossil specimen of *Vincelestes neuquenianus* (Macrini *et al.*, 2007).**

In the disputed group Condylarthra, considered to be composed by a series of primitive ungulates from the Paleocene-Eocene periods, *Hyopsodus lepidus* (family Hyopsodontinae) presents an osseous tentorium in the shape of a thick crest of bone (Orliac *et al.*, 2012). Tentorial ossification has also been found in four genera of Notoungulata from the families Oldfieldthomasiidae (*Oldfieldthomasia*), Hegetotheriidae (*Paedotherium*), Interatheriinae (*Cochilius*), and Notohippidae (*Rhynchippus*) (McPhee, 2014; Dozo and Martínez, 2015). In notungulates, the osseous tentorium is formed by the confluence of the petrosal crest, the supraoccipital, and the parietal bone (McPhee, 2014).

The ossification of the tentorium cerebelli has been also observed in creodont fossils, a group of basal carnivores that appeared in the Late Cretaceous and became extinct in the Miocene (Feldhamer *et al*., 2015). Polly (1993) affirmed that the osseous tentorium differed in shape and position between Creodonta and Carnivora, but could be considered homologous, since it served to separate the cerebral hemispheres and the cerebellum in both cases. To illustrate the differences, a detailed description of the osseous tentorium of *Hyaenodon exiguus* (Creodonta: Hyaenodontidae) and its comparison with the Canid tentorium is transcribed in full below:

"[…] the tentorium cerebelli […] is formed by the basisphenoid, alisphenoid, squamosal, and parietal. The tentorium meets the floor of the braincase anterior to the foramen ovale, considerably anterior to its position in Carnivora. In *Canis*, the tentorium meets the floor of the braincase posterior to the foramen ovale and is formed by a crest of the petrosal

which is inclined posterodorsally at the rear of the cranial cavity. In *Hyaenodon*, the tentorium is located anterior to the petrosal and there is no petrosal crest. It is more vertical and more anteriorly placed in *Hyaenodon* than in *Canis*, concomitant with the smaller, more anteriorly placed cerebral hemispheres in *Hyaenodon*." (Polly, 1993)

A much older account (Wortman, 1894) describes ossification of the tentorium of *Patriofelis ferox* (a species from another family of Creodonta: Oxyaenidae) as extremely limited or even non-existent.

## 3.4. Discussion

This extensive review includes most of the literature currently available and supplements the data with findings from the Grant Museum in an attempt to provide a more comprehensive account about ossification of the falx and the tentorium in Mammalia. After gathering this data together for the first time, the two hypotheses outlined in the introduction can now be revisited and discussed in more detail, either to see if there is any supporting evidence or to dismiss them.

### *3.4.1. Dural ossification as a result of diet*

As discussed before, Nojima (1988) created a distinction between the dural folds that ossified prenatally and those that ossified during the course of aging; he named these carnivore type and dolphin type. Dural ossification as a consequence of dietary intake would obviously only provide a viable explanation for species of the second group, which mainly includes some cetaceans (Delphinidae and Phocoenidae) and primates (Cebidae) because, although it is known that maternal diet is a factor which potentially affects the osseous development of the offspring (Hurley, 1969; Shrader and Zeman, 1973), no evidence seems to indicate that it can produce consistent ossification of the soft dural structures (and, anyway, it could not account for the uniformity exhibited across individuals of the same groups, such as Felids). The carnivore type is much better-represented than the dolphin type, because it encompasses all Carnivora, Sirenia, Perissodactyla (Equidae), Marsupialia (Macropodidae) and some Cetacea (Physeteridae and Ziphiidae). In the embryology of humans, the lateral parts of the tentorium cerebelli begin its basal development after circa 41 days. Both lateral parts become fused at a later

stage forming the full tentorium (O'Rahilly *et al.*, 1986). The development of the falx cerebri occurs simultaneously in two independent portions, an anterior and a posterior part. They both fuse together early (after circa 51 days; O'Rahilly *et al.*, 1986). According to a study of Tsitouridis *et al.* (2006) which analyzed 40 human specimens, disconnected ossification is more frequent in the anterior part of the structure. However, it must be noted that, in species classified in the Carnivore type, falx ossification mostly occurs in the caudal region, which is the one that develops from the dorsolateral continuation of the tentorium in humans (O'Rahilly *et al.*, 1986), and also the part that usually ossifies in groups such as pinnipeds and the genus ursus, in which the osseous portion of the falx marks a continuation with the tentorial process (Nojima, 1990c). Unfortunately, apart from isolated references in the literature (for example in the case of *Madoqua* (Artiodactyla; Poggesi *et al.*, 1982)), there is little information about the prenatal stages of the dural folds so, currently, information for many mammalian orders is missing.

Nojima (1988) initially suggested that the gradual ossification of the falx and tentorium that characterised the dolphin type could be a consequence of an excess intake of vitamin D, calcium and phosphorous, and he supported this hypothesis by arguing that the standard diet of a captive bottlenose dolphin would cause vitamin D toxicity in most mammals. However, he later retracted this hypothesis when he found out ontogenetic ossification of the tentorium cerebelli in captive Spider monkeys (*Ateles*) which had been fed throughout life with a diet with no particular high contents of vitamin D and compared it with the unossified tentorium of other primate species which had been fed with similar diets (Nojima, 1990a).

Despite this conclusion, the hypothesis deserves a closer scrutiny, not only because of the discrepancies between Nojima and other authors concerning ossification among the Platyrrhini, but also because it has been demonstrated that an inadequate intake of vitamins – not limited to vitamin D – calcium and minerals in a diet may result in bone alterations and, in some cases, cranial thickening (Chandra *et al.*, 1999; O'Regan and Kitchener, 2005; Palacios, 2006). There are many nutrients that are related with bone health and bone remodelling, including, but not limited to, vitamins A, B, C, D and K, calcium, proteins, magnesium, phosphorous, fluoride and copper (Palacios, 2006), but it must be borne in mind that these nutrients interact with one another and that merely observing isolated levels of consumption of one of them may not be sufficient. For example, boron and iron increase absorption of other nutrients, such as vitamin D and

calcium (Palacios, 2006). Considering all types of soft-tissue mineralization, it appears that other vitamins may be involved. For example, vitamin K insufficiency can cause severe calcification of soft tissues (Theuwissen *et al.*, 2012), although it does not necessarily induce calcification of the dura mater, let alone ossification. There is no doubt that the species belonging to the Carnivore type manifest proper osseous dural folds, and little in the case of species pertaining to the Dolphin type. Nojima (1990b) stated that the osseous falx and tentorium of Spotted Dolphins were not formed by calcareous depositions, but proper bone. However, this is much more difficult to assess in the case of the disconnected patches of osseous (or osseous-like) tissue found in humans or discovered in both *Felis silvestris catus* specimens that were dissected for this Thesis (see Chapter 4 and, particularly, Figure 4.2) because the two conditions are virtually indistinguishable in radiology. Because of this, Batnitzky *et al.* (1974) performed histological analyses of the falx on 18 autopsies and found that, in all cases, the tissue was membranous bone complete with bone marrow elements. Similar results were reported by Sands *et al.* (1987). Debnath *et al.* (2009) also described a case of falx cerebri ossification which consisted "of two peripheral layers of compact osseous tissue delimiting a central layer of medullary osseous tissue." Some authors (Tsitouridis *et al.*, 2006; Tubbs *et al.*, 2006) even regard "calcification" as a misnomer. Because of this, and because calcification does not have any mechanical significance in the context of this current study, only proper ossification will be take into account here. Nevertheless, specific effects of an inadequate consumption of an isolated nutrient have been frequently studied, and two of these – high levels of calcium and vitamin D, and deficiency of vitamin A – have been linked with osseous alterations of dural folds and therefore may provide grounds to support the diet hypothesis.

In the case of high levels of vitamin D, which were originally proposed by Nojima (1988) as a possible cause for post-natal ossification in dolphins and porpoises, evidence in humans does indeed confirm that it may result in dural fold ossification (DeWind, 1961; Schey, 1974; Davies *et al.*, 1986; these papers frequently refer to dural "calcification", but see Section 2.5.7). However, almost-complete ossification in the manner of Delphinidae or Phocoenidae is extremely rare in humans, where it tends to appear in disconnected patches of bone, and not necessarily linked with hypervitaminosis D (for a more detailed account of this phenomenon, see Chapter 2).

Another driver of dural fold ossification may be the consumption of a diet *low* in vitamin A. Hypovitaminosis A seems to cause an increase in osteoblastic activity, provoking alterations in bone growth, especially in the cranial bones (Gallina *et al.*, 1970). In particular, the effects of hypovitaminosis A have been well-studied in lions (*Panthera leo*) (Chandra *et al.*, 1999; Hartley *et al.*, 2005; Gross-Tsubery *et al.*, 2010) where, in many cases, the normal osseous tentorium cerebelli and associated bones (parietals, occipital) had been thickened (Figure 3.27 and Figure 3.28). However, although the lack of vitamin A seems to be the primary cause, other explanations have been proposed for this syndrome, such as developmental malformations or viral infections (Gross-Tsubery *et al.*, 2010). The syndrome mostly affects felids because they cannot convert β carotene into vitamin A and therefore are more sensitive to deficiencies in their diet (Schweigert *et al.*, 2002). Other examples of this effect in the literature include cheetah (*Acinonyx jubatus*) (De Risio *et al.*, 2010) and common household cats (*Felis silvestris catus*) (Espadas *et al.*, 2017), but there are occurrences of non-felid species as well, such as dogs (*Canis lupus familiaris*) (Mellanby, 1941). The normal condition in canids is a partial ossification of the tentorium, contrary to felids where ossification is complete, so it is interesting that a lack in vitamin A produces ossification in the structure. Hypovitaminosis A has also been identified in sea otters (*Enhydra lutris nereis*), with one of the symptoms being an irregular thickening of the calvaria, but not specifically the tentorium (Leger *et al.*, 2011). So far, pigs (*Sus scrofa*) seem to be the only example where ossification was produced in a previously unossified tentorium as a consequence of vitamin A deficiency (Jubb *et al.*, 1993).

**Figure 3.27. Saggital section of *Panthera leo* with thickening of the occipital bone and tentorium cerebelli (after Chandra *et al.*, 1999).**
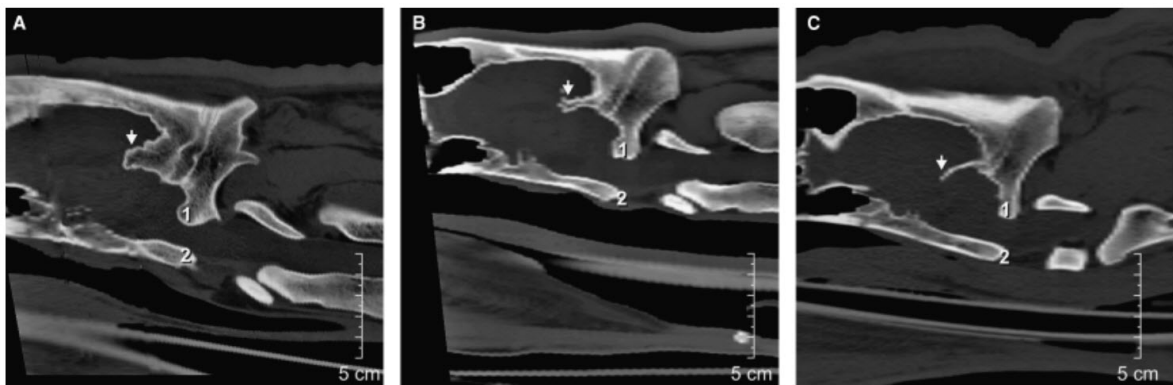


**Figure 3.28. CT midsagittal views of the posterior end of the skulls of three specimens of *Panthera leo*. The left and middle images shows the thickening of the osseous tentorium cerebelli (white arrow). The specimen of the right shows the normal condition. Also, note the abnormal thickening of the occipital bone (Gross-Tsubery *et al.*, 2010).**

It has been reported that hypovitaminosis A causes thickening of the soft dura mater as well. For example, Gallina *et al.* (1970) reported that the dura mater was thicker in calves (*Bos taurus*) that had been subjected to a diet poor on vitamin A for 16 weeks after birth when compared with a control group. This thickening, manifested in the manner of dura mater fibrosis, has been confirmed in a different study (Van der Lugt and Prozesky, 1989). It also seems that the opposite is true, and that an increase in vitamin A

consumption produced a decrease in the weight of the soft tentorium cerebelli (Gorgacz *et al.*, 1971).

Despite the evidence that a diet low in vitamin A may be a cause of dural ossification in otherwise healthy individuals, there are a number of reasons that cast doubt on the idea. Firstly, most accounts refer to the thickening of the tentorium, either osseous or soft, but there is very limited evidence of ossification in the case of the soft tentorium, just fibrosis. The only two exceptions are the ossification in pigs (Jubb *et al.*, 1993) and perhaps the mention of tentorial "calcification" in dogs by Mellanby (1941), although in the latter it is not entirely clear if the author was referring to a normal condition of the animals or a phenomenon of clinical significance. Secondly, although the thickening of the tentorium is one of the main effects of the lack of vitamin A, it does not appear in isolation; other alterations in bones of the skull, the mandible and the cervical vertebrae are referred in the studies. Thirdly, vitamin A deficiency causes medical problems other than bone thickening, some of them quite severe, such as lack of coordination, convulsions and blindness (Bartsch *et al.*, 1975; Gross-Tsubery *et al.*, 2010). It is also important to note that, while hypervitaminosis D may produce ossification both in the falx cerebri and tentorium cerebelli, all studies of hypovitaminosis A refer to an increase in thickness of the tentorium but they do not mention changes in the falx. Therefore, it may be concluded that, although there is evidence of tentorium alterations as a consequence of different nutrient intakes, there is currently insufficient support in the literature to sustain the diet hypothesis; but the idea cannot be ruled out completely until more systematic studies have been undertaken.

In this regard, there are some parallels suggested across taxa; for example, the various myrmecophagous orders – Pilosa (belonging to the superorder Xenarthra), Pholidota and Tubulidentata – that share a similar diet and an ossified tentorium cerebelli, despite not being closely related phylogenetically. The aardwolf (*Proteles cristata*) can also be included, a carnivoran with a primary diet of termites. Myrmecophages are an example of evolutionary convergence and exhibit multiple morphological adaptations (Feldhamer *et al*., 2015). They could represent a good case of study of the proposed hypothesis because of their monodiet, but even in specialized feeders that are forced to consume a limited array of prey it is extremely problematic to link diet with dural ossification. One of the primary issues is that, despite all efforts, the nutrient requirements of most species in the wild are currently unknown (Cabana *et al.*, 2017). A related

problem is that, although referred to as myrmecophages, it would be more accurate to characterize these mammals as specialized insectivores which consume social insects of low nutritional value opportunistically, because the majority of them do not feed exclusively on ants or termites (Delsuc *et al*., 2014). Even disregarding this, there is a high number of ant species and their nutritional composition may vary enormously (Pekár and Mayntz, 2014). Lastly, it should be noted that there are also exceptions among myrmecophages: both the Giant anteater (Myrmecophagidae) and echidnas (Tachyglossidae) do not exhibit tentorial ossification, despite sharing a similar diet.

### *3.4.2. Dural ossification as a result of behavioural causes*

The fact that most Carnivora share such a distinctive trait as an osseous tentorium cerebelli, and some an osseous falx, is suggestive of a common connecting factor. An ossified tentorium can also be found in some marsupials, such as the thylacine (*Thylacinus cynocephalus*), and in extinct Creodonta, all of which occupy predatorial niches in different times and locations (Janis *et al*., 1998; Figueirido and Janis, 2011). Initially, therefore, ossification appears to be another example of morphological convergence. Moreover, FE analyses of the cranium of *Felis silvestris catus* reveal a slight increase in stress at the back of the skull during biting when an osseous tentorium cerebelli is absent (Sellés de Lucas *et al.*, 2018; Chapter 5), which confirms that the osseous tentorium does indeed play a mechanical role during feeding. These results may be of some significance, but more research across different taxa with multiple morphologies is required before it can be concluded that tentorial ossification represent an adaptation for predatorial biting.

Beyond biting there are many other behaviours in which ossified dural folds may have some mechanical significance for the skull. Perhaps one of the most obvious is locomotion, and certain kinetic movements, particularly those which involve sudden accelerations and decelerations; for example, related to hopping or bounding, such as the ones that characterize kangaroos and wallabies, which possess an ossified tentorium. Heteromyidae also share this same method of travelling, which is very rare among rodents, and exhibit tentorial ossification. In fact, Nikolai (1983) has already suggested that the osseous tentorium of Heteromyidae may serve a functional role linked to that bipedal locomotion. However, this hypothesis is weakened after considering that other

species such as rabbits, characterised by a bounding locomotion, do not possess ossified tentoria (Klintworth, 1968), although it could be argued that the combination of bipedalism and hopping that kangaroos and kangaroo-rats share differs from the bounding movement of rabbits (Lovegrove, 2004). Nonetheless, another potential criticism for the hypothesis can be easily raised: most Diprotodontia have ossified tentoria but do not share the same method of locomotion as kangaroos and wallabies.

Another factor related to locomotion that might intuitively seem important is speed and, specifically, maximum running speed, although possibly acceleration to and deceleration from that maximum speed, rather than absolute speed itself, may have more relevance. There is little data on this in the literature, and it is difficult to measure the speed of an animal in the wild, and then unclear as to whether the animal is moving at its maximum capabilities. Those studies which have measured speed frequently use different methods, which may also be problematic when comparing data (Garland, 1983; Iriarte-Díaz, 2002).

To support the hypothesis that maximum speed may be an important factor in dural ossification, it is well known that most Carnivora can reach relatively high speeds as part of their predatory activities. Among Heteromyidae, the Merriam's kangaroo rat (*Dipodomys merriami*), with a speed of 32 km/h, is also one of the fastest members among Rodentia for which data has been gathered. Also, tentorial ossification is present among some Perissodactyla (horses, zebras, etc.), with absolute maximum running speeds of ~70 km/h (Garland, 1983). However, most herbivores lack tentorial ossification (Nojima, 1990c) despite some species being able to reach higher maximum speeds, which weighs against this hypothesis. For example, a Blackbuck (*Antilope cervicapra*) can reach 105 km/h, which is very close to the impressive 110 km/h of cheetahs (*Acinonyx jubatus*) (Garland, 1983). Contrary to the order Carnivora, the dural condition in Artiodactyla has not receive the same amount of interest, so there is still some uncertainty about ossification in this regard, but the current investigation has confirmed the lack of an osseous tentorium in a specimen of *Odocoileus virginianus*; the closely related *Odocoileus hemionus* has an absolute maximum running speed of 61 km/h (Garland, 1983). On the other hand, not all members of Carnivora are so fast (bears, for example), and even among felids, maximum speeds vary considerably amid species, from the record of the cheetah to more modest values of under 60 km/h in tigers and lions (Garland, 1983). This is similar to the speed a European rabbit can reach (*Oryctolagus cuniculus*), but in

contrast to carnivores, rabbits do not exhibit tentorial ossification. Given the existence of so many counterexamples, it seems that a link between tentorial ossification and maximum running speed lacks support.

Apart from this, there are other dynamic behaviours that may potentially affect the endocranium and the brain, but they are equally problematic. One of them is the impact received by bulls while fighting during the rut (Nojima, 1990c) or the potential falls as a consequence of an arboreal method of locomotion, as in the case of many species of Primates. However, there does not seem to be a clear correlation between dural ossification and any of these behaviours.

Aquatic or semiaquatic animals represent a special case, given that an ossified falx cerebri is most commonly present in marine, lotic or lacustrine mammals. Among Carnivora it can be found in Otariidae, Phocidae and Odobenidae, and in many cetaceans, which includes Ziphiidae, Delphinidae, Monodontidae and Phocoenidae. Moreover, it is present in all extant Sirenia studied, and even in Ornithorhynchidae. It may seem tempting to try to find some correlation between the aquatic habitat and the ossification of this structure, but there are also cases that support the contrary. For example, the ossified falx is absent in several families of Cetacea (in Balaenopteridae, Eschrichtiidae, Balaenidae, Kogiidae and Platanistidae) and is also missing in mammals which share the same lacustrine habitat as platypuses, such as some Mustelidae. In contrast, Ursidae also have a partially ossified falx cerebri despite not belonging to these habitats.


## 3.5. Conclusions and future research

The purpose of this chapter was firstly to bring together and comment upon previous evidence of dural ossification reported in the scientific literature and arrange them in a systematic manner, a task that so far had never been undertaken. Secondly, this material was supplemented with data from observations of specimens of the Grant Museum, adding new species for which ossification information had not previously been described elsewhere. Thirdly, in the light of all this compiled and new data, the chapter tested the validity of two hypotheses that were proposed in the past to provide an explanation for the condition. Finally, based on this work, recommendations are made for possible future research directions to reveal the still unexplained presence of dural ossifications. After considering a wide variety of cases there does not appear to be a single, straightforward

explanation for dural ossification in mammals, because for each one of the two hypotheses proposed – dietary or behavioural – there exists a group of counterexamples. Consequently, future research in this area faces two possible alternatives:

The first one would be to consider that dural ossification is a multicausal phenomenon and, as a consequence, deserves an equally multicausal explanation. After all, the process of ossification and its degree varies greatly across species, families and orders, and sometimes even across individuals of the same species. If that was the case, then for example, Nojima (1988) could be right in his first assumption, because tentorial ossification in *Ateles* monkeys may not be related with high consumption of calcium and vitamin D but, at the same time, it could be the primary cause for this condition in Cetacea.

The second possibility would be to consider that dural ossification is not linked to either diet or behavioural causes, and hence there is an alternative explanation for the wide arrange of ossifications present in mammals. For example, a proposal that has not been explored here is that perhaps there is a link between ossification, particularly tentorial ossification, and encephalization quotients. Moreover, there is also plenty of variation between the extent and fibrosity of the soft dural folds in mammals, and therefore, in some species, ossification may be indeed impossible due to this or any other related factors.

Before confirming or dismissing these two possibilities, more focused and systematic research is required. A larger number of species must be studied (with multiple specimens from the same species, and recording sex, to assess interspecies variation and sexually dimorphic variation, respectively) to fill the gaps that still persist in some mammalian groups. This would also ideally include the study of embryos at various stages and new-borns, sub-adults, etc., to help better differentiate among the Carnivore and Dolphin type dural folds. It would also involve the FE analyses of a larger number of specimens in a similar manner that the one conducted with the cranium of *Felis silvestris catus* and even experimental work with diets with different amounts of nutrients. It is a challenging task, almost certainly the reason why the phenomenon has remained understudied for such a long time.

Moreover, and possibly more importantly, it still remains to be explained why or how the alteration of the dura material properties of the falx and the tentorium would contribute in an adaptation to increase the performance of predatory behaviour or

presumably preventing injuries during fast movements, biting or locomotion. Except for the slight decrease of stress in the posterior area of the skull found in FE analyses (Sellés de Lucas *et al.*, 2018), there is no evidence yet in the literature to support this. In fact, the presence of ossified dural folds may even have some disadvantages. It has been suggested that the osseous tentorium cerebelli may act as a contributing factor for herniation in horses (Schmidt and Ondreka, 2018). Also, in certain cases where a unilateral increase in intracranial pressure takes place, such as subfalcine herniation, an ossified falx cerebri might hypothetically will be less able to displace brain tissue, because bone is less flexible than soft dura, thus potentially increasing the risk of medical problems (Tubbs *et al.*, 2006).

# Chapter 4. Finite element modelling of a common cat skull (*Felis silvestris catus*)

In this chapter, the creation of a digital model of a *Felis silvestris catus* skull is described. The aim was to produce a multi-purpose model that could be used to test various hypotheses related to the role that thin bony structures and soft tissues play in the biomechanics of the cranium. Thus, the *Felis silvestris catus* model was constructed to include structures such as the nasal turbinates, periodontal ligament and dura mater (including the falx cerebri and the tentorium cerebelli), together with a basic reconstruction of the felid neck muscles. In the latter case, the purpose was to examine quantitatively the biomechanical role of the falx and the tentorium and the effects its ossification might play under various biting regimes. The details of this study are included in Chapter 5.

## 4.1. Creation of the *in silico* model

The head of an adult *Felis silvestris catus* specimen, obtained from a deceased animal donated to the Liverpool Institute of Veterinary Science for teaching and research, was scanned in an X-Tek HMX 160 microCT (µ-CT) system at the University of Hull, UK (scan resolution 61.7 µm in all three axes). The sex of the specimen is unknown, as the body was not used in this study. A second *Felis silvestris catus* specimen obtained under the same circumstances was also used for dissection in order to gather additional data. From now on, it will be referred as the second specimen or the "control" specimen.

The stack of .TIFF images obtained from µ-CT scanning was then imported into Avizo (Version 9.0.1, Visualization Science Group) where segmentation of the different structures was achieved using a semi-automatic method, combining algorithms with further manual refinements. The skull was intact, apart from the cusp of the left canine tooth which was reconstructed digitally, while the first left premolar was also absent (no action was taken in this case, as it did not play any relevant role in the analyses). The mandible was also segmented in order to reconstruct jaw-closing muscle orientations. The nasal turbinates were represented independently and identified as a different structure, as was the nasal septum. Where possible, the delicate structures that compose the cribriform

plate and the ethmoturbinates were maintained. The trabecular bone was visible in the CT scans and individual trabeculae were segmented. Voids in the trabecular bone and the empty spaces between the nasal turbinates were filled with a general filling material to simulate the presence of generic soft tissues, which also prevented errors during the FE solution arising from disconnected fragments of trabeculae. The cranial cavity was also filled with another material to reconstruct the gross volume of the brain and to allow modelling of the dura mater covering its surface at a later stage. However, as no other intermediate layers were modelled, this endocast should be regarded as a simplification of the brain, since it was connected directly to the bone in the model, and therefore the endocast surface strains are likely to be oversensitive to changes in bone strain. This therefore prevents a more detailed analysis of the effects that the ossified dural folds might pose on this particular structure. The periodontal ligament (PDL) was included by covering the tooth roots and their proximal surfaces with a 3-4 voxel-wide layer of tissue (0.19-0.25 mm; McCormack *et al.*, 2017). Although the ossified tentorium forms a continuum with the parietal bone (Figure 4.1), it was carefully segmented as an independent structure (from where it attaches to the internal parietal wall) in order to allow testing with different material properties during the analyses.
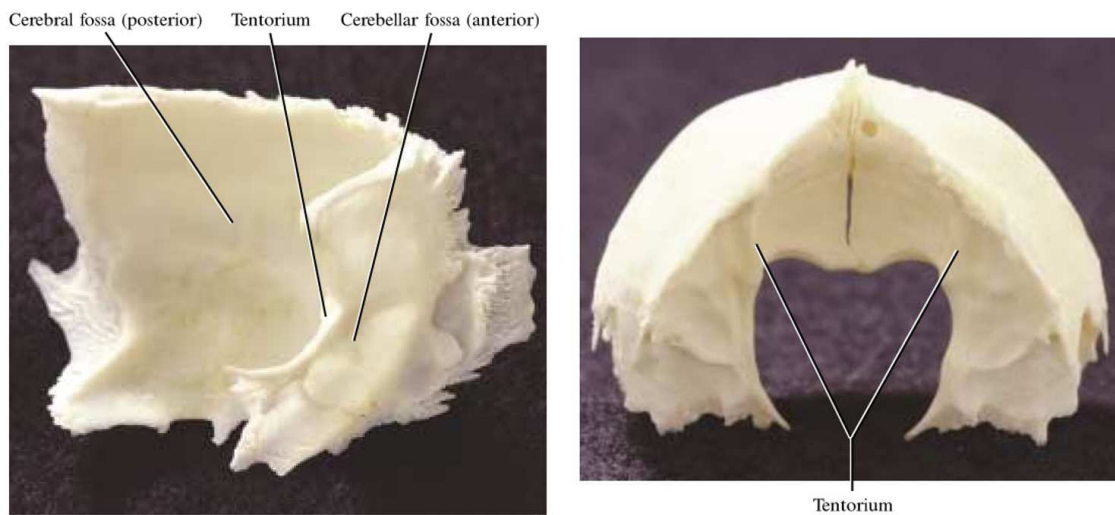


**Figure 4.1. Left: medial view of the right parietal of the cat; Right: caudal view of paired parietals (after Sebastiani and Fishbeck, 2005).**

The falx cerebri was visible to some extent in the CT scans allowing it to be reconstructed in the final model (Figure 4.2, left). The most probable cause for this was that the specimen's falx was partially ossified in its posterior region, and therefore discernible in the scanned images. Although the ossification was unexpected in this species, it may not be such a rare occurrence, since dissection of the second specimen (Figure 4.2, right) also revealed what seemed to be similar patches of ossification (although no further analyses were carried to confirm their precise composition). Moreover, in its posterior end, where the falx cerebri attaches to the midline of the tentorium cerebelli, two thin sheets of tissue were also observed (Figure 4.3. **Above: CT scans of the specimen modelled, showing the two thin sheets of tissue found. Below: Posterior view showing the same structure after a parasagittal cut of the second specimen.**) both in the scans and in the control specimen after performing the parasagittal cut, presumably further increasing the attachment strength of the structure.



**Figure 4.2. Left: Coronal view of a CT scan image which shows two oval shapes following the midline. Right: parasagittal cut of the control specimen, with possible patches of ossification (highlighted in red).**
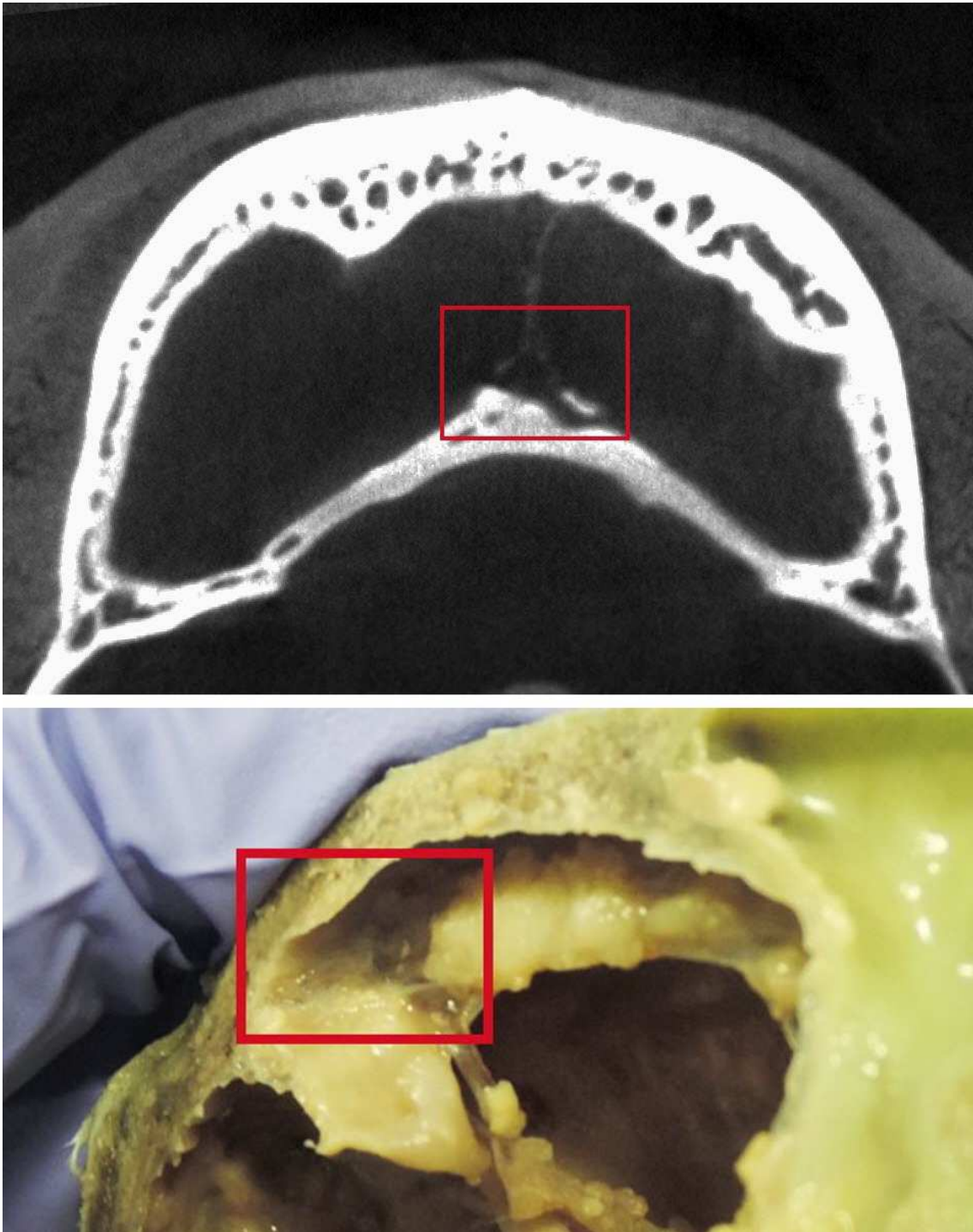
**Figure 4.3. Above: CT scans of the specimen modelled, showing the two thin sheets of tissue found. Below: Posterior view showing the same structure after a parasagittal cut of the second specimen.**

After segmentation in Avizo, various surface models were created with different numbers of surface triangles until the desired number of tetrahedral elements were

achieved in the final grid model. Each surface model had to be modified in order to improve the tetrahedral quality and remove all intersections before converting it into a final grid model suitable for finite element analysis (Avizo User's Guide, 2018). This stage of the process proved to be extremely difficult and time consuming, as several of the resulting models failed to generate a grid file despite the grid parameters being within the range recommended by the software. The final model had more than 12 million surface triangles and nearly 5.9 million high order (quadratic) tetrahedral elements. The full list of structures segmented in Avizo, together with additional ones modelled in ANSYS at a later stage (see Chapter 5) and their corresponding material properties, are summarized in Table 5.1.

Avizo landmark tools were used to define the origin and insertion areas of the muscles, with the data required for this step gathered during the dissection of the two specimen heads (see next section).

## 4.2. Masticatory muscles

Household cat anatomy, including precise muscular origin and insertion attachments (Figure 4.4), is well known and has been thoroughly described in literature. The anatomical descriptions below have been taken from various sources: Diogo et *al.*, 2012; Hartstone-Rose *et al.*, 2012; Sebastiani and Fishbeck, 2005; Laison *et al.*, 2001; and Turnbull, 1970; and are based on the dissection of the two specimen heads performed in the laboratory. The left side of the specimen scanned previously was dissected together with the second cat's head, in order to gain confidence and insight into specific anatomical characteristics of the species, and also to assess the weight of each individual muscle. Due to conflicts in muscle nomenclature, the same terminology employed by Hartstone-Rose *et al.* (2012) is used, which follows closely the one used by Turnbull (1970).
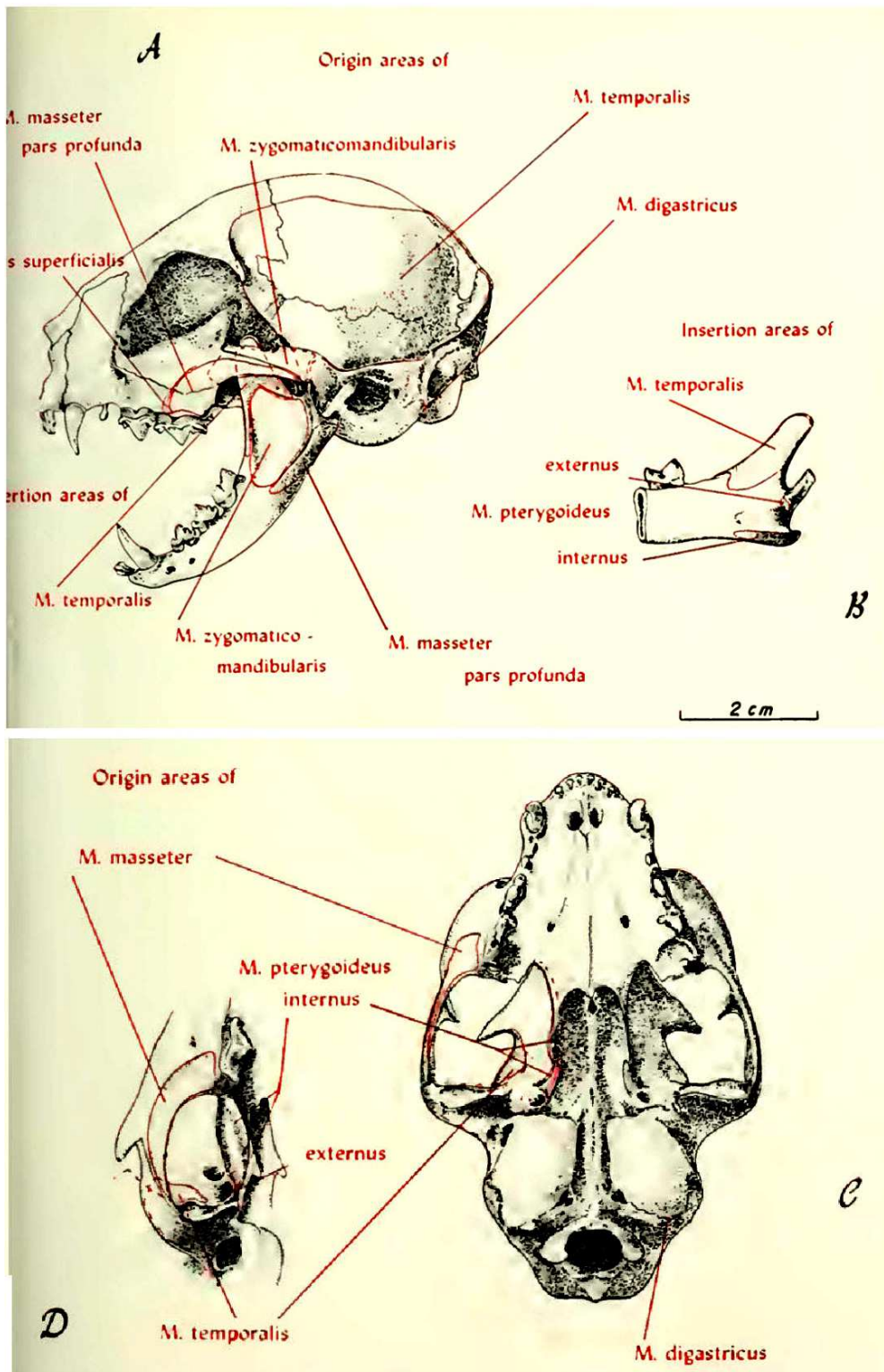
**Figure 4.4. Felis silvestris catus skull origin and insertion areas of the masticatory muscles. Lateral view (A). Medial view of the distal part of the jaw (B). Ventral view (C). Ventrolateral view of a skull detail (D) (After Turnbull, 1970).**

**Temporalis.** The temporalis is a massive muscle complex which occupies the temporal fossa and typically contributes to half of the total mass of the masticatory musculature (Table 4.). It has its origin in the temporal bone (although a few fibres also originate from the zygomatic arch) and inserts into the coronoid process of the jaw. The temporalis group has three further divisions: the zygomatic temporalis, the superficial temporalis and the deep temporalis (Figure 4.5, left). The superficial temporalis is covered by the temporal fascia, a sheet of thick fibrous tissue (Figure 4.5, right).



**Figure 4.5. Left: Right deep temporalis of the modelled specimen. Right: Temporal fascia in the control specimen.**

**Masseter.** The masseter muscle complex completely covers the posterior border of the mandible. It has its origin in the lateral and ventral surfaces of the zygomatic arch, and inserts into the masseteric fossa, extending into adjacent areas of the mandible as well. While some authors consider the zygomatico-mandibularis a completely different muscle, others treat it as the deepest layer of the masseter (Hartstone-Rose *et al*., 2012). It is covered by a thick aponeurosis and inserts on the lateral surface of the mandibular ramus. Sebastiani and Fishbeck (2005) identified the presence of three separate layers in the masseter with different fibre directions, while Turnbull (1970) identified two distinct layers, with the zygomatico-mandibularis the third. In the dissections, it was observed that the masseter of *Felis silvestris catus* is formed from up to five different layers (Figure 4.6). These results are consistent with some other references that identified at least six masseter layers in other felid species or have described between two and six layers in various mammalian species (Hartstone-Rose *et al*., 2012). For the purposes of the current research the most external layer will be referred as the superficial masseter and the

deepest one as the zygomatico-mandibularis, grouping all the remaining layers as part of a single "deep masseter".



**Figure 4.6. One of the layers of the masseter muscle in the second specimen, partially removed.**

**Pterygoideus.** The pterygoid complex is composed of pterygoideus externus and internus (or medial). The former is a relatively small muscle located in a ventral position with respect to the temporalis, and with an origin that extends from the external pterygoid fossa of the palatine to the foramen rotundum of the basisphenoid bone, and which inserts on the medial surface of the head of the condyle. The pterygoideus internus originates on the internal pterygoid fossa and in the lower border of the infratemporal fossa and inserts in the angular process of the mandible and in the pterygoideus externus.

## 4.3. Dissection data

The relative sizes of the muscles of the two specimens and those values reported in the literature were consistent although, interestingly, the whole muscle mass of the second specimen was 2.5 times greater, thus potentially 36% larger in each direction. Note the

pterygoid group was damaged in the second specimen, hence its weight was approximated by multiplying the value of the scanned specimen by the scaling factor of 2.5 (see Table 4.).

|  | Scanned specimen | | Second specimen | | Turnbull (1970) values | |
|---|---|---|---|---|---|---|
| Masseter group | 2.7 g | 29.3% | 7 g | 30.4% | 2.4 g | 35.2% |
| Temporalis group | 5.3 g | 57.6% | 13 g | 56.5% | 3.70 g | 54.3% |
| Pterygoid group | 1.2 g | 13% | (1.2×2.5 = 3 g) | 13% | 0.72 g | 10.5% |
| **Total weight** | **9.2 g** | | **23 g** | | **6.82 g** | |

**Table 4.1. Muscle group weights and percentage contributions for the specimens considered.**

## 4.4. Calculation of the muscle physiological cross-sectional areas (PCSA)

Muscle contributions to feeding appear to be relatively consistent across carnivorans, and the values for *Pantera onca* (temporalis, 64.1%; masseter, 28.3%; pterygoideus, 7.6%) have been already used for FE analyses of other species as diverse as *Felis lybica*, *Neofelis nebulosa* and *Panthera Leo* (Slater and Van Valkenburgh, 2009, following Davis, 1955). However, the cat's lineage in particular is known for having a wider skull with a stronger masseter than other felids (Sicuro and Oliveira, 2011), so taking this data at face value for *Felis silvestris catus* may mean an underrepresentation of the relative contribution of this muscle. To improve accuracy in the final model, we preferred measuring the specimen's muscles directly and then use the information gathered to estimate physiological cross-sectional area and muscle force (Table 4.2 and Table 4.3). In order to achieve this, the muscles were placed in a 10% formaldehyde solution and stored in a fridge for one month, at which time they were digested in a 30% nitric acid solution for 72 hours in order to separate the individual muscle fibres. The acid was then substituted with a 50% aqueous glycerol solution to stop the digestion process. Ten to fifteen random fibres for each muscle were isolated, photographed and subsequently measured with the software ImageJ (Schneider *et al*., 2012) to estimate mean fibre length.

| Muscle (scanned specimen) | Mean fibre length (mm) | Weight (g) | PCSA (cm²) | Overall contribution (%) | Muscle force (N) |
|---|---|---|---|---|---|
| Superficial masseter | 7.70 | 1.6 | 1.97 | 17.4% | 49.17 |
| Deep masseter | 8.33 | 0.3 | 0.34 | 3.3% | 8.50 |
| Zygomatico-mandibularis | 6.40 | 0.8 | 1.18 | 8.7% | 29.57 |
| Zygomatico-temporalis | 11.90 | 0.5 | 2.49 | 5.4% | 62.3 |
| Deep temporalis | 10.03 | 2.0 | 1.89 | 21.7% | 47.17 |
| Superficial temporalis | 14.10 | 2.8 | 1.88 | 30.4% | 47.00 |
| Pterygoid group | 10.55 | 1.2 | 1.08 | 12.0% | 26.92 |

**Table 4.2. Muscle fibre length, weight and PCSA values of the scanned specimen together with calculated muscle force and individual muscle contributions to total muscle force.**

| Muscle (second specimen) | Mean fibre length (mm) | Weight (g) | PCSA (cm²) |
|---|---|---|---|
| Superficial masseter | 10.43 | 4.1 | 3.72 |
| Deep masseter | 11.91 | 0.9 | 0.72 |
| Zygomatico-mandibularis | 7.66 | 2.0 | 2.47 |
| Zygomatico-temporalis | 14.36 | 2.5 | 1.65 |
| Deep temporalis | 14.57 | 5.2 | 3.38 |
| Superficial temporalis | 15.56 | 5.3 | 3.23 |

**Table 4.3. Muscle fibre length, weight and PCSA values of the second specimen.**

The muscle physiological cross-sectional areas (PCSA) were then calculated using the following formula (Murphy and Beardsley, 1974):

$$PCSA = \frac{muscle\ mass\ (g)}{density\ (g/cm^3)\ \times\ fibre\ length\ (cm)}$$

The muscle density was estimated to be 1.0564 g/cm³, a value taken from Murphy and Beardsley (1974) for the cat soleus, which has also been used in studies of cat neck muscles (Wickland *et al.*, 1991) and felid masticatory analysis (Hartstone-Rose *et al.*, 2012). Different values have been proposed for the intrinsic muscle tension (strength) produced by mammalian skeletal muscle cross-section, which is typically reported to range from 10 N/cm² to 50 N/cm². An intermediate value of 30 N/cm² was chosen for a

feline bite force estimation study by Hartstone-Rose *et al*. (2012). A possible alternative is the 2.3 N/cm$^2$ used by Spector *et al.* (1980) for the cat soleus. Muscle force was calculated for the scanned specimen using the following formula:

$$Muscle\ force = PCSA\ (cm^2) \times tension\ per\ unit\ CSA\ (kg/cm^2)$$

For the muscle insertions the mandible was positioned at a gape angle of approximately 0 degrees, i.e. complete occlusion. Because the specimen's head was not completely symmetric, landmarks were manually placed on both sides of the skull, left and right side (instead of mirroring them) in order to maximise accuracy. A variable number of insertion points, between two and sixteen, were used for each muscle depending on its size. After calculating the Cartesian components of each force, a bespoke routine coded in R (Version 3.3.3; R Development CORE TEAM R, 2008) was employed to format the spatial information into ANSYS commands (Mechanical APDL, 14.5.7, ANSYS Inc., Canonsburg, PA, USA).

## 4.5. Dura mater

The dura mater was simulated in ANSYS by selecting all the surface elements of the brain endocast material and creating a covering layer of shell elements (ANSYS SHELL 181). Shell elements are a simple but effective way to model thin structures such as the dura, with the ability to easily modify section data being useful for assigning different thicknesses to the structure during sensitivity tests. Although the dura actually extends over the brain and around the spinal cord, only the part that enclosed the brain was considered in this model, hence the dura was discontinued before reaching the infratentorial region (Figure 4.7).
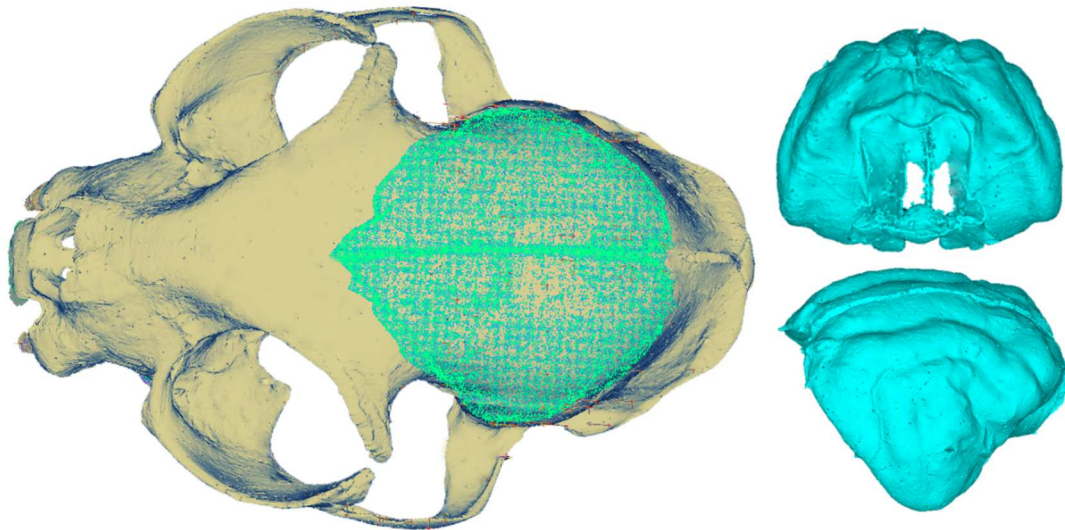
**Figure 4.7. Dura mater superimposed in green over a representation of the cat's cranium. Right top and bottom: frontal and lateral view of the model representation of the dura mater.**

## 4.6. Muscle wrapping

Accurate modelling of the muscle geometry is essential to examine the loading of skulls, but is often treated rather casually in biomechanical studies, where for example muscles are frequently simulated as simple force vectors applied directly to nodes of the bone surface. These studies may oversimplify the complex nature of muscle structure, as an individual muscle can attach closely over an area of the skull surface (Liu *et al.*, 2012) and wrap around the bone. For our analyses and based on the muscle dissections, only the superficial temporalis was modelled in this way, due to the fact that the rest of the masticatory muscles were found to follow approximately straight paths. Muscle wrapping was deemed necessary for the superficial temporalis, however, given the origin area of the muscle and the curvature of the parietal and the temporal bones in the cat's cranium.

Bespoke muscle wrapping solutions have been devised for different software. For example: the program BoneLoad for Strand7 FE software (Grosse *et al.*, 2007), loading data taken from MDA simulations for ANSYS models (Curtis *et al.*, 2008), and an algorithm developed for VoxFE (Liu *et al.*, 2012). Following a similar approach, we created a semi-automatic procedure in ANSYS to handle a muscle lying over a curvilinear surface. The process involves the creation of a series of paths each consisting of a line of

short "hairs" using ANSYS LINK180 (truss-type) elements positioned perpendicular to the bone surface (see Figure 4.8). Landmarks for each individual hair were defined manually in Avizo and later imported into ANSYS. The node at the outer end of each hair was then connected together to its neighbours with further link elements, thereby creating muscle strands wrapping around the cranium. The total force specified for the superficial temporalis muscle was then divided by the number of strands, and the resulting force then applied to the last node of each strand. An example of the code used is available in Appendix 2: ANSYS code for the muscle wrapping method.
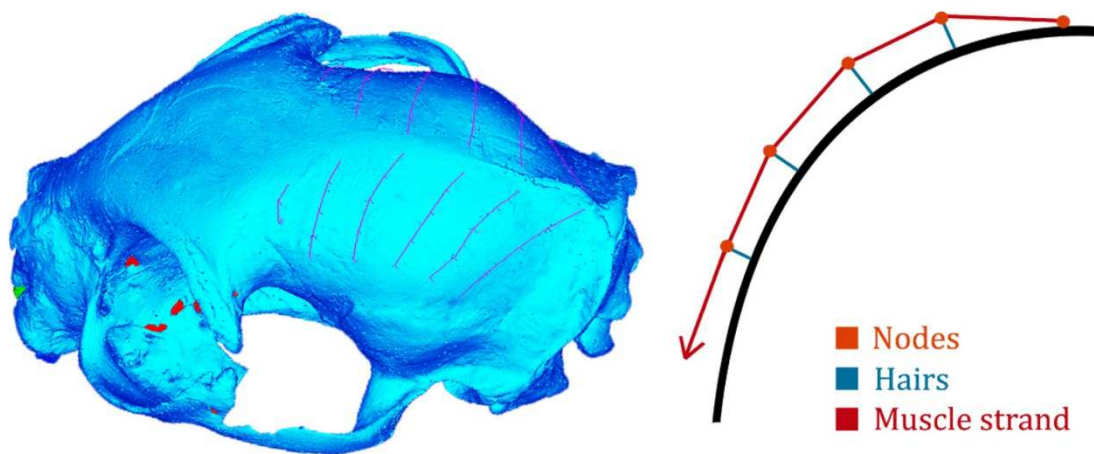


**Figure 4.8. Left: Final distribution of the link elements (dark blue) over the cat's cranium model representing the superficial temporalis. Right: schematic drawing of the muscle wrapping solution representing the hairs and nodes of a single muscle strand in frontal view.**

### 4.7. Neck modelling

During household cat mastication, the head also moves vertically and laterally, which requires the activation of the *semispinalis capitis* muscles (*biventer cervicis* m. and *complexus* m.) in the neck. At the same time, neck muscles play an important role in prey capture, where downward and upward movements increase penetration force of lower and upper canines, respectively. In addition to this, torsion movements may aid in tearing meat from carcasses (Gorniak and Gans, 1980). These nuchal muscles responsible for neck action are attached to the occipital, the mastoid region of the temporal and the posterior part of the parietal (Buckland-Wright, 1978). Despite the fact that cervical musculature plays an important role in many feeding actions, it is rarely taken into

account in biomechanical analyses. One of the main reasons may be due to the inherent complexity of its structure and distribution. An exception to this, however, can be found in McHenry *et al.* (2007), where neck muscles were modelled as part of intrinsic and extrinsic load analyses in two felid species (*Panthera leo* and the extinct *Smilodon fatalis*). They achieved it by using more than a hundred beam elements in each model.

For our analyses, neck modelling was necessary to apply extrinsic loads more accurately, given the importance of the posterior part of the head where neck muscles are attached. As in McHenry *et al.* (2007), the neck muscles were not used to apply forces but to hold the cranium in place; nonetheless, our approach differs methodologically to the one described in their paper (see the detailed explanation below).

Table 4.4 includes the full list of neck muscles modelled. It was created by gathering anatomical data from Reighard and Jennings (1901), Wickland *et al.* (1991) and Sebastiani and Fishbeck (2005). *The rectus capitis* group, which is composed of three individual muscles (*major, medius* and *minor*) was considered as a single unit for the analyses, while the *obliquus capitis caudalis*, with its origin on the atlas vertebra (C1), was not modelled. The number of landmarks per muscle, used to define the number of strands, was based on the size of the neck origin areas. As the original vertebrae and scapula were not preserved in the specimen, two octagons with different sizes were modelled and imported into Avizo to provide a surface for easier placement of the insertion landmarks. A small octagon was positioned at the approximate location of the axis vertebra (C2) and a larger one at the scapula, closely following the bone's orientation (Figure 4.9). The purpose of the octagons was only to provide topological information (vertex and sides) to place the landmarks more easily. The neck muscle origin and insertion landmarks were then imported into ANSYS and used for the pullback and lateral shake analyses. Muscle strands were defined as flexible link elements with equivalent soft tissue material properties (see following chapter).

| Muscle | Origin | Insertion | Landmarks IDs |
|---|---|---|---|
| **Cleidomastoid** | Apex and caudal area of the mastoid process of the temporal bone. | Clavicle. | 26 |
| **Levator scapulae ventralis** | Two heads: One from the atlas, the other from the basioccipital close to the tympanic bulla. | The two heads unite. Then inserts into metacromion and insfraspinous fossa (scapula). | 13 |
| **Longus capitis** | Basioccipital bone medial to the tympanic bulla. | C5 | 1 |
| **Longissimus capitis** | Mastoid process of the temporal bone. | C5 according to Wickland *et al*. (1991). C4 to C7 according to Sebastiani and Fishbeck (2005). | 12 |
| **Rectus capitis (three muscles: major, medius, minor)** | Midpoint of lambdoidal ridge to lateral point ¼ or 1/3 away from the mastoid process. | C1 and C2. | 23, 24, 25 |
| **Sternomastoid** | Lateral half of the lambdoidal ridge and mastoid area of the temporal bone until reaching mastoid process. | Anterior end of the manubrium. | 2, 3, 4 |
| **Splenius** | Lambdoidal ridge from midline to mastoid process. | Three attachments: midorsal line of neck, C6 and T1. | 8, 9, 10, 11 |
| **Occipitoscapularis (rhomboideus capitis)** | Few mm from the midline of lambdoidal ridge to half of the way from mastoid process. | Dorsal border of scapula. | 5, 6, 7 |
| **Biventer cervicis (spinalis capitis)** | Skull near the center of lambdoidad ridge. | T1 | 14, 15 |
| **Complexus (semispinalis capitis)** | Median third of the lambdoidal crest. | C6 according to Wickland *et al*. (1991). C3 to C7 and T1 to T3 according to Sebastiani and Fishbeck (2005). | 16, 17 |
| **Obliquus capitis cranialis (obliquus superior)** | Parallel to lambdoidal ridge, from 1 cm to midline | C1 | 18, 19, 20, 21, 22 |

| | to caudal side of the mastoid process. | | |
|---|---|---|---|
| **Obliquus capitis caudalis (obliquus inferior) (not used in these analyses)** | C1 | C2 | |

**Table 4.4. Full list of neck muscles considered, together with their origins and insertions, and their corresponding landmarks.**
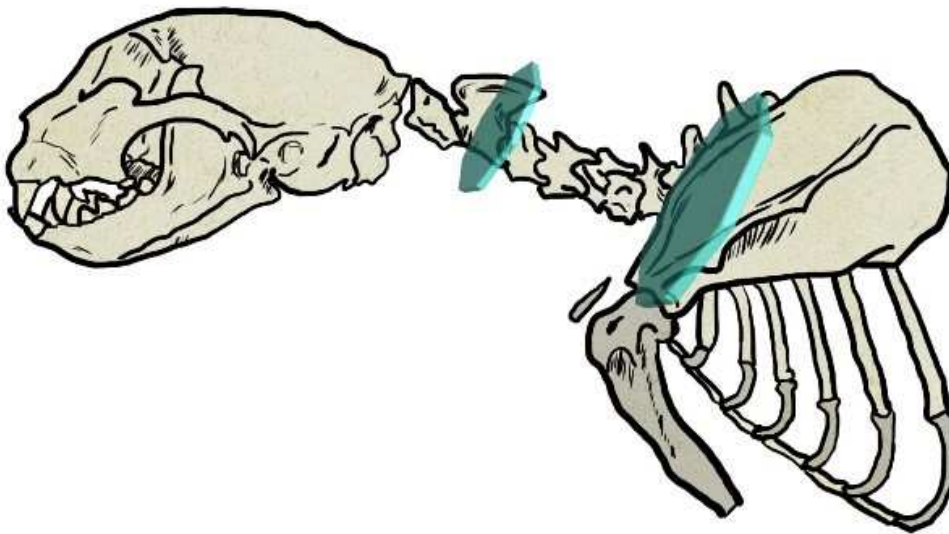


**Figure 4.9. Schematic drawing with head-neck orientation and relative size, position and orientation of the two octagons created for the muscle insertion landmarks.**
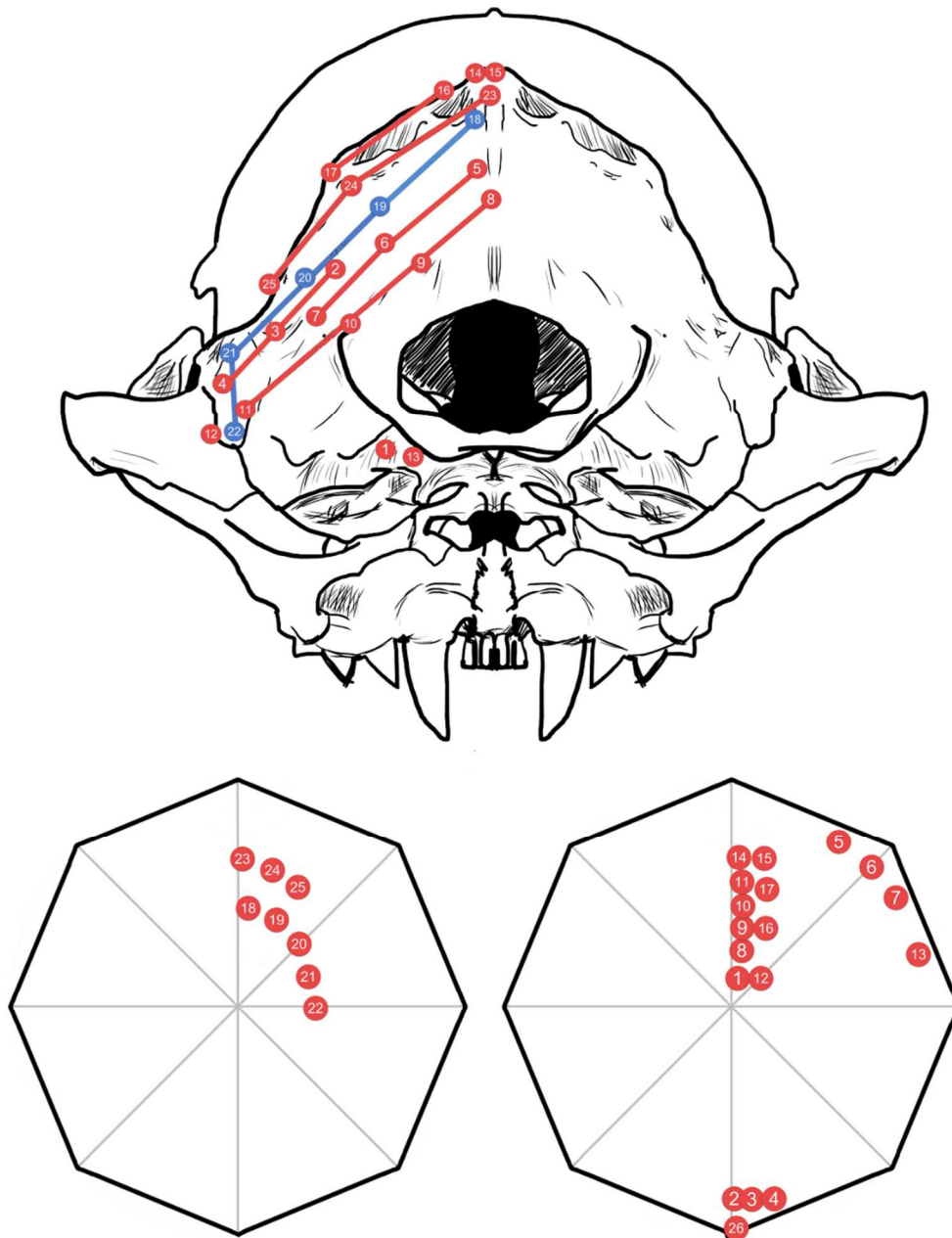
**Figure 4.10. Top: Posterior view of the cat cranium with landmark origin information. Bottom: Insertion landmarks for the neck muscles. Left octagon represents the attachments in the atlas and axis. Right octagon represents attachments in the remaining vertebrae, together with the clavicle and the scapula. See Table 4 for key to muscle insertion landmarks.**

## 4.8. Conclusions

The work described in this chapter is intended to provide a model for FE analyses of a series of biological structures usually neglected in other studies. Because it must fit a multipurpose research, it has become one of the most complete non-human FE models to date, as it comprises not only bone and dura mater, but also trabecular structures, the falx cerebri and the tentorium cerebelli, the turbinates, the nasal septum and the periodontal ligament. Concerning muscle action, it also includes muscle wrapping of the superior temporalis and simulates the support of the neck. The model will be complemented in the next chapter with a full set of biting regimes, intrinsic and extrinsic bites, both unilateral and bilateral. Despite its complexity, the *Felis silvestris catus* model also has certain limitations. Perhaps the more notorious one is the presence of a brain endocast instead of a true model of the brain, as it prevents the analysis of stresses in the brain as a consequence of variations in material properties of the falx cerebri and tentorium cerebelli. Another limitation in this sense is the absence of a layer of cerebrospinal fluid (CSF), which would also be necessary in the model before the effects in the brain could be taken into consideration.

In Chapter 5, the *Felis silvestris catus* model will be used to test the role of the dura mater and the dural folds during feeding activities. In Chapter 6, the model will serve to ponder the effects of the modelling of the periodontal ligament, the nasal septum and the turbinates.

# Chapter 5. An assessment of the role of the falx cerebri and tentorium cerebelli in carnivorans

The falx cerebri and the tentorium cerebelli are two projections of the dura mater in the cranial cavity which ossify to varying degrees in some mammalian species. The idea that ossification of these structures may be necessary to support the loads arising during feeding has been proposed and dismissed in the past, but never tested quantitatively. To address this, a biomechanical model of a domestic cat (*Felis silvestris catus*) skull was created and the material properties of the falx and tentorium were varied for a series of loading regimes incorporating the main masticatory and neck muscles during biting.

Under these loading conditions, ossification of the falx cerebri does not have a significant impact on the stress in the cranial bones. In the case of the tentorium, however, a localised increase in stress was observed in the parietal and temporal bones, including the tympanic bulla, when a non-ossified tentorium was modelled. These effects were consistent across the different analyses, irrespective of loading regime. The results suggest that ossification of the tentorium cerebelli may play a minor role during feeding activities by decreasing the stress in the back of the skull.

## 5.1. Introduction

The dura mater is a fibrous membrane that covers the brain and the spinal cord. It further extends into the cranial cavity in the shape of four folds of projections, two of which are the falx cerebri and the tentorium cerebelli. The falx cerebri divides the two cerebral hemispheres, while the tentorium separates the cerebral lobes from the underlying cerebellum (Figure 5.1). Both the falx and tentorium are commonly found across a variety

of mammal species, albeit not necessarily with the same degree of development (Klintworth, 1968). Moreover, some species exhibit an ossified falx or an ossified tentorium; occasionally both. Ossification can also be a prenatal or a postnatal process, and these differences in developmental patterns led Nojima (1988) to discriminate between the prenatal carnivore type (e.g. Marsupialia, Sirenia, Carnivora) and the postnatal dolphin type (some Cetacea and Primates). The degree of tentorial ossification also varies across species. In carnivorans, the level of ossification ranges from none in the striped skunk (*Mephitis mephitis*), to partial (Canidae), or complete, as in members of the Felidae (Nojima, 1990c).
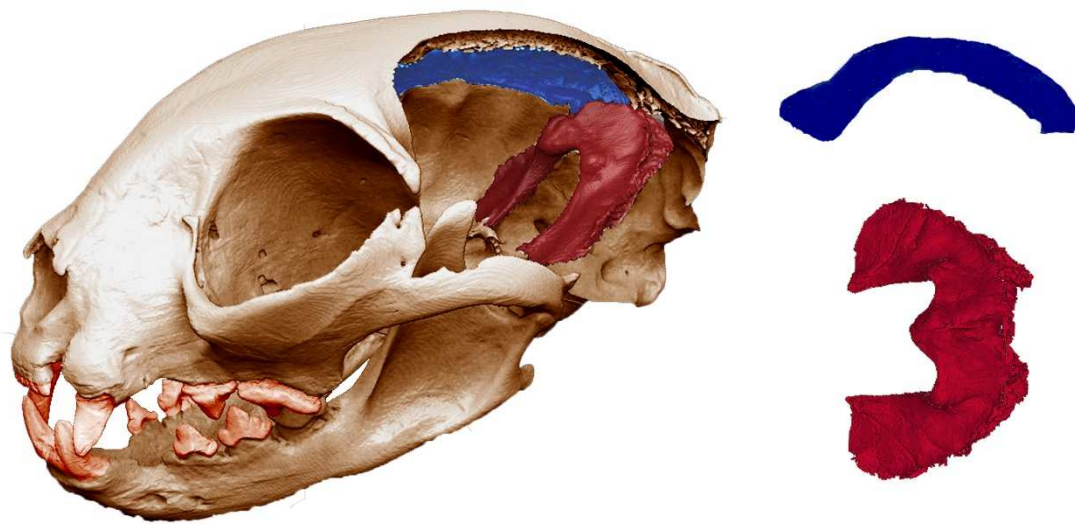


**Figure 5.1. Left: The skull used for the *in silico* model after performing a virtual parasagittal cut in the braincase to reveal the falx cerebri and the tentorium cerebelli (displayed in blue and red, respectively). Top right: Falx cerebri in medial-lateral view. Bottom right: Tentorium cerebelli in dorsal view.**

The functional role of the ossification of these structures remains unclear. The hypothesis that an ossified tentorium in carnivorans aids in the protection of the brain during locomotion and feeding has been dismissed in the past, largely based on evidence that other animal groups which perform similar activities, such as herbivores and rodents, do not exhibit ossification (Nojima, 1990c). However, this is founded on casual observation, and to date no specific analysis has been performed to support or reject it. In this study, we examine quantitatively the biomechanical role that the falx and the tentorium play in the mammalian skull, and any particular effects for Carnivora that the

ossification may offer under different biting regimes. In order to achieve this, we developed a detailed finite element (FE) model of a domestic cat (*Felis silvestris catus*) skull which included the falx and tentorium (the creation process is described in detail in Chapter 4).

The most widely accepted hypothesis is that Felidae are composed of two main lineages: the Machairodontinae, commonly known as sabretoothed cats, and the Felinae, or true cats (Turner and Anton, 1997; Christiansen, 2008). The first felid-like carnivore species appeared on the Oligocene Period, around 35 million years ago (Johnson *et al.*, 2006); however, all the living felid species, which are members of the Felinae subfamily, first appeared in the late Miocene. *Felis silvestris* is a polytypic species that includes various different subspecies which can produce viable offspring when crossed: *Felis silvestris lybica*, *Felis silvestris ornata*, and perhaps *Felis silvestris bieti*. The domestic household cat can be considered an additional subspecies, under the name *Felis silvestris catus* (Driscoll *et al.*, 2007).

Domestic cats have a shortened rostrum (even shorter when compared with other members of the same group), which provides an increased mechanical advantage and enhanced bite force generation, permitting them to kill prey more quickly (Kitchener *et al.*, 2010; Van Valkenburgh *et al.*, 2014). The patterns of masticatory cycles in cats will necessarily differ depending on food size and consistency, and the force exerted will vary across the mandible when the length of the out-force moment arm is reduced (for example, bite force at the canine tips in *Felis silvestris catus* is 73.3 N and 118.1 N at the carnassial eocone; data obtained from Christiansen and Wroe, 2007).

The use of this particular species has two main advantages: it is widely available for study and, being a felid, it has a fully ossified tentorium, in contrast to other carnivorans. Over the last 20 million years, felids have maintained a similar body plan (Kitchener *et al.*, 2010), a fact that has made this group especially popular for allometric studies (Slater and Van Valkenburgh, 2009). Following this general trend, the ossified tentorium of the domestic cat's skull is also very similar to those of other felids. In these species, such as in other carnivorans, the tentorium ossifies during fetal development (Nojima, 1988). In an adult *Felis silvestris catus*, the thickness of this structure ranges from 0.6 to 1.7 mm, the lateral wings being less thick than the midline and the margins (Siegel, 1974).

## 5.2. Methods

A solid model of the skull of a *Felis silvestris catus* was produced in Avizo. Then, a finite element model was generated and imported into ANSYS, together with muscle force data and orientation, and the dura mater and neck structures were recreated (see Chapter 4 for details).

### *5.2.1. Material properties*

Table 5.1 includes the complete list of material properties used. The model was assigned bone material properties taken from the cortical bone of domestic dogs (i.e. Young's modulus $E = 13.7$ GPa; $v = 0.30$), following Slater and Van Valkenburgh (2009) in which these values were applied to various felid species. To the best of our knowledge, there are no material property data for the cat's dura in the literature, but human values are well known and were selected as a reasonable approximation ($E = 31.5$ MPa; $v = 0.45$ (after Kleiven and Holst, 2002). The same applies to the periodontal ligament (PDL; $E = 50$ MPa; $v = 0.49$) which was taken from Rees and Jacobsen (1997). A value of 0.5 MPa was assigned to the remaining generic soft tissues (Huempfner-Hierl *et al.*, 2015), including the brain endocast, link elements and filling materials ($v = 0.45$). All material properties assigned to the different tissues were assumed to be isotropic, homogeneous, and linear elastic, as it has been demonstrated that models using these properties still produce reasonable estimates of the stress and strain distributions (Strait *et al.*, 2005; Bright and Rayfield, 2011). Although nonlinear modelling is desirable in FE analyses of biological systems, in general, linear models are preferred in studies of functional morphology (for a detailed explanation, see Section 9.4). Concerning the dura mater, a study by Kegel *et al.*, (2018) noted its strong nonlinearity advising that nonlinear solutions should be used even at low strain values. Also, Walsh *et al.* (2018) reported local anisotropy in the dura mater of pigs in the sagittal sinus and the parietal regions. Nevertheless, both Kegel *et al.* (2018) and Walsh *et al.* (2018) confirmed that bulk dura mater exhibit isotropic behaviour. Both these papers are concerned primarily with models for assessing traumatic brain injuries, where strains are usually orders of magnitude higher than in biting analyses, but nonetheless their conclusions should be taken into account when interpreting the results obtained in this study. Also, the current study focuses on a comparison of different versions of the same model by varying the material properties of

the structures of interest, so any potential minor inaccuracies in the material properties will not be critical as long as the property values are realistic and constant in both versions. Validation for the *Felis silvestris catus* model, although desirable, was not possible given the characteristics and limitations of the study. The specimens used had been preserved in a solution of formaldehyde (see Chapter 4), hence testing for material properties of the tissue would not give the accurate *in vivo* values. A great effort was put into obtaining a fresh specimen for subsequent analyses, but unfortunately after many false leads this proved to be unachievable. This is a typical limitation of many functional morphology type of studies (see Chapter 9 for a more detailed discussion). Nevertheless, because specific material property data for *Felis silvestris catus* were not available, sensitivity tests were undertaken for the soft tissues, to assess their impact on the results (see below). All these tests were performed for a bilateral canine bite.

| Material | Elastic Modulus (MPa) | Poisson Ratio | Taken from |
|---|---|---|---|
| Bone | 13,700 | 0.3 | Slater and Van Valkenburgh, 2009 (dogs) |
| Teeth | 13,700 | 0.3 | |
| Brain endocast | 0.5 | 0.45 | |
| Dura, falx, tentorium | 31.5 | 0.45 | Kleiven and Holst, 2002 (humans) |
| PDL | 50 | 0.49 | Rees and Jacobsen, 1997 (humans) |
| Link elements | 0.5 | 0.45 | |
| Generic soft tissue | 0.5 | 0.45 | Huempfner-Hierl *et al.,* 2015 (humans) |

**Table 5.1. Material properties for the cat model.**

### 5.2.2. Boundary conditions

The skull model was subjected to bilateral and unilateral canine and carnassial bites with different falx and tentorium material properties simulating either soft dural or hard osseous tissues in various combinations (see Table 5.2). All felids are hypercarnivores (Meachen-Samuels and Van Valkenburgh, 2009) relying almost exclusively on vertebrate prey. As a consequence of this dietary specialization, they also exhibit a reduced dentition, the most important teeth being the upper and lower carnassials, which

correspond to the maxillary fourth premolar and mandibular first molar. Biting and grasping are mostly done with the incisors and the canines, while the carnassials are used for cutting and tearing food after the killing, as they are strategically located close to the insertion of the masticatory muscles (Buckland-Wright, 1978; Orsini and Hennet, 1992; Reiter and Soltero-Rivera, 2014; Figure 5.2, right). The hinge articulation of the lower jaw is also in line with the intersection between the carnassials (Turner and Anton, 1997).

Given these varied behaviours it is important to run multiple biting simulations because the cranium will deform in different ways depending on factors such as loading position and force magnitudes (Curtis *et al.*, 2013). For the bilateral canine analyses, one node was constrained dorso-ventrally at the tip of each canine, with one node at the left glenoid fossa constrained in all degrees of freedom and the opposite node on the right side constrained in two directions (anterior-posteriorly and dorso-ventrally). These minimal constraints reduce the risk of artefacts from over-constraining the model (Dumont *et al.*, 2005, Grosse *et al.*, 2007). For the unilateral canine analyses, only the node at the tip of the left canine was constrained. For the carnassial analyses the same configuration at the glenoid fossae was maintained, but the anterior constraints were located at the notch between the paracone and the metacone of each carnassial (left carnassial in the case of the unilateral biting; Figure 5.2, left).
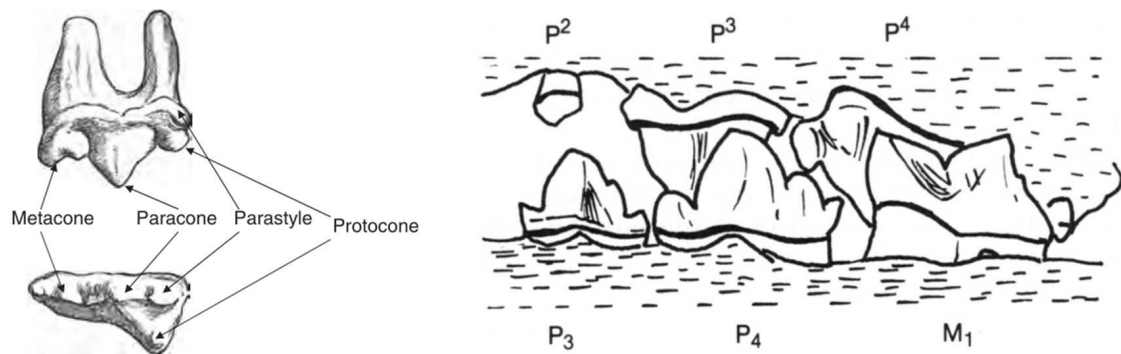


**Figure 5.2. Left: Carnassial tooth drawing of *Panthera tigris* (Kitchener *et al.*, 2010). Right: Representation of the scissor-like occlusion of the carnassials from a lingual view (Orsini and Hennet, 1992).**

Additionally, two extrinsic loading regimes were applied to the model, one to simulate a pullback movement, the other a lateral pull. Similar types of analyses have been performed in previous studies of felids (Wroe, 2008; Slater and Van Valkenburgh,

2009), but using different approaches. Here, the extrinsic loading conditions were applied in combination with biting by applying the muscle forces *and* reaction forces at the glenoid fossae and the canines for bilateral biting as predicted by the previous analyses. (In theory, these forces place the loaded skull in perfect equilibrium, however due to unavoidable rounding errors in the software, there will inevitably be some, albeit negligible, out-of-balance force). In addition, while the bite force loading was maintained, further loads were superimposed to simulate the pullback or lateral pull action, thereby replicating the loading of the skull *in vivo*. Two constraint conditions were applied; one with, and one without the neck. For the first model, without the neck, three locations on the posterior cranium were minimally constrained; two at the occipital condyles and the third located between them, over the foramen magnum. One node was constrained in all degrees of freedom, the second in only two directions (anterior-posteriorly and dorso-ventrally), while the third (over the foramen magnum) was constrained anterior-posteriorly only. In the second variation, when the neck was modelled, all nodes corresponding to the muscle insertion points were constrained in all degrees of freedom. For the pullback simulation, once a bite force loading and the constraint option had been specified, an arbitrary pullback force of 25 N was applied to the upper posterior area of each canine, directed in a posterior-anterior direction, and subjecting the skull to tensional forces. For the lateral pull, the same force was applied to the left lateral surface of the canines. Thus, the two loading analyses were carried out with and without the neck structure, and the differences compared. A schematic representation of the loads and constraints applied to the model can be seen in Figure 5.3.
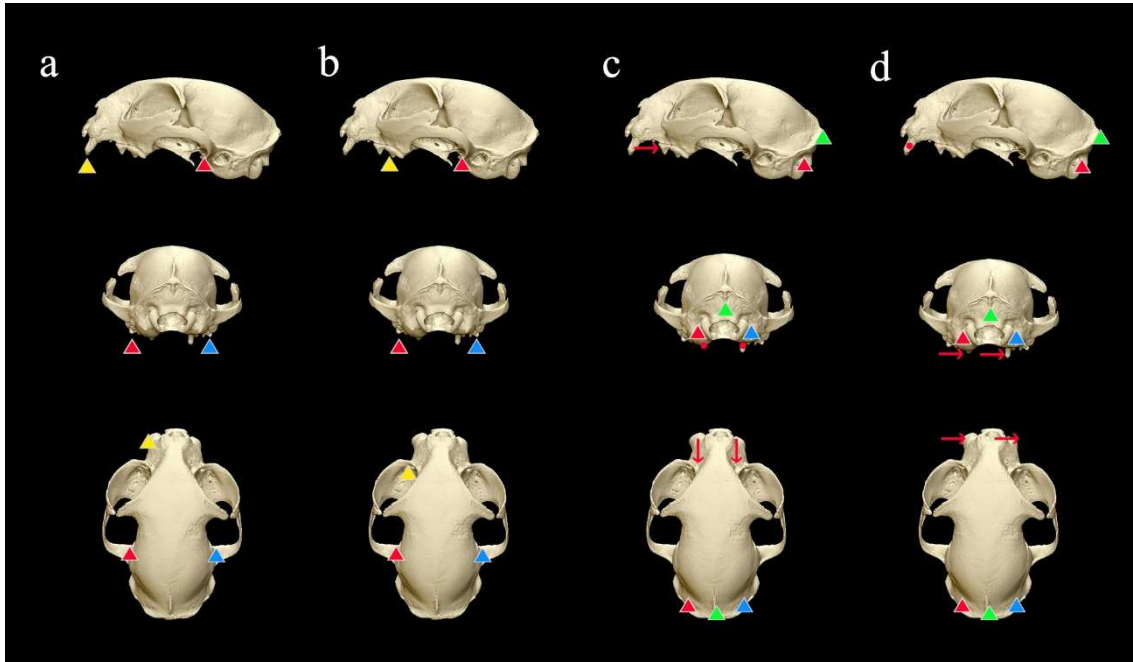
**Figure 5.3. Constraints and some of the loads applied to the *Felis silvestris catus* model in different biting regimes: (a) unilateral canine, (b) unilateral carnassial, (c) pullback biting (with no neck) and (d) lateral shake (with no neck). Bilateral canine and carnassial biting are identical to (a) and (b) but the constraints are applied to both teeth. Loads in the extrinsic regimes with the neck modelled are identical to (c) and (d), but constraints are not applied directly to the skull, but to the two hexagons described in the main text. Colour legend of the constraints is as follows: only dorso-ventrally (yellow); only anterior-posteriorly (green); anterior-posteriorly and dorso-ventrally (blue); in all degrees of freedom (red).**

| Loading regime (intrinsic) | HF/HT | HF/ST | SF/HT | SF/ST |
|---|---|---|---|---|
| Canine bilateral biting | ✓ | ✓ | ✓ | ✓ |
| Canine unilateral biting | ✓ | ✓ | ✓ | ✓ |
| Carnassial bilateral biting | ✓ | ✓ | ✓ | ✓ |
| Carnassial unilateral biting | ✓ | ✓ | ✓ | ✓ |
| **Loading regime (extrinsic)** | **HF/HT** | **HF/ST** | **SF/HT** | **SF/ST** |
| Pullback biting (no neck) | | | ✓ | ✓ |
| Pullback biting (neck) | | | ✓ | ✓ |
| Lateral shake (no neck) | | | ✓ | ✓ |
| Lateral shake (neck) | | | ✓ | ✓ |

**Table 5.2. List of intrinsic and extrinsic analyses performed with corresponding variations in material properties (HF: hard/osseous falx; HT: hard/osseous tentorium; SF: soft falx; ST: soft tentorium).**

The value used for the force of the extrinsic analyses (25 N applied on each canine, hence a total of 50 N) has to be regarded as an approximation because, as far as we know, there is no data on what this force could be in this *Felis* species. The much larger value of 298 N used in Slater and van Valkenburgh (2009) was based on a previous study with a dingo. In their analyses, they used the same value for their three models so that "force to surface area ratios were held constant among models within each set of extrinsic load cases, allowing comparison of relative performance among the three taxa". If an adult Dingo weights about 16 kg (Behrendorff *et al*., 2016), a similar force applied to a medium sized cat of 3 kg (e.g. see Moseby and Read, 2006 or Hall and MacGregor, 1937) would be approximately 56 N, which is close to the 50 N value we used. The cat specimen scanned was also probably smaller than average, since the second specimen we dissected was 2.5 times larger; but only the head was preserved, so the actual weight is unknown. However, for a mass of 2.5 kg, the pullback force would be approximately twice the cat's body weight. In relation to the bite force, a pullback force of 50 N is approximately half of 101.1 N predicted by the model for a bilateral canine biting. Thus, although we don't have an *in vivo* pull back force, a value of 50 N seems reasonable in relation to these other parameters.

As stated above, the total maximum bite force predicted by the model, measured at the tip of the canines for a canine bilateral bite, was 101.1 N, while the unilateral carnassial bite force was predicted to be 175.8 N. By using a modified version of the dry skull method (Thomason, 1991), Sakamoto *et al.* (2009) estimated a canine bite force of 177 N based on the skull width of fourteen specimens of *Felis silvestris catus* (median skull width, 62 mm; the skull width of our model is 75 mm, measured across the zygomatic arches, following Sakamoto and Ruta, 2012). In contrast, using the same dry skull method, Christiansen and Wroe (2007, skull width not provided) reported a lower value of 73.3 N.

Performance of the skulls was evaluated by considering von Mises stress because this measure has been employed previously to assess skull behaviour (including earlier research in felid cranial biomechanics, such as McHenry *et al.* (2007), Wroe (2008) and Slater and Van Valkenburgh, (2009)). Von Mises stress is also convenient because it is a scalar function combining the three principal stresses, is related to the von Mises failure criterion, and is useful for comparing the performance of complex 3D geometries.

Due to the large number of comparative analyses performed in this study, difference plots are used to present the results in an easy and concise manner, and in such a way that even small differences in stress values become immediately evident (Figure 5.4), as has been used in previous research (McCormack *et al*., 2017). For the difference plots, the following convention is used for all the results: the minuend of the subtraction is always the model with the osseous material properties while the subtrahend is the model with the soft tissue material properties. Thus negative values (cold colours) represent areas in which stress is lower in the osseous model, and positive values (warm colours) are areas in which stress is higher in the osseous model, and areas with no significant stress differences are centred around green. More even stress distributions and lower stress values represent a structure more adapted to withstand stresses under a particular loading regime (Slater and Van Valkenburgh. 2009).
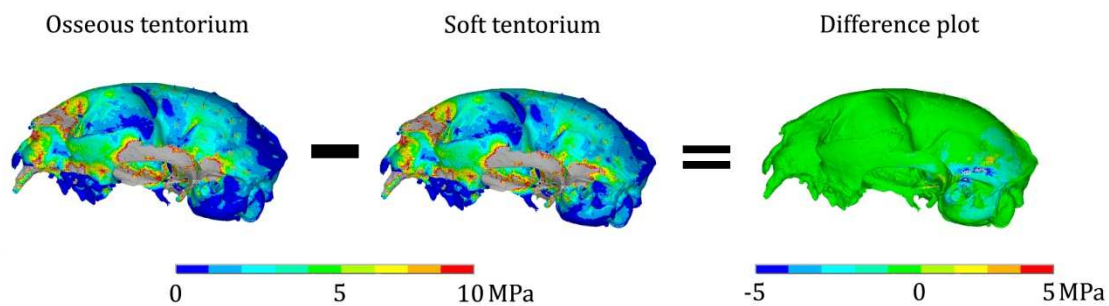


**Figure 5.4. Explanation of how the difference plots in this study were generated. The von Mises stress values predicted by the model with the soft tentorium are subtracted from those of the model with the osseous tentorium to create a difference plot. In the difference plots, cold colours represent areas in which stress in the model with the osseous tentorium is lower and vice versa with the warmer colours.**

### 5.2.3. Sensitivity tests

Since specific material property data for *Felis silvestris catus* were not available for the analyses, comprehensive sensitivity tests were undertaken to assess the likely accuracy of the results (see Table 5.3). All these tests were performed for a bilateral canine bite. Dura mater thickness of 0.55 mm was taken from Cotton *et al.* (2016) for humans, but further sensitivity tests with homogeneous thickness values of 0.2 mm and 1.5 mm were also undertaken. Considering the dura mater elastic modulus (standard value 31.5 MPa

for humans; value taken from Kleiven and Holst, 2002), we also ran analyses for 3 MPa and 300 MPa, and for the generic soft tissue (0.5 MPa, taken from Huempfner-Hierl *et al.,* 2015) which were also varied within a reasonable range: 5 MPa, 50 MPa and 500 MPa. All these values were tested independently.

| Sensitivity test | Values tested | Standard value used |
|---|---|---|
| Young's Modulus (MPa) of dura mater | 3, 31.5, 300 | 31.5 MPa [1] |
| Thickness (mm) of dura mater | 0.2, 0.55, 1.5 | 0.55 mm [2] |
| Young's modulus (MPa) of other soft tissues | 0.5, 5, 50, 500 | 0.5 MPa [3] |

**Table 5.3. Sensitivity test values for the dura mater and other soft tissues (which also include the filling materials and the link elements). [1] Kleiven and Holst, 2002, [2] Cotton *et al.*, 2016, [3] Huempfner-Hierl *et al.*, 2015.**

The preliminary sensitivity tests demonstrated that neither the stress magnitude nor distribution were significantly affected by the variations considered. As a result, detailed stress plots are not presented here, and the following summarizes the outcome of those investigations. Changes in dura mater thickness did not lead to any discernable differences in the stress pattern and magnitude in the bone. Similarly, no meaningful differences were noticed between dura mater elastic modulus values of 3 MPa and 30 MPa, but there was a slight decrease in stress in the skull roof area for a value of 300 MPa, as would be expected. The sensitivity tests also demonstrated that using the higher elastic modulus value for the (soft tissue) cavity filling materials resulted in lower stresses across the skull, but the changes were negligible between the range of 0.5 MPa and 50 MPa.

A discussion about the biomechanical role of the periodontal ligament is covered separately in Chapter 6.

Sensitivity tests were also carried out to assess the importance of wrapping the superficial temporalis to better reflect the way the muscle covers and loads the cranial vault. Previous studies (Grosse *et al.*, 2007; Curtis *et al.*, 2008; Liu *et al.*, 2012) have demonstrated that applying muscle wrapping in the temporalis muscle for bats and macaques respectively reduces peak stresses slightly, but the basic distribution of stress

patterns remains unaltered. These studies assumed a uniform distribution of the muscle strands, as did the cat model, with the muscle force divided equally between the strands in the three cases. Liu *et al.* (2012) did however note that, despite the fact that this may not alter the results significantly, other studies have shown that higher loads are located in the anterior fibres of the muscle.

In the current analysis, imperceptible variations in stress distribution were observed through the model (Figure 5.5), (ignoring local artefacts caused by the attachment of the muscle "hairs" of each wrapping strand). During bilateral canine biting, changes in bite force between the models with and without muscle wrapping, as measured at the tip of both canines, were also negligible (< 1 N). Increasing the number of muscle strands would have distributed the loading more evenly over the bone, but it seems highly unlikely that it would have changed the overall conclusion of this test, as the direction of the resultant force would not change.
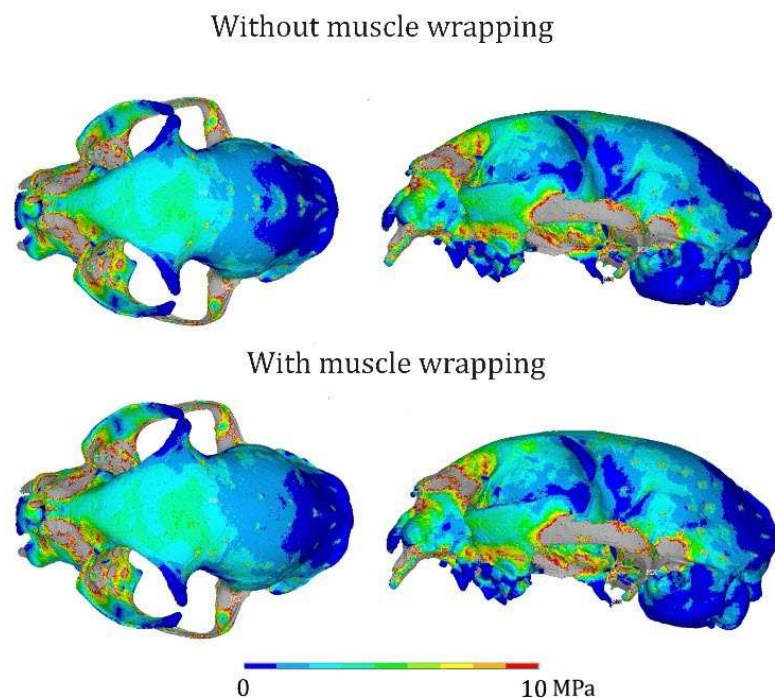


**Figure 5.5. The *Felis silvestris catus* model before and after application of muscle wrapping of the superficial temporalis.**

## 5.3. Results

After the sensitivity tests, the model was subjected to a series of intrinsic and extrinsic loading regimes in which canine and carnassial biting were simulated. Considering the models with a soft falx and an ossified tentorium first (*i.e.* the natural condition in *Felis silvestris catus*), for bilateral canine biting the simulation stresses were equally high in the rostrum, the zygomatic arches and the palatine and presphenoid bones (Appendix 3. Additional contour plots for *Felis silvestris catus*, Figure A1, left columns). In the rostrum, the nasal bones experience lower stresses than the surrounding bones, with the stress transmitted through the maxilla and into the frontal bone, until it reaches the approximate location of the coronal suture, where it dissipates. Regions of low or no stress can be identified within the parietal and interparietal bones, the tympanic bullae and the postorbital processes. In the carnassial bilateral biting simulation, stress in the rostrum and the palatine were greatly reduced but remained constant in the zygomatic arches, and seemed to be slightly higher throughout the orbit and in certain areas of the zygomatic bone. With unilateral biting, either with canine or carnassial teeth, stresses were higher on the working side both in the rostrum and the cranial roof (Appendix 3. Additional contour plots for *Felis silvestris catus*, Figure A1, right columns). It is also worth noting that the stress at the back of the skull remains invariant for all these loading regimes. In the case of the extrinsic loads with an ossified tentorium, the pullback loading regime seemed to most closely replicate the simple bilateral bite (Appendix 3. Additional contour plots for *Felis silvestris catus*, Figure A2). For the lateral pull, higher stresses manifested in the skull roof of the side opposite to the applied force. The largest differences between the two sides seemed to be located in the frontal bone and postorbital processes. Slight variations of stress magnitude were detected with the inclusion of the neck muscles in the analyses for both cases, but there were no meaningful differences in stress distribution.

When models with ossified structures are compared to those with soft structures, differences in stress distribution and magnitude in cranial bone are also uncommon, regardless of the biting regime. Changes in the material properties of the falx cerebri do not lead to any discernible variations in the external skull stress patterns. However, difference plots demonstrate that the models with an ossified tentorium consistently exhibit lower stress values in the parietal and temporal bones, including the tympanic bulla (Figure 5.6 and Figure 5.7), with slight or minor differences depending on the particular regime. To provide further detail about the differences, 40 nodes at three sample

locations of approximately 0.5 mm diameter were probed (Figure 5.8) for both ossified and non-ossified tentorium models during a bilateral canine biting regime. The greatest decrease in stress was 2.11 MPa at the inferior region of the temporal bone. Also, locally high stresses are observed in the interparietal and the sagittal crest for the lateral pull plus biting regime with no neck. These appear to be a consequence of the oversimplified constraints applied, causing the load path to be focussed through those regions, because the equivalent version with neck muscles does not display them, and therefore they probably don't have mechanical significance. It is worth noting that stresses in the rostrum and the anterior area of the skull roof remained unaltered for all cases tested.
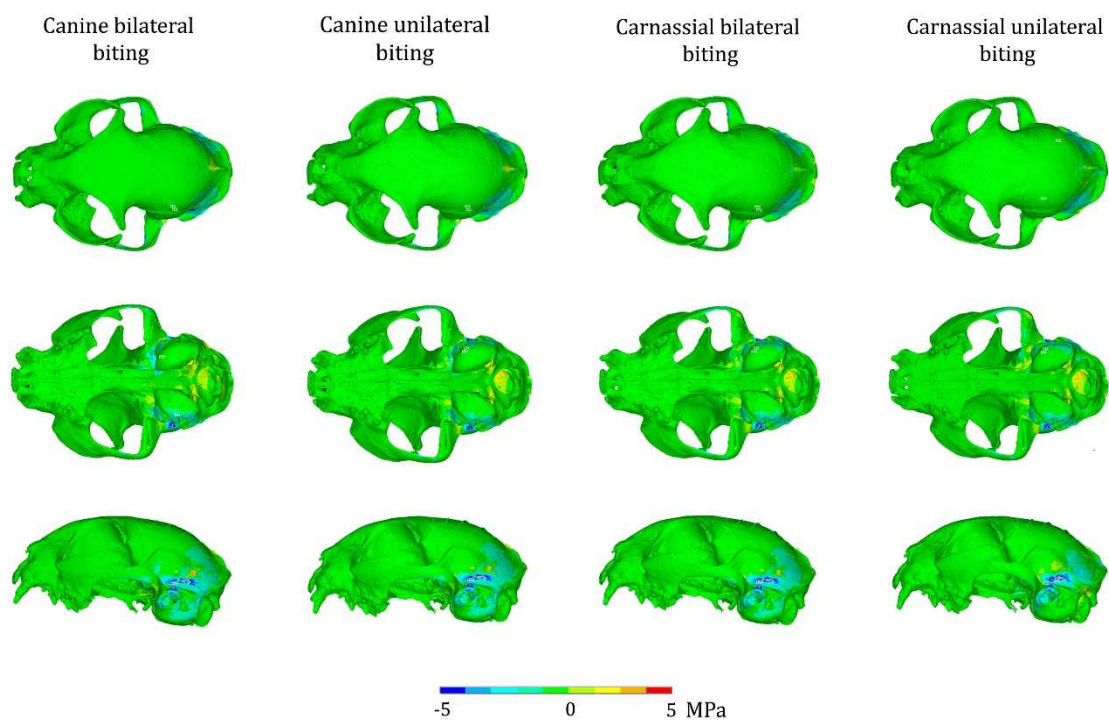


**Figure 5.6. Von Mises stress difference plots for the (intrinsic) biting analyses, comparing osseous and soft tentorium models.**
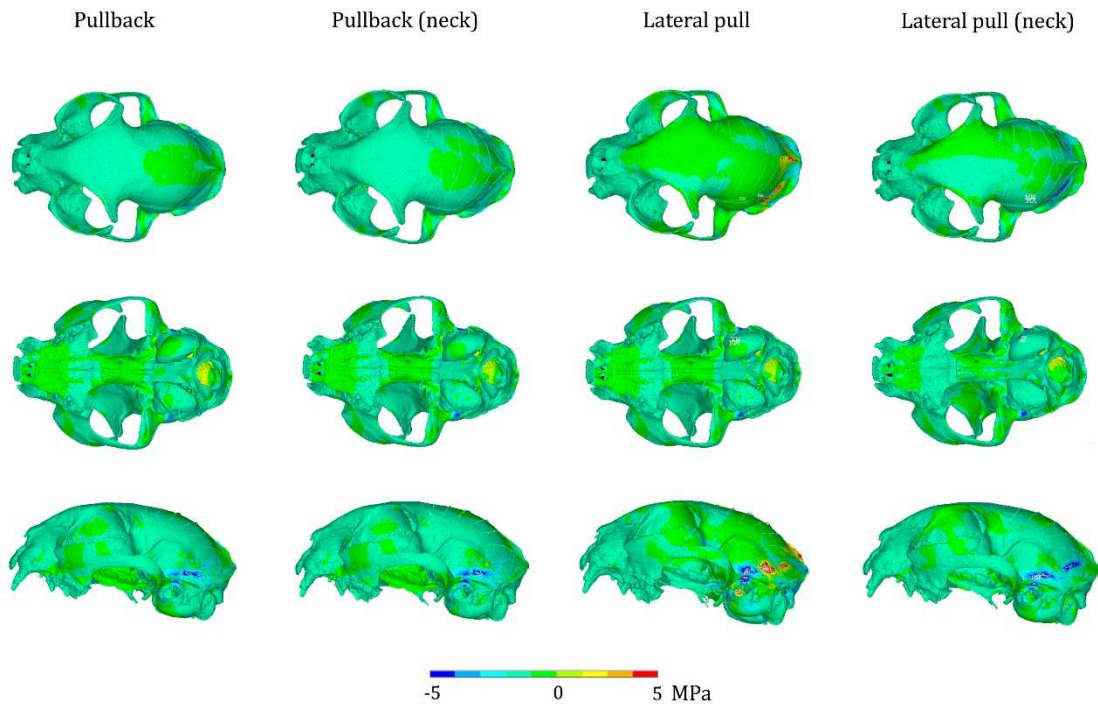
**Figure 5.7. Von Mises stress difference plots for extrinsic analyses (biting plus pulling/tearing loads) comparing osseous and soft tentorium models for models with and without neck muscles.**
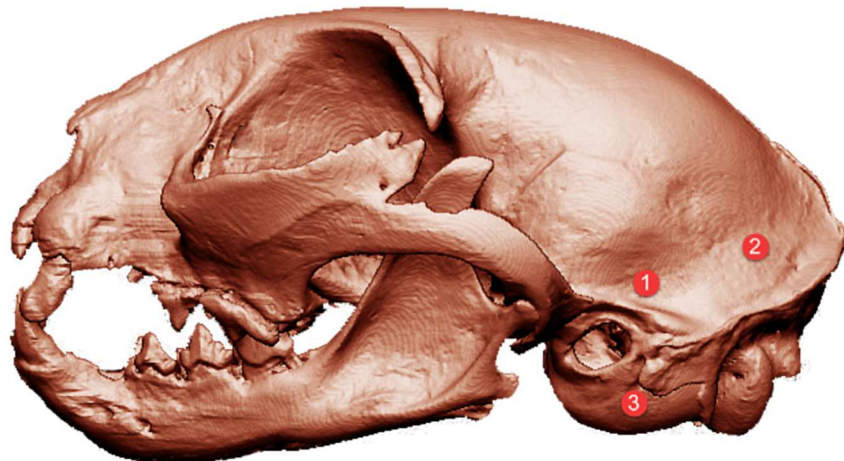


**Figure 5.8. Location of the regions where values of von Mises stress were probed for a bilateral canine biting regime with both osseous and soft tentorium. In each region, the difference values of 40 individual nodes were calculated and then averaged. The decrease in stress in the ossified tentorium model was as follows: Region 1 = 2.11 MPa; Region 2 = 1.13 MPa; Region 3 = 0.11 MPa. The diameter of each region probed was approximately 0.5 mm.**

Examination of the stresses in the tentorium of both ossified and non-ossified versions (Figure 5.9 and Appendix 3. Additional contour plots for *Felis silvestris catus*, Figure A3; note the different scales of the contour plots) shows that higher stresses are located anteriorly, with peak stress values in the area in contact with the parietal wall, and lower values in the borders of the tentorial notch. Apart from these differences in magnitude, the actual stress distribution remains unchanged for the different material properties and biting regimes. In the falx cerebri (Figure 5.10), the stress is more unevenly distributed, but appears to be higher at the anterior third (especially in the soft falx cerebri) and the posterior end, particularly in the osseous falx for all regimes except the carnassial unilateral biting, and in the soft falx for both canine bites. The stresses in the osseous falx and tentorium are to varying degrees of magnitude higher than those in the versions with soft tissue material properties, but in the extrinsic biting regimes (Appendix 3. Additional contour plots for *Felis silvestris catus*, Figure A4) the soft falx seems to experience higher stresses overall. Moreover, adding or removing the dura mater layer over the brain endocast surface does not seem to have any effects on the results. In general, the cranial vault of the cat skull does not experience meaningful amounts of tension or compression (Appendix 3. Additional contour plots for *Felis silvestris catus*, Figure A5), but the area of the temporal bone where the tentorium is located is subjected to compressive stresses. Compression is also visible in the tentorium cerebelli wings and in the posterior end of the midline, at the attachment of the falx cerebri.
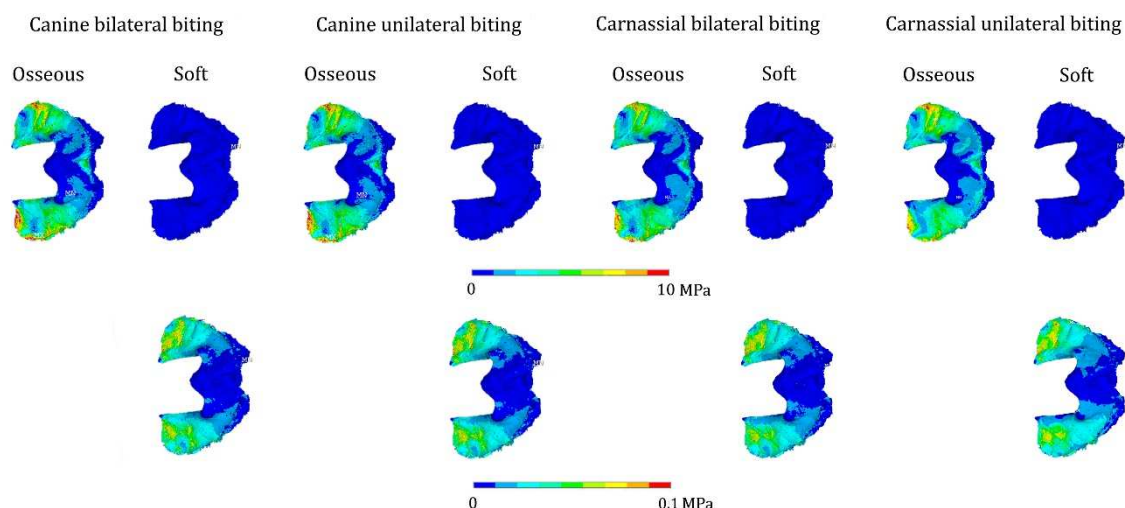


**Figure 5.9. von Mises stress plots for the tentorium cerebelli. Top row: Osseous and soft tentorium in dorsal view for all intrinsic regimes. Bottom row: Soft tentorium**

**for the same loading regimes as the top row, but with adjusted contour levels to reveal the stress patterns.**
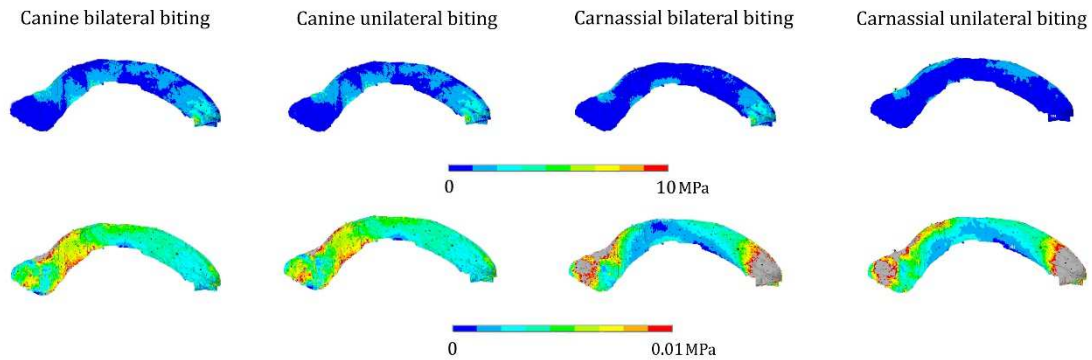


**Figure 5.10. von Mises stress plots for the falx cerebri. Top row: osseous falx cerebri in medial-lateral view for all intrinsic regimes. Bottom row: soft falx cerebri for the same analyses, but with adjusted contour levels to reveal the stress patterns.**

## 5.4. Discussion

The aim of this research was to test whether the presence of the osseous falx or tentorium played a significant role in reducing stress in the cranial bones under different biting regimes in *Felis silvestris catus*. It was observed that changing their material properties did lead to a considerable reduction of stress in the originally softer structures (Figure 5.9 and Figure 5.10, and Appendix 3. Additional contour plots for *Felis silvestris catus*, Figure A3 Figure A4) but we did not observe the same effect in the cranial bone when considering the model as a whole.

In the case of the falx cerebri, the alteration of its material properties did not lead to any changes in the von Mises stress pattern of the cranium. According to the CT scans, the patches of ossification in the falx of the original specimen are located primarily in the middle to posterior regions of the structure (in the case of the non-scanned specimen, ossification nodules appear in the middle section; see Figure 4.2). Thus there does not seem to be any correlation between their location and the predicted stress pattern from the FE analyses (Figure 5.10 and Appendix 3. Additional contour plots for *Felis silvestris*

123

*catus*, Figure A4) and, in any case, it seems unlikely that these isolated nodules have any mechanical significance, since they appear disconnected from the cranial roof. For the tentorium cerebelli, the stress is concentrated at the end of both "wings" of the structure (Figure 5.9 and Appendix 3. Additional contour plots for *Felis silvestris catus*, Figure A3).

Stress differences between models with ossified and non-ossified tentoria were limited to the back of the skull, and specifically to the bones adjacent to the tentorium (parietal and temporal, including the tympanic bulla), and perhaps indicates that the tentorium may play a minor role during feeding. The difference in stress magnitude is however small (see Figure 5.8) and therefore these results should be treated with caution. A more detailed model is necessary to assess the specific effects that this reduction in stress may pose on the brain. The area of interest at the back of the skull initially suggested a link between the neck muscles, as they are primarily attached to this region, but the extrinsic analyses that incorporated the neck did not reveal any meaningful differences. A recent study by McIntosh and Cox (2016) demonstrates that, for mole-rats, a progressive increase in gape leads to a decrease in stress in the anterior regions of the cranium and an increase posteriorly. As felids are known to exhibit high values of maximum gape (61.3° in *Felis chaus* (Christiansen and Adolfssen, 2005), a closely related species to *Felis silvestris catus*), it is possible that analyses with higher gape angles may reveal a more significant role for an ossified tentorium.

The use of simple linear elastic properties for the falx and the tentorium is one of the limitations of the current analysis. In particular for this study, the non-ossified materials are assumed to resist loads equally in both tension and compression, whereas in reality they will be much stiffer in tension. As a result, the model may overestimate their influence. Since the stiffness of these structures is orders of magnitude less than that of bone and their thicknesses are much smaller, their effect will be minimal, as demonstrated by the sensitivity studies. We believe therefore that this simplification does not alter the overall conclusions of the study. Also, the recent study by Kegel *et al.* (2018) observed that the dura mater behaves nonlinearly even at low strain values, hence the inclusion of nonlinearity in future studies of soft dural folds would be advisable. This would not affect the results of the present work however, because the bulk dura mater covering the brain in the case of *Felis silvestris catus* was proved to have a negligible influence on general cranial stress patterns, but it would presumably be important when considering the study

of the soft dural folds themselves. Walsh *et al.* (2018) refers to local variations in stiffness for the dura mater covering the brain, and these variations would also affect the dural folds, and potentially alter the patterns of stress represented in figures 5.9 and 5.10 (and the corresponding figures in Appendix 3) but, as there are no data available concerning regional differences in isotropy/anisotropy in the dural folds in felid species to date (properties of the dura mater are not only related with age, but also varied among different species; Kegel *et al.*, 2018), this point cannot be investigated further. Moreover, for a full ossified tentorium cerebelli, as is the case of *Felis silvestris catus*, the assignment of material properties for a soft tentorium can only be based on assumptions.

Of the four different intrinsic biting regimes considered (Appendix 3. Additional contour plots for *Felis silvestris catus*, Figure A1), the unilateral carnassial bite generates the highest peak stresses, being particularly high in the orbital region (although see Chapter 7 for the scaling of the muscle force of models and an explanation of the triangle of support). From simple lever mechanics, it is evident that carnassial bites will generate higher forces than canine ones (for example, 118.1 N *vs.* 73.3 N, as calculated by Christiansen and Wroe (2007); 180.6 N *vs.* 101.1 N in our model for the bilateral carnassial bite). The results from this study show that the most efficient biting regime in *Felis silvestris catus* is the carnassial bilateral bite, as this is the one that generates the highest bite forces while experiencing the lowest overall stresses and the lowest peak stresses. In nature, biting and grasping are mostly carried out with the incisors and canines, while the carnassials are used for cutting and tearing food (Buckland-Wright, 1978; Orsini and Hennet, 1992; Reiter and Soltero-Rivera, 2014). However, according to Orsini and Hennet (1992), the upper jaw is larger than the lower in cats and therefore, for the teeth of both sides to be joined during mastication, the mandible has to be brought to one side, so it is highly doubtful that this type of carnassial bilateral bite will ever be used in nature. Force variation between bilateral and unilateral carnassial bites (180.6 N *vs.* 175.8 N) seems to be, in any case, negligible.

The skull shape of felids is rather conservative (Sicuro and Oliveira, 2011; Chamoli and Wroe, 2011). Some researchers have developed FE models of extinct sabre-toothed cats and other felids (McHenry *et al.*, 2007; Wroe, 2008; Slater and Van Valkenburgh, 2009; Chamoli and Wroe, 2011) where biting regimes were based upon the cat's masticatory cycles and hunting behaviour. These studies demonstrated that felid skulls also exhibit similar stress patterns when biting, and that stress is largely confined

to the rostrum, the mandible and the zygomatic arch region. Our results follow a similar trend and replicate the ones obtained by Slater and Van Valkenburgh (2009; see Figure 5.11) from the cranium of *Felis lybica*, a closely related species, and also largely agree with the classic experimental study of a *Felis silvestris catus* cranium performed by Buckland-Wright (1978).
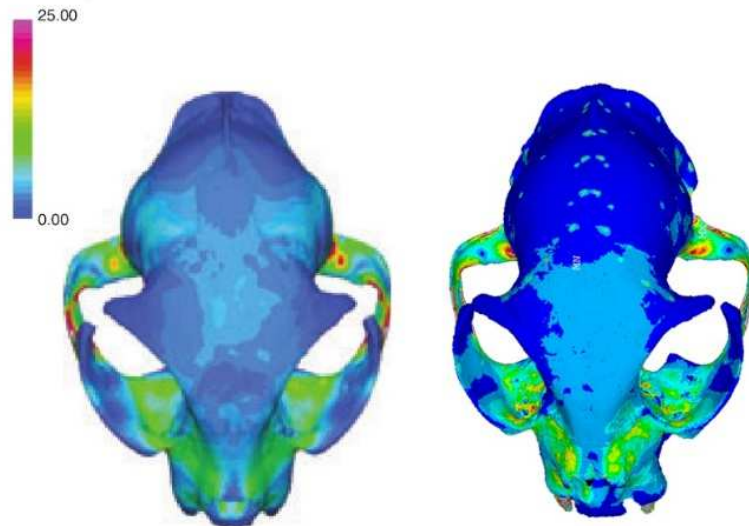


**Figure 5.11. von Mises stress analyses for a bilateral canine biting comparison. Left, *Felis silvestris lybica* (African wildcat). Right, *Felis silvestris catus* (Domestic cat). Left image from Slater and Van Valkenburgh (2009).**

According to the literature, the most probable function for the tentorium cerebelli is to withstand the weight of the cerebral hemispheres (Bull, 1969; and see references in Jeffery, 2002), given that it is present in birds and mammals, and that both groups are characterised by a more developed brain than other tetrapods. Even when closely comparing different mammal species (see Klintworth, 1968, table 1 for the tentorial indices; reproduced in Chapter 2, Table 2.2 in this thesis), it seems reasonable to infer a relationship between tentorium development and encephalization quotient (Jerison, 1973), using values of tentorial index as indicators (the tentorium is considered to be more developed as the length of the straight sinus increases). The lower values are consistently present in orders with low brain quotients, such as Rodentia, Lagomorpha and Chiroptera, and increase in Carnivora, Cetacea and Primates (Boddy *et al.*, 2012). The function of the falx cerebri may be to constrain the brain and limit displacement and rotation inside the

cranium (Kumaresan and Radhakrishnan, 1996; Snell, 2010). However, the presence of a bony falx and tentorium defies a simple explanation. The degree of ossification varies among different species and groups and it can develop before or after birth (Klintworth, 1968; Nojima, 1990a). In carnivorans, an ossified tentorium cerebelli is present in almost all species, with the exception of *Mephitis*. It is more developed in Felidae, Viverridae and Hyaenidae, where the structure is fully ossified and crosses the petrosa, than in other groups such as Phocidae or Canidae, where ossification does not reach the base of the skull (Nojima, 1990c). An ossified falx is present in all pinnipeds, but also in the genus *Ursus* (Nojima, 1990c). Sometimes the condition manifests in species that normally exhibit a soft-tissue falx and tentorium: for example, partial falx ossification is relatively frequent in humans (around 10% of the adult population (Tanaka and Takeuchi, 1974; Debnath *et al.*, 2009)) and tentorium ossification, while rarer, also exists (Tanaka and Takeuchi, 1974; Tubbs *et al.*, 2012).

In the analyses presented, all intrinsic and extrinsic biting regimes consistently resulted in the same pattern of stress across the cranium, which suggests that the function of the dural ossifications is not related to the forces exerted by struggling prey or in the action of pulling or tearing a carcass. However, feral *Felis silvestris catus* mostly feed on small prey such as birds, mice and even some invertebrates (Bradshaw, 2006), therefore similar tests should be run on larger predatory felids before completely ruling out a protective role for the dural ossifications during prey handling and feeding. This is especially important given the fact that small felids have proportionally larger braincases (Christiansen, 2008) and that may have a meaningful effect on the results. A new model with a more detailed brain would also help to resolve whether the stress reductions observed in the back of the skull lead to a corresponding decrease in the stress of the brain. Equally, it is important to note that the skulls of carnivorans in general, and felids in particular, are subjected to forces other than those associated with feeding, such as the ones resulting from acceleration or deceleration. In the past, various functional hypotheses have been proposed for the ossified falx and tentorium in carnivorans, notably that they serve as an extra protection for the brain to avoid injuries during locomotion (particularly relevant in the case of felids) or during mastication (Nojima, 1990c). Nojima's argument to dismiss this is based on the fact that most carnivorans manifest ossification but most herbivores do not, despite displaying a wide range of different speeds and behaviours. This still remains a strong case, but perhaps future research should

focus on these and other alternative loading situations in order to address the role of the osseous falx and tentorium.


## 5.5. Conclusions

Under the loading conditions tested, it can be concluded that ossification of the falx cerebri does not have a meaningful impact in the bones of the cranium, but the non-ossified tentorium results in a localised stress increase in the parietal and temporal bones, including the tympanic bulla. The increase was consistent in all the analyses performed, either intrinsic or extrinsic. These results suggest that ossification of the tentorium cerebelli may play a minor role during feeding activities by decreasing the stress in the back of the skull. However, models with different topographies and behaviours, and particularly those specifically designed to test the effects on the brain, must be developed in the future to further assess the hypothesis that tentorial ossification in mammals – or, at least, in Carnivora – has a meaningful mechanical role during feeding.

From this study, however, it can also be concluded that the inclusion of certain structures in the skull ignored in most biomechanical analyses (as it is the case of the falx cerebri and the tentorium cerebelli) may have a previously unperceived effect in other regions of the model. This idea will be explored further and becomes the main focus of the following chapter.

# Chapter 6. Additional structures in the *Felis silvestris catus* cranium: the role of the PDL, the nasal turbinates and the nasal septum in cranial biomechanics studies.

This chapter presents other analyses performed with the *Felis silvestris catus* skull model, which include the periodontal ligament, the nasal turbinates and the osseous part of the nasal septum. The aim of this work is to test the impact of including small or secondary anatomical structures usually neglected in most finite element analyses studies. The results show small variations in stress levels in the lower part of the rostrum (specifically in the alveolar region) and the palatine bone after removing or modifying the PDL elastic properties. The removal of the nasal turbinates and the osseous nasal septum have a more extensive effect on the skull, producing an increase of stress in the palatine foramens and surrounding regions, in the maxilla and also in the temporal bone. Modelling of these structures therefore has an impact on the magnitude of the results, although they do not significantly alter the stress patterns observed in the skull.

## 6.1. Introduction

A model is a simplified representation of reality, and finite element models when applied in fields such as Biology, Medicine, Biomedical Engineering and Palaeontology, frequently include simplifications of the biological structures that they intend to replicate. Simplification in itself may not be a problem, but an oversimplification may lead to unexpectedly inaccurate results. Because of this, many researchers perform both validation studies (which in most cases are difficult to execute for a variety of reasons, including cost, availability and so-forth), sensitivity tests and convergence tests (although the latter have become less relevant in recent times, as the increase of computing power has allowed researchers to easily create meshes with several million elements). It is also known that cranial soft tissues can play a key role in the function of the skull, for example by facilitating kinesis (Rayfield, 2007); this has been demonstrated in the case of patent sutures in bony structures (i.e. not fused but still connected by soft tissue), which can work together to redistribute strain (Curtis *et al.*, 2013).

Nonetheless, most cranial FE studies still focus only on the major bone elements and neglect the small osseous structures or biological tissues other than bone, which may also influence the biomechanics of the cranium. There are obvious reasons for this: firstly, the already time-consuming process of FE model creation greatly increases hand-in-hand with its complexity. For example, the turbinates are ignored in most FE studies due to their inherent complexity and the difficulties in obtaining accurate geometry in the final model (e.g. Dumont *et al.*, 2011; Dzialo *et al.*, 2013). However, the potential importance of modelling the inner sinus and the nasal walls in finite element analyses in a *Homo sapiens* skull was demonstrated by Toro-Ibacache *et al.* (2016), where the model with these structures more closely fitted *in vitro* data. Secondly, the cost of the technology necessary to perform these analyses may be prohibitive in some studies – although the advances in computing power referred above have greatly reduced the time and cost in recent years. And, thirdly, it is frequently difficult to ascertain the material properties of these structures, since most biological tissues are nonlinear and often anisotropic (Humphrey, 2003; Einstein *et al.*, 2003).

In this study the biomechanical role of some of the structures that are frequently absent from cranial FE models is assesed, and in particular the effects of models with and without the structure of interest on the von Mises stress distribution. The following sections provide a brief overview of the structures analysed, together with an account of some previous studies that have considered them either as part of some experimental work or with FE analyses, and the conclusions reached.

### *6.1.1. The periodontal ligament*

The periodontal ligament (or PDL) connects the roots of teeth with the alveolar socket and serves as a way to redistribute loads produced during mastication into the alveolar processes (Poiate *et al.*, 2009). As a result of its anisotropy and heterogeneity, to accurately estimate the mechanical properties of the PDL has proved to be a very complex task for researchers. Different studies have proposed Young's modulus values that span from 0.01 to 1750 MPa and from 0.28 to 0.49 for Poisson's ratio (Fill *et al.*, 2011). This variability in the literature, which not only occurs in humans, appears to be a factor of different parameters, such as geometry, type of loading, area of the PDL selected etc. (Rees, 2001; Fill *et al.*, 2011). In fact, it has even been argued that the periodontal

ligament of each individual tooth possesses its own particular biomechanical properties (Fill *et al.*, 2011).

Previous research has analysed the mechanical role that the modelling of the PDL may play in the osseous structures that support the teeth in more generalist head biomechanical analyses. A study which focused on the cranium of a brown capuchin (*Cebus apella*) confirmed that the effect of the PDL was localised in the alveolar bone that surrounds the teeth and that it did not extend to other areas of the structure, therefore not affecting the integrity of the skull (Wood *et al.* 2011). On the other hand, Gröning *et al.* (2011) analysed a human mandible, and demonstrated an overall reduction of the stiffness on the whole bone, results that are supported by a previous FE validation study by Marinescu *et al.* (2005). Despite the discrepancy, the results of Wood *et al.* (2011) and Gröning *et al.* (2011) fundamentally agree in that neglecting the modelling of the PDL may produce overstiffening. The differences on the effect of the modelling of the PDL in both studies are probably a logical consequence of the different geometries of the mandible and the cranium, and also of the much higher stiffness of the latter.

### 6.1.2. The felid turbinates

The turbinates are bony plates covered with epithelium and located in the nasal chambers. They can be divided into three, depending on the bone from which they originate: ethmoturbinates arise from the ethmoid, nasoturbinates from the nasal and maxilloturbinates from the maxilla (Figure 6.1). It is suggested that the ethmoturbinates are related to the sense of smell, and the maxilloturbinates and perhaps the nasoturbinates help preserve body water and heat, the latter by directing air to the former (Van Valkenburgh *et al.*, 2004, 2011). The reduced rostrum of felids means they have reduced nasal regions compared to other carnivorans (e.g. dogs) as well and consequently have smaller olfactory lobes in their brains (Turner and Anton, 1997). Despite the fact that the sense of smell plays a lesser role than sight or hearing for hunting, it is still nevertheless important for communication with other members of the species (Kitchener *et al.*, 2010).
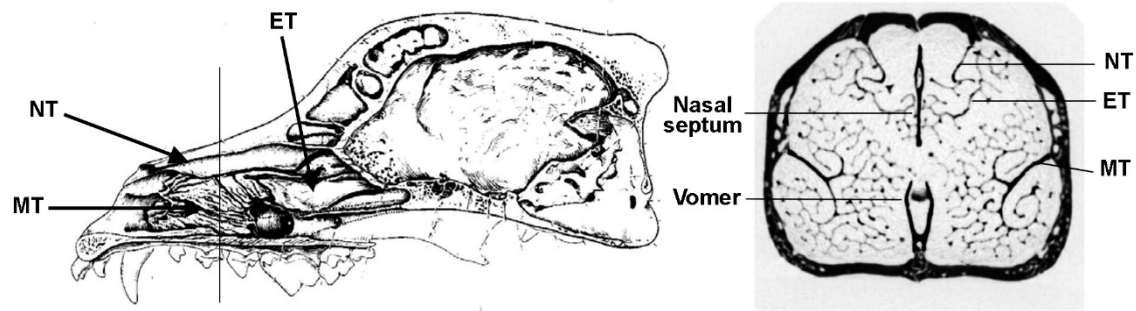
**Figure 6.1.** *Canis familiaris* **skull in sagittal section (left) and inverted CT image of a coronal section of a *Vulpes macrotis* (right) with the locations of the ethmoturbinates (ET), maxilloturbinates (MT) and nasoturbinates (NT); (after Van Valkenburgh *et al.*, 2004).**

### 6.1.3. The nasal septum

The nasal septum has osseous and cartilaginous parts. The former is composed of the perpendicular plate of the ethmoid bone, together with the vomer, and the latter is located in the more rostral area (Sebastiani and Fishbeck, 1998). An experimental study with pigs (*Sus scrofa*) reached the conclusion that the cartilage of the nasal septum may help absorb loads during mastication, as strain magnitudes in the area were considerably higher than in adjacent bony regions, but it did not serve as a vertical strut to prevent collapse of the nasal cavity as it has been sometimes hypothesized (Dayeh *et al.*, 2009). In contrast, a previous study on a human skull found high stresses and deformation in the hard palate and the posterior part of the osseous nasal septum during mastication (Hilloowala and Kanth, 2007). Since the cartilaginous part of the nasal septum was not visible in the CT scans of the cat skull modelled here, it was not considered in the following analysis. Only the effect of the osseous part was tested in the final model.

### 6.2. Methods

The PDL of the *Felis silvestris catus* specimen was also not visible in the CT scans, so it was recreated by covering the proximal surface of each tooth and its corresponding root with a 3 or 4 pixel-width sheet of tissue, and given isotropic homogeneous and linear elastic properties. This 3 or 4 voxel width (0.19-0.25 mm, agreeing with McCormack *et al.*, 2017) is a minimum requirement to ensure there was no contact between bone and

teeth and for the creation of reasonably shaped elements. It did however have the undesirable effect that, in certain areas, these pixels had to be removed from the teeth surface or the alveolar region, therefore unnaturally altering the geometry of these structures. For a detailed account of the creation process of the digital *Felis silvestris catus* model, see Chapter 4.

For the investigation into the effects of the periodontal ligament, successive analyses of the cat's cranium were performed using different Young Modulus values for the PDL (of 0.1 MPa, 1 MPa and 50 MPa). To simulate a scenario in which the PDL was not modelled, another analysis was performed where bone material properties were applied (using $E = 13.7$ GPa and $\nu = 0.30$, following Slater and Van Valkenburgh, 2009). For the turbinates and the nasal septum, analyses were performed before and after removal of the structure of interest. This was achieved by altering the material Young's modulus and Poisson ratio of these to match the surrounding generic soft tissue that was used as a filling material for the model (whose effects were also examined in Chapter 4). Therefore, the filling material was preserved in both analyses (with and without the turbinates). All the analyses were performed by simulating a bilateral canine biting regime. A full account of the material properties used and the loading conditions of the *Felis silvestris catus* model can be found in Chapter 5.

It is also worth mentioning that there is variability in the thickness of both the nasal septum and the turbinate individual structures. In the nasal septum, the most common width thickness can span from 10 to 20 pixels (i.e. 0.62-1.24mm). In the case of the turbinates, the approximate width of the structures can be as low as 3-4 pixels or as high as 15-20.
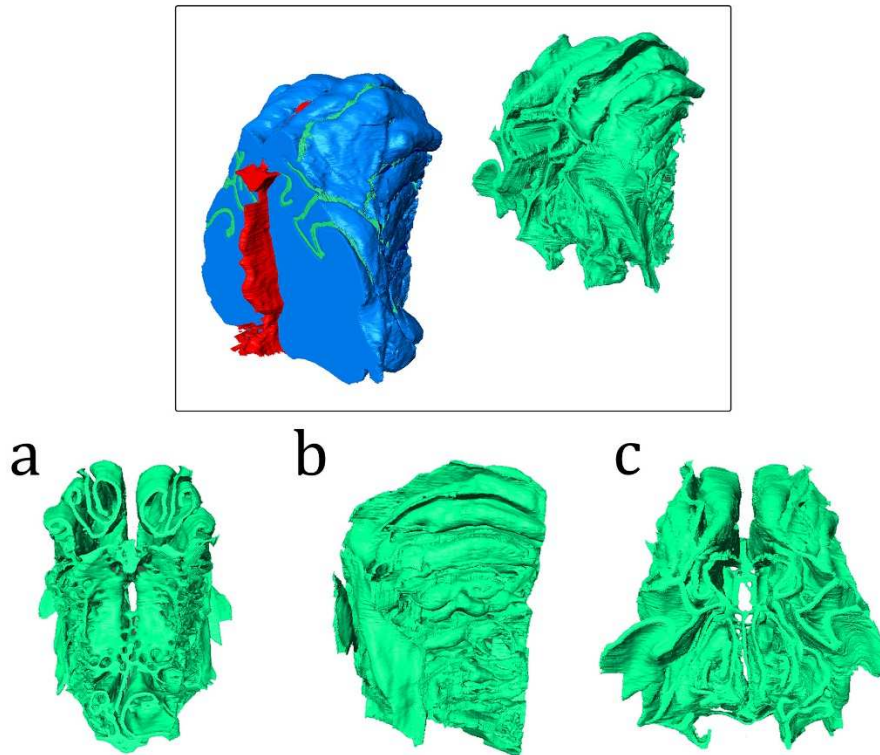
**Figure 6. 2. Above: Subset of the cat's cranium model showing the filling material surrounding the turbinates (blue), the turbinates (green) and the osseous part of the nasal septum (red), together with the separated turbinates (in green). Below: Turbinates in posterior (a), lateral (b) and anterior (c) view.**

## 6.3. Results

### 6.3.1. Periodontal ligament

When comparing the models with different material properties for the periodontal ligament, some trends are visible (Figure 6.3). Firstly, there are differences but they are minor and localised. The areas that seem to be most affected by the variation in the PDL properties are the rostrum (particularly the maxilla and the alveolar region) and the palatine bone. However, in all cases the changes appear to have a negligible impact on the general cranial biomechanics of the model, as they barely alter the pattern of the stress results. Secondly, despite the same overall loading pattern, a gradual reduction in stress is still noticeable when the PDL's Young Modulus is increased. Thirdly, assigning low values could potentially alter the results in more significant ways than omitting to model the PDL at all. This last conclusion, perhaps the most meaningful, becomes self-evident

when comparing the analyses: the 1 MPa model has more extensive areas of stresses in the palatine region and also exhibits minor differences in the superior and posterior orbital walls. On the contrary, differences between the 50 MPa model and the osseous PDL model are minimal across the cranium, and therefore agree with the results of Wood *et al*. (2011).
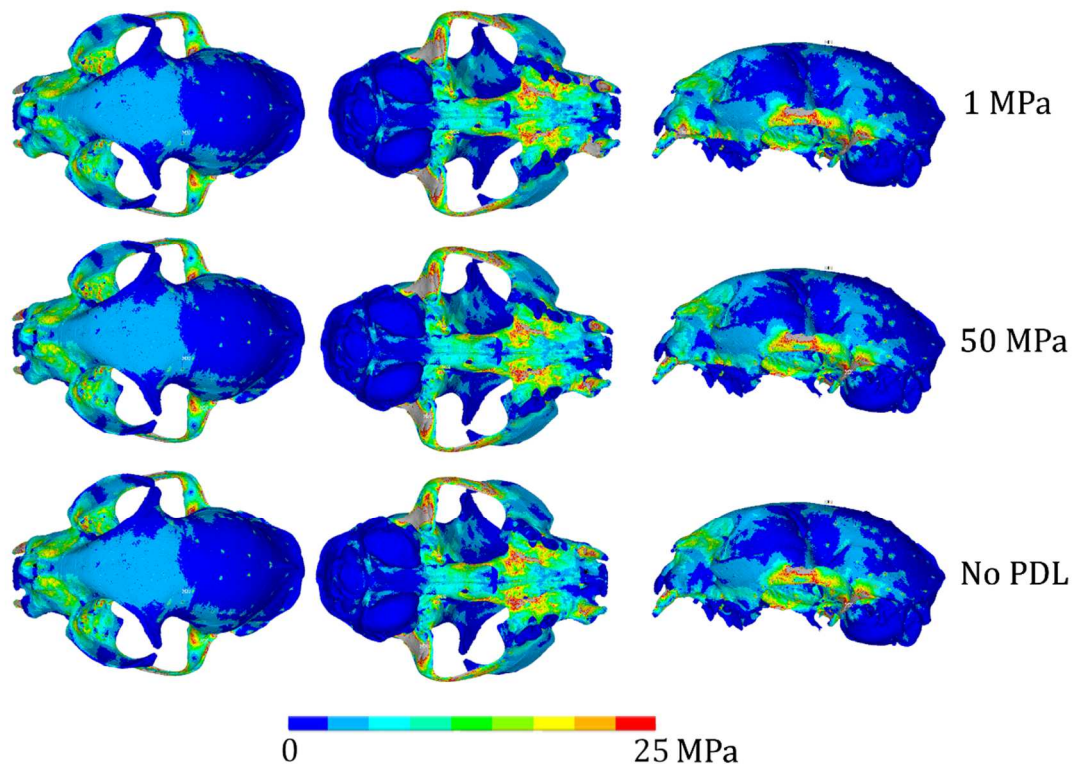


**Figure 6.3. von Mises stress distribution (bilateral canine biting regime) for the periodontal ligament with various elastic modulus values: 1 MPa (top row), 50 MPa (middle row), 13,700 MPa or bone material properties (bottom row).**

### 6.3.2. Turbinates and nasal septum

The removal of the turbinates in the cranial model of *Felis silvestris catus* leads to an increase in stress in the cranium, which is most pronounced in the palatine and surrounding areas, in the maxilla and, surprisingly, in the temporal bone (Figure 6.4; see Chapter 5 for an explanation of the difference plots). However, and at the same time, there is also an opposite, and less marked, decrease in stress in the anterior part of the palatine,

specifically between both posterior palatine foramens, as well as in other areas of the zygomatic bone and the maxilla.
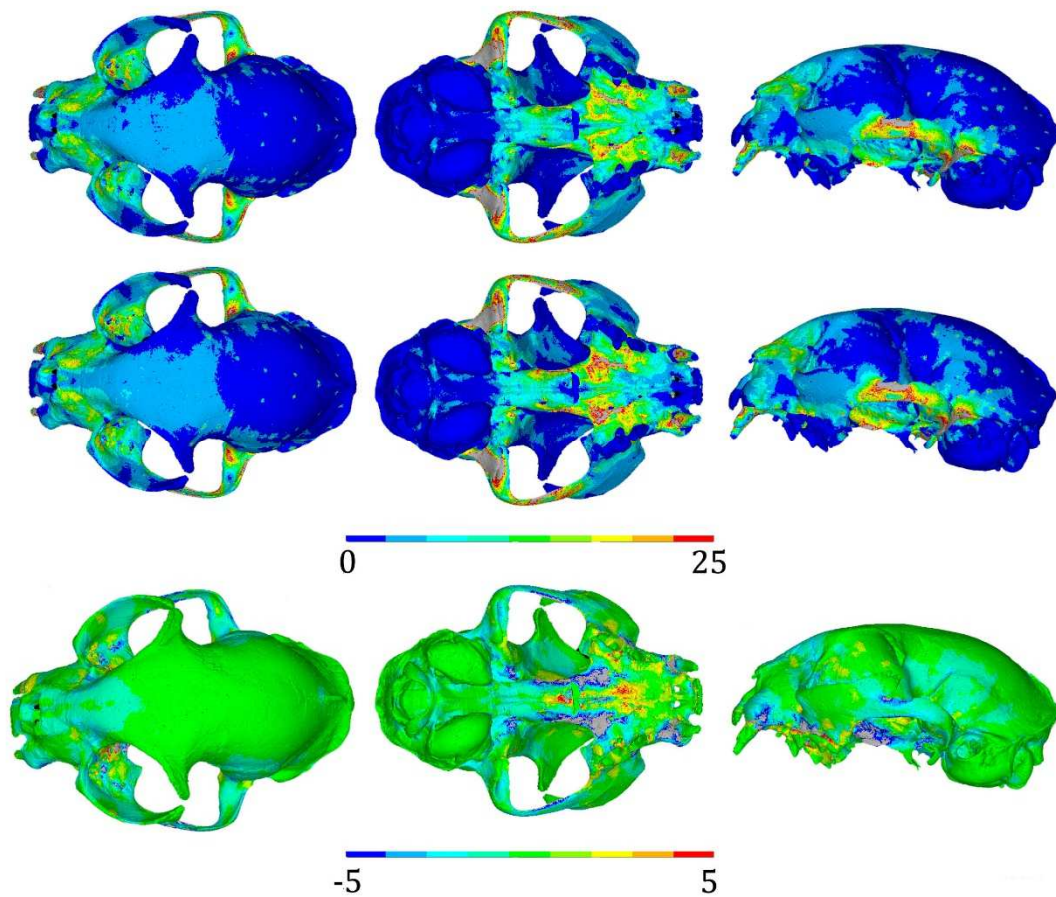


**Figure 6.4. von Mises stress plots (under a bilateral canine biting regime) for the turbinates. Top row: Model with turbinates. Middle row: Model without turbinates. Bottom row: difference plots.**

Similarly, removing the osseous nasal septum also has an impact on the overall level of stress in the cranium, with an increase observed when the septum is absent and a similar decrease in the same areas described above (Figure 6.5). Globally, the effects of removing the nasal septum are very similar to the effects of removing the turbinate structures.
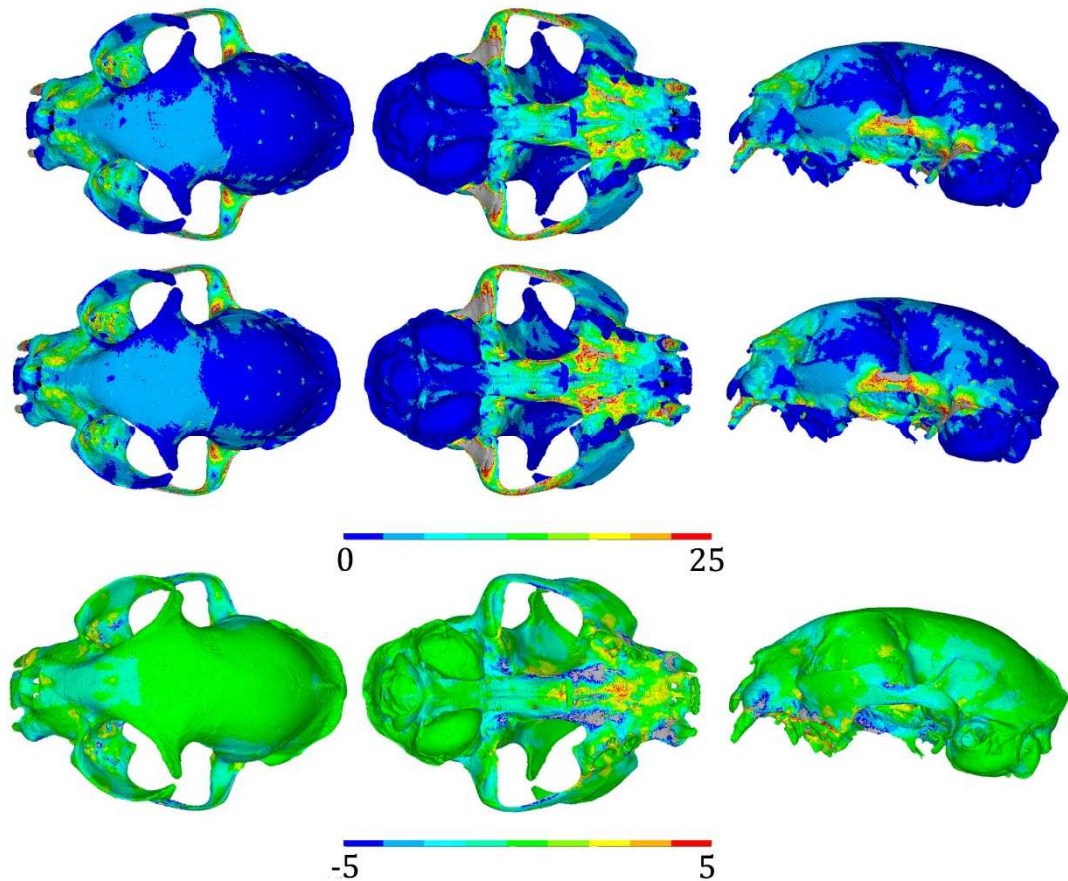
**Figure 6.5. von Mises stress analyses (bilateral canine biting regime) for the nasal septum. Top row: model with nasal septum. Middle row: model without nasal septum. Bottom row: difference plots.**

## 6.4. Discussion

### 6.4.1. Periodontal ligament

The analyses above seem to suggest that altering the material values of the PDL homogeneously may have a minor but still undesirable effect in the FE results of cranial biomechanics, especially with low Young modulus values. This effect can be seen more clearly in the ventral detail of Figure 6.6 below. The areas of peak stresses in the canines and the surrounding regions are much more extensive in the model using a PDL with Young modulus of 1 MPa than in the model with no PDL or with a PDL of 50 MPa. These results agree with those found by Wood *et al*. (2011); in particular, if the focus of the study is the bone in the neighbourhood of the teeth or the teeth themselves, then the PDL

should be modelled. If however, the study is not specifically concerned with the area of the crania around the teeth, then it may not be necessary to include the PDL. (These conclusions cannot be extrapolated to analyses of the mandible, which are much less rigid structures as mentioned previously).
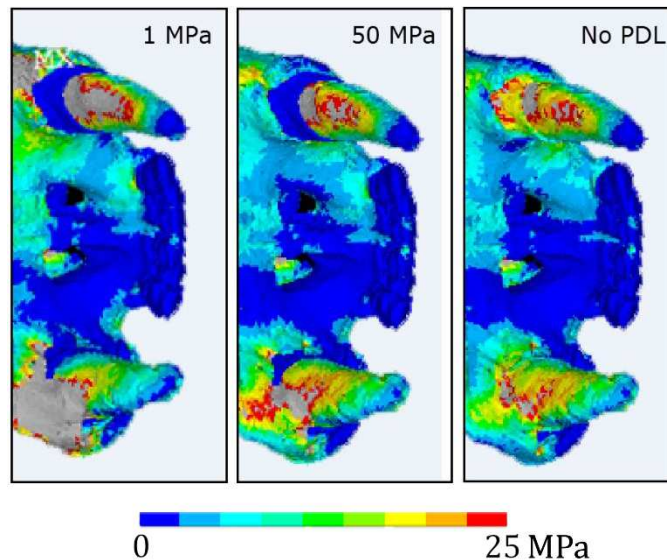


**Figure 6.6. Detail from Figure 6.3; ventral views showing the local effects that the alteration of material properties of the periodontal ligament has on the canine teeth and alveolar region.**

Another important factor that perhaps has not been sufficiently taken into account is the morphological differences amongst mammal crania, because geometrical variability will inevitably lead to different responses to stress and the significance of the same structures within those crania may vary. Tetrapod crania exhibit considerable variability and different geometries may adopt different biomechanical approaches. Wood *et al.* (2011) pointed out that the area primarily affected by the inclusion of the PDL depends on the length of the tooth roots. Thus, not only might a premolar bite be expected to have a different effect to a canine bite because the location differs, but also the roots vary considerably in size. The length of the different teeth roots also differs between species and animal groups. Even among felids, tooth roots can have critical impact in cranial biomechanics. This poses the question of what importance the PDL might play in an extreme case, such as the extinct sabre-toothed species displayed in Figure 6.7 where the tooth takes up such a large part of the cranium volume. These animals were investigated

by Wroe *et al*. (2013); unfortunately, they didn't model the PDL, but it seems likely that its inclusion would have a significant effect on the stresses.
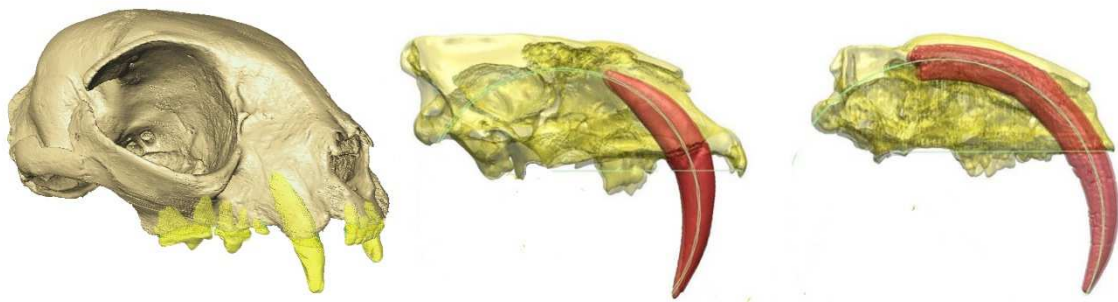


**Figure 6.7.** *Felis silvestris catus* **(left),** *Smilodon fatalis* **(middle) and** *Thylacosmilus atrox* **(right) cuts showing the extension of the canine tooth and its corresponding root, in yellow and red, respectively. In such extreme examples, the modelling of the PDL might be a very important factor to take into account (middle and right images adapted from Wroe** *et al.***, 2013).**

### 6.4.2. Turbinates and nasal septum

The function of the cartilaginous septum as a reinforcement to support facial integrity or as a load-absorbing structure during mastication has been the focus of various academic works (Sarnat and Wexler, 1996; Al Dayeh *et al*., 2009). However, the osseous part of the nasal septum and the turbinates have not received the same attention (with the exception of Toro-Ibacache *et al.* (2016) whose work support the results obtained here). From the results of this study it seems that both the osseous part of the nasal septum and the nasal turbinates help to increase skull integrity in the cranium of *Felis silvestris catus*. Thus, the omission of either the turbinates or the osseous part of the nasal septum in analyses will lead to a general increase in stress, which is not only confined to the rostral and palatal areas, but, unexpectedly, also extends to the posterior part of the skull. There is also a decrease of stress in the palatine, rostrum and zygomatic, that is worth noting. The effect is likely to be accumulative, so a model without any of these structures will lead to even greater or lower stresses in the regions affected.

Apart from the additional segmentation effort, there is no reason to exclude these structures in future FE analyses, particularly the osseous part of the nasal septum. Their omission appears to have a significant effect in different parts of the cranium, and

therefore the accurate modelling of both the turbinates and the septum would appear to be important. Moreover, felids are characterised by their short rostrums (Turner and Anton, 1997), so it is possible that the effects of omitting the nasal septum and the turbinates in finite element analyses may be more significant in species with longer snouts.

## 6.5. Conclusions

This chapter has focused on the analyses of the effect that some cranial structures – the periodontal ligament, the nasal turbinates and the osseous part of the nasal septum – may pose on general cranial biomechanics. The decision to include or disregard each of these structures will depend on the specific motivation of the study in question and the areas of the cranium that are of interest. In the analyses performed here, a minor localised effect is observed with the addition of the periodontal ligament and the variation of its material properties. A more significant change in the stress patterns of the cranium was found if the nasal turbinates or osseous part of the nasal septum were not present, so the modelling of these structures in future FE models of skulls seems to be advisable.

# Chapter 7. Human head model creation and preliminary analyses

## 7.1. Introduction

One of the main aims of this research was to investigate the role of soft tissues in human cranial biomechanics. This chapter introduces the finite element (FE) model of a human head used in that investigation, together with some of the preliminary analyses and results. The FE model was developed from a digital anatomical human head model, the multimodal imaging-based detailed anatomical model (MIDA) which was created by Iacono *et al.* (2015; FDA, Center for Devices and Radiological Health, IT'IS Foundation) and includes over 150 structures of the head and neck.

This chapter comprises a detailed description of the development of such FE model. It also describes the unilateral molar bite simulation that was investigated and discusses the overall stress distribution in the cranium arising from such a biting action. The analyses also include a comparison between the hypothetical case where maximum forces are applied in all muscles and a simulation with more representative, asymmetrically scaled muscle forces. The chapter concludes with an investigation to assess the effects that modelling bulk soft tissues, such as skin and muscles, has in FE biting analyses.

In the following chapter, the FE model is then used to test the role of the postorbital bars and septa structures.

## 7.2. Methods and techniques

The MIDA anatomical human head model created by Iacono *et al.* (2015) from a twenty-nine year old female volunteer, has been made available for public use and integrates data from different sources: a T1- and two T2- weighted MRIs (Magnetic Resonance Imaging) with 500 μm isotropic resolution, a series of MRA scans (Magnetic Resonance Angiography) to capture the vascular structures, and DTI (Diffusion Tensor Imaging) for the most detailed tissues of the brain. The MIDA model has already been used in other studies, such as those performed by Howell and McIntyre (2017), Bächinger *et al.* (2017) and Liu *et al.* (2017) for varied purposes.

The data had to be adapted to suit the particular needs of the present study, which required the following steps. Firstly, the *NII* file[3] supplied by Iacono and colleagues was loaded into AVIZO 9.4, thus generating a 16-bit colormap with each of the structures represented as a different greyscale value. The structures of interest were then separated (segmented) from each other by defining a different AVIZO label (identifier) for each. Some structures were simplified and combined depending on their importance in the study. Thus the cranium was segmented as a single structure, while the brain and eyes were simplified and both defined as single homogenous materials, thereby ignoring any sub-structures. The postorbital bar and the postorbital septa were segmented separately from the rest of the skull to allow their functions to be tested independently, as were the mandible and the cervical vertebrae. The upper teeth were manually separated from the lower ones. The temporalis/temporoparietalis muscle was segmented individually and separated after reaching the approximate height of the zygomatic arch in order to allow the definition of a surface for modelling the temporal fascia at a later stage. A minor modification was made to the MIDA model with the most posterior end of this muscle being deleted, since it extended much further posteriorly than appeared to be the case in other anatomical depictions and dissection photographs from the literature. The remaining structures were considered to be part of a single material of generic soft tissue, including the skin, the remaining muscles, the fat pads and the vascular tissues. The articular disc of the temporomandibular joint was modelled as an approximately oval shape in the connection between the mandibular condyle and the mandibular fossa. The periodontal ligament (PDL) was not modelled because the previous analyses (see Chapter 6 and the bibliography mentioned therein) revealed that inclusion of the PDL only had a very localised effect. Finally, all the structures from the MIDA model were digitally trimmed to the height of the upper lip in the anterior part and approximately to the lower surface of the atlas vertebra in the posterior part (Figure 7.1).

---

[3] NII (or NIfTI, Neuroimaging Informatics Technology Initiative) is a format commonly used for multi-dimensional neuroimaging data.
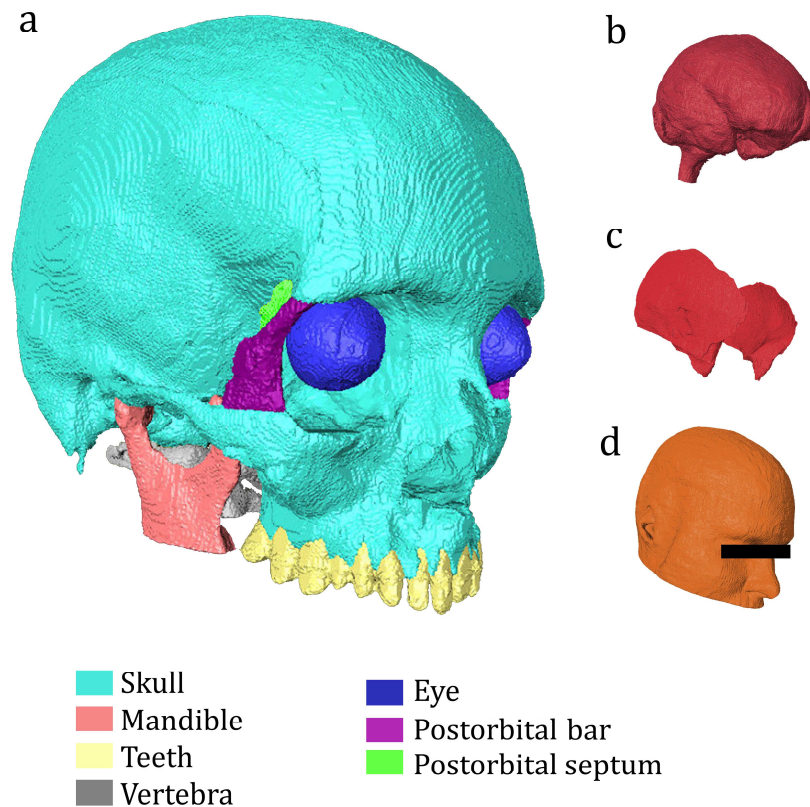
**Figure 7.1. The MIDA model of Iacono *et al.* (2015) after being adapted to suit the research purposes of this study. (a) All skeletal tissues modelled plus the eyes, (b) brain, (c) temporalis/temporoparietalis muscle, (d) bulk tissues of the head. The articular disk is not visible in the images.**

The FE model was generated by using the meshing module available in AVIZO 9.4, with a high mesh density in the structures most important for the analyses, and a lower number in the generic soft tissues, the brain and the vertebrae. Overall, the final FE model generated by this approach included approximately 5.3 million higher-order tetrahedral elements.

### 7.2.1. Material properties

The material properties used in the FE model are summarised in Table 7.1. Trabecular spaces with individual trabeculae were present in the MIDA model, and hence a single value for Young's modulus was specified for all the osseous materials in the skull, mandible and cervical vertebrae. A range of values for bone has been used in previous

FE analyses, which is not surprising given that bone properties vary significantly within an individual and between individuals. Thus, elastic modulus values ranging over 8 GPa (Tse *et al.*, 2015), 13.7 GPa (Pinheiro and Alves, 2015) and 15 GPa (Horgan and Gilchrist, 2003) have been used in previous studies, with Poisson ratio values that span from 0.22 (Horgan and Gilchrist, 2003; Ho and Kleiven, 2009; Tse et al., 2015) to 0.3 (Hirose *et al*, 2006; Pinheiro and Alves, 2015).

Toro-Ibacache *et al.* (2016) measured the Young Modulus of the maxillary tuberosity and the zygomatic arch with a nano-hardness tester and obtained values of 16.3 ± 3.7 GPa and of 21.9 ± 2.7 GPa respectively. In another study, the mean elastic modulus for a set of 10 human mandibles was measured by using a pulse transmission technique, and ranged between 12.7 and 22.8 GPa (Schwartz-Dabney and Dechow, 2003). An intermediate value of 17 GPa with a Poisson's ratio of 0.3 was therefore chosen as it has been used in several previous studies (e.g. Strait *et al.*, 2005; Kupczik *et al.*, 2009; Curtis *et al.*, 2011; Gröning *et al.*, 2011; Toro-Ibacache *et al.*, 2016 and others), including those carried out at the University of Hull, thereby facilitating comparison of those results with the current study.

Similarly, there is no consensus in the literature about the material property values of the articular disc of the temporo-mandibular joint (TMJ), hence this study follows Beek *et al.* (2000) using an elastic modulus of 6 MPa and Poisson's ratio of 0.4, which was chosen after considering values used by various studies. Property values for the temporal fascia were obtained from Curtis *et al.* (2011). The temporal fascia is composed of two layers: a superficial layer which nearly covers the lateral aspect of the skull, and a deep layer which closely covers the temporalis muscle and is confined to its limits. Both layers are histologically indistinguishable and share similar elastic properties (Wormald and Alun-Jones, 1991). For the modelling of the human head, the thickness of this structure was estimated from measurements taken on a cadaveric specimen at 6 intervals along the fascia before and after it divides (Gröning, unpublished data). Before the division, the fascia measured 30.43 μm in thickness, and aftwerwards, the deep temporal fascia measured 7.61 μm and the superficial measured 18.06 μm. However, in the model, the superficial layer was not separated from the deep one, hence we used a constant value of 30 μm thickness for the shell elements.

Since humans possess a postorbital bar rather than a postorbital ligament (as would be the case in many other animal species), any value assigned to the latter must necessarily be speculative. In the current model, therefore, a value for the collateral ligaments of human ankle joints measured by Siegler *et al.* (1988, table 2) and averaged to be 265 MPa was used. The Poisson's ratio was taken from tendon values from Ozkaya and Nordin (1999) which has been used for ligaments in other studies (for example, Wu, 2012). Other flesh and skin tissue values were obtained from Huempfner-Hierl *et al.* (2015), but a series of sensitivity analyses was also performed for values 0.5, 5, 50 and 500 MPa. The results of these variations in the soft tissues are discussed in the following results and discussion section.

Teeth have different elastic modulus values depending on the region investigated. The outer surface of enamel has a modulus of typically 75 GPa, while bulk dentine varies between 15 to 30 GPa when measured in different areas of the tooth, and the small area under the dentine, sometimes called the 'soft zone' is between 3 and 9 GPa or even lower (Barak *et al.*, 2009). Here an intermediate value of 50 GPa was used, following Toro-Ibacache *et al.* (2016) who applied this mean value from various sources to a series of FE models of the human head, such as this one.

Brain is also heterogeneous; however, there are FE studies that have considered the brain as homogeneous and linearly isotropic. The range of values that has been used is summarised in Tse (2013, table 9), with elastic modulus that vary from 0.0667 MPa to 0.675 MPa and a Poisson's ratio of 0.48 or 0.49. For the purposes of these analyses (that do not undertake a close examination of the stresses in the brain) the upper values have been used, which generally agree with the upper elastic modulus values used for other soft tissues in the model.

The human eyes are complex structures composed of different parts, each one with their own individual material properties. Among them, the cornea, lens, vitreous, sclera and retina are the most important from a biomechanical point of view (Aloy *et al.*, 2017). However, for the purposes of this model, values from Schutte *et al.* (2006), in which eyes were modelled as a single material, were taken; hence, an elastic modulus of 0.5 MPa and Poisson's ratio of 0.4 was chosen.

| Structure | Young's modulus | Poisson's ratio | Reference |
|---|---|---|---|
| Skull | 17,000 MPa | 0.3 | Strait *et al.*, 2005 |
| Mandible | 17,000 MPa | 0.3 | Strait *et al.*, 2005 |
| Vertebrae | 17,000 MPa | 0.3 | Strait *et al.*, 2005 |
| Teeth | 50,000 MPa | 0.3 | Toro-Ibacache *et al.*, 2016 |
| Brain | 0.675 MPa | 0.49 | Tse, 2013 |
| Bulk soft tissues | 0.5 MPa | 0.45 | Huempfner-Hierl *et al.*, 2015 |
| Eyes | 0.5 MPa | 0.4 | Schutte *et al.*, 2006 |
| Temporal fascia | 148 MPa | 0.3 | Curtis *et al.*, 2011 |
| Postorbital ligament | 265 MPa | 0.4 | Siegler *et al.*, 1988; Ozkaya and Nordin, 1999 |
| Articular disk of the TMJ | 6 MPa | 0.4 | Beek *et al.*, 2000 |

**Table 7.1. Material properties used for the human head model. All materials were assumed to be linearly elastic and isotropic.**

### 7.2.2. Bite force

The following procedure was followed to simulate biting. First, a series of landmarks was created in AVIZO on the cranium at the areas of origin of the masticatory muscles, while the mandible (positioned in total occlusion) was used as a surface for placing the insertion landmarks in order to recreate the muscle strand orientation. Physiological cross-sectional area (PCSA) values for the muscles were taken from van Eijden *et al.* (1997) and then multiplied by 32 N/mm$^2$, the intrinsic muscle stress of human jaw muscles as calculated by Weijs and Hillen (1985). The same PCSA and muscle stress values were used by Gröning *et al.* (2011), with the resultant muscle forces used in Table 7.2. These maximum (unscaled) muscle force values are also similar to the values used by Wroe *et al.* (2010; supplementary material, table S2).

Subsequently, the maximum muscle values were scaled based on clenching obtained by electromyography (EMG) from various independent studies, but gathered together by Nelson (1986; Table II). This electromyographic data represents voluntary clenching and was used to scale the maximum theoretical muscle force values obtained from the PCSA in order to get a more realistic simulation of human biting. Each muscle

was multiplied by its scaling factor, which depends on its degree of activation. For the purposes of the scaling, the temporalis muscle was divided into three different regions. Unfortunately, there is no consensus about the precise structure of this muscle in humans. Some researchers consider that it has one single layer, others that it has two different layers or parts (superficial and deep or anterior and posterior), or three separate parts (for a detailed historiographical discussion, see Gaudy *et al.* (2002) and Sedlmayr *et al.* (2009)). Gaudy *et al.* (2002) also described differences in orientation between the orbital part and the temporal part of the muscle. In the orbital part, muscle fibres were vertical in the anterior area and positioned more horizontally in the posterior area, while in the temporal part they were horizontal. For the purposes of this study, and in order to perform the necessary calculations for Table 7.2, the temporalis was divided into three regions of equivalent size, following Van Eijden *et al.* (1996) who separated the temporalis into six different portions. The decision to separate the temporalis in this way allows the scaling values provided by Nelson (1986) to be applied: the anterior temporalis used by Nelson corresponds to the first two portions of the muscle described by Van Eijden *et al.* (1996), the middle temporalis to the second pair, and the posterior temporalis to the last two. These scaled values were then divided equally among the number of landmarks (and strands) that composed each muscle in the model.

| Muscle | PCSA | Maximum muscle force (N) | Scaling factors (Right/Left) | |
|---|---|---|---|---|
| Superficial masseter | 6.82 ± 1.04 | 218.2 | 0.72 | 0.60 |
| Deep masseter | 3.49 ± 0.82 | 111.7 | 0.72 | 0.60 |
| **Masseter (total)** | **10.31 ± 1.41** | **329.9** | **0.72** | **0.60** |
| Anterior temporalis | 5.25 ± 1.28 | 168 | 0.73 | 0.58 |
| Middle temporalis | 4.29 ± 0.74 | 137.3 | 0.66 | 0.67 |
| Posterior temporalis | 3.71 ± 1.05 | 118.7 | 0.59 | 0.39 |
| **Temporalis (total)** | **13.25 ± 3.30** | **424** | | |
| **Medial pterygoid** | **6.00 ± 1.24** | **192** | **0.84** | **0.60** |
| **Lateral pterygoid (inferior head)** | **2.82 ± 0.66** | **90.2** | **0.30** | **0.65** |

**Table 7.2. Maximum muscle force calculated from each muscle's PCSA (after van Eijen *et al.*, 1996 and 1997). Scaling factors from Nelson (1986).**

### 7.2.3. Boundary conditions

Tooth identification in humans uses the following system: I1, I2, C1, P3, P4, M1, M2, and M3 (where M3 corresponds to the wisdom tooth). Incisors (I) are used for cutting and biting during mastication, the canines (C) pierce and tear, while the role of the molars (M) is to grind the food with the premolars (P) assisting the molars and the canines in their respective functions (Bath-Balog and Fehrenbach, 1997). The average maximum bite force measured voluntarily in an *in vivo* experiment between human incisors is typically 140-200 N (Hellsing, 1980), 120-350 N for the canine teeth (Lyons and Baxendale, 1990) and 600-750 N for the molars (Hagberg, 1987), while Tortopidis *et al.* (2002) reported 428 N (s.d. 132 N) in unilateral bite force in the molar area. Hence bite force increases anterior-posteriorly across the oral cavity. Individual tooth values have also been measured by using single tooth transducers (Ferrario *et al.*, 2004), who reported lower values but a similar progression in force increase (see Table 7.3) and confirmed a symmetry between left and right sides of the dental arch. This study also confirmed that men had larger bite forces than women for every individual tooth considered.

| Tooth | I1 | I2 | C1 | P3 | P4 | M1 | M2 |
|-------|-----|-----|-----|-----|-----|-----|-----|
| **Women** | | | | | | | |
| Mean (N) | 93.88 | 95.75 | 119.68 | 178.54 | 206.01 | 234.46 | 221.71 |
| SD | 38.16 | 36.59 | 42.58 | 77.20 | 86.52 | 70.53 | 73.08 |
| **Men** | | | | | | | |
| Mean (N) | 146.17 | 139.30 | 190.31 | 254.08 | 291.36 | 306.07 | 294.30 |
| SD | 44.44 | 51.40 | 79.36 | 72.20 | 57.29 | 41.99 | 55.92 |

**Table 7.3. Single tooth bite forces for men and women (after Ferrario *et al.*, 2004, table 1).**

The analysis in the current research was designed for a single biting regime at the right first molar (M1). Thus, constraints were applied to a single node at each temporomandibular joint in the FE model of the cranium. One of these nodes was constrained in all degrees of freedom with the other in two directions (anterior-posteriorly and dorso-ventrally), thereby applying minimal constraints to the joints. The molar tooth was only constrained dorso-ventrally. This is the same configuration as that applied to the previous *Felis silvestris catus* model (see Chapter 5).

An analysis performed with the model using the unscaled (maximum) muscle forces returned a bite force of 979.2 N at M1. After scaling, the reaction force at the same tooth was found to be 625 N, which is at the higher end of the experimental values reported previously in the literature, but also similar to the bite force values predicted by Gröning *et al.* (2011) for M1 (524 N and 554 N without and with the periodontal ligament in place, respectively). These differences could arise because either a larger sized skull is modelled in the current analysis, or the lines of action of the muscle forces are different.

## 7.3. Results and discussion

### 7.3.1. Temporomandibular joint forces and bite forces

When simulating a unilateral bite, some FE models (Wroe *et al*., 2010, Cox *et al.*, 2011, for example) assume equal (maximum) activity of the muscles on both sides of the skull, which is not observed *in vivo* (Nelson, 1986; table II). For example, the force of the working side masseter in *Macaca Fascicularis* exceeds the force of the balancing side by a factor of typically 2-3, depending on the power of the bite and the type of food and of jaw movement (Hylander *et al*., 1992).

This can be explained by considering the constrained lever model proposed by Greaves (1978). When performing a unilateral bite, the adductor muscle forces produce reaction forces at the tip of the tooth and at the temporo-mandibular joints, forming a triangle "of support" (Figure 7.2). For the bite to be stable, the line of action of the resultant vector must lie within this triangle, so the three points are all in compression. This is not a problem with bilateral bites, or unilateral bites with the incisor, canine or premolar teeth, but the position of the bite point changes significantly with molar bites so that the resultant could fall outside the triangle of support. When this happens, distractive (tensile) forces are generated in the temporomandibular joint at the working side, pulling the joint apart and therefore risking disarticulation of the jaw. For this reason, mammals reduce the force exerted by the balancing side when chewing unilaterally, so the resultant vector is drawn in the direction of the working side and back into the triangle of support (Ledogar *et al*., 2016).
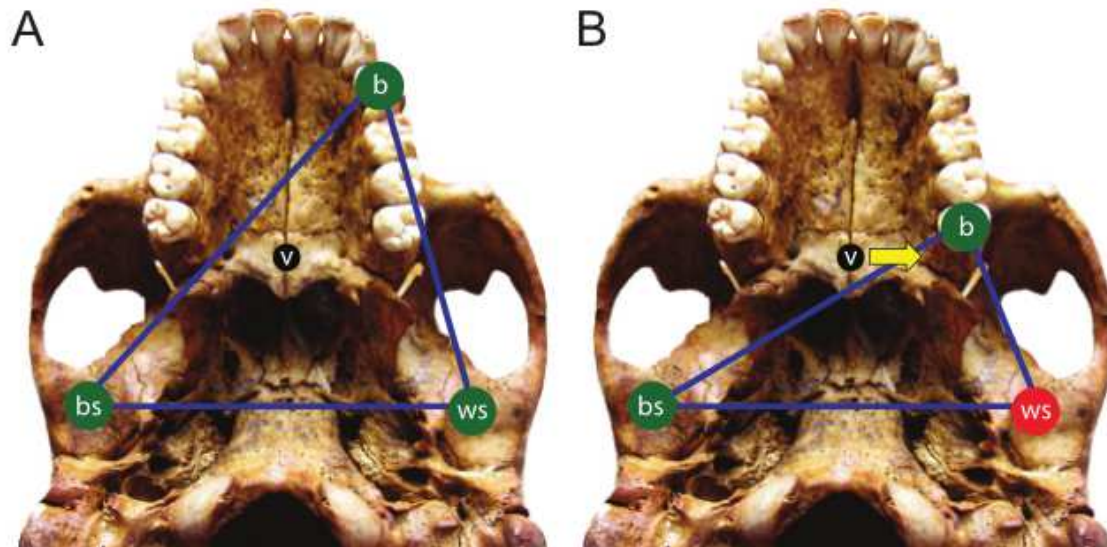
**Figure 7.2. Triangle of support representing the constrained lever model of jaw biomechanics for a premolar bite (A) and a molar bite (B). ws: working side, bs: balancing side, b: bite point, v: the resultant vector of the action of the jaw adduction muscles. (After Ledogar *et al.*, 2016).**

In the model with maximum muscle forces applied, the symmetric high force values of the jaw adduction muscles cause the resultant force to lie outside the triangle of support. This is seen in

Table **7.4** by looking at the component of the reaction force at the working side $TMJ_{WS}$ along the dorsoventral axis, which has a negative value of -8.56N (i.e. acting in a ventral direction), indicating a tensile force on the cranium. In contrast, in the model with scaled muscles the same component of the reaction force at $TMJ_{WS}$ has a positive value (indicating a compressive force) of 72.24 N.

Table **7.4** gives all the components of the reaction force values at both TMJs. Note also, for the model with scaled muscles the reaction forces only decrease slightly in $TMJ_{WS}$ (less than 20 N) but dramatically at $TMJ_{BS}$ or balancing side (almost 200 N).

|  | Model with unscaled muscles | | | Model with muscles scaled | | |
|---|---|---|---|---|---|---|
| **Total BF** | 979.22 | | **Reaction force** | 625.04 | | **Reaction force** |
| **TMJ$_{WS}$** | X | -219.02 | 219.37 | X | -186.5 | 200 |
| | Y | -8.56 | | Y | 72.24 | |
| **TMJ$_{BS}$** | X | -275.58 | 524.79 | X | -200.05 | 336.44 |
| | Y | 446.61 | | Y | 270.5 | |

**Table 7.4. Total bite force, reaction forces at both temporomandibular joints (TMJ) and XY components using unscaled and scaled muscle forces (units in N). TMJ$_{WS}$ corresponds to the working side, and TMJ$_{BS}$ to the balancing side.**

### 7.3.2. Stress distributions

The M1 bite produces high stresses in the zygomatic arches and the postorbital bars in both models (Figure 7.3). While in the balancing (left) side, high stresses are located in the anterior part of the temporal bone, in the working (right) side, high stresses manifest more anteriorly, in the sphenoid bone and in the lower area of the temporal. The laterals of the right orbit also clearly experience high stresses, particularly in the model using maximum muscle forces. As expected, stress is also high in the right side of the maxilla above the bite point, but also in the ethmoid bone and the left lacrimal, but is diffused before reaching the nasal bone. The lower region of the nasal has been found by many studies to be an area that experiences high stresses when biting and is regarded as a type of 'pillar' or 'frame' resisting compression (see references in Ledogar *et al.*, 2016). This is also confirmed in the present analyses and its effect can be seen in the third principal stress plots (Figure 7.4). Ledogar *et al.* (2016) reported high levels of tension in this area for a premolar bite, which is also observed below with an M1 bite (see Figure 7.4 for the first principal stress plots). It is also worth noting that stresses remain low across all of the cranial vault.
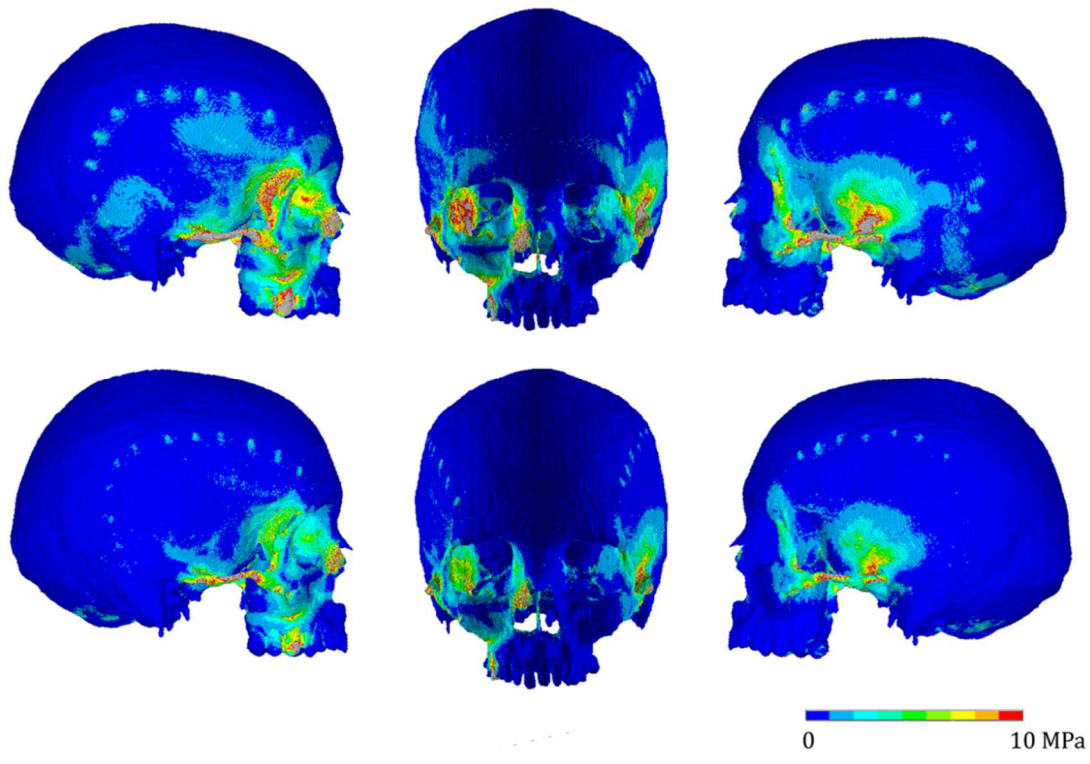
**Figure 7.3. von Mises stress distributions for a unilateral M1 bite. Top row shows the stress using maximum muscle forces; bottom row shows the stress distribution with the scaled muscle forces.**

Closer inspection of the first principal stress plots for the scaled muscle forces (Figure 7.3, above) shows that a tensile force occurs in both postorbital bars and in the temporal bone on the left side. In contrast, on the right side, the area under the nasal bone is subjected to tension, as are the lower and lateral aspects of the right orbit and the posterior end of the right zygomatic arch. The third principal stress plots (Figure 7.4, below) show more extensive compression forces affecting both lateral sides of the skull and increasing across the whole extension of the zygomatic arches. Also, high compression forces are found in the working side in the biting molar and the lower maxilla above it, in a continuum that ascends the right side of the rostrum and finally dissipates in the frontal bone at the approximate height of the supraorbital foramen. Compression is also observed in the right postorbital septum and in the ethmoid bone. In the FE study carried out by Ledogar *et al.* (2016) examining M2 biting, the highest tensile strains were observed in the working postorbital bar (almost three times higher than in the corresponding point of the working side). In the current model, we see a similar tension

in both postorbital bars, which seems to increase towards the inferior end of the structure, although peak tensions at the working postorbital bar seems more extensive. At the same time, Ledogar *et al.* (2016) refers to lower values in adjacent regions, such as the zygomatic body, which to some extent is also observed in the figures below.
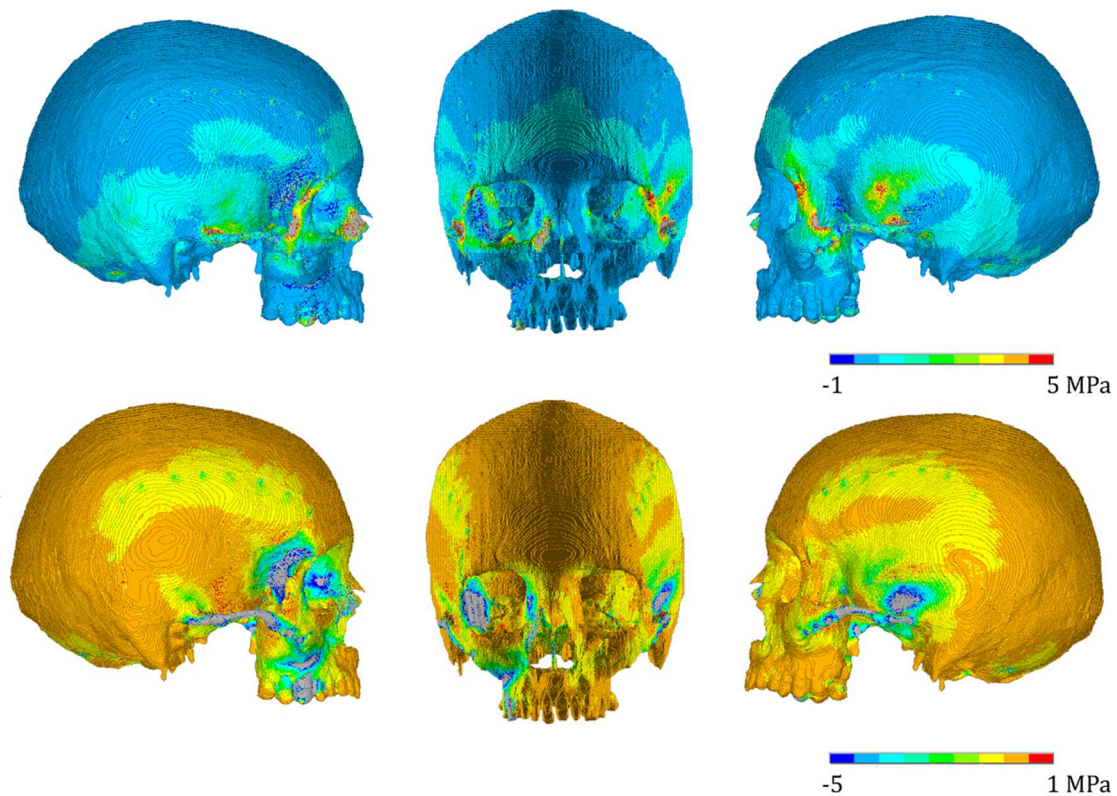


**Figure 7.4. Principal stress plots from a unilateral M1 bite using the scaled muscle forces. Upper row: 1st principal stress (most tensile stress); lower row: 3rd principal stress (most compressive stress).**

### 7.3.3. The effects of including bulk soft tissues in FE analyses

Most earlier FE models that focus on simulation of biting behaviour neglect the inclusion of other soft tissues of the human head that surround the cranial bones and yet they contribute a significant proportion of the mass of the object. As a consequence, the effect that these tissues may have on the results remained unexplored thus far. To test their effect in the current study, the MIDA digital data was processed in AVIZO and meshed so that the bulk soft tissues could be included in the FE model, as described in Section 7.2.

153

To test the sensitivity of the results to the stiffness of the soft tissues, their overall Young's modulus value was varied with the following values: 0.5, 5, 50 and 500 MPa. Figure 7.5 compares the resultant von Mises stress for an M1 bite (with scaled muscles). As expected, the results show how stress in the bone structures of the cranium is (largely uniformly) reduced as the elastic module of the bulk soft tissues increases. The effects, however, only seem significant for values of $E > 50$ MPa, much higher than the default soft tissue modulus of 0.5 MPa (Table 7.1) used in this analysis and values used in previous FE models of the cranium (0.5 MPa in Huempfner-Hierl *et al.*, 2015; 1 MPa in Zhang *et al.*, 2001; 2.2 MPa in Gladilin *et al.*, 2004). Therefore, it seems unnecessary to include the bulk soft tissues to improve the accuracy of the FE models. These results have been confirmed by similar tests performed on a rat head where bulk soft tissues were simulated to assess their influence in the analyses (Sharp *et al.*, 2018).
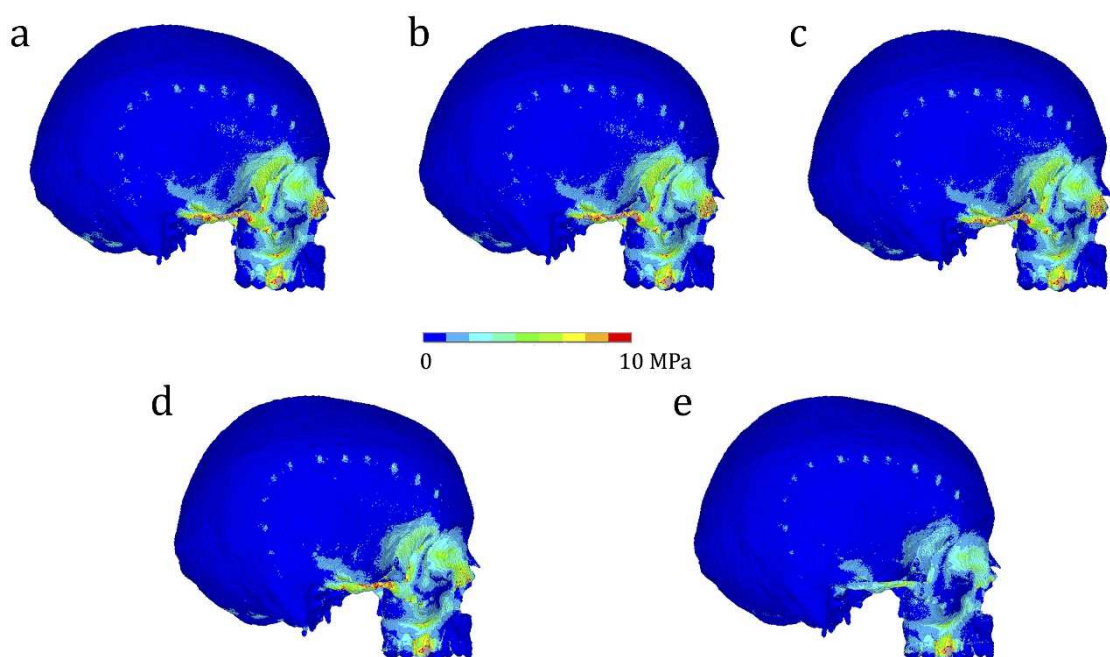


**Figure 7.5. The influence of bulk soft tissues on the von Mises stress distribution in the cranium during an M1 bite. (a) No external soft tissues modelled; (b) to (e) Elastic modulus of the bulk soft tissues varied as follows: 0.5 MPa, 5 MPa, 50 MPa and 500 MPa.**

It still remains to be tested whether these soft tissue structures play a more important role in other species with thicker skin, a stiffer skin, or different arrangements

of the soft tissues under the dermis. They also might be expected to be more significant in open, space-frame type skull structures, such as those found in reptiles, rather than the closed skulls of mammals. Young modulus values compiled and reported by Greven *et al.* (1995) from the skin of fish, reptiles and amphibian species can be seen in

Table **7.5**, with some *E* values above 50 MPa. Even taking this data into account, the effect identified in the current analyses does not alter the general stress distribution patterns of the bone tissue, but rather seem instead to decrease stress overall. However, this reduction in stress may be important for bone remodelling and consequently to define bone shape overall. Moreover, although the values from

Table **7.5** refer to skin, soft tissues surrounding the cranial bones are obviously not limited to skin, but involve muscles with different densities, cartilage, fascial tissue etc. Furthermore, in the case of reptiles, for example, the lack of facial musculature or thick subcutaneous tissue between the skin and bone may make the role of skin more significant than in mammals. Also, the presence of scales or osteoderms will inevitably add a stiffening effect to the surface, but how that effects the stress distribution in the underlying bone needs further, specific analyses.

| Species | Skin elastic modulus (MPa) |
|---|---|
| Rainbow trout (*Salmo gairdneri*) | 13.9 to 870 |
| Tokay gecko (*Gekko gecko*) | 42 |
| Turnip-tailed gecko (*Thecadactylus rapicauda*) | 82.5 |
| African clawed frog (*Xenopus laevis*) | 10.4 to 38.4 |

**Table 7.5. Elastic modulus values of compiled by Greven *et al.* (1995).**

**7.4. Conclusions**

The purpose of this chapter was to introduce the FE model developed from the MIDA anatomical human head model created by Iacono *et al.* (2015), including the modelling process, the material properties and boundary conditions. The model has been first tested with a molar unilateral bite and the bite force generated have been compared with previous experimental data as well as the results from the digital model of another study (Gröning *et al.*, 2011).

At the same time, this study presents a comparison of the model with maximum activation of muscle forces with one in which the forces from the mastication muscles have been reduced after taking into account scaling factors. This process has been already performed in FE analyses in the past (Gröning *et al.*, 2011), but its use has not become extensive, probably because of the lack of data for most species. Moreover, the FE model has also been used to test the role of bulk tissues during biting. The results confirm that, when bulk tissues are included in the model, the stress in the bone is reduced in an apparently uniform manner as the Young modulus of the bulk soft tissues increases. However, in reality, with the relatively low modulus of the soft tissues in a human head, this effect is minimal, but it may become more significant for some species with particularly thick skins and/or more open, space-frame type skull constructions.

In the following chapter, the human FE head model is used to examine the biomechanical role of the postorbital bar, the postorbital ligament and the postorbital septum.

# Chapter 8. The role of the postorbital bar and septum in the human skull

## 8.1. Introduction

The postorbital bar is an ossified arch which is usually formed by the articulation of orbital processes from the frontal and zygomatic bones. It surrounds the side of the eye and forms part of the circular orbit (Smith *et al*., 2013). This structure has evolved multiple times across different taxa and is common to all primates. Many other mammalian groups lack a full postorbital bar, in which case the structure is formed by a postorbital process of variable length and completed by a postorbital ligament, with which if creates a continuum (Heesy, 2005). Anthropoids (and the genus *Tarsius*, although only partially) have also developed a postorbital septum, an osseous structure which separates the temporal fossa from the orbit (Cartmill, 1980).

Previous research has focused on the specific role of the bars (Curtis *et al.*, 2007 in felids; Parisi, 2010 in protosimians) or the septa (Ross and Hylander, 1996; Nakashige *et al.*, 2011, in owl monkeys and macaques, respectively). In the current study, both structures are analysed together, to examine the hypothesis that they both perform a similar mechanical role of protecting the contents of the orbit during feeding. It doesn't appear that an FE study of this nature has been carried out before and the contribution of these structures to the cranium of modern humans has not been assessed. The advantages of carrying out such *in silico* investigations is the ability to test conditions that are not present in nature. Therefore, to assess the mechanical role of the postorbital bar and the septum, the structures of interest were removed and compared to the intact results, examining the changes in the strain distributions in the skull and the deformation of the orbit and eye.

There is still some controversy as to why both the bar and the septum evolved, although the studies performed during the last two decades (Noble *et al.*, 2000; Ravosa *et al.* 2000a, 2000b; Heesy, 2005; Heesy *et al.*, 2007; Jašarević *et al.*, 2010) seem to have reached a consensus to support the idea that the increase in orbital convergence produces a rearrangement of the mastication muscles that, during contraction, may create oculomotor disruption (Cartmill, 1970; 1980). In this hypothesis, the substitution of a

postorbital ligament with a postorbital bar and the closure of the orbit by the septum is regarded as a system to avoid distortion in the orbital margins of animals with convergent orbits during mastication. For a full review of the different competing hypotheses and the state of the question, see Chapter 2.

In any case, the main objective of the analyses performed in this current study is to assess the mechanical role of the postorbital bars and postorbital septa structures as they currently exist in humans and, tentatively, to extend these conclusions to extant anthropoids. The intention is not to support or refute evolutionary hypotheses about why these structures evolved in the first place, since that cannot be properly investigated using only this single specimen.

## 8.2. Methods

All the analyses were performed by simulating a single bite at the right first molar (M1). Five different model variations were considered: one without any modifications to the cranium; one after removing the postorbital bars; one after removing the septa and substituting the postorbital bars for postorbital ligaments; one after removing the postorbital septa; and a model with both the postorbital bars and the postorbital septa removed.

In order to assess strain variation in the different analyses, the model was probed at 9 locations in the skull (Figure 8.1. ). This was performed by selecting 40 to 60 surface nodes in each location of interest (typically covering an area of 0.5 mm) and examining the average maximum principal strain (S1), minimum principal strain (S3), von Mises strain and maximum shear strain over that area. The areas probed were the dorsal orbital regions, the ethmoid bones, the postorbital bars and the zygomatic arches, in both the working side and the balancing side. A single location was also probed in the interorbital area. Some of these locations were chosen following Nakashige *et al.* (2011) in order to be able to compare the results with the ones from that study. The displacement of both sides of the skull was also examined by selecting a node in both inferolateral orbital regions (indicated by a crosshair in Figure 8.1. ). These nodes are strategically located near the inferolateral orbital angle at the intersection of a horizontal plane which traverses through the inferior part of the orbital margin and a vertical plane which passes through the lateral orbital margin. The vertical displacement is measured to assess the

displacement ratio between the working side and the balancing side on each analysis. The closer to 1 the ratio, the more similar the displacement between both sides. The same procedure was used by in Nakashige *et al.* (2011), again facilitating comparisons with that paper.
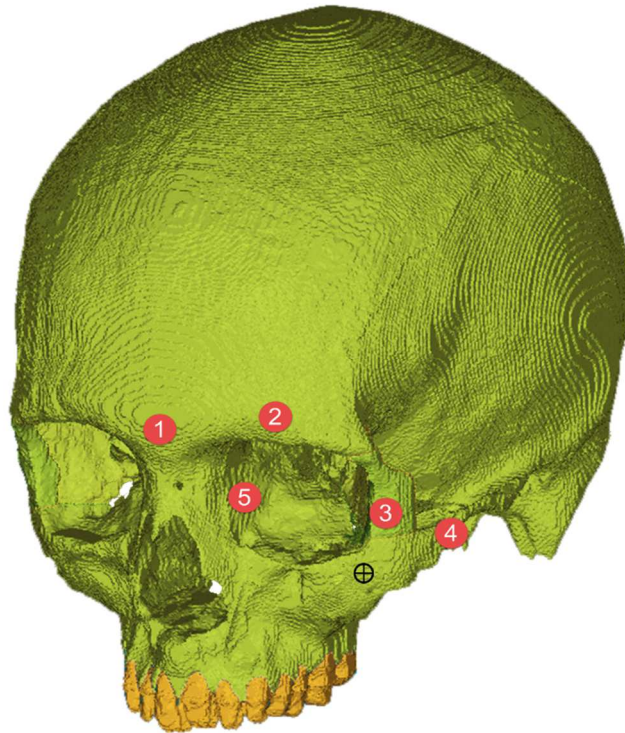


**Figure 8.1. Human head model with the approximate location of the regions where strain data were gathered (only the regions probed on the left side are shown). [1] interorbital region, [2] dorsal orbital region, [3] postorbital bar [4] zygomatic arch, [5] ethmoid bone. The location of the inferolateral node used to measure skull displacement is represented with a crosshair.**

To assess eye deformation during biting, the following approach was used: firstly, two nodes were selected, one on the superior and one on the inferior sides of the eyeball. Then, the relative vertical displacement was calculated after each bite (subtracting the displacement of the inferior node from the superior node value). Negative values then indicate the amount of compression in millimeters in the dorsoventral axis, while positive values indicate tension. A percentage deformation was determined by comparing the eye diameter before and after the analyses, where the diameter of the eyes of the model were

measured from the coordinates of the two nodes selected. On the WS, the undeformed diameter was found to be 23.9 mm, while on the BS it was 23.6 mm. This agrees well with the value quoted in Bekerman *et al.*, 2014, which reports that the human eye measures ≈ 23.7 mm in the vertical direction). The deformation results for the different models are given in Table 8.3.

A full and detailed description of the methods used to create the human head model, including material properties, boundary conditions, sensitivity tests and preliminary analyses, can be found in Chapter 7.

## 8.3. Results

Removal of the postorbital septa has a slight but noticeable effect in the von Mises strain distribution (Figure 8.2, b). On the working side, strain is increased in the postorbital bar and seems to transmit part of the load to the temporal. Peak strains are also visible in the superior area of both postorbital bars. Even more significantly, strain increases in the ethmoid and the lacrimal bones of the working side and, to a lesser extent, in the body of the zygomatic bone. The missing septa do not alter tensile strains in a meaningful manner, but the ethmoid and the lacrimal become subjected to additional compressive forces (Figure 8.3).
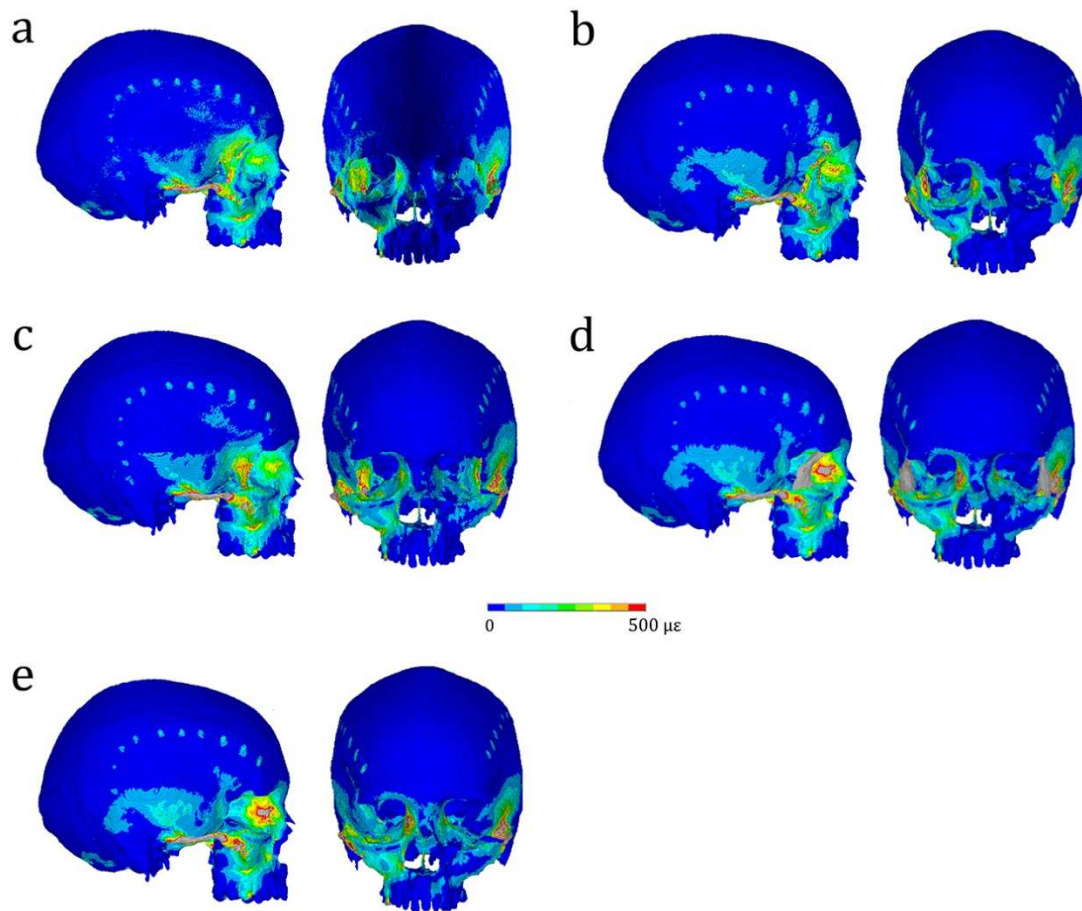
**Figure 8.2. von Mises strain distribution with different postorbital bars and postorbital septa configurations: (a) reference model with intact postorbital bars and postorbital septa; (b) after removal of the postorbital septa only; (c) after removal of the postorbital bars only; (d) after removal of the postorbital septa and substitution of the posorbital bars for postorbital ligaments; (e) after removal of both postorbital bars and postorbital septa.**

Removal of the postorbital bars while maintaining the postorbital septa in place (Figure 8.2c) has a similar effect on the results as removal of the septa. Strain is increased in the lacrimal and the ethmoid, and in the body of the zygomatic bone. The absence of the bars also leads to high strains in the septum. On this occasion, the increase is also visible in the balancing side, although to a lesser extent. When simulating a postorbital ligament by varying the material properties of the postorbital bars (Figure 8.2d), strains further increase in all the areas referred to previously (lacrimal, ethmoid, zygomatic arches and body of the zygomatic bone). Moreover, peak strains appear in the lacrimal

and ethmoid bones of the working side. Subsequent complete removal of the postorbital bars (Figure 8.2e) further confirms this trend.
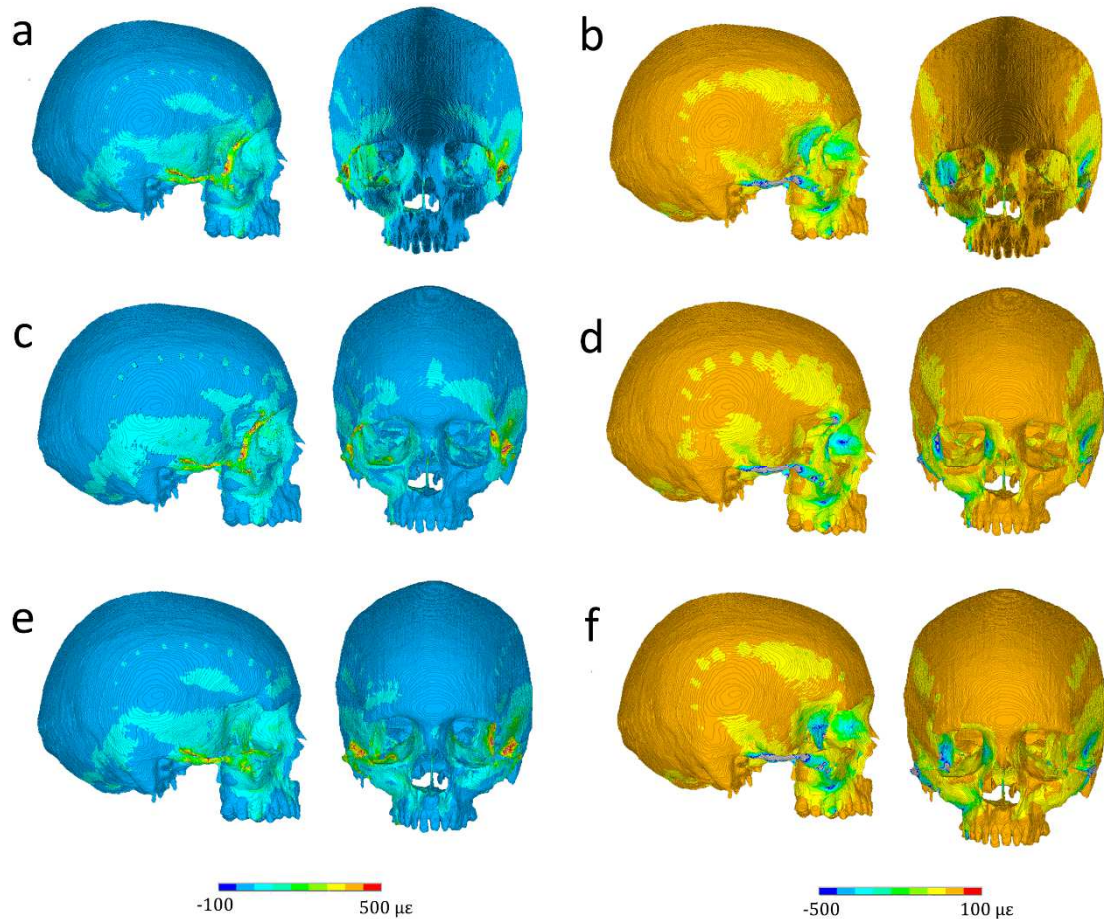


**Figure 8.3. (a, b) analysis simulating a unilateral bite at the first molar (M1) position. (c, d) same analyses after removal of the postorbital septum, but not the bar. (e, f) same analyses after removal of the postorbital bar, but not the septum. (a, c, e) 1st principal (most tensile) strain); (b, d, f) 3rd principal (most compressive) strain.**

This increase in strain is confirmed when comparing specific nodal values for the regions probed in the different analyses (Table 8.1 and 8.2). In both sides of the cranium, von Mises strain increases when the septa and bars are removed, or when substituting the later for postorbital ligaments. The highest strains are invariably found in the model with both the bars and the septa removed. This remains true for all regions tested. The highest absolute values of von Mises strain is found in both zygomatic arches (2480 µε for the

162

working side and 1520 με for the balancing side). However, the greatest change is found in the dorsal orbital area and the ethmoid bone on the balancing side, where strain values are increased by a factor of four when both structures are removed. The dorsal orbital is also the area with the greatest increase on the working side.

|  | BALANCING SIDE | | | | WORKING SIDE | | | |
|---|---|---|---|---|---|---|---|---|
|  | S1 | S3 | von Mises Strain | Max Shear Strain | S1 | S3 | von Mises Strain | Max Shear Strain |
| Dorsal orbital | | | | | | | | |
| Reference model | 13 | -13.8 | 20.1 | 26.8 | 26.1 | -31.7 | 44.6 | 57.8 |
| Postorbital ligaments | 23.8 | -25.7 | 39.3 | 49.5 | 29.6 | -35.1 | 49.3 | 64.7 |
| Without bars | 23.3 | -26.4 | 39.2 | 49.7 | 33.8 | -36.5 | 53.5 | 70.3 |
| Without septa | 24.6 | -21.3 | 32.4 | 45.9 | 41.9 | -41.9 | 66.2 | 83.8 |
| With no bars or septa | 67.5 | -49.1 | 85 | 116.6 | 72.8 | -89.8 | 126 | 162.6 |
| Ethmoid bone | | | | | | | | |
| Reference model | 42.7 | -40.3 | 61.5 | 83 | 92.1 | -138 | 174 | 230.1 |
| Postorbital ligaments | 98.7 | -85.5 | 137 | 184.2 | 117 | -173 | 214 | 290 |
| Without bars | 104 | -91.8 | 145 | 195.8 | 120 | -180 | 221 | 300 |
| Without septa | 27.7 | -16.6 | 37.6 | 44.3 | 135 | -185 | 242 | 320 |
| With no bars or septa | 227 | -122 | 269 | 349 | 176 | -258 | 332 | 434 |
| Postorbital bar | | | | | | | | |
| Reference model | 205 | -94.6 | 215 | 299.6 | 301 | -298 | 429 | 599 |
| Postorbital ligaments | 907 | -457 | 939 | 1364 | 548 | -554 | 756 | 1102 |
| Without bars |  |  |  |  |  |  |  |  |
| Without septa | 367 | -202 | 407 | 569 | 481 | -478 | 662 | 959 |
| With no bars or septa |  |  |  |  |  |  |  |  |
| Zygomatic arch | | | | | | | | |
| Reference model | 507 | -439 | 748 | 946 | 867 | -1270 | 1630 | 2137 |
| Postorbital ligaments | 714 | -620 | 1030 | 1334 | 1250 | -1590 | 2210 | 2840 |
| Without bars | 722 | -632 | 1040 | 1354 | 1260 | -1620 | 2240 | 2880 |
| Without septa | 541 | -455 | 778 | 996 | 827 | -1590 | 1770 | 2417 |
| With no bars or septa | 1110 | -937 | 1520 | 2047 | 1160 | -2270 | 2480 | 3430 |

**Table 8.1. (In previous page). Strain values (in με) for the different locations probed in the model for: maximum principal strain (S1), minimum principal strain (S3), von Mises strain and maximum shear strain, and under various conditions (reference model, substitution of the postorbital bars for ligaments, removal of the postorbital bars, removal of the postorbital septa, and removal of both the postorbital bars and septa). For the specific locations of the regions probed, see Figure 8.1. .**

| | S1 | S3 | von Mises Strain | Max Shear Strain |
|---|---|---|---|---|
| | Dorsal interorbital | | | |
| Reference model | 9.5 | -12.7 | 17.1 | 22.2 |
| Postorbital ligaments | 13.7 | -16.4 | 21.5 | 30.1 |
| Without bars | 14.5 | -17 | 22.4 | 31.5 |
| Without septa | 12.0 | -15.8 | 21.6 | 27.8 |
| With no bars or septa | 22.9 | -28.1 | 36.4 | 51 |

**Table 8.2. Strain values (in με) for the dorsal interorbital for: maximum principal strain (S1), minimum principal strain (S3), von Mises strain and maximum shear strain, and under various conditions.**

When considering deformation of the eye in the different models, Table 8.3 shows compression of the ocular orbit on the working side, with values generally following the trends observed in the cranium strains. The reference model experiences a 0.063% compression of the eye of the working side. The value increases but remains relatively unchanged after replacement of the bars for a ligament and complete removal of the bars. However, when the septa are removed (but not the bars), the deformation increases to 0.098%, and increases further to 0.17% when both the bars and septa are removed. While these are apparently very small values, the latter is an increase in diametral compression of 276% compared to the reference model. In contrast, the eye on the balancing side experiences a smaller compression during a normal M1 bite with the reference skull, but increasing tensile deformation for the modified models, up to 0.071%. It is also worth noting, though, that the tensile deformation in the balancing side is approximately half the compression experienced on the working side.

| Analysis | Working side | | Balancing side | |
|---|---|---|---|---|
| | DM  (mm) | % deformation | DM (mm) | % deformation |
| Reference model | -0.015127 | -0.063% | -0.001474 | -0.006% |
| Postorbital ligaments | -0.016222 | -0.068% | 0.001344 | 0.006% |
| Without bars | -0.016117 | -0.067% | 0.001812 | 0.008% |
| Without septa | -0.023576 | -0.098% | 0.000571 | 0.002% |
| With no bars or septa | -0.041759 | -0.174% | 0.016676 | 0.071% |

**Table 8.3. Deformation of the eyes of the reference and the different modified models. DM (diametral deformation). Negative values indicate compression of the eye; positive values indicate tension. The percentages changes are with respect to the initial eye diameter.**

Regarding distortion of the orbit, data from the two nodes at the inferolateral orbital angle of the skull was gathered from the reference model and the model with the septa removed (Table 8.4). Results show that the ratio of the distortion of the working and balancing sides is closest to one in the anteroposterior direction for both analyses, with the largest difference in the ratios of the mediolateral displacement. As indicated by the vertical ratio, the reference model has a more symmetrical displacement (closest to 1) than the model with the septa removed. There are also greater vertical and anteroposterior displacements in the balancing side than in the working side for both analyses.

| Inferolateral orbital node | Working side (WS) | | | Balancing side (BS) | | | Ratio (WS/BS) | | |
|---|---|---|---|---|---|---|---|---|---|
| | X | Y | Z | X | Y | Z | X | Y | Z |
| Reference model | 0.026 | -0.018 | -0.007 | 0.021 | -0.051 | -0.002 | 1.24 | 0.35 | 3.13 |
| No septa analysis | 0.031 | -0.013 | -0.012 | 0.024 | -0.067 | -0.007 | 1.30 | 0.19 | 1.67 |

**Table 8.4. Displacements of the node located at the inferolateral orbital angle, in millimetres. X: anteroposterior axis (positive displacements are towards the left (balancing) side; Y: vertical axis, Z: mediolateral axis (negative displacements are directed posteriorly).**

**8.4. Discussion**

The goal of this investigation was to evaluate the mechanical role of the postorbital bar and postorbital septum in the human cranium by assessing the effect of removing the structures or altering the mechanical properties of the tissues *in silico*, thus replicating configurations that are not possible to reproduce *in vivo*.

The results support the idea that in *Homo Sapiens* both the bars and the septa strengthen the orbits, protect the eye from distortion during unilateral biting and generally help to reduce strains in the various areas of the cranium where values were gathered, such as the zygomatic arches, the ethmoid bones and the postorbital bars (in the case of the septa). A more detailed discussion of these results follows.

*8.4.1. Effects in strain after removal of the postorbital bars and/or septa*

Nakashige *et al.* (2011) examined the role of the postorbital septum by performing FE analyses in the cranium of two macaques (*Macaca fascicularis*) and, in particular, tested the hypothesis that removal of the septa would result in an increase in the magnitude of strain in the regions of the supraorbital torus and the postorbital bars. They found minor strain increases in parts of the areas, but they did not correspond to the ones identified in the previous *in vivo* and *in vitro* experiments of Ross and Hylander (1996). Given that the magnitude of the strain in these regions was very low (see below for possible explanations), they concluded that the postorbital septa did not play a meaningful mechanical role supporting the orbital region in extant anthropoids.

In the case of the current human model, after removal of the postorbital septa there was no apparent strain increase in the supraorbital, but there was a noticeable increase in the postorbital bars, an occurrence previously observed by Ross and Hylander (1996). In fact, after examining the postorbital bars for the different scenarios studied here (Figure 8.4) it can be concluded that stress increases with removal of the postorbital septa, whether the postorbital bars are bony or replaced with a ligament.[4] This is observed in

---

[4] Heesy *et al.* (2006) considered the mechanical difference between large postorbital processes and full postorbital bars negligible. Therefore it must be noted than in the altered version of the human model, the length of the postorbital processes are minimal, as the whole postorbital bars were substituted for postorbital

both the working side and the balancing side. Moreover, elimination of the postorbital septa leads to a strain increase in the medial orbital wall of the working side, as well as in the zygomatic process of the frontal bone (Figure 8.2b).
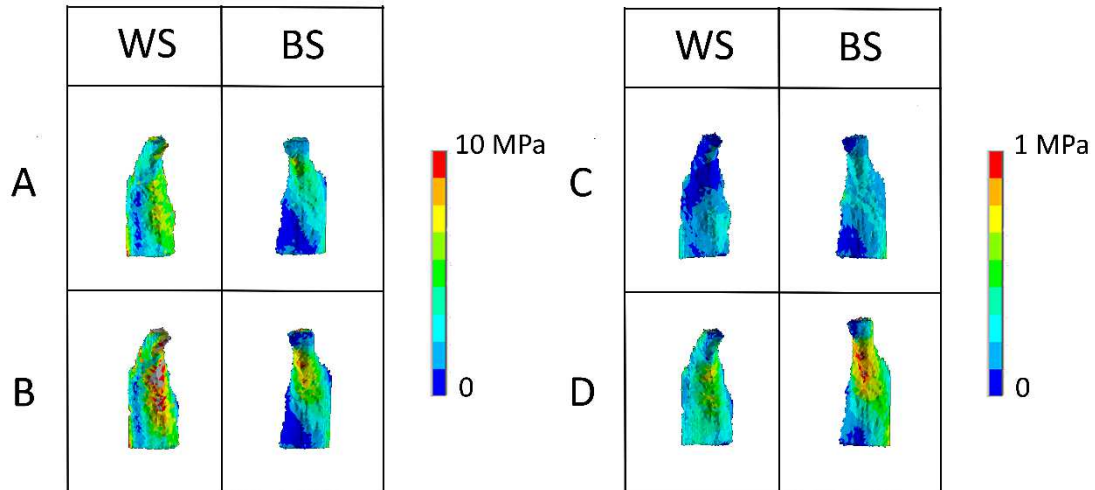


**Figure 8.4. Comparison of von Mises stress in the postorbital bar in frontal view. (a) reference model with intact postorbital bars and septa. (b) after removal of the postorbital septa. (c) simulation of the postorbital ligament in presence of the postorbital septa. (d) simulation of the postorbital ligament with absence of postorbital septa. WS corresponds to the right or working side and BS corresponds to left or balancing side.**

One of the hypothesis tested in Nakashige *et al.* (2011) was that the presence of postorbital septa helps to reduce deformation in the orbits when performing a unilateral bite, where the two sides of the skull deform in different manners as a consequence of their different loading conditions. To test this hypothesis, Nakashige *et al.* (2011) recorded the displacement of two nodes located in the inferolateral region of the orbit for both an intact skull and one in which the septa was removed, and calculated the ratios between working and balancing side displacements. Their results confirm the hypothesis, as the displacement ratios in the vertical axis were more asymmetrical (more different to

ligaments. Consequently, an increase in the length of the postorbital processes will alter these results, possibly reducing strain in the cranium in the same manner that closed postorbital bars do.

1) in their (macaque) model without the septa (Nakashige *et al.*, 2011; table 3).[5] This is also true for the human model examined here, with the ratio of the reference model closer to 1 (0.35) than in the analysis with the septa removed (0.19; see Table 8.4). In the current study, a greater vertical displacement is also observed in the balancing side (WS: -0.018 mm; BS: -0.051 mm for the reference model and WS: -0.013 mm; BS: -0.067 for the analysis with the septa removed), which was also predicted by Nakashige *et al.* (2011), but not confirmed in their results. Therefore, the current study supports the idea that the postorbital septum helps minimize asymmetrical deformation when the skull is subjected to unilateral loading of the molar teeth.

The results of our experiments differ from those from Nakashige *et al.* (2011) in the fact that we recorded higher values of strain overall. For example, in the postorbital bar of the working side in their model of a macaque skull before removal of the septa, their maximum shear strain value (93 µε) is noticeably lower than that observed in this human model (599 µε). However, Nakashige *et al.* (2011) refer to values as high as 194 µε from Ross (unpublished data) for the same location. The authors of the study observe that the macaque specimen had a more developed supraorbital torus and postorbital bars, hence explaining the discrepancy between their values and those provided by other studies. Therefore, a further explanation for this disparity between Nakashige *et al.* (2011) and the results from this study may simply be the fact that macaque skulls are more robust than those of humans.

Concerning the postorbital bar, Parisi (2010) observed a reduction in strain in the zygomatic arch after removal of the bars in *Eulemur fulvus* while simulating a unilateral first molar bite, but it was accompanied by an increase of strain in the orbital wall (Figure 8.5). In the current study, this does not lead to a reduction in strain in the zygomatic arch (Figure 8.2b and d), and a slight increase is observed along the body of the zygomatic bone. However, in agreement with Parisi (2010) strain increases are seen in the orbital wall, specifically in the lacrimal and the ethmoid bones of the working side.

---

[5] When comparing Nakashige *et al.* (2011) values with the ones in our study it should be bore in mind that the working side in our human model is the right one, while in in the macaque model the right side corresponds with the balancing side. Therefore, the Z axis (mediolateral) is inverted and positive displacements in the human model are towards the balancing side.
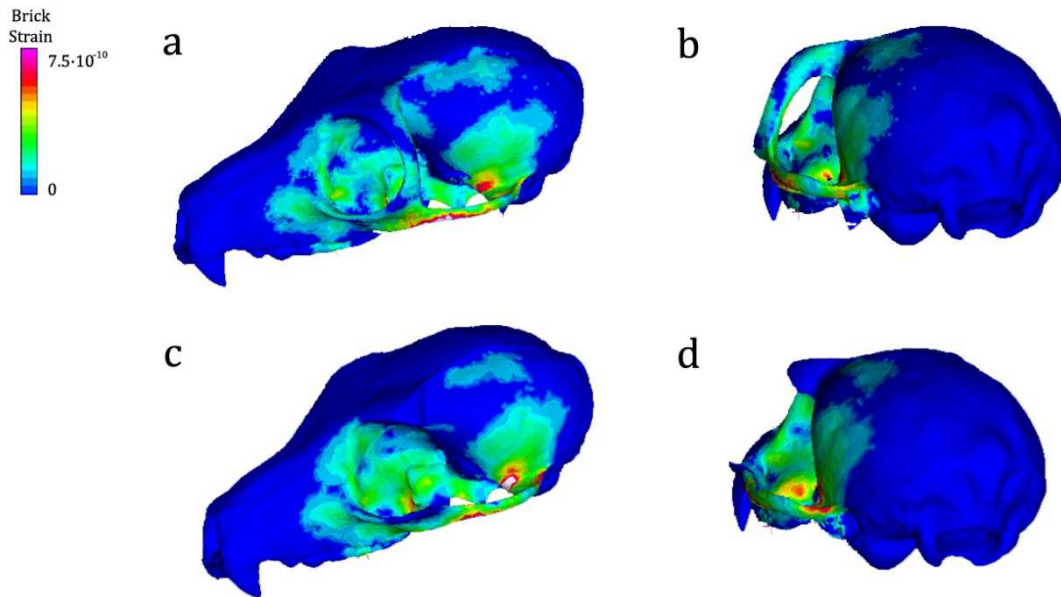
**Figure 8.5. (a, b): von Mises stress distribution from an *Eulemur fulvus* model. (c, d): The same model after removal of the postorbital bar. Adapted from Parisi (2010).**

Most FE models of anthropoids show high strains in the orbit, either during unilateral premolar or unilateral molar bites (see Ledogar *et al.* (2016) for modern humans or Smith *et al.* (2015) which includes FE models for *P. troglodytes*, *A. africanus* and *P. boisei*). It is worth noting that the orbital lamina of the ethmoid bone (also referred to as "lamina papyracea" due to its paper-thin configuration) is one of the most delicate structures in the skull and, together with the inferior wall of the orbit, fractures easily as a consequence of trauma (Song *et al.*, 2009; Figure 8.6). The orbital lamina, as opposed to the orbital floor, is strengthened by the presence of ethmoid air cells "which reinforce the medial wall like corrugated paper or a beehive" (Brady *et al.*, 2001). Given the fact that higher orbit strains in the reference model also occur in the ethmoid area, this biological reinforcement of the lamina papyracea may serve as a system to withstand forces generated during mastication. From the current results it seems clear that both the postorbital bars and septa also greatly help to reduce strain in this fragile area of the human skull.
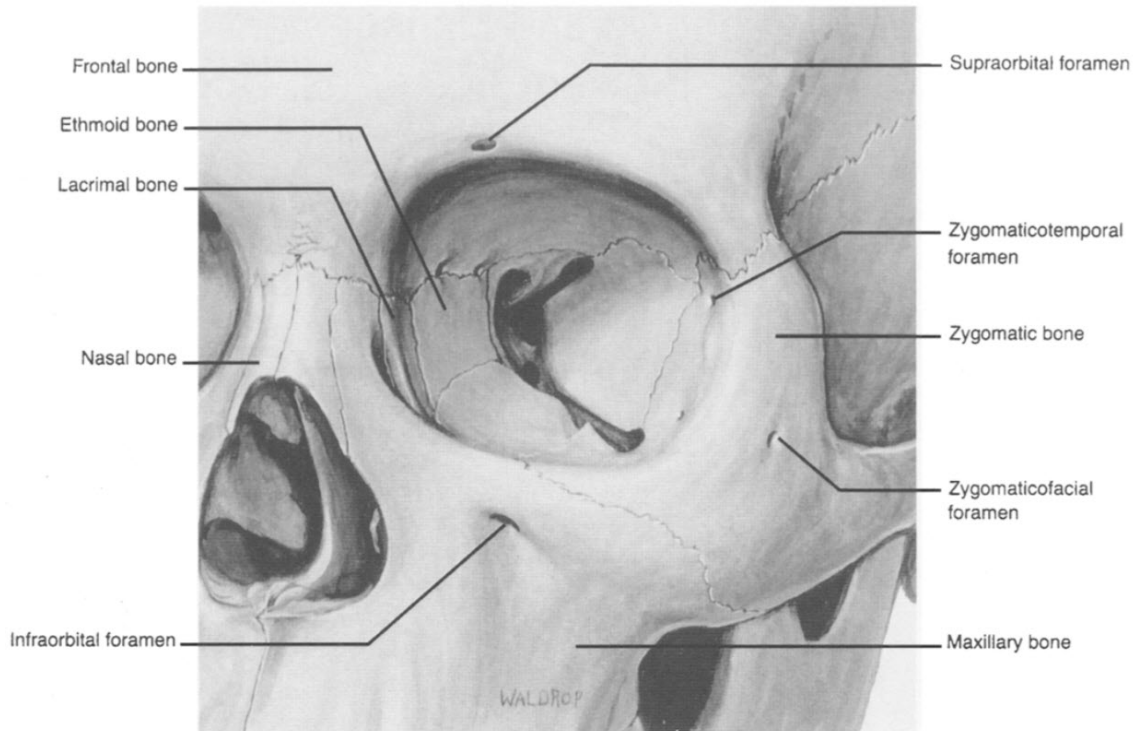
**Figure 8.6. Frontal view of the orbital bones (Brady *et al*., 2001, after Dutton, 1994).**

It would be premature to use these results to infer why the postorbital septum evolved in anthropoids, because the cranial geometry of basal anthropoids is different from those of extant species – both macaques (Nakashige *et al.*, 2011) and humans (this study). Nevertheless, the fact that removal of either the postorbital bar or the septum leads to an increase in strain in the same areas of the skull seems to suggest that they perform a similar mechanical role in protecting the medial aspect of the working side orbit from compression forces arising from mastication – although, of course, they may perform other roles as well. The effects are cumulative, and the removal of both bars and septa leads to a further increase in strain in the same regions mentioned. The postorbital bar has evolved independently multiple times, and because the septa is a secondary structure evolved only in anthropoids (and *Tarsius* in a lesser degree), it is not unreasonable to think that the latter may enhance the supporting role of the former. This suggestion seems to be supported by the results obtained by Ross and Hylander (1996), although the authors of that study and those of the more recent FE study by Nakashige *et al.* (2011) conclude that the postorbital septa no longer play a significant mechanical role in extant anthropoids.

### 8.4.2. Eye distortion and ocular stability

Distortion of the eye is also observed after removal of the postorbital bars and postorbital septa, particularly after removal of the latter. When removing both the bars and the septa, this distortion results in a 276% increase in compression of the eye in the working side (i.e. 0.174% of the eye diameter or 0.042 mm) and a corresponding vertical tension in the balancing side (of 0.071% or 0.016 mm). In reality, however, the tensile effect may not occur *in vivo*, because the model assumes a perfect connection between all materials, and hence the tissues supporting the eye may in fact separate, thereby relieving the tensile forces. Curiously, the removal of the bars does not produce as much compression as removal of the septa. Cartmill's hypothesis (1970, 1980) proposes that the increase in orbital convergence, as observed in Primates, would lead to vision distortion as a consequence of the action of the mastication muscles. This would, in turn, produce the eventual substitution of the postorbital ligament for an ossified postorbital bar, and also to the formation of a postorbital septum. The research of Heesy *et al.* (2006) suggests that the presence of the postorbital septum may help to alleviate displacements of the eyes, which our results also seem to confirm. From his study, Heesy and colleagues concluded that the presence of a postorbital bar and septum served as a way to avoid deformation of the orbit, as already suggested by Cartmill (1970), but by itself it was not sufficient to maintain the normal oculomotor function when mastication muscles were contracted. As a result, they also concluded that in order to avoid the effects of diplasia and oscillopsia, variations in the position of the eyes as a consequence of feeding were corrected by other mechanisms of the extraocular motor system that compensated for these displacements.

The results of this study demonstrate that, in humans, both structures help to protect the orbit and stiffen the lateral orbit walls, albeit to different degrees. There are, however, some caveats in our analyses that must be taken into account. Firstly, eyes are a complex structure with multiple interrelated parts, each one with different material properties (Aloy *et al.*, 2017). For the sake of this investigation, we created the eyes of the human model as a single structure with homogeneous material properties, following Schutte *et al.* (2006). In addition, as mentioned above, all materials were assumed to be perfectly connected which will fairly represent interfaces in compression, but not necessarily those that experience tension. The magnitudes of the deformation of the eyes in this model, therefore, may not be accurate compared to *in vivo* values. The same can be argued about the tissues that surround the eyes inside the orbit, which in our model

were regarded as generic soft tissues. In the future, the use of more detailed material properties would be necessary to fully address these questions.

## 8.5. Conclusions

In humans, the presence of both the postorbital bars and the postorbital septa protect the contents of the orbit and prevent distortion of the ocular globe when performing unilateral molar bites. A more detailed model, particularly one that takes into account the complexities of the ocular structures and its surrounding environment, may help to confirm these results in the future and also provide specific more accurate quantitative information about the nature of the deformation and the effects it may have in vision. At the same time, the bar and the septum in humans help reduce strain in other regions of the cranium. For example, the presence of the septa reduces strain in the postorbital bars, as was previously demonstrated by the experiments performed by Ross and Hylander (1996). Of particular interest is the fact that strain increases in the ethmoid area or "lamina papyracea" when the bars or the septa are removed. Since this is such a fragile region, it seems logical that the presence of these structures would help to dissipate strain in this particular area. Moreover, the postorbital septum also helps to minimize asymmetrical deformation between the working and balancing sides when performing a unilateral bite with the molar teeth.

Therefore, it can be concluded that, at least in the case of humans, both the postorbital bars and the postorbital septa serve as a system to protect the orbit and avoid eye distortion, but they also accomplish an important mechanical role in the cranium, helping to reduce strain in areas such as the zygomatic arches and the ethmoid bone; in some cases, decreasing it by a factor of four. However, these conclusions cannot be extended to other extant anthropoids or to infer evolutionary patterns based on these results. For the former, a more inclusive study will be necessary, one that analyses several extant anthropoid species within the same experimental framework. For the later, it would be necessary to perform analyses on models of basal anthropoids.

# Chapter 9. Discussion

This chapter presents an overview of all the work conducted throughout this thesis in which the results are discussed and put into a broader context, taking into account the current literature of the field. Given that all results from the analyses have already been discussed extensively in the previous chapters, only the major points will be presented and sometimes expanded here.

## 9.1. Comparative anatomy of the ossification of the dural folds and its role in cranial biomechanics

Chapter 3 and Chapter 5 present a new review and examination of dural ossification by considering questions that have remained largely unanswered since they were presented, first tangentially in Gordon Klintworth's paper about the anatomy and phylogeny of the tentorium cerebelli (1968) and then in more detail in several works by Takao Nojima (1988, 1990a, 1990b and 1990c). Chapter 3 discusses and collates all available references concerning the dural condition with many previously undescribed species, and confirms that ossification of the falx cerebri is shared by Ornithorhynchidae, some members of Ursidae, Otariidae, Phocidae and Odobenidae among Carnivora, Physeteridae, Ziphiidae, Delphinidae and Phocoenidae among Cetacea, Sirenia, and a single and dubious case found in a specimen of the genus Propithecus (Chapter 3, Figure 3.11; Grant Museum, sp. Z405). Ossification of the tentorium cerebelli is much more common, appearing as a trait in several members of marsupials and in Cetacea, in Xenarthra, in many primates, in almost all Carnivorans (with the sole exemption of Mephitidae), in Equidae, Tubulidentata, Pholidota, and in certain members of Artiodactyla (*Camelus dromedarius* and *Madoqua phillipsi*) and Rodentia (at least in Heteromyidae). The degree of ossification in each case, however, is extremely variable.

In light of these results, it is clear that ossification of the falx cerebri and/or the tentorium cerebelli has taken place independently at various times and in different lineages (Macrini *et al.*, 2007). However, despite presentation of over 250 extant species in one review for the first time (Appendix 1. Dural folds condition in extant species) and many other extinct ones, there are still many phylogenetic gaps and many genus for which

the condition of the falx cerebri and the tentorium cerebelli is unknown. Given the elusive nature of ossification, which in some cases may be associated with external causes, observation of a single specimen for each species or genus is probably not enough, so a study with a larger scope in mind would be necessary to reconstruct an evolutionary story of the condition.

Concerning the origin and nature of the ossification, two main hypotheses were considered in this work. Although both of them have already been examined and disregarded by Nojima in the past (1988; 1990a; 1990c), the current advances in the field and the new body of work compiled here justified a second consideration.

The first hypothesis proposed that postnatal dural fold ossification may be related with either a high dietary intake of food rich in calcium, phosphorus and vitamin D, such as is the case in some species of Cetacea (Nojima, 1988), or a diet poor in vitamin A because there is some evidence that vitamin A deficiency causes cranial bone thickening (Chandra *et al.*, 1999; Hartley *et al.*, 2005, and many others), thickening of the soft dura mater (Gallina *et al.*, 1970; Van der Lugt and Prozesky, 1989) and at least one instance in which it produced ossification in a previous unossofied tentorium cerebelli (Jubb *et al.*, 1993). This hypothesis was disregarded partly because pathologies associated with hipervitaminosis D and hypovitaminosis A do not seem compatible with anatomical descriptions of postnatally-developed dural folds. In humans, dural fold ossification has been better studied, and a link has been established between hipervitaminosis D and dural ossification (DeWind, 1960; Schey, 1974; Davies *et al*., 1986), but it normally appears as disconnected patches of bone, and not continuous or complete as is the case in Delphinidae or Phocoenidae. On the other hand, hypovitaminosis A in felids and other mammals, does not merely produce thickening of the tentorium, but is frequently joined by alterations in other bones of the skull, the mandible and the cervical vertebrae. Moreover, hypovitaminosis A causes further medical problems, such as lack of coordination, convulsions and blindness (Bartsch *et al.*, 1975; Gross-Tsubery *et al.*, 2010) which are not observed in species in which postnatal ossification of the dural folds appears to be commonplace.

The second hypothesis proposes a link between ossification and behavioural causes, perhaps suggesting a functional role, either due to locomotion (for example, hopping or bounding), speed, or as a consequence of inhabiting an aquatic or semiaquatic environment. After careful consideration, none of these possibilities seem to have enough

support to withstand closer scrutiny. Although various groups with an osseous falx or tentorium seem to share some of these traits, there are many counterexamples that also must be taken into consideration.

An obvious scenario of this hypothesis is the idea that ossification, particularly ossification of the tentorium cerebelli in Carnivorans, may be related with biting or feeding behaviour. This is reinforced by the fact that many mammals that have occupied predatorial niches share the same trait (not only Carnivora, but some Marsupials, such as the recently extinct thylacine, and much older members of the Order Creodonta) initially supporting the possibility that the osseous tentorium in these groups could represent a case of morphological convergence. This was put to test by simulating various intrinsic and extrinsic biting regimes, both unilateral and bilateral, in an FE model of a common household cat (*Felis silvestris catus*), varying the material properties of both the falx cerebri and the tentorium cerebelli to represent the ossified and the unossified structures. Chapter 4 describes the creation of such a model, which also takes into consideration the neck muscles for the extrinsic biting regimes, and Chapter 5 presents the boundary conditions applied, the analyses performed, and the results obtained.

These results showed that changing the material properties to simulate the ossified falx and tentorium does indeed lead to a substantial reduction in the von Mises stress in the structures themselves, but it has a much more modest effect in the cranium as a whole. The ossified falx cerebri does not have any visible effect in the stress patterns, and differences between models with ossified and non-ossified tentoria were restricted to the posterior area of the cranium: in the parietal and temporal, including the tympanic bulla. This localised reduction of stress may suggest that the tentorium plays a minor role during biting, but all intrinsic and extrinsic analyses were consistent in reproducing this reduction of von Mises stress, perhaps indicating as well that ossification is not related to the forces exerted by struggling prey or in the action of tearing a carcass.

## 9.2. The role of the postorbital bars, ligaments and septa in the human cranium

In Chapter 8 the biomechanical roles of the postorbital bars, the postorbital ligaments and the postorbital septa during unilateral molar biting in a *Homo sapiens* skull were analysed. This was achieved by removing the structures of interest and comparing the results to the ones performed with the cranium intact by examining the changes in von Mises strain.

The postorbital bar has evolved independently multiple times in various taxa and is present in all primates, but the previous state of the structure is an osseous postorbital process completed with a postorbital ligament (Heesy, 2005; Smith *et al*., 2013). The postorbital septa, which separates the temporal fossa from the orbit, is a secondary osseous structure that has only evolved in anthropoids, and *Tarsius* in a lesser grade (Cartmill, 1980).

So far, several hypotheses (summarized in Chapter 2) have been proposed to explain the mechanical role of these structures. According to the results of the FE analyses performed in this project, the bars and the septa collaborate to reduce strains in several areas of the *Homo sapiens* cranium. Removal of the septa also has the effect of increasing strain in the postorbital bars, both in the working side and in the balancing side, and in the medial orbital wall of the working side and the zygomatic process of the frontal bone. The presence of the septa also strengthens the orbits and protects the eye from distortion during unilateral biting, confirming previous results by Nakashige *et al* (2011). Moreover, in the human head model, the septa minimizes the asymmetrical deformation arising from a molar bite and reduces the distortion of the eye, an effect that also takes place with the removal of the postorbital bars, albeit their contribution is much less. In *Homo sapiens*, therefore, it seems that the septa, and the bars, although in a lesser degree, protect the orbit and stiffen the lateral orbit walls, but these results must be treated cautiously, among other factors because of the simplified manner in which the eyes were modelled.

Removal of the postorbital bars while maintaining the septa has similar effects in the human head model. An increase in strain is observed in the lacrimal, the ethmoid and the body of the zygomatic bone, as well as the septum. After replacing the postorbital bars with ligaments, strain increases more in all these areas and peak strains appear in the lacrimal and ethmoid bones of the working side. Removing both the bars and the septa increase strain even more, in what it looks like a cumulative effect. The highest strain values are observed in the zygomatic arches, reaching 1520 µɛ in the balancing side and 2480 µɛ in the working side. Moreover, the ethmoid bone, which experiences 4.4 times the strain in the balancing side and 2.3 times in the working side (compared to the reference model) with von Mises strain values of 269 µɛ and 332 µɛ respectively), is a region particularly fragile of the human skull (Brady *et al.*, 2001; Song *et al.*, 2009), and both the bars and the septa seem to aid in the protection of this delicate area.

## 9.3. Improving the accuracy of digital finite element models

One of the main aims of this project was to test a wide range of different anatomical structures that have been either neglected from previous finite element models or whose effects in the results are not completely understood or sufficiently studied yet. The purpose of this was to help establish the level of detail that needs to be included in FE models of the cranium.

The research has confirmed that some of the structures studied does not appear to impact the general von Mises stress or strain patterns of the cranium significantly, as is the case of the dura mater that encloses the brain (Chapter 4), the falx cerebri (Chapter 5) and the periodontal ligament (Chapter 6) in the *Felis silvestris catus* model, and the bulk soft tissues (Chapter 7) included in the *Homo sapiens* model. However, even in these cases, the results must be treated with caution and the nature and focus of each analysis considered carefully, also bearing in mind that different geometries may produce different results. For example, not modelling the PDL has a localised effect on the surrounding alveolar region of the *Felis silvestris catus* model. This may not be important in a study that is only concerned with global stresses across the skull (as in Wood *et al.* 2011 or the research carried out in Chapter 5), but could be of great importance in a different study that considers the mandible and not the cranium (such as Gröning *et al.*, 2011). Moreover, in certain species, such as extinct sabre-toothed cats, the large depth of the tooth sockets may well be expected to modify the stress and strain fields if the PDL is not included, so different species may require different strategies and further testing. In the same sense, the inclusion of the bulk soft tissues that surround the cranium may be irrelevant for most mammalian species, but it still remains to be confirmed if that is the case in species with either dermal plates or high elastic module skins, such as some fishes, amphibians or reptiles.

On the other hand, the tests performed in Chapter 6 seem to confirm that both the nasal turbinates and the osseous part of the nasal septum do indeed influence the results obtained in FE analyses, and their omission produces unnatural high stresses in the cranium overall. This is true in particular in the palatine and surrounding areas, and in the maxilla and in the temporal bone, but, at the same time, a decrease in stress is observed in the anterior area of the palatine as well as in other parts of the zygomatic bone and the maxilla. While it is expected that the septum can easily be modelled with the rest of the bones of the skull, this is not the case for the turbinates, because of the time-consuming

segmentation process to extract their geometry and the difficulties in fully capturing their complexity in the first place (as is the case with the struts of trabecular bone). For example, the nasal turbinates were not included in studies by Dumont *et al.* (2011) in the models of a saddleback tamarin (*Saguinus fuscicollis*) and a common marmoset (*Callithrix jacchus*), or in Dzialo *et al.* (2014) in a model of a common chimpanzee (*Pan troglodytes*).

Additionally, the current study examined two further aspects in the FE models: a simple muscle wrapping technique with the superficial temporalis of the *Felis silvestris catus* skull (Chapter 4 and Chapter 5) and the scaling down of the muscle forces in the human head skull (Chapter 7). Muscle wrapping has been applied in other studies before (Grosse *et al.*, 2007; Curtis *et al.*, 2008; Liu *et al.*, 2012) and found to result in a slight reduction in peak stress, but not altering the general stress patterns of the skull. In the analyses performed for this project, the patterns of stress also remained largely unchanged, but the reduction of peak stresses was not observed.

In contrast, the comparison between unscaled (all fully activated) and scaled (physiologically activated) muscle forces in the *Homo sapiens* FE head model, did reveal important differences. For example, total bite force was reduced by about a third (from 979.2 N to 625 N) for unilateral biting at the first molar and, logically, strain was also reduced considerably in both the working side and the balancing side. This indicates that simple application of maximum muscle forces does not completely replicate in vivo conditions accurately as it may produce variations in the magnitude and/or distribution of strain, and realistic, scaled (physiologically representative) muscle forces should be applied when possible.

Finally, although the results concerning the postorbital ligaments, bars and septa have been already discussed in this chapter, it should be noted that they may also be of importance when taking account of intraspecific variation. For example, although the most usual condition in the *Felis silvestris catus* species is the presence of postorbital processes with pairing postorbital ligaments, these processes can, on certain specimens, close into complete postorbital bars (a specimen with this characteristics was described by Heesy *et al.*, 2007 and is not, by any means, an exceptionally abnormal condition). Results obtained in Chapter 8 in the *Homo sapiens* head model seem to suggest that, at least in the geometry of a human cranium, the presence of postorbital bars helps reduce strain more effectively than the combination of the postorbital processes and postorbital

ligaments (but see Heesy *et al.*, 2007). Although nowadays intraspecific variation is rarely considered in vertebrate finite element studies (Bright, 2014), the increasing ease in the FE model creation process does facilitate studies with multiple specimens of the same species, and therefore assessment of intraspecific variation will probably become more widespread in the near future.

## 9.4. Research shortcomings: Validation, material properties and other caveats

Biological tissues behave in an extremely complex manner (Godinho *et al*., 2017). In fact, "most soft tissues exhibit a nonlinear, inelastic, heterogeneous, anisotropic character that varies from point to point, from time to time and from individual to individual" (Humphrey, 2003). As a consequence, it is often difficult for researchers to access accurate and reliable details of the mechanical properties of the materials they simulate. This applies to bone, as well as other biological tissue such as some of the ones used in the models of this thesis. Moreover, there is no data available for the great majority of extant vertebrate species. A good example of this difficulty is the extreme variation in the Young's modulus values of the periodontal ligament reported in other studies, which range between 0.01 to 1750 MPa (Fill *et al.*, 2011; see Chapter 6). To mitigate uncertainty in material properties in the current project, careful sensitivity tests were undertaken for the following materials: dura mater, periodontal ligament and both the internal and external bulk soft tissues (see Chapter 5 and Chapter 7).

Uncertainty in the definition of material properties can be tested and partially resolved through validation of the models via experimental studies. Although desirable, it is very difficult, sometimes impossible (as in the case of fossils or due to ethical issues), to test mechanical properties in biological specimens, so researchers frequently rely on hypotheses about the material properties of a given model (Gil Espert *et al.*, 2015; Toro-Ibacache *et al.*, 2016). In fact, FE validation studies are rarely carried out. Five years ago, according to Bright (2014), with the exception of primate species, they had only been performed in alligators, pigs, elephants, ostriches and finches. To the best of my knowledge, no validation studies in Felid species are currently available and, although a great effort was put into obtaining fresh specimens from various sources including veterinary practices and animal shelters to perform post-mortem *in vitro* experiments, none of them ultimately provided a specimen. For this reason, special attention was paid

to sensitivity tests to alleviate the lack of specific data for the *Felis silvestris catus* model and the opportunity to undertake comparative experimental studies.

Of course, even when data are indeed available, they will be subject-specific and may rely on further assumptions, for example in post-mortem experiments when replicating the action of physiological loadings, or in *in vivo* experiments when deciding in which areas to capture strain data. Digital Speckle Pattern Interferometry (DSPI) partly overcomes this limitation by sampling over a larger area, but still only a small fraction of the specimen is sampled (Toro-Ibacache *et al.*, 2016).

Bone, which is necessarily considered in all studies of cranial biomechanics while other tissues and structures such as some of the ones included in this project are frequently ignored, it is a heterogeneous material (with varying properties across the skull and varying proportions of cortical and trabecular bone) and anisotropic (with properties that vary with orientation). In addition, the overall shape of a bone and its curvature may vary, subtly changing the orientation of the primary material property axes (Strait *et al*., 2005).

Nonetheless, most biomechanical studies assume cranial bone has homogeneous, isotropic and linear elastic material properties (for example: Grosse *et al*., 2007; Wroe *et al.*, 2010; Dumont *et al.*, 2011, Nakashige *et al.*, 2011; Curtis *et al.*, 2011; Gröning *et al.*, 2011; Wang *et al.*, 2012; Oldfield *et al.*, 2012; Cox *et al.*, 2015; McCurry *et al.*, 2015; Fortuny *et al.*, 2016; but there are many others). This simplification has been assumed with other biological tissues as well, as indeed it has the current study. For example, the dura mater (Takhounts *et al.*, 2003; Cai *et al.*, 2018), the articular disk (Beek *et al.*, 2000; Commisso *et al.*, 2015), the bulk soft tissues (Huempfner-Hierl *et al.*, 2015) or the periodontal ligament (Gröning *et al.*, 2011). The implications of this assumption are rarely tested, although Wood *et al.* (2011) investigated the effect of modelling the PDL with hyperelastic or viscoelastic properties and demonstrated that, as far as stresses and strains were concerned, differences with linear elastic properties, such as the one used in Chapter 6, were undiscernible. Although sensitivity studies comparing structures with linear and nonlinear elastic properties would have been desirable in the current research, they were outside the scope of this project. The nonlinear models reviewed in Section 2.6 either consider a single structure, so they are interested in local stresses rather than general cranial loading patterns, or are focused on assessing the effects of traumatic brain injuries. As discussed in Chapter 5, the higher strain rates that occur in vehicle crashes or sports injuries make the use nonlinear solutions more important than in biting analyses, where

much lower strain rates are involved. It also must be borne in mind that models created for testing trauma are, in general, much less detailed (with fewer elements) than those used to assess functional morphology, and therefore the inclusion of nonlinearity has a less pronounced impact in the solution phase.

One of the first studies to investigate the effect of simplifications in digital FE models of crania, and perhaps the most widely cited by researchers, was the work of Strait *et al.* (2005), in which they performed various sensitivity analyses using a skull model of a *Macaca fascicularis*. From their results they concluded that: (i) models with isotropic and linear bone properties can be used confidently to assess the general distribution of stress or strain, but (ii) the results must be treated with caution if absolute values are required. The first part of the assertion is supported by Porro *et al.* (2013) in a model of a mandible of *Alligator mississippiensis*, by Gil Espert *et al.* (2015) in models of bovine mandibles and by Toro-Ibacache *et al.* (2016) and Godinho *et al*. (2017) in human crania. Most of the analyses performed in this current research are comparative, involving an assessment of the effects of alterations or inclusion/exclusion of various tissues and structures, and hence can be viewed with confidence. The second part of the assertion is again supported by Porro *et al.* (2013) and Godinho *et al.* (2017) who found that absolute strain magnitudes were higher and lower in their respective FE models compared to their experimental counterparts.[6] Therefore, absolute values of stress or strain presented in this thesis should be treated with caution. For example, the strain values for the postorbital bars in Chapter 8 can be used with confidence in a comparison between the different human models, but not to investigate questions related with bone remodelling.

Other limitations of the modelling process have been explicitly stated and discussed in the corresponding chapters. These include the brain material in the endocranial cavity in *Felis silvestris catus*, which should not be used to investigate the strains in the brain, since it is connected directly to the bone, thus making its surface oversensitive to changes in bone strain (Chapter 5 and Chapter 6). In a similar manner, the tensional forces distorting the eye in the *Homo sapiens* model (Chapter 8) may not be an accurate representation of reality, given the perfect connection between the materials

---

[6] In contrast, however, Rayfield (2011) found good correlation even in strain orientation and magnitude between *in vitro* and *in silico* experiments performed over ostriches jaws, although the geometry of the models and loads applied were simpler in that case.

of the eyes and the supporting soft tissues in the model, which *in vivo* might separate from the eye to relieve these tensional forces.

# Chapter 10. Conclusions and future work

## 10.1. Conclusions

The aim of this research was to investigate various elements and structures of the mammalian head whose effects remain insufficiently studied in finite element analyses. The work contributed to a larger project focused on the biomechanical role of cranial soft tissues in both reptiles and mammals. Such structures were considered both in terms of their functional role and as part of the general functioning of the FE model that included them, i.e. to assess if they alter the general results of the analyses in a significant manner and therefore if they should be modelled even in studies which aim to test hypotheses unrelated with those structures.

With this main objective in mind, two multi-purpose FE models were used, each with the intention of answering specific questions. The first was a model of a *Felis silvestris catus*, the second a model of *Homo sapiens*. After performing the corresponding investigations and analyses, the key findings of this thesis are summarized below:

- Previous hypotheses concerning ossification of the falx cerebri and/or the tentorium cerebelli in various lineages of mammals still lack support today after analysing them under the light of new findings. The causes of ossification and its possible mechanical role are currently largely unknown.

- In the cranium of a *Felis silvestris catus*, the osseous tentorium seems to play a minor and localised role in reducing stress in the parietal and temporal bones during feeding activities. These effects were consistent across several different analyses, irrespective of loading regime.

- The modelling of the PDL and the variation of its material properties has a localised effect in the alveolar region but do not alter the general pattern of stress in the *Felis silvestris catus* cranium.

- The inclusion of generic bulk soft tissues in FE models do not have a meaningful effect in the results. Stress is reduced as the elastic modulus of the bulk soft tissues increases, but it remains to be tested whether they may have a more significant role in species with thicker or stiffer skins, or with different arrangements of soft tissues.

- In contrast, it is advisable to include the nasal turbinates and/or the osseous part of the nasal septum in future FE models. The *omission* of either of these structures leads to a general increase in stress, not only confined to the rostral and palatal areas, but extending posteriorly in the skull, in combination with a (smaller) decrease in stress in the palatine, rostrum and zygomatic regions.

- In the *Homo sapiens* model, both the postorbital bars and the postorbital septa protect the contents of the orbit and prevent distortion of the ocular globe when performing unilateral molar bites, while also reducing strain in other areas of the cranium.

- The presence of the postorbital septa reduce strain in the postorbital bars and minimize asymmetric deformation between the working and balancing sides in unilateral molar bites.

## 10.2. Future work

This study has provided one of the first insights into the modelling of some biological structures usually neglected in FE analyses of skulls. The complexity of FE models will undoubtedly increase in the future, and the modelling of structures other than bone, particularly other soft tissues of the head, will gradually become more common. More sensitivity studies are necessary to assess how anisotropy and nonlinearity affects the results of FE analyses, but at the same time, more experimental data are urgently needed to provide the validation of these and other studies.

Concerning the causes of ossification of the dural folds and the assessment of its mechanical role, there are several directions in which further research may be useful in the future. To start with, there are many gaps in our knowledge of falx and tentorial ossification in multiple mammal lineages, and many species where our current knowledge is based on examination of a single specimen. Therefore, in order to perform statistical analyses or attempt to reconstruct phylogenetic trees, for example, it is important to widen our knowledge in this area. Ideally, this would be complemented not only with the study of osseous specimens, but with the observation of full ontogenetical sequences and even with experimental work. Moreover, to confirm that the osseous tentorium cerebelli has a role in the reduction of the stress in the back of the skull in Carnivora during biting, other FE analyses must be carried out. This would allow not only the hypothesis to be tested

further, but also different cranial geometries and different tentorial ossifications and configurations to be examined. More accurate modelling of the brain, and in particular the brain-skull interface, is also necessary in order to gather data from this structure, because one of the main functions of the falx and the tentorium are to support and hold the brain in place.

Finally, in order to verify the hypotheses about the origins of the septa, the reason why they evolved and their mechanical role, future FE studies need to focus on models of extinct basal anthropoids. In the same way, to further assess the function of the combination of the postorbital process and postorbital ligament it is important to test this arrangement in mammalian species other than *Homo*.

# References

Abensperg-Traun, M. & Boer, E.D. 1992, "The foraging ecology of a termite-and ant-eating specialist, the echidna Tachyglossus aculeatus (Monotremata: Tachyglossidae)", *Journal of Zoology,* vol. 226, no. 2, pp. 243-257.

Adeeb, N., Deep, A., Griessenauer, C.J., Mortazavi, M.M., Watanabe, K., Loukas, M., Tubbs, R.S. & Cohen-Gadol, A.A. 2013, "The intracranial arachnoid mater", *Child's Nervous System,* vol. 29, no. 1, pp. 17-33.

Adeeb, N., Mortazavi, M.M., Tubbs, R.S. & Cohen-Gadol, A.A. 2012, "The cranial dura mater: a review of its history, embryology, and anatomy", *Child's Nervous System,* vol. 28, no. 6, pp. 827-837.

Aiello, L. & Dean, C. 1990, *An introduction to human evolutionary anatomy,* London, Academic Press.

Al Dayeh, A.A., Rafferty, K.L., Egbert, M. & Herring, S.W. 2009, "Deformation of nasal septal cartilage during mastication", *Journal of Morphology,* vol. 270, no. 10, pp. 1209-1218.

Aloy, M., Adsuara, J., Cerdá-Durán, P., Obergaulinger, M., Esteve-Taboada, J., Ferrer-Blasco, T. & Montés-Micó, R. 2017, "Estimation of the mechanical properties of the eye through the study of its vibrational modes", *PloS One,* vol. 12, no. 9, pp. 1-19.

Al-Sagair, O. & ElMougy, S. 2002, "Post-natal Development in the Linear and Tric Morphometrics of the Camelidae Skull", *Anatomia, Histologia, Embryologia,* vol. 31, no. 4, pp. 232-236.

Anderson, P.S., Bright, J.A., Gill, P.G., Palmer, C. & Rayfield, E.J. 2011, "Models in palaeontological functional analysis", *Biology Letters,* vol. 8, no. 1, pp. 119-122.

Bachinger, M., Zerbi, V., Moisa, M., Polania, R., Liu, Q., Mantini, D., Ruff, C. & Wenderoth, N. 2017, "Concurrent tACS-fMRI Reveals Causal Influence of Power Synchronized Neural Activity on Resting State fMRI Connectivity", *The Journal of*

*Neuroscience : the official journal of the Society for Neuroscience,* vol. 37, no. 18, pp. 4766-4777.

Barak, M.M., Geiger, S., Chattah, N.L., Shahar, R. & Weiner, S. 2009, "Enamel dictates whole tooth deformation: a finite element model study validated by a metrology method", *Journal of Structural Biology,* vol. 168, no. 3, pp. 511-520.

Barbarino, G., Jabareen, M., Trzewik, J., Nkengne, A., Stamatas, G. & Mazza, E. 2009, "Development and validation of a three-dimensional finite element model of the face", *Journal of Biomechanical Engineering,* vol. 131, no. 4, pp. (041006)1-11.

Bartsch, R.C., Imes, G.D., Jr & Smit, J.P. 1975, "Vitamin A deficiency in the captive African lion cub Panthera loe (Linnaeus, 1758)", *The Onderstepoort Journal of Veterinary Research,* vol. 42, no. 2, pp. 43-54.

Bath-Balogh, M., Fehrenbach, M.J. & Thomas, P. 1997, *Illustrated dental embryology, histology, and anatomy,* Philadelphia, Saunders.

Batnitzky, S., Powers, J. & Schechter, M. 1974, "Falx "calcification"– Does this exist?", *Neuroradiology,* vol. 7, no. 5, pp. 255-260.

Beek, M., Koolstra, J., Van Ruijven, L. & Van Eijden, T. 2000, "Three-dimensional finite element analysis of the human temporomandibular joint disc", *Journal of Biomechanics,* vol. 33, no. 3, pp. 307-316.

Behrendorff, L., Leung, L.K., McKinnon, A., Hanger, J., Belonje, G., Tapply, J., Jones, D. & Allen, B.L. 2016, "Insects for breakfast and whales for dinner: the diet and body condition of dingoes on Fraser Island (K'gari)", *Scientific Reports,* vol. 6, pp. 1-12.

Bekerman, I., Gottlieb, P. & Vaiman, M. 2014, "Variations in eyeball diameters of the healthy adults", *Journal of Ophthalmology,* vol. 2014, pp. 1-5.

Benton, M. 2005, *Vertebrate palaeontology,* Oxford, Blackwell Publishing.

Bermejo, A., Gonzalez, O. & Gonzalez, J. 1993, "The pig as an animal model for experimentation on the temporomandibular articular complex", *Oral Surgery, Oral Medicine, Oral Pathology,* vol. 75, no. 1, pp. 18-23.

Boddy, A., McGowen, M., Sherwood, C., Grossman, L., Goodman, M. & Wildman, D. 2012, "Comparative analysis of encephalization in mammals reveals relaxed constraints on anthropoid primate and cetacean brain scaling", *Journal of Evolutionary Biology,* vol. 25, no. 5, pp. 981-994.

Boessenecker, R.W., Perry, F.A. & Geisler, J.H. 2015, "Globicephaline whales from the Mio-Pliocene Purisima Formation of central California, USA", *Acta Palaeontologica Polonica,* vol. 60, no. 1, pp. 113-123.

Bradshaw, D., Ivarsson, J., Morfey, C. & Viano, D.C. 2001, "Simulation of acute subdural hematoma and diffuse axonal injury in coronal head impact", *Journal of Biomechanics,* vol. 34, no. 1, pp. 85-94.

Bradshaw, J.W. 2006, "The evolutionary basis for the feeding behavior of domestic dogs (Canis familiaris) and cats (Felis catus)", *The Journal of Nutrition,* vol. 136, no. 7 Suppl, pp. 1927S-1931S.

Brady, S.M., McMann, M.A., Mazzoli, R.A., Bushley, D.M., Ainbinder, D.J. & Carroll, R.B. 2001, "The diagnosis and management of orbital blowout fractures: update 2001", *The American Journal of Emergency Medicine,* vol. 19, no. 2, pp. 147-154.

Brichtová, E., Jiroušek, O. & Gál, P. 2009, "Finite element model of the human head validated by the reconstruction of a real child sport accident", *Scripta Medica,* vol. 82, no. 3, pp. 175.

Bright, J.A. 2014, "A review of paleontological finite element models and their validity", *Journal of Paleontology,* vol. 88, no. 4, pp. 760-769.

Bright, J.A. 2012, "The importance of craniofacial sutures in biomechanical finite element models of the domestic pig", *PLOS One,* vol. 7, no. 2, pp. 1-12.

Bright, J.A. & Rayfield, E.J. 2011, "The response of cranial biomechanical finite element models to variations in mesh density", *The Anatomical Record,* vol. 294, no. 4, pp. 610-620.

Broughton, M. & Fyfe, G.M. 2013, "The superficial musculoaponeurotic system of the face: a model explored", *Anatomy Research International,* vol. 2013, pp. 1-5.

Bruner, E. 2004, "Geometric morphometrics and paleoneurology: brain shape evolution in the genus Homo", *Journal of Human Evolution,* vol. 47, no. 5, pp. 279-303.

Bryant, H.N. 1991, "Phylogenetic relationships and systematics of the Nimravidae (Carnivora)", *Journal of Mammalogy,* vol. 72, no. 1, pp. 56-78.

Bryant, H.N., Russell, A.P. & Fitch, W.D. 1993, "Phylogenetic relationships within the extant Mustelidae (Carnivora): appraisal of the cladistic status of the Simpsonian subfamilies", *Zoological Journal of the Linnean Society,* vol. 108, no. 4, pp. 301-334.

Buckland-Wright, J. 1978, "Bone structure and the patterns of force transmission in the cat skull (Felis catus)", *Journal of Morphology,* vol. 155, no. 1, pp. 35-61.

Bull, J.W. 1969, "Tentorium cerebelli", *Proceedings of the Royal Society of Medicine,* vol. 62, no. 12, pp. 1301-1310.

Burgin, C.J., Colella, J.P., Kahn, P.L. & Upham, N.S. 2018, "How many species of mammals are there?", *Journal of Mammalogy,* vol. 99, no. 1, pp. 1-14.

Butler, P., Mitchell, A.W. & Ellis, H. 1999, *Applied radiological anatomy,* Cambridge, Cambridge University Press.

Cabana, F., Plowman, A., Van Nguyen, T., Chin, S., Wu, S., Lo, H., Watabe, H. & Yamamoto, F. 2017, "Feeding Asian pangolins: An assessment of current diets fed in institutions worldwide", *Zoo Biology,* vol. 36, no. 4, pp. 298-305.

Cai, Z., Xia, Y., Bao, Z. & Mao, H. 2019, "Creating a human head finite element model using a multi-block approach for predicting skull response and brain pressure",

*Computer Methods in Biomechanics and Biomedical Engineering,* vol. 22, no. 2, pp. 169-179.

Camens, A.B. 2010, "Were early Tertiary monotremes really all aquatic? Inferring paleobiology and phylogeny from a depauperate fossil record", *Proceedings of the National Academy of Sciences of the United States of America,* vol. 107, no. 4, pp. E12; author reply E13.

Cartmill, M. 1980, "Morphology, function, and evolution of the anthropoid postorbital septum" in *Evolutionary biology of the New World monkeys and continental drift* Springer, New York, pp. 243-274.

Cartmill, M. 1970, "The orbits of arboreal mammals: a reassessment of the arboreal theory of primate evolution", Ph.D. Thesis. The University of Chicago.

Chamoli, U. & Wroe, S. 2011, "Allometry in the distribution of material properties and geometry of the felid skull: Why larger species may need to change and how they may achieve it", *Journal of Theoretical Biology,* vol. 283, no. 1, pp. 217-226.

Chandra, A.S., Papendick, R.E., Schumacher, J., Homer, B.L. & Wollenman, P. 1999, "Cerebellar herniation in captive lions (Panthera leo)", *Journal of Veterinary Diagnostic Investigation,* vol. 11, no. 5, pp. 465-468.

Chen, Y. & Ostoja-Starzewski, M. 2010, "MRI-based finite element modeling of head trauma: spherically focusing shear waves", *Acta Mechanica,* vol. 213, no. 1-2, pp. 155-167.

Christiansen, P. 2008, "Evolution of skull and mandible shape in cats (Carnivora: Felidae)", *PLoS One,* vol. 3, no. 7, pp. 1-8.

Christiansen, P. & Adolfssen, J.S. 2005, "Bite forces, canine strength and skull allometry in carnivores (Mammalia, Carnivora)", *Journal of Zoology,* vol. 266, no. 2, pp. 133-151.

Christiansen, P. & Wroe, S. 2007, "Bite forces and evolutionary adaptations to feeding ecology in carnivores", *Ecology,* vol. 88, no. 2, pp. 347-358.

Colbert, M.W., Racicot, R. & Rowe, T. 2005, "Anatomy of the cranial endocast of the bottlenose dolphin, Tursiops truncatus, based on HRXCT", *Journal of Mammalian Evolution,* vol. 12, no. 1-2, pp. 195-207.

Cotton, R., Pearce, C.W., Young, P.G., Kota, N., Leung, A., Bagchi, A. & Qidwai, S. 2016, "Development of a geometrically accurate and adaptable finite element head model for impact simulation: the Naval Research Laboratory–Simpleware Head Model", *Computer Methods in Biomechanics and Biomedical Engineering,* vol. 19, no. 1, pp. 101-113.

Cox, P.G. 2008, "A quantitative analysis of the Eutherian orbit: correlations with masticatory apparatus", *Biological Reviews,* vol. 83, no. 1, pp. 35-69.

Cox, P.G., Rayfield, E.J., Fagan, M.J., Herrel, A., Pataky, T.C. & Jeffery, N. 2012, "Functional evolution of the feeding system in rodents", *PLoS One,* vol. 7, no. 4, pp. 1-11.

Cox, P.G., Rinderknecht, A. & Blanco, R.E. 2015, "Predicting bite force and cranial biomechanics in the largest fossil rodent using finite element analysis", *Journal of Anatomy,* vol. 226, no. 3, pp. 215-223.

Cua, A., Wilhelm, K. & Maibach, H. 1990, "Elastic properties of human skin: relation to age, sex, and anatomical region", *Archives of Dermatological Research,* vol. 282, no. 5, pp. 283-288.

Cunningham, J.A., Rahman, I.A., Lautenschlager, S., Rayfield, E.J. & Donoghue, P.C. 2014, "A virtual world of paleontology", *Trends in Ecology & Evolution,* vol. 29, no. 6, pp. 347-357.

Cunningham, J.A., Rahman, I.A., Lautenschlager, S., Rayfield, E.J. & Donoghue, P.C. 2014, "A virtual world of paleontology", *Trends in Ecology & Evolution,* vol. 29, no. 6, pp. 347-357.

Curtis, N., Kupczik, K., Fagan, M. & Evans S.E. 2007, Finite Element Modelling of the Cat Skull. *8th International Congress of Vertebrate Morphology (ICVM-8)*, Paris, France, 16-21 July 2007, p. 1063.

Curtis, N., Kupczik, K., O'higgins, P., Moazen, M. & Fagan, M. 2008, "Predicting skull loading: applying multibody dynamics analysis to a macaque skull", *The Anatomical Record: Advances in Integrative Anatomy and Evolutionary Biology: Advances in Integrative Anatomy and Evolutionary Biology,* vol. 291, no. 5, pp. 491-501.

Curtis, N., Witzel, U., Fitton, L., O'higgins, P. & Fagan, M. 2011, "The mechanical significance of the temporal fasciae in Macaca fascicularis: an investigation using finite element analysis", *The Anatomical Record,* vol. 294, no. 7, pp. 1178-1190.

Curtis, N., Jones, M., Evans, S., O'higgins, P. & Fagan, M. 2013, "Cranial sutures work collectively to distribute strain throughout the reptile skull", *Journal of the Royal Society Interface,* vol. 10, no. 86, pp. 1-8.

DAVIES, M., MAWER, E.B. & FREEMONT, A.J. 1986, "The osteodystrophy of hypervitaminosis D: A metabolic study", *QJM: An International Journal of Medicine,* vol. 61, no. 1, pp. 911-919.

De Bonis, L., Peigné, S., Guy, F., Likius, A., Makaye, H.T., Vignaud, P. & Brunet, M. 2009, "A new mellivorine (Carnivora, Mustelidae) from the Late Miocene of Toros Menalla, Chad", *Neues Jahrbuch für Geologie und Paläontologie-Abhandlungen,* vol. 252, no. 1, pp. 33-54.

De Risio, L., Beltran, E., de Stefani, A., Holloway, A. & Matiasek, K. 2010, "Neurological dysfunction and caudal fossa overcrowding in a young cheetah with hypovitaminosis A", *The Veterinary Record,* vol. 167, no. 14, pp. 534-536.

Debnath, J., Satija, L., George, R.A., Vaidya, A. & Sen, D. 2009, "Computed tomographic demonstration of unusual ossification of the falx cerebri: a case report", *Surgical and Radiologic Anatomy,* vol. 31, no. 3, pp. 211-213.

Deck, C. & Willinger, R. 2009, "The current state of the human head finite element modelling", *International Journal of Vehicle Safety,* vol. 4, no. 2, pp. 85-112.

Degrange, F.J., Tambussi, C.P., Moreno, K., Witmer, L.M. & Wroe, S. 2010, "Mechanical analysis of feeding behavior in the extinct "terror bird" Andalgalornis steulleti (Gruiformes: Phorusrhacidae)", *PloS One,* vol. 5, no. 8, pp. e11856.

Delsuc, F., Ctzeflis, F.M., Stanhope, M.J. & Douzery, E.J. 2001, "The evolution of armadillos, anteaters and sloths depicted by nuclear and mitochondrial phylogenies: implications for the status of the enigmatic fossil Eurotamandua", *Proceedings of the Royal Society of London. Series B: Biological Sciences,* vol. 268, no. 1476, pp. 1605-1615.

Delsuc, F., Metcalf, J.L., Wegener Parfrey, L., Song, S.J., González, A. & Knight, R. 2014, "Convergence of gut microbiomes in myrmecophagous mammals", *Molecular Ecology,* vol. 23, no. 6, pp. 1301-1317.

DEWIND, L.T. 1961, "Hypervitaminosis D with osteosclerosis", *Archives of Disease in Childhood,* vol. 36, pp. 373-380.

Diogo, R., Pastor, F., De Paz, F., Potau, J.M., Bello-Hellegouarch, G., Ferrero, E.M. & Fisher, R.E. 2012, "The head and neck muscles of the serval and tiger: homologies, evolution, and proposal of a mammalian and a veterinary muscle ontology", *The Anatomical Record: Advances in Integrative Anatomy and Evolutionary Biology,* vol. 295, no. 12, pp. 2157-2178.

Dong, W. 2008, "Virtual cranial endocast of the oldest giant panda (Ailuropoda microta) reveals great similarity to that of its extant relative", *Naturwissenschaften,* vol. 95, no. 11, pp. 1079-1083.

Dozo, M.T. & Martínez, G. 2015, "First digital cranial endocasts of late Oligocene Notohippidae (Notoungulata): implications for endemic South American ungulates brain evolution", *Journal of Mammalian Evolution,* vol. 23, no. 1, pp. 1-16.

Driscoll, C.A., Menotti-Raymond, M., Roca, A.L., Hupe, K., Johnson, W.E., Geffen, E., Harley, E.H., Delibes, M., Pontier, D., Kitchener, A.C., Yamaguchi, N., O'brien, S.J. & Macdonald, D.W. 2007, "The Near Eastern origin of cat domestication", *Science (New York, N.Y.),* vol. 317, no. 5837, pp. 519-523.

Dumont, E.R., Davis, J.L., Grosse, I.R. & Burrows, A.M. 2011, "Finite element analysis of performance in the skulls of marmosets and tamarins", *Journal of Anatomy,* vol. 218, no. 1, pp. 151-162.

Dumont, E.R., Piccirillo, J. & Grosse, I.R. 2005, "Finite-element analysis of biting behavior and bone stress in the facial skeletons of bats", *The Anatomical Record Part A: Discoveries in Molecular, Cellular, and Evolutionary Biology: An Official Publication of the American Association of Anatomists,* vol. 283, no. 2, pp. 319-330.

Dwek, J.R. 2010, "The periosteum: what is it, where is it, and what mimics it in its absence?", *Skeletal Radiology,* vol. 39, no. 4, pp. 319-323.

Dzialo, C., Wood, S.A., Berthaume, M., Smith, A., Dumont, E.R., Benazzi, S., Weber, G.W., Strait, D.S. & Grosse, I.R. 2014, "Functional implications of squamosal suture size in Paranthropus boisei", *American Journal of Physical Anthropology,* vol. 153, no. 2, pp. 260-268.

Edwards, C. & Marks, R. 1995, "Evaluation of biomechanical properties of human skin", *Clinics in Dermatology,* vol. 13, no. 4, pp. 375-380.

Einstein, D., Reinhall, P., Nicosia, M., Cochran, R. & Kunzelman, K. 2003, "Dynamic finite element implementation of nonlinear, anisotropic hyperelastic biological membranes", *Computer Methods in Biomechanics & Biomedical Engineering,* vol. 6, no. 1, pp. 33-44.

El Allali, K., Achaâban, M. & Ouassat, M. 2017, "Anatomy of the dromedary head skeleton revisited", *Journal of Morphological Sciences,* vol. 34, no. 2, pp. 073-088.

Emry, R.J. & Skinner, M.F. 1970, "A North American Oligocene pangolin and other additions to the Pholidota". *Bulletin of the AMNH*; vol. 142, article 6, pp. 455-510.

Espadas, I., Ricci, E., McConnell, F. & Sanchez-Masian, D. 2017, "MRI, CT and histopathological findings in a cat with hypovitaminosis A", *Veterinary Record Case Reports,* vol. 5, no. 3, pp. 1-5.

Evans, H.E. & De Lahunta, A. 2013, *Miller's anatomy of the dog,* China, Elsevier Health Sciences.

Fagan, M. & Lee A. J. C. 1986, "Role of the collar on the femoral stem of cemented total hip replacements - a finite element investigation". *Journal of Biomedical Engineering*, no. 8, pp. 295-304.

Feijo, A. & Cordeiro-Estrela, P. 2016, "Taxonomic revision of the Dasypus kappleri complex, with revalidations of Dasypus pastasae (Thomas, 1901) and Dasypus beniensis Lonnberg, 1942 (Cingulata, Dasypodidae)", *Zootaxa,* vol. 4170, no. 2, pp. 271-297.

Feldhamer, G.A., Drickamer, L.C., Vessey, S.H., Merritt, J.F. & Krajewski, C. 2007, *Mammalogy: adaptation, diversity, ecology,* Baltimore, James Hopkins University Press.

Feneis, H. & Dauber, W. 2000, *Pocket Atlas of Human Anatomy.* Stuttgart and New York, Thieme.

Fernandes, F.A., Tchepel, D., Alves de Sousa, Ricardo J & Ptak, M. 2018, "Development and validation of a new finite element human head model: Yet another head model (YEAHM)", *Engineering Computations,* vol. 35, no. 1, pp. 477-496.

Ferrario, V., Sforza, C., Serrao, G., Dellavia, C. & Tartaglia, G. 2004, "Single tooth bite forces in healthy young adults", *Journal of Oral Rehabilitation,* vol. 31, no. 1, pp. 18-22.

Figueirido, B. & Janis, C.M. 2011, "The predatory behaviour of the thylacine: Tasmanian tiger or marsupial wolf?", *Biology Letters,* vol. 7, no. 6, pp. 937-940.

Fill, T.S., Carey, J.P., Toogood, R.W. & Major, P.W. 2011, "Experimentally determined mechanical properties of, and models for, the periodontal ligament: critical review of current literature", *Journal of Dental Biomechanics,* vol. 2011, pp. 1-10.

Finarelli, J.A. & Goswami, A. 2009, "The evolution of orbit orientation and encephalization in the Carnivora (Mammalia)", *Journal of Anatomy,* vol. 214, no. 5, pp. 671-678.

Fortuny, J., Marcé-Nogué, J., Steyer, J., de Esteban-Trivigno, S., Mujal, E. & Gil, L. 2016, "Comparative 3D analyses and palaeoecology of giant early amphibians (Temnospondyli: Stereospondyli)", *Scientific Reports,* vol. 6, pp. 30387.

Gallina, A., Helmboldt, C., Frier, H., Nielsen, S. & Eaton, H. 1970, "Bone growth in the hypovitaminotic A calf", *The Journal of Nutrition,* vol. 100, no. 1, pp. 129-141.

Garland, T. 1983, "The relation between maximal running speed and body mass in terrestrial mammals", *Journal of Zoology,* vol. 199, no. 2, pp. 157-170.

Gaudin, T.J. & Wible, J.R. 1999, "The entotympanic of pangolins and the phylogeny of the Pholidota (Mammalia)", *Journal of Mammalian Evolution,* vol. 6, no. 1, pp. 39-65.

Gaudy, J., Zouaoui, A., Bri, P., Charrier, J. & Laison, F. 2002, "Functional anatomy of the human temporal muscle", *Surgical and Radiologic Anatomy,* vol. 23, no. 6, pp. 389-398.

Geisler, J.H., Sanders, A.E. & Luo, Z. 2005, "A new protocetid whale (Cetacea: Archaeoceti) from the late middle Eocene of South Carolina", *American Museum Novitates,* vol. 2005, no. 3480, pp. 1-68.

Ghassemi, A., Prescher, A., Riediger, D. & Axer, H. 2003, "Anatomy of the SMAS revisited", *Aesthetic Plastic Surgery,* vol. 27, no. 4, pp. 258-264.

Gil Espert, L., Marcé Nogué, J. & Sánchez Romero, M. 2015, "Insights into the controversy over materials data for the comparison of biomechanical performance in vertebrates", *Palaeontologia Electronica,* vol. 18.1. no. 10A, pp. 1-24.

Gingerich, P.D. Zalmout, I.S & Domning, D.P. 2010, "Sirenia". In Werdelin, L. & Sanders W.J. (ed.), *Cenozoic Mammals of Africa,* California, University of California Press, pp. 147-160.

Girard, M. J., Suh, J. K. F., Bottlang, M., Burgoyne, C. F., & Downs, J. C., 2011, "Biomechanical changes in the sclera of monkey eyes exposed to chronic IOP elevations", *Investigative ophthalmology & visual science*, Vol. *52*, no. 8, pp. 5656-5669.

Gladilin, E., Zachow, S., Deuflhard, P. & Hege, H. 2004, "Anatomy-and physics-based facial animation for craniofacial surgery simulations", *Medical and Biological Engineering and Computing,* vol. 42, no. 2, pp. 167-170.

Godinho, R.M., Toro-Ibacache, V., Fitton, L.C. & O'Higgins, P. 2017, "Finite element analysis of the cranium: Validity, sensitivity and future directions", *Comptes Rendus Palevol,* vol. 16, no. 5-6, pp. 600-612.

González Guarda, E. A. 2009. "Sobre la presencia de Mephitidae (Carnivora, Mammalia) en el Pleistoceno Superior de Chile: Primer registro confirmado", Ph.D. Thesis. Universidad Austral de Chile.

Gorgacz, E., Rousseau Jr, J., Frier, H., Hall Jr, R. & Eaton, H. 1971, "Composition of the dura mater in chronic bovine hypervitaminosis A", *The Journal of Nutrition,* vol. 101, no. 11, pp. 1541-1546.

Gorniak, G.C. & Gans, C. 1980, "Quantitative assay of electromyograms during mastication in domestic cats (Felis catus)", *Journal of Morphology,* vol. 163, no. 3, pp. 253-281.

Greaves, W. 1985, "The mammalian postorbital bar as a torsion-resisting helical strut", *Journal of Zoology,* vol. 207, no. 1, pp. 125-136.

Greaves, W. 1978, "The jaw lever system in ungulates: a new model", *Journal of Zoology,* vol. 184, no. 2, pp. 271-285.

Greven, H., Zanger, K. & Schwinger, G. 1995, "Mechanical properties of the skin of Xenopus laevis (Anura, Amphibia)", *Journal of Morphology,* vol. 224, no. 1, pp. 15-22.

Gröning, F., Fagan, M. & O'Higgins, P. 2011, "The effects of the periodontal ligament on mandibular stiffness: a study combining finite element analysis and geometric morphometrics", *Journal of Biomechanics,* vol. 44, no. 7, pp. 1304-1312.

Gröning, F., Fagan, M. & O'Higgins, P. 2011, "The effects of the periodontal ligament on mandibular stiffness: a study combining finite element analysis and geometric morphometrics", *Journal of Biomechanics,* vol. 44, no. 7, pp. 1304-1312.

Grosse, I.R., Dumont, E.R., Coletta, C. & Tolleson, A. 2007, "Techniques for modeling muscle-induced forces in finite element models of skeletal structures", *The Anatomical Record: Advances in Integrative Anatomy and Evolutionary Biology:*

*Advances in Integrative Anatomy and Evolutionary Biology,* vol. 290, no. 9, pp. 1069-1088.

Gross-tsubery, R., Chai, O., Shilo, Y., Miara, L., Horowitz, I.H., Shmueli, A., Aizenberg, I., Hoffman, C., Reifen, R. & Shamir, M.H. 2010, "Computed tomographic analysis of calvarial hyperostosis in captive lions", *Veterinary Radiology & Ultrasound,* vol. 51, no. 1, pp. 34-38.

Groves, C. & Shekelle, M. 2010, "The genera and species of Tarsiidae", *International Journal of Primatology,* vol. 31, no. 6, pp. 1071-1082.

Haagenson, M., Kirberger, R., Hartley, M. & Sweers, L. 2005, "Diagnosis of suspected hypovitaminosis A using magnetic resonance imaging in African lions (Panthera leo)", *Journal of the South African Veterinary Association,* vol. 76, no. 3, pp. 132-137.

Hagberg, C. 1987, "Assessments of bite force: a review" *Journal of Craniomandibular Disorders*, vol. 1, no. 3, p. 162.

Hall, S. 2014, *Basic biomechanics,* New York, McGraw-Hill Higher Education.

Hall, V. & MacGregor, W. 1937, "Relation of kidney weight to body weight in the cat", *The Anatomical Record,* vol. 69, no. 3, pp. 319-331.

Hamann, M.C.J., Sacks, M.S. & Malinin, T.I. 1998, "Quantification of the collagen fibre architecture of human cranial dura mater", *The Journal of Anatomy,* vol. 192, no. 1, pp. 99-106.

Hannula, M., Narra, N., Onnela, N., Dastidar, P. & Hyttinen, J. 2014, "A multi-tissue segmentation of the human head for detailed computational models", *Engineering in Medicine and Biology Society (EMBC), 2014 36th Annual International Conference of the IEEE*, pp. 2484-2487.

Hartmann, U. & Kruggel, F. 1999, "Transient analysis of the biomechanics of the human head with a high-resolution 3D finite element model", *Computer Methods in Biomechanics and Biomedical Engineering,* vol. 2, no. 1, pp. 49-64.

Hartstone-Rose, A., Perry, J.M. & Morrow, C.J. 2012, "Bite force estimation and the fiber architecture of felid masticatory muscles", *The Anatomical Record,* vol. 295, no. 8, pp. 1336-1351.

He, T., Friede, H. & Kiliaridis, S. 2002, "Macroscopic and roentgenographic anatomy of the skull of the ferret (Mustela putorius furo)", *Laboratory Animals,* vol. 36, no. 1, pp. 86-96.

Heesy, C.P. 2005, "Function of the mammalian postorbital bar", *Journal of Morphology,* vol. 264, no. 3, pp. 363-380.

Heesy, C.P., Ross, C.F. & Demes, B. 2007, "Oculomotor stability and the functions of the postorbital bar and septum" in Ravosa, M.J., Dagosto, M. (ed.) *Primate origins: adaptations and evolution*, New York, Springer, pp. 257-283.

Hellsing, G. 1980, "On the regulation of interincisor bite force in man", *Journal of Oral Rehabilitation*, vol. 7, no. 5, pp. 403-411.

Hemae, K.M. 1967, "Masticatory function in the mammals", *Journal of Dental Research,* vol. 46, no. 5, pp. 883-893.

Herman, G.T. 2009, *Fundamentals of computerized tomography: image reconstruction from projections,* Dordrecht, Heidelberg, London and New York Springer Science & Business Media.

Herring, S.W. 2007, "Masticatory muscles and the skull: a comparative perspective", *Archives of Oral Biology,* vol. 52, no. 4, pp. 296-299.

Herring, S.W., Rafferty, K.L., Liu, Z.J. & Lemme, M. 2011, "Mastication and the postorbital ligament: dynamic strain in soft tissues", *Integrative and Comparative Biology,* vol. 51, no. 2, pp. 297-306.

Herring, S.W., Rafferty, K.L., Liu, Z.J. & Lemme, M. 2011, "Mastication and the postorbital ligament: dynamic strain in soft tissues", *Integrative and Comparative Biology,* vol. 51, no. 2, pp. 297-306.

Herring, S.W., Rafferty, K.L., Liu, Z.J. & Marshall, C.D. 2001, "Jaw muscles and the skull in mammals: the biomechanics of mastication", *Comparative Biochemistry and Physiology Part A: Molecular & Integrative Physiology,* vol. 131, no. 1, pp. 207-219.

Hilloowala, R. & Kanth, H. 2007, "The transmission of masticatory forces and nasal septum: structural comparison of the human skull and Gothic cathedral", *CRANIO®,* vol. 25, no. 3, pp. 166-171.

Hirose, M., Tanaka, E., Tanaka, M., Fujita, R., Kuroda, Y., Yamano, E., Van Eijden, T.M. & Tanne, K. 2006, "Three-dimensional finite-element model of the human temporomandibular joint disc during prolonged clenching", *European Journal of Oral Sciences,* vol. 114, no. 5, pp. 441-448.

Ho, J. & Kleiven, S. 2009, "Can sulci protect the brain from traumatic injury?", *Journal of Biomechanics,* vol. 42, no. 13, pp. 2074-2080.

Holz, P. 2014, "Monotremata (Echidna, Platypus)", *Fowler's Zoo and Wild Animal Medicine,* vol. 8, pp. 247-255.

Horgan, T.J. & Gilchrist, M.D. 2003, "The creation of three-dimensional finite element models for simulating head impact biomechanics", *International Journal of Crashworthiness,* vol. 8, no. 4, pp. 353-366.

Horgan, T. & Gilchrist, M.D. 2003, "The creation of three-dimensional finite element models for simulating head impact biomechanics", *International Journal of Crashworthiness,* vol. 8, no. 4, pp. 353-366.

Horovitz, I. & MacPhee, R.D. 1999, "The quaternary Cuban platyrrhineParalouatta varonaiand the origin of Antillean monkeys", *Journal of Human Evolution,* vol. 36, no. 1, pp. 33-68.

Hoursan, H., Ahmadian, M.T., Barari, A. & Beidokhti, H.N. 2013, "Modelling and Analysis of the Effect of Angular Velocity and Acceleration on Brain Strain Field in Traumatic Brain Injury", *ASME 2013 International Mechanical Engineering Congress and* Exposition, American Society of Mechanical Engineers, pp. 1-7.

Howell, B. & McIntyre, C.C. 2017, "Role of soft-tissue heterogeneity in computational models of deep brain stimulation", *Brain Stimulation,* vol. 10, no. 1, pp. 46-50.

Huang, J., Raymond, D., Shen, W., Stuhmiller, J., Crawford, G. & Bir, C. 2011, "Development and Validation of a Subject-Specific Finite Element Model for Skull Fracture Assessment", *ASME 2011 International Mechanical Engineering Congress and* Exposition, American Society of Mechanical Engineers, pp. 1-10.

Huempfner-Hierl, H., Bohne, A., Schaller, A., Wollny, G. & Hierl, T. 2015, "Does facial soft tissue protect against zygomatic fractures? Results of a finite element analysis", *Head & Face Medicine,* vol. 11, no. 1, pp. 21.

Humphrey, J.D. 2003, "Continuum biomechanics of soft biological tissues", *Proceedings of the Royal Society of London.Series A: Mathematical, Physical and Engineering Sciences,* vol. 459, no. 2029, pp. 3-46.

Hylander, W.L., Johnson, K.R. & Crompton, A. 1992, "Muscle force recruitment and biomechanical modeling: an analysis of masseter muscle function during mastication in Macaca fascicularis", *American Journal of Physical Anthropology,* vol. 88, no. 3, pp. 365-387.

Iacono, M.I., Neufeld, E., Akinnagbe, E., Bower, K., Wolf, J., Oikonomidis, I.V., Sharma, D., Lloyd, B., Wilm, B.J. & Wyss, M. 2015, "MIDA: a multimodal imaging-based detailed anatomical model of the human head and neck", *PloS One,* vol. 10, no. 4, pp. 1-35.

Ichishima, H. & Kimura, M. 2013, "New material of Haborophocoena toyoshimai (Odontoceti: Phocoenidae) from the lower Pliocene Embetsu Formation of Hokkaido, Japan", *Paleontological Research,* vol. 17, no. 2, pp. 127-138.

Ichishima, H. & Kimura, M. 2005, "Haborophocoena toyoshimai, a new early Pliocene porpoise (Cetacea; Phocoenidae) from Hokkaido, Japan", *Journal of Vertebrate Paleontology,* vol. 25, no. 3, pp. 655-664.

Iriarte-Diaz, J. 2002, "Differential scaling of locomotor performance in small and large terrestrial mammals", *The Journal of Experimental Biology,* vol. 205, no. 18, pp. 2897-2908.

Iwamoto, M., Nakahira, Y., Tamura, A., Kimpara, H., Watanabe, I. & Miki, K. 2007, "Development of advanced human models in THUMS", *Proc. 6th European LS-DYNA Users' Conference*, pp. 47.

Janis, C.M., Scott, K.M., Jacobs, L.L., Gunnell, G.F. & Uhen, M.D. 1998, *Evolution of tertiary mammals of North America: Volume 1, terrestrial carnivores, ungulates, and ungulate like mammals,* Cambridge, Cambridge University Press.

Jašarević, E., Ning, J., Daniel, A.N., Menegaz, R.A., Johnson, J.J., Stack, M.S. & Ravosa, M.J. 2010, "Masticatory loading, function, and plasticity: a microanatomical analysis of mammalian circumorbital soft-tissue structures", *The Anatomical Record: Advances in Integrative Anatomy and Evolutionary Biology,* vol. 293, no. 4, pp. 642-650.

Jeffery, N. 2002, "Differential regional brain growth and rotation of the prenatal human tentorium cerebelli", *Journal of Anatomy,* vol. 200, no. 2, pp. 135-144.

Jeffery, N., Ryan, T.M. & Spoor, F. 2008, "The primate subarcuate fossa and its relationship to the semicircular canals part II: Adult interspecific variation", *Journal of Human Evolution,* vol. 55, no. 2, pp. 326-339.

Jerison, H. 1973, *Evolution of the Brain and Intelligence*, New York and London, Academic Press.

Johnson, W.E., Eizirik, E., Pecon-Slattery, J., Murphy, W.J., Antunes, A., Teeling, E. & O'Brien, S.J. 2006, "The late Miocene radiation of modern Felidae: a genetic assessment", *Science,* vol. 311, no. 5757, pp. 73-77.

Jones, M.E., Gröning, F., Dutel, H., Sharp, A., Fagan, M.J. & Evans, S.E. 2017, "The biomechanical role of the chondrocranium and sutures in a lizard cranium", *Journal of the Royal Society Interface,* vol. 14, no. 137, pp. 1-13.

Jubb, K.V.F., Kennedy, P.C. & Palmer, N. 1993, *Pathology of domestic animals,* vol. 1, San Diego, Academic Press.

Kalra, A. 2018, "Developing FE Human Models From Medical Images" in Yang, K. (ed.), *Basic Finite Element Method as Applied to Injury Biomechanics,* London, San Diego, Cambridge and Oxford, Academic Press, pp. 389-415.

Kang, H., Willinger, R., Diaw, B.M. & Chinn, B. 1997, "Validation of a 3D anatomic human head model and replication of head impact in motorcycle accident by finite element modeling", *Proceedings: Stapp Car Crash Conference,* Society of Automotive Engineers SAE, pp. 329-338.

Kardong, K.V. 1995, *Vertebrates: comparative anatomy, function, evolution,* New York, McGraw-Hill.

Kay, R.F., Simons, E. & Ross, J.L. 2008, "The basicranial anatomy of African Eocene/Oligocene anthropoids. Are there any clues for platyrrhine origins?" in Fleagle, J.G, Gilbert, C. C. (ed.), *Elwyn Simons: A Search for Origins* Springer, New York, pp. 125-158.

Kay, R.F., Thewissen, J. & Yoder, A.D. 1992, "Cranial anatomy of Ignacius graybullianus and the affinities of the Plesiadapiformes", *American Journal of Physical Anthropology,* vol. 89, no. 4, pp. 477-498.

De Kegel, D., Vastmans, J., Fehervary, H., Depreitere, B., Vander Sloten, J., & Famaey, N., 2018, "Biomechanical characterization of human dura mater", *Journal of the mechanical behavior of biomedical materials*, Vol. 79, pp. 122-134.

Kermack, K., Mussett, F. & Rigney, H. 1981, "The skull of Morganucodon", *Zoological Journal of the Linnean Society,* vol. 71, no. 1, pp. 1-158.

Kidwell, C.S., Chalela, J.A., Saver, J.L., Starkman, S., Hill, M.D., Demchuk, A.M., Butman, J.A., Patronas, N., Alger, J.R. & Latour, L.L. 2004, "Comparison of MRI and CT for detection of acute intracerebral hemorrhage", *Jama,* vol. 292, no. 15, pp. 1823-1830.

Kielan-Jaworowska, Z. 1996, "Characters of multituberculates neglected in phylogenetic analyses of early mammals", *Lethaia,* vol. 29, no. 3, pp. 249-266.

Kielan-Jaworowska, Z., Cifelli, R.L. & Luo, Z. 2004, *Mammals from the age of dinosaurs: origins, evolution, and structure,* Columbia, Columbia University Press.

Kimpara, H., Nakahira, Y., Iwamoto, M. & Miki, K. 2006, "Investigation of anteroposterior head-neck responses during severe frontal impacts using a brain-spinal cord complex FE model", *Stapp Car Crash Journal,* vol. 50, pp. 509.

Kitchener, A.C., Van Valkenburgh, B., Yamaguchi, N., Macdonald, D. & Loveridge, A. 2010, "Felid form and function" in MacDonald, D. & Loveridge, A. (ed.), *Biology and conservation of wild felids,* Oxford, Oxford University Press, pp. 83-106.

Kleiven, S. & von Holst, H. 2002, "Consequences of head size following trauma to the human head", *Journal of Biomechanics,* vol. 35, no. 2, pp. 153-160.

Klintworth, G.K. 1968, "The comparative anatomy and phylogeny of the tentorium cerebelli", *The Anatomical Record,* vol. 160, no. 3, pp. 635-641.

König, H.E. & Liebich, H. 2005, *Anatomía de los animales domésticos: texto y atlas en color,* Buenos Aires, Bogota, Caracas, Madrid, Mexico and Sao Paulo Ed. Médica Panamericana.

Kumaresan, S. & Radhakrishnan, S. 1996, "Importance of partitioning membranes of the brain and the influence of the neck in head injury modelling", *Medical and Biological Engineering and Computing,* vol. 34, no. 1, pp. 27-32.

Kupczik, K. 2008, "Virtual biomechanics: basic concepts and technical aspects of finite element analysis in vertebrate morphology", *Journal of Anthropological Sciences,* vol. 86, no. 4, pp. 193-198.

Laison, F., Lautrou, A., Azérad, J., Pollin, B. & Lévy, G. 2001, "Superficial architecture of the jaw-closing muscles of the cat (Felis catus): the temporo-masseteric complex", *Comptes Rendus de l'Académie des Sciences-Series III-Sciences de la Vie,* vol. 324, no. 9, pp. 855-862.

Landini, L., Positano, V. & Santarelli, M. 2018, *Advanced image processing in magnetic resonance imaging,* Boca Raton, London, New York, Taylor & Francis.

Ledogar, J.A., Dechow, P.C., Wang, Q., Gharpure, P.H., Gordon, A.D., Baab, K.L., Smith, A.L., Weber, G.W., Grosse, I.R. & Ross, C.F. 2016, "Human feeding biomechanics: performance, variation, and functional constraints", *PeerJ,* vol. 4, pp. 1-9.

Li, X., Sandler, H., & Kleiven, S., 2017, "The importance of nonlinear tissue modelling in finite element simulations of infant head impacts", *Biomechanics and modeling in mechanobiology*, Vol. 16, no. 3, pp. 823-840.

Lieberman, D. 2011, *The evolution of the human head,* Harvard, Harvard University Press.

Lieberman, D.E., McBratney, B.M. & Krovitz, G. 2002, "The evolution and development of cranial form in Homosapiens", *Proceedings of the National Academy of Sciences of the United States of America,* vol. 99, no. 3, pp. 1134-1139.

Liu, J., Shi, J., Fitton, L.C., Phillips, R., O'Higgins, P. & Fagan, M.J. 2012, "The application of muscle wrapping to voxel-based finite element models of skeletal structures", *Biomechanics and Modeling in Mechanobiology,* vol. 11, no. 1-2, pp. 35-47.

Liu, Q., Farahibozorg, S., Porcaro, C., Wenderoth, N. & Mantini, D. 2017, "Detecting large-scale networks in the human brain using high-density electroencephalography", *Human Brain Mapping,* vol. 38, no. 9, pp. 4631-4643.

Lovegrove, B.G. 2004, "Locomotor mode, maximum running speed, and basal metabolic rate in placental mammals", *Physiological and Biochemical Zoology: PBZ,* vol. 77, no. 6, pp. 916-928.

Lyons, M. F., & Baxendale, R. H. 1990, "A preliminary electromyographic study of bite force and jaw-closing muscle fatigue in human subjects with advanced tooth wear", *Journal of Oral Rehabilitation*, vol. *17*, no. 4, pp. 311-318.

MacManus, D. B., Pierrat, B., Murphy, J. G., & Gilchrist, M. D., 2017, "Protection of cortex by overlying meninges tissue during dynamic indentation of the adolescent brain", *Acta biomaterialia*, Vol. 57, pp. 384-394.

MacPhee, R.D. 2014, "The serrialis bone, interparietals,"X" elements, entotympanics, and the composition of the notoungulate caudal cranium", *Bulletin of the American Museum of Natural History,* vol. 2014, no. 384, pp. 1-70.

Macrini, T.E., Rowe, T. & Archer, M. 2006a, "Description of a cranial endocast from a fossil platypus, Obdurodon dicksoni (Monotremata, Ornithorhynchidae), and the relevance of endocranial characters to monotreme monophyly", *Journal of Morphology,* vol. 267, no. 8, pp. 1000-1015.

Macrini, T.E. 2006b, *The evolution of endocranial space in mammals and non-mammalian cynodonts,* P.h.D. Thesis, The University of Texas.

Macrini, T.E., Rougier, G.W. & Rowe, T. 2007, "Description of a cranial endocast from the fossil mammal Vincelestes neuquenianus (Theriiformes) and its relevance to the evolution of endocranial characters in therians", *The Anatomical Record,* vol. 290, no. 7, pp. 875-892.

Macrini, T.E. 2009, "Description of a digital cranial endocast of Bathygenys reevesi (Merycoidodontidae; Oreodontoidea) and implications for apomorphy-based diagnosis of isolated, natural endocasts", *Journal of Vertebrate Paleontology,* vol. 29, no. 4, pp. 1199-1211.

Madhukar, A. & Ostoja-Starzewski, M. 2019, "Finite element methods in human head impact simulations: a review", *Annals of Biomedical Engineering,* pp. 1-23.

Malizos, K.N. & Papatheodorou, L.K. 2005, "The healing potential of the periosteum: molecular aspects", *Injury,* vol. 36, no. 3, pp. S13-S19.

Mao, H., Zhang, L., Jiang, B., Genthikatti, V.V., Jin, X., Zhu, F., Makwana, R., Gill, A., Jandir, G. & Singh, A. 2013, "Development of a finite element human head model partially validated with thirty five experimental cases", *Journal of Biomechanical Engineering,* vol. 135, no. 11, pp. (111002)1-15.

Marinescu, R., Daegling, D.J. & Rapoff, A.J. 2005, "Finite-element modeling of the anthropoid mandible: the effects of altered boundary conditions", *The Anatomical Record Part A: Discoveries in Molecular, Cellular, and Evolutionary Biology: An Official Publication of the American Association of Anatomists,* vol. 283, no. 2, pp. 300-309.

Martin, L.D. 1980, "Functional morphology and the evolution of cats", *Transactions of the Nebraska Academy of Sciences,* VIII, pp. 141-154.

May-Collado, L.J., Kilpatrick, C.W. & Agnarsson, I. 2015, "Mammals from 'down under': a multi-gene species-level phylogeny of marsupial mammals (Mammalia, Metatheria)", *PeerJ,* vol. 3, pp. 1-27.

McCormack, S.W., Witzel, U., Watson, P.J., Fagan, M.J. & Gröning, F. 2017, "Inclusion of periodontal ligament fibres in mandibular finite element models leads to an increase in alveolar bone strains", *PloS One,* vol. 12, no. 11, pp. 1-23.

McCurry, M.R., Evans, A.R. & McHenry, C.R. 2015, "The sensitivity of biological finite element models to the resolution of surface geometry: a case study of crocodilian crania", *PeerJ,* vol. 3, pp. 1-16.

McHenry, C.R., Wroe, S., Clausen, P.D., Moreno, K. & Cunningham, E. 2007, "Supermodeled sabercat, predatory behavior in Smilodon fatalis revealed by high-resolution 3D computer simulation", *Proceedings of the National Academy of Sciences of the United States of America,* vol. 104, no. 41, pp. 16010-16015.

McIntosh, A.F. & Cox, P.G. 2016, "The impact of gape on the performance of the skull in chisel-tooth digging and scratch digging mole-rats (Rodentia: Bathyergidae)", *Royal Society Open Science,* vol. 3, no. 10, pp. 160568.

McManus, J.J. 1974, "Didelphis virginiana", *Mammalian Species,* no. 40, pp. 1-6.

Meachen-Samuels, J. & Van Valkenburgh, B. 2009, "Craniodental indicators of prey size preference in the Felidae", *Biological Journal of the Linnean Society,* vol. 96, no. 4, pp. 784-799.

Mellanby, E. 1941, "Skeletal changes affecting the nervous system produced in young dogs by diets deficient in vitamin a", *The Journal of Physiology,* vol. 99, no. 4, pp. 467-486.

Meredith, R.W., Westerman, M. & Springer, M.S. 2008, "A timescale and phylogeny for "Bandicoots" (Peramelemorphia: Marsupialia) based on sequences for five nuclear genes", *Molecular Phylogenetics and Evolution,* vol. 47, no. 1, pp. 1-20.

Miller, L. E., Urban, J. E., & Stitzel, J. D., 2017, "Validation performance comparison for finite element models of the human brain", *Computer methods in biomechanics and biomedical engineering*, Vol. 20, no. 12, pp. 1273-1288.

Ming, T.K. 2013, *Development of a Realistic Finite Element Model of Human Head and its Applications to Head Injuries,* P.h.D. Thesis, National University of Singapore.

Moazen, M., Curtis, N., O'Higgins, P., Jones, M.E., Evans, S.E. & Fagan, M.J. 2008, "Assessment of the role of sutures in a lizard skull: a computer modelling study", *Proceedings of the Royal Society B: Biological Sciences,* vol. 276, no. 1654, pp. 39-46.

Moseby, K. & Read, J. 2006, "The efficacy of feral cat, fox and rabbit exclusion fence designs for threatened species protection", *Biological Conservation,* vol. 127, no. 4, pp. 429-437.

Moss, M.L. & Young, R.W. 1960, "A functional approach to craniology", *American Journal of Physical Anthropology,* vol. 18, no. 4, pp. 281-292.

Murphy, R.A. & Beardsley, A.C. 1974, "Mechanical properties of the cat soleus muscle in situ", *The American Journal of Physiology,* vol. 227, no. 5, pp. 1008-1013.

Nakashige, M., Smith, A.L. & Strait, D.S. 2011, "Biomechanics of the macaque postorbital septum investigated using finite element analysis: implications for anthropoid evolution", *Journal of Anatomy,* vol. 218, no. 1, pp. 142-150.

Nelson, G. 1986, *Three dimensional computer modeling of human mandibular mechanics*, P.h.D. Thesis, University of British Columbia.

Nikolai, J.C. & Bramble, D.M. 1983, "Morphological structure and function in desert heteromyid rodents", *Great Basin Naturalist Memoirs,* pp. 44-64.

Noble, V.E., Kowalski, E.M. & Ravosa, M.J. 2000, "Orbit orientation and the function of the mammalian postorbital bar", *Journal of Zoology,* vol. 250, no. 3, pp. 405-418.

Nojima, T. 1990c, "A morphological consideration of the relationships of pinnipeds to other carnivorans based on the bony tentorium and bony falx", *Marine Mammal Science,* vol. 6, no. 1, pp. 54-74.

Nojima, T. 1990b, "The relationship between development of the bony falx and bony tentorium in cetaceans and their diets", *Scientific Reports of Cetacean Research,* vol. 1, pp. 39-61.

Nojima, T. 1990a, "Developmental pattern of the bony tentorium of spider monkeys (Ateles)", *Primates,* vol. 31, no. 1, pp. 137-141.

Nojima, T. 1988, "Developmental pattern of the bony falx and bony tentorium of spotted dolphins (Stenella attenuata) and the relationship between degree of development and age", *Marine Mammal Science,* vol. 4, no. 4, pp. 312-322.

Oldfield, C., McHenry, C., Clausen, P., Chamoli, U., Parr, W., Stynder, D. & Wroe, S. 2012, "Finite element analysis of ursid cranial mechanics and the prediction of feeding behaviour in the extinct giant A griotherium africanum", *Journal of Zoology,* vol. 286, no. 2, pp. 171-171.

O'rahilly, R., Müller, F., & Nat, D. R., 1986, "The meninges in human development", *Journal of Neuropathology & Experimental Neurology*, Vol. 45, no. 5, pp. 588-608.

O'Regan, H.J. & Kitchener, A.C. 2005, "The effects of captivity on the morphology of captive, domesticated and feral mammals", *Mammal Review,* vol. 35, no. 3-4, pp. 215-230.

Orliac, M.J., Argot, C. & Gilissen, E. 2012, "Digital cranial endocast of Hyopsodus (Mammalia, "Condylarthra"): a case of Paleogene terrestrial echolocation?", *PLoS One,* vol. 7, no. 2, pp. 1-10.

Orsini, P. & Hennet, P. 1992, "Anatomy of the mouth and teeth of the cat", *Veterinary Clinics of North America: Small Animal Practice,* vol. 22, no. 6, pp. 1265-1277.

Owen, R. 1866, *On the Anatomy of Vertebrates: Birds and mammals,* London, Longmans, Green and Company.

Ozkaya, N., Nordin, M., Goldsheyder, D. & Leger, D. 2012, *Fundamentals of Biomechanics,* New York, Springer.

Pailler-Mattei, C., Bec, S. & Zahouani, H. 2008, "In vivo measurements of the elastic mechanical properties of human skin by indentation tests", *Medical Engineering & Physics,* vol. 30, no. 5, pp. 599-606.

Palacios, C. 2006, "The role of nutrients in bone health, from A to Z", *Critical Reviews in Food Science and Nutrition,* vol. 46, no. 8, pp. 621-628.

Palma, R.E. & Spotorno, A.E. 1999, "Molecular systematics of marsupials based on the rRNA 12S mitochondrial gene: the phylogeny of Didelphimorphia and of the living fossil microbiotheriid Dromiciops gliroides Thomas", *Molecular phylogenetics and evolution,* vol. 13, no. 3, pp. 525-535.

Parisi, D. 2010, *The Mechanical Function of the Postorbital Bar in Eulemur fulvus Analyzed Using Finite Element Analysis*, Senior Thesis, University of Albany.

Pekár, S. & Mayntz, D. 2014, "Comparative analysis of the macronutrient content of Central European ants (Formicidae): Implications for ant-eating predators", *Journal of Insect Physiology,* vol. 62, pp. 32-38.

Pinheiro, M. & Alves, J. 2015, "The feasibility of a custom-made endoprosthesis in mandibular reconstruction: implant design and finite element analysis", *Journal of Cranio-Maxillofacial Surgery,* vol. 43, no. 10, pp. 2116-2128.

Poggesi, M., Mannucci, P. & Simonetta, A. 1982, "Development and morphology of the skull in the Dik-Diks (genus Madoqua Ogilby, Artiodactyla, Bovidae)", *Monitore Zoologico Italiano.Supplemento,* vol. 17, no. 1, pp. 191-217.

Poiate, Isis A Venturini P, de Vasconcellos, A.B., de Santana, R.B. & Poiate, E. 2009, "Three-dimensional stress distribution in the human periodontal ligament in masticatory, parafunctional, and trauma loads: finite element analysis", *Journal of Periodontology,* vol. 80, no. 11, pp. 1859-1867.

Polly, P.D. 1993, *Hyaenodontidae (Creodonta, Mammalia) and the position of systematics in evolutionary biology,* P.h.D. Thesis, University of California at Berkeley.

Porro, L.B., Metzger, K.A., Iriarte-Diaz, J. & Ross, C.F. 2013, "In vivo bone strain and finite element modeling of the mandible of Alligator mississippiensis", *Journal of Anatomy,* vol. 223, no. 3, pp. 195-227.

Rai, R., Iwanaga, J., Shokouhi, G., Oskouian, R.J. & Tubbs, R.S. 2018, "The Tentorium Cerebelli: A Comprehensive Review Including Its Anatomy, Embryology, and Surgical Techniques", *Cureus,* vol. 10, no. 7, pp. 1-13.

Rao, S.R., Rao, T.R., Ovchinnikov, N., McRAE, A. & Rao, A.V.C. 2007, "Unusual isolated ossification of falx cerebri: a case report", *Neuroanatomy,* vol. 6, pp. 54-55.

Rauschmann, M.A., Huggenberger, S., Kossatz, L.S. & Oelschlaeger, H.H. 2006, "Head morphology in perinatal dolphins: a window into phylogeny and ontogeny", *Journal of Morphology,* vol. 267, no. 11, pp. 1295-1315.

Ravosa, M.J., Johnson, K.R. & Hylander, W.L. 2000a, "Strain in the galago facial skull", *Journal of Morphology,* vol. 245, no. 1, pp. 51-66.

Ravosa, M.J., Noble, V.E., Hylander, W.L., Johnson, K.R. & Kowalski, E.M. 2000b, "Masticatory stress, orbital orientation and the evolution of the primate postorbital bar", *Journal of Human Evolution,* vol. 38, no. 5, pp. 667-693.

Rayfield, E.J. 2011, "Strain in the ostrich mandible during simulated pecking and validation of specimen-specific finite element models", *Journal of Anatomy,* vol. 218, no. 1, pp. 47-58.

Rayfield, E.J. 2007, "Finite element analysis and understanding the biomechanics and evolution of living and fossil organisms", *Annual Review of Earth Planetary Science,* vol. 35, pp. 541-576.

Rees, J. 2001, "An investigation into the importance of the periodontal ligament and alveolar bone as supporting structures in finite element studies", *Journal of Oral Rehabilitation,* vol. 28, no. 5, pp. 425-432.

Rees, J. & Jacobsen, P. 1997, "Elastic modulus of the periodontal ligament", *Biomaterials,* vol. 18, no. 14, pp. 995-999.

Reighard, J.E. & Jennings, H.S. 1901, *Anatomy of the Cat,* New York, H. Holt.

Reiter, A.M. & Soltero-Rivera, M.M. 2014, "Applied feline oral anatomy and tooth extraction techniques: an illustrated guide", *Journal of Feline Medicine and Surgery,* vol. 16, no. 11, pp. 900-913.

Richmond, B.G., Wright, B.W., Grosse, I., Dechow, P.C., Ross, C.F., Spencer, M.A. & Strait, D.S. 2005, "Finite element analysis in functional morphology", *The Anatomical Record Part A: Discoveries in Molecular, Cellular, and Evolutionary Biology: An Official Publication of the American Association of Anatomists,* vol. 283, no. 2, pp. 259-274.

Ridgway, S.H., Carlin, K.P., Van Alstyne, K.R., Hanson, A.C. & Tarpley, R.J. 2016, "Comparison of Dolphins' Body and Brain Measurements with Four Other Groups of Cetaceans Reveals Great Diversity", *Brain, Behavior and Evolution,* vol. 88, no. 3-4, pp. 235-257.

Rohen, J.W., Yokochi, C. & Lütjen-Drecoll, E. 2006, *Color atlas of anatomy: a photographic study of the human body,* Philadelphia and Baltimore, Schattauer Verlag.

Rommel, S.A., Pabst, D.A. & McLellan, W.A. 2009, "Skull anatomy" in Würsig, B., Thewissen, J.G.M. & Kovacs K.M. (ed.), *Encyclopedia of marine mammals*, London, San Diego, Cambridge and Oxford, Academic Press, pp. 1033-1047.

Ross, C.F. & Hylander, W.L. 1996, "In vivo and in vitro bone strain in the owl monkey circumorbital region and the function of the postorbital septum", *American Journal of Physical Anthropology: The Official Publication of the American Association of Physical Anthropologists,* vol. 101, no. 2, pp. 183-215.

Rowe, T., Rich, T.H., Vickers-Rich, P., Springer, M. & Woodburne, M.O. 2008, "The oldest platypus and its bearing on divergence timing of the platypus and echidna clades", *Proceedings of the National Academy of Sciences of the United States of America,* vol. 105, no. 4, pp. 1238-1242.

Ruan, J.S., Khalil, T.B. & King, A.I. 1993, "Finite element modeling of direct head impact", *37th Stapp Car Crash Conference Proceedings-P-269, SAE 1993 Transactions: Journal of Passenger Cars-V102-6.*

Saban, R. 1975, "Structure of the ear region in living and subfossil lemurs" in Tattersall, Ian & Sussman, R.W. (ed.), *Lemur biology,* New York and London, Plenum Press, pp. 83-110.

Sabet, A.A., Christoforou, E., Zatlin, B., Genin, G.M. & Bayly, P.V. 2008, "Deformation of the human brain induced by mild angular head acceleration", *Journal of Biomechanics,* vol. 41, no. 2, pp. 307-315.

Sakamoto, M., Lloyd, G. & Benton, M. 2010, "Phylogenetically structured variance in felid bite force: the role of phylogeny in the evolution of biting performance", *Journal of Evolutionary Biology,* vol. 23, no. 3, pp. 463-478.

Sakamoto, M. & Ruta, M. 2012, "Convergence and divergence in the evolution of cat skulls: temporal and spatial patterns of morphological diversity", *PLoS One,* vol. 7, no. 7, pp. 1-13.

Saldino, R. M., & Di Chiro, G., 1974, "Tentorial calcification", *Radiology*, Vol. 111, no. 1, pp. 207-210.

Salles, L.O. 1992, "Felid phylogenetics: extant taxa and skull morphology (Felidae, Aeluroidea)", *American Museum Novitates*; no. 3047, pp. 2-67.

Sands, S. F., Farmer, P., Alvarez, O., Keller, I. A., Gorey, M. T., & Hyman, R. A., 1987, "Fat within the falx: MR demonstration of falcine bony metaplasia with marrow formation", *Journal of computer assisted tomography*, Vol. 11, no. 4, pp. 602-605.

Santana, S. & Lofgren, S. 2013, "Does nasal echolocation influence the modularity of the mammal skull?", *Journal of Evolutionary Biology,* vol. 26, no. 11, pp. 2520-2526.

Sarnat, B.G. & Wexler, M.R. 1966, "Growth of the face and jaws after resection of the septal cartilage in the rabbit", *American Journal of Anatomy,* vol. 118, no. 3, pp. 755-767.

Sarvghad-Moghaddam, H., Karami, G. & Ziejewski, M. 2014, "The Effects of Directionality of Blunt Impacts on Mechanical Response of the Brain", *ASME 2014 International Mechanical Engineering Congress and Exposition,* American Society of Mechanical Engineers, pp. V003T03A013.

SCHEY, W.L. 1974, "Intracranial calcifications in childhood: frequency of occurrence and significance", *American Journal of Roentgenology,* vol. 122, no. 3, pp. 495-502.

Schmidt, V. 2015, *Comparative anatomy of the pig brain: an integrative magnetic resonance imaging (MRI) study of the porcine brain with special emphasis on the external morphology of the cerebral cortex*, P.h.D. Thesis, Giessen University.

Schmidt, M. & Ondreka, N. 2018, "Hydrocephalus in Animals", in Cinalli G., Ozek M. & Sainte-Rose C. (ed.), *Pediatric Hydrocephalus,* Springer, pp. 1-53.

Schneider, C.A., Rasband, W.S. & Eliceiri, K.W. 2012, "NIH Image to ImageJ: 25 years of image analysis", *Nature Methods,* vol. 9, no. 7, pp. 671.

Schutte, S., van den Bedem, Sven PW, van Keulen, F., van der Helm, Frans CT & Simonsz, H.J. 2006, "A finite-element analysis model of orbital biomechanics", *Vision Research,* vol. 46, no. 11, pp. 1724-1731.

Schwartz-Dabney, C.a. & Dechow, P. 2003, "Variations in cortical material properties throughout the human dentate mandible", *American Journal of Physical Anthropology: The Official Publication of the American Association of Physical Anthropologists,* vol. 120, no. 3, pp. 252-277.

Schweigert, F.J., Raila, J., Wichert, B. & Kienzle, E. 2002, "Cats absorb β-carotene, but it is not converted to vitamin A", *The Journal of Nutrition,* vol. 132, no. 6, pp. 1610S-1612S.

Sebastiani, A. & Fishbeck, D.W. 2005, *Mammalian anatomy: the cat,* Colorado, Morton Publishing Company.

Sedlmayr, J.C., Kirsch, C.F. & Wisco, J.J. 2009, "The human temporalis muscle: superficial, deep, and zygomatic parts comprise one structural unit", *Clinical Anatomy,* vol. 22, no. 6, pp. 655-664.

Sellés de Lucas, V., Dutel, H., Evans, S.E., Gröning, F., Sharp, A.C., Watson, P.J. & Fagan, M.J. 2018, "An assessment of the role of the falx cerebri and tentorium cerebelli in the cranium of the cat (Felis silvestris catus)", *Journal of The Royal Society Interface,* vol. 15, no. 147, pp. 1-9.

Sharp, A.C., Dutel, H., Crumpton, N., Fagan, M. & Evans, S.E. 2018. "The role of soft tissues in a biomechanical model of the rat cranium", *Society of Integrative and Comparative Biology (SICB) Annual Meeting*, San Francisco, USA.

Shoshani, J. & McKenna, M.C. 1998, "Higher taxonomic relationships among extant mammals based on morphology, with selected comparisons of results from molecular data", *Molecular Phylogenetics and Evolution,* vol. 9, no. 3, pp. 572-584.

Sicuro, F.L. & Oliveira, L.F.B. 2011, "Skull morphology and functionality of extant Felidae (Mammalia: Carnivora): a phylogenetic and evolutionary perspective", *Zoological Journal of the Linnean Society,* vol. 161, no. 2, pp. 414-462.

Siegel, J.M. 1974, "A stereotaxic map of the bony tentorium of the cat", *Physiology & Behavior,* vol. 13, no. 5, pp. 715-717.

Siegler, S., Block, J. & Schneck, C.D. 1988, "The mechanical characteristics of the collateral ligaments of the human ankle joint", *Foot & Ankle,* vol. 8, no. 5, pp. 234-242.

Slater, G. & Van Valkenburgh, B. 2009, "Allometry and performance: the evolution of skull form and function in felids", *Journal of Evolutionary Biology,* vol. 22, no. 11, pp. 2278-2287.

Smith, A.L., Benazzi, S., Ledogar, J.A., Tamvada, K., Pryor Smith, L.C., Weber, G.W., Spencer, M.A., Lucas, P.W., Michael, S. & Shekeban, A. 2015, "The Feeding Biomechanics and Dietary Ecology of P aranthropus boisei", *The Anatomical Record,* vol. 298, no. 1, pp. 145-167.

Smith, N.B. & Webb, A. 2010, *Introduction to medical imaging: physics, engineering and clinical applications,* Cambridge, Cambridge university press.

Smith, T.D., Deleon, V.B. & Rosenberger, A.L. 2013, "At birth, tarsiers lack a postorbital bar or septum", *The Anatomical Record,* vol. 296, no. 3, pp. 365-377.

Snell, R.S. 2010, *Clinical neuroanatomy,* Baltimore and Philadelphia, Lippincott Williams & Wilkins.

Solano, M. & Brawer, R.S. 2004, "CT of the equine head: technical considerations, anatomical guide, and selected diseases", *Clinical Techniques in Equine Practice,* vol. 3, no. 4, pp. 374-388.

Song, W.K., Lew, H., Yoon, J.S., Oh, M. & Lee, S.Y. 2009, "Role of medial orbital wall morphologic properties in orbital blow-out fractures", *Investigative Ophthalmology & Visual Science,* vol. 50, no. 2, pp. 495-499.

Soons, J., Herrel, A., Genbrugge, A., Adriaens, D., Aerts, P. & Dirckx, J. 2012, "Multi-layered bird beaks: a finite-element approach towards the role of keratin in stress dissipation", *Journal of the Royal Society Interface,* vol. 9, no. 73, pp. 1787-1796.

Spector, S. A., Gardiner, P. F., Zernicke, R. F., Roy, R. R., & Edgerton, V. R., 1980, "Muscle architecture and force-velocity characteristics of cat soleus and medial gastrocnemius: implications for motor control", *journal of Neurophysiology*, vol. 44 no. 5, pp. 951-960.

St. Leger, J.A., Righton, A.L., Nilson, E.M., Fascetti, A.J., Miller, M.A., Tuomi, P.A., Goertz, C.E. & Puschner, B. 2011, "Vitamin A deficiency and hepatic retinol levels

in sea otters, Enhydra lutris", *Journal of Zoo and Wildlife Medicine,* vol. 42, no. 1, pp. 98-104.

Stitzel, J. D., Duma, S. M., Cormier, J. M., & Herring, I. P., 2002, *A nonlinear finite element model of the eye with experimental validation for the prediction of globe rupture* (No. 2002-22-0005). SAE Technical Paper.

Takhounts, E.G., Eppinger, R.H., Campbell, J.Q. & Tannous, R.E. 2003, "On the development of the SIMon finite element head model", *Stapp Car Crash Journal,* vol. 47, pp. 107.

Tambusso, P.S. & Farina, R.A. 2015a, "Digital endocranial cast of Pampatherium humboldtii (Xenarthra, Cingulata) from the late Pleistocene of Uruguay", *Swiss Journal of Palaeontology,* vol. 134, no. 1, pp. 109-116.

Tambusso, P.S. & Fariña, R.A. 2015b, "Digital cranial endocast of Pseudoplohophorus absolutus (Xenarthra, Cingulata) and its systematic and evolutionary implications", *Journal of Vertebrate Paleontology,* vol. 35, no. 5, pp. e967853.

Tanaka, Y. & Takeuchi, K. 1974, "Dural Calification from the Neurosurgical Point of View", *Neurologia Medico-Chirurgica,* vol. 14, supplement, pp. 5-10.

Theuwissen, E., Smit, E., & Vermeer, C., 2012, "The role of vitamin K in soft-tissue calcification", *Advances in Nutrition*, Vol. 3, no. 2, pp. 166-173.

Thomason, J. 1991, "Cranial strength in relation to estimated biting forces in some mammals", *Canadian Journal of Zoology,* vol. 69, no. 9, pp. 2326-2333.

Tohno, Y., Tohno, S., Minami, T., Moriwake, Y., Yamada, M., Furuta, K., Yamada, M., Haga, S. & Yamamoto, H. 2000, "Differences in the mineral contents between falx cerebri and tentorium cerebelli", *Biological Trace Element Research,* vol. 78, no. 1-3, pp. 43-52.

Toledo, P.M.d. & Domning, D.P. 1989, "Fossil Sirenia (Mammalia: Dugongidae) from the Pirabas Formation (Early Miocene), northern Brazil.", *O Boletim do Museu Paraense Emílio Goeldi*, vol. 1, no. 2, pp. 119-146.

Toms, S. R., & Eberhardt, A. W., 2003, "A nonlinear finite element analysis of the periodontal ligament under orthodontic tooth loading", *American Journal of Orthodontics and Dentofacial Orthopedics*, Vol. 123, no. 6, pp. 657-665.

Toro-Ibacache, V., Fitton, L.C., Fagan, M.J. & O'Higgins, P. 2016, "Validity and sensitivity of a human cranial finite element model: implications for comparative studies of biting performance", *Journal of Anatomy,* vol. 228, no. 1, pp. 70-84.

Tortopidis, D., Lyons, M., Baxendale, R. & Gilmour, W. 1998, "The variability of bite force measurement between sessions, in different positions within the dental arch", *Journal of Oral Rehabilitation,* vol. 25, no. 9, pp. 681-686.

Truong, D.Q., Magerowski, G., Pascual-Leone, A., Alonso-Alonso, M. & Bikson, M. 2012, "Finite Element study of skin and fat delineation in an obese subject for transcranial Direct Current Stimulation", *Engineering in Medicine and Biology Society (EMBC), 2012 Annual International Conference of the IEEE,* pp. 6587.

Tse, K.M., Tan, L.B., Lim, S.P. & Lee, H.P. 2015, "Conventional and complex modal analyses of a finite element model of human head and neck", *Computer Methods in Biomechanics and Biomedical Engineering,* vol. 18, no. 9, pp. 961-973.

Tse, K.M., Tan, L.B., Lim, S.P. & Lee, H.P. 2015, "Conventional and complex modal analyses of a finite element model of human head and neck", *Computer Methods in Biomechanics and Biomedical Engineering,* vol. 18, no. 9, pp. 961-973.

Tsitouridis, I., Natsis, K., Goutsaridou, F., Tsitouridis, K., Tarazi, L., Chondromatidou, S., Papapostolou, P., Papastergiou, C. & Emmanouilidou, M. 2006, "Falx Cerebri Ossification: CT and MRI Evaluation", *The Neuroradiology Journal,* vol. 19, no. 5, pp. 621-628.

Tubbs, R.S., Kelly, D.R., Lott, R., Salter, E.G. & Oakes, W.J. 2006, "Complete ossification of the human falx cerebri", *Clinical Anatomy,* vol. 19, no. 2, pp. 147-150.

Tubbs, R.S., Mortazavi, M.M., Miller, J., Shoja, M.M., Loukas, M. & Cohen-Gadol, A.A. 2012, "Ossification of the Human Tentorium Cerebelli", *Biomedicine International,* vol. 3, no. 1, pp. 34-38.

Turnbull, W.D. 1970, "Mammalian masticatory apparatus", *Fieldiana: Geology,* vol. 18, no. 2.

Turner, A. & Antón, M. 1997, *The big cats and their fossil relatives: an illustrated guide to their evolution and natural history,* New York, Columbia University Press.

Van der Lugt, Jaco J & Prozesky, L. 1989, "The pathology of blindness in new-born calves caused by hypovitaminosis A", *Onderstepoort Journal of Veterinary Research*, no. 56, pp. 99-109.

Van Eijden, T.M., Koolstra, J.H. & Brugman, P. 1996, "Three-dimensional structure of the human temporalis muscle", *The Anatomical Record: An Official Publication of the American Association of Anatomists,* vol. 246, no. 4, pp. 565-572.

Van Eijden, T., Korfage, J. & Brugman, P. 1997, "Architecture of the human jaw-closing and jaw-opening muscles", *The Anatomical Record: An Official Publication of the American Association of Anatomists,* vol. 248, no. 3, pp. 464-474.

Van Valkenburgh, B., Curtis, A., Samuels, J.X., Bird, D., Fulkerson, B., Meachen-Samuels, J. & Slater, G.J. 2011, "Aquatic adaptations in the nose of carnivorans: evidence from the turbinates", *Journal of Anatomy,* vol. 218, no. 3, pp. 298-310.

Van Valkenburgh, B., Pang, B., Bird, D., Curtis, A., Yee, K., Wysocki, C. & Craven, B.A. 2014, "Respiratory and olfactory turbinals in feliform and caniform carnivorans: the influence of snout length", *The Anatomical Record,* vol. 297, no. 11, pp. 2065-2079.

Van Valkenburgh, B., Theodor, J., Friscia, A., Pollack, A. & Rowe, T. 2004, "Respiratory turbinates of canids and felids: a quantitative comparison", *Journal of Zoology,* vol. 264, no. 3, pp. 281-293.

Vaughan, T., Ryan, J. & Czaplewski, N. 2015, *Mammalogy,* New York, Jones & Bartlett Learning.

Walsh, D. R., Ross, A. M., Malijauskaite, S., Flanagan, B. D., Newport, D. T., McGourty, K. D., & Mulvihill, J. J., 2018, "Regional mechanical and biochemical properties of the porcine cortical meninges", *Acta biomaterialia*, Vol. 80, pp. 237-246.

Wang, Q., Wood, S.A., Grosse, I.R., Ross, C.F., Zapata, U., Byron, C.D., Wright, B.W. & Strait, D.S. 2012, "The role of the sutures in biomechanical dynamic simulation of a macaque cranial finite element model: implications for the evolution of craniofacial form", *The Anatomical Record: Advances in Integrative Anatomy and Evolutionary Biology,* vol. 295, no. 2, pp. 278-288.

Warburton, N. & Travouillon, K. 2016, "The biology and palaeontology of the Peramelemorphia: a review of current knowledge and future research directions", *Australian Journal of Zoology,* vol. 64, no. 3, pp. 151-181.

Ward, C.C. & Thompson, R.B. 1975, "The development of a detailed finite element brain model*", SAE Technical Paper 751163*, pp. 3238-3252.

Weickenmeier, J. 2015, *Investigation of the Mechanical Behavior of Facial Soft Tissues*, P.h.D. Thesis, ETH Zurich.

Weijs, W. & Hillen, B. 1985, "Physiological cross-section of the human jaw muscles", *Cells Tissues Organs,* vol. 121, no. 1, pp. 31-35.

Westerman, M., Krajewski, C., Kear, B.P., Meehan, L., Meredith, R.W., Emerling, C.A. & Springer, M.S. 2016, "Phylogenetic relationships of dasyuromorphian marsupials revisited", *Zoological Journal of the Linnean Society,* vol. 176, no. 3, pp. 686-701.

Wickland, C., Baker, J. & Peterson, B. 1991, "Torque vectors of neck muscles in the cat", *Experimental Brain Research,* vol. 84, no. 3, pp. 649-659.

Witzel, U. 2011, "Virtual synthesis of the skull in Neanderthals by FESS" in Condemi, S. & Weniger, G. (ed.), *Continuity and Discontinuity in the Peopling of Europe*, London and New York, Springer, pp. 203-211.

Wood, S.A., Strait, D.S., Dumont, E.R., Ross, C.F. & Grosse, I.R. 2011, "The effects of modeling simplifications on craniofacial finite element models: the alveoli (tooth sockets) and periodontal ligaments", *Journal of Biomechanics,* vol. 44, no. 10, pp. 1831-1838.

Wormald, P. J., & Alun-Jones, T. 1991, "Anatomy of the temporalis fascia", *The Journal of Laryngology & Otology*, vol. 105, no. 7, pp. 522-524.

Wortman, J.L. 1894, "Osteology of Patriofelis, a Middle Eocene creodont", *Bulletin of the AMNH*, vol. 6, article 5, pp. 129-165.

Wroe, S. 2008, "Cranial mechanics compared in extinct marsupial and extant African lions using a finite-element approach", *Journal of Zoology,* vol. 274, no. 4, pp. 332-339.

Wroe, S., Chamoli, U., Parr, W.C., Clausen, P., Ridgely, R. & Witmer, L. 2013, "Comparative biomechanical modeling of metatherian and placental saber-tooths: a different kind of bite for an extreme pouched predator", *PLoS One,* vol. 8, no. 6, pp. 1-9.

Wroe, S., Ferrara, T.L., McHenry, C.R., Curnoe, D. & Chamoli, U. 2010, "The craniomandibular mechanics of being human", *Proceedings of the Royal Society B: Biological Sciences,* vol. 277, no. 1700, pp. 3579-3586.

Wu, S.G. 2012, "Developing a Three Dimensional Finite Element Model of the Anterior Cruciate Ligament to Examine the Risk Factors for Women during the Sidestep Cutting Maneuver", BsC Project, Worcester Polytechnic Institute.

Yan, W. & Pangestu, O.D. 2011, "A modified human head model for the study of impact head injury", *Computer Methods in Biomechanics and Biomedical Engineering,* vol. 14, no. 12, pp. 1049-1057.

Yang, K.H., Mao, H., Wagner, C., Zhu, F., Chou, C.C. & King, A.I. 2011, "Modeling of the brain for injury prevention" in Bilson, L.E. (ed.), *Neural tissue biomechanics,* Heidelberg, Dordrecht, London and New York, Springer, pp. 69-120.

Yue, X., Wang, L., Sun, S., & Tong, L., 2008, "Viscoelastic finite-element analysis of human skull-dura mater system as intracranial pressure changing", *African Journal of Biotechnology*, Vol. *7*, no. 6, pp. 689-695.

Zandian, A., Clarke, P., Tubbs, R. & Loukas, M. 2014, "A partially ossified falx cerebri", *Folia Morphologica,* vol. 73, no. 3, pp. 363-365.

Zhang, L., Yang, K.H. & King, A.I. 2001, "Comparison of brain responses between frontal and lateral impacts by finite element modeling", *Journal of Neurotrauma,* vol. 18, no. 1, pp. 21-30.

Ziegler, A., Kunth, M., Mueller, S., Bock, C., Pohmann, R., Schröder, L., Faber, C. & Giribet, G. 2011, "Application of magnetic resonance imaging in zoology", *Zoomorphology,* vol. 130, no. 4, pp. 227-254.

Zienkiewicz, O.C., 1971. *The Finite Element Method in Engineering Science*, London, McGraw Hill.

# Appendices

**Appendix 1. Dural folds condition in extant species**

The following table includes all the extant species discussed in Chapter 3, noting the presence or absence of ossified dural folds. Taxonomy mainly follows Vaughan *et al.*, (2015). Discrepancies in literature concerning the presence of an ossified tentorium in some species of Primates have been marked as "NO/YES" (the "no" indicating the first reference; in all cases, Nojima, 1990b). Those specimens observed in the Grant Museum in which the presence of the osseous tentorium could not be univocally identified has been marked as "Uncertain".

| SUPERORDER/ORDER/ INFRAORDER | FAMILY | GENUS | SPECIES | OSSIF. FALX | OSSIF. TENTORIUM | REFERENCES |
|---|---|---|---|---|---|---|
| Monotremata | Tachyglossidae | Tachyglossus | *Tachyglossus aculeatus* | NO | NO | Grant, 1834;  Macrini et al., 2006 |
| Monotremata | Tachyglossidae | Zaglossus | *Zaglossus bartoni/brujini* | NO | NO | Grant, 1834 |
| Monotremata | Ornithorhynchidae | Ornithorhynchus | *Ornithorhynchus anatinus* | YES | NO | (Nojima, 1990a (after Owen 1866); Macrini, 2006) |
| Didelphimorphia | Didelphidae | Didelphis | *Didelphis virginiana* |  | NO | Klintworth, 1968 |
| Dasyuromorphia | Thylacinidae | Thylacinus | *Thylacinus cynocephalus* | NO | YES | Grant Museum, sp. Z90 |
| Dasyuromorphia | Dasyuridae | Antechinus | *Antechinus flavipes* | NO | NO | Grant Museum, sp. specimen Z98b |
| Peramelemorphia | Peramelidae | Perameles | *Perameles nasuta* | NO | UNCERTAIN | Grant Museum, sp. Z1684 |
| Peramelemorphia | Peramelidae | Isoodon sp | *Isoodon sp* | NO | UNCERTAIN | Grant Museum, sp. Z1751 |
| Diprotodontia | Phascolarctidae | Phascolarctos | *Phascolarctos cinereus* | NO | UNCERTAIN | Grant Museum, sp. Z699 |
| Diprotodontia | Vombatidae | Vombatus | *Vombatus ursinus* | NO | YES | Grant Museum, sp. Z68 |
| Diprotodontia | Phalangeridae | Trichosurus | *Trichosurus vulpecula* | NO | UNCERTAIN | Grant Museum, sp. Z100 |
| Diprotodontia | Macropodidae | Macropus | *Macropus brownii* | NO | YES | Klintworth, 1968; Nojima, 1988 |
| Diprotodontia | Macropodidae | Dendrolagus | *Dendrolagus sp* |  | YES | Nojima, 1988 |
| Diprotodontia | Macropodidae | Macropus | *Macropus giganteus* | NO | YES | Grant Museum, sp. Z1681 |
| Diprotodontia | Macropodidae | Macropus | *Macropus fuliginosus* | NO | YES | Grant Museum, sp. Z1210 |
| Diprotodontia | Pseudocheiridae | Pseudocheirus sp | *Pseudocheirus sp* | NO | UNCERTAIN | Grant Museum, sp. Z74 |
| Diprotodontia | Petauridae | Dactylopsila | *Dactylopsila trivirgata* | NO | UNCERTAIN | Grant Museum, sp. Z72 |
| Xenarthra | Megalonychidae | Choloepus | *Choloepus didactylus* | NO | NO | Grant Museum, sp. Z130a |
| Xenarthra/cingulata | Dasypodidae | Dasypus | *Dasypus kappleri* |  | YES | Feijó and Cordeiro-Estrela, 2016 |
| Xenarthra/cingulata | Dasypodidae | Dasypus | *Dasypus pastasae* |  | YES | Feijó and Cordeiro-Estrela, 2016 |
| Xenarthra/cingulata | Dasypodidae | Dasypus | *Dasypus beniensis* |  | YES | Feijó and Cordeiro-Estrela, 2016 |
| Xenarthra/cingulata | Dasypodidae | Dasypus | *Dasypus novemcinctus* | NO | YES | Grant Museum, sp. Z134 |
| Xenarthra | Myrmecophagidae | Myrmecophaga | *Myrmecophaga tridactyla* | NO | NO | Grant Museum, sp. Z1554 |
| Insectivora | Tenrecidae | Tenrec | *Tenrec ecaudatus* | NO | NO | Grant Museum, sp. Z3064 |
| Insectivora | Tenrecidae | Setifer | *Setifer setosus* | NO | NO | Grant Museum, sp. Z610 |
| Insectivora | Erinaceidae | Echinosorex | *Echinosorex gymnura* | NO | NO | Grant Museum, sp. Z606 |
| Insectivora | Talpidae | Talpa | *Talpa europaea* | NO | NO | Grant Museum, sp. Z600a |

| SUPERORDER/ORDER/ INFRAORDER | FAMILY | GENUS | SPECIES | OSSIF. FALX | OSSIF. TENTORIUM | REFERENCES |
|---|---|---|---|---|---|---|
| Chiroptera | Pteropodidae | Rousettus | *Rousettus aegyptiacus* | NO | NO | Dissection (personal observation) |
| Chiroptera | Vespertilionidae | | *Nycticeius humeralis* | | NO | Klintworth, 1968 |
| Primates | Lemuridae | Lemur | *Lemur catta/ Eulemur mongoz* | NO | NO | Nojima, 1990b |
| Primates | Lemuroidea | Daubentonia | *Daubentonia madagascariensis* | | YES | Saban in Tattersall and Sussman, ed., 1975 |
| Primates | Galagidae | Galago sp | *Galago sp* | NO | NO | Grant Museum, sp. Z2361 |
| Primates | Lorisidae | Loris | *Loris tardigradus* | NO | NO | Nojima, 1990b |
| Primates | Lorisidae | Nycticebus | *Nycticebus Coucang* | NO | NO | Nojima, 1990b |
| Primates | Lorisidae | Galago | *Galago senegalensis* | NO | NO | Nojima, 1990b |
| Primates | Cheirogaleidae | Cheirogaleus sp | *Cheirogaleus sp* | UNCERTAIN | NO | Grant Museum, sp. Z411 |
| Primates | Indriidae | Propithecus sp | *Propithecus sp* | NO | NO | Grant Museum, sp. Z405 |
| Primates | Tarsiidae | Tarsius | *Tarsius sp* | | NO | Horovitz and McPhee, 1999 |
| Primates | Cercopithecidae | Erythrocebus | *Erythrocebus patas* | NO | NO | Nojima, 1990b; Horovitz and McPhee, 1999 |
| Primates | Cercopithecidae | Macaca | *Macaca mulatta* | NO | NO | Nojima, 1990b; Horovitz and McPhee, 1999 |
| Primates | Cercopithecidae | Macaca | *Macaca fascicularis / M. fuscata* | NO | NO | Nojima, 1990b; Horovitz and McPhee, 1999 |
| Primates | Cercopithecidae | Cercopithecus | *Cercopithecus aethiops* | NO | NO | Nojima, 1990b; Horovitz and McPhee, 1999 |
| Primates | Cercopithecidae | Chaeropithecus | *Chaeropithecus papio* | NO | NO | Nojima, 1990b; Horovitz and McPhee, 1999 |
| Primates | Cercopithecidae | Papio cynocephalus | *Papio cynocephalus* | NO | NO | Nojima, 1990b; Horovitz and McPhee, 1999 |
| Primates | Cercopithecidae | Mandrillus | *Mandrillus leucophaeus* | NO | NO | Nojima, 1990b; Horovitz and McPhee, 1999 |
| Primates | Cercopithecidae | Theropithecus | *Theropithecus gelada* | NO | NO | Nojima, 1990b; Horovitz and McPhee, 1999 |
| Primates | Cercopithecidae | Cercopithecus | *C. ascanius / C. cephus / C. mitis* | NO | NO | Nojima, 1990b; Horovitz and McPhee, 1999 |
| Primates | Cercopithecidae | Colobus | *Colobus badius* | NO | NO | Nojima, 1990b |
| Primates | Cercopithecidae | Nasalis | *Nasalis larvatus* | NO | NO | Nojima, 1990b |

| SUPERORDER/ORDER/ INFRAORDER | FAMILY | GENUS | SPECIES | OSSIF. FALX | OSSIF. TENTORIUM | REFERENCES |
|---|---|---|---|---|---|---|
| Primates | Cercopithecidae | Presbytis | *Presbytis entellus / P. obscura* | NO | NO | Nojima, 1990b |
| Primates | Hominidae | Pongo | *Pongo pygmaeus* | NO | NO | Nojima, 1990b |
| Primates | Hominidae | Gorilla | *Gorilla gorilla* | NO | NO | Nojima, 1990b |
| Primates | Hominidae | Pan | *Pan troglodytes / Pan Paniscus* | NO | NO | Nojima, 1990b |
| Primates | Hylobatidae | Hylobates lar (Lar gibbon) | *Hylobates lar* | NO | NO | Nojima, 1990b; Horovitz and McPhee, 1999 |
| Primates | Callitrichidae | Callithrix | *Callithrix jacchus* | NO | NO/YES | Nojima, 1990b; Horovitz and McPhee, 1999; Kay *et al.*, 2008 |
| Primates | Callitrichidae | Saguinus | *Saguinus nigricollis/ S. oedipus* | NO | NO/YES | Nojima, 1990b; Horovitz and McPhee, 1999; Kay *et al.*, 2008 |
| Primates | Callitrichidae | Leontopithecus | *Leontopithecus rosalia* | NO | NO/YES | Nojima, 1990b; Horovitz and McPhee, 1999; Kay *et al.*, 2008 |
| Primates | Callitrichidae | Callimico | *Callimico goeldii* | | NO/YES | Horovitz and McPhee, 1999, Kay *et al.*, 2008 |
| Primates | Callitrichidae | Cebuella | *Cebuella sp* | | NO/YES | Horovitz and McPhee, 1999, Kay *et al.*, 2008 |
| Primates | Cebidae | Saimiri | *Saimiri sciureus* | NO | NO/YES | Nojima, 1990b; Horovitz and McPhee, 1999 |
| Primates | Cebidae | Cebus | *Cebus albifrons / C. apella* | NO | NO/YES | Nojima, 1990b; Horovitz and McPhee, 1999; Kay *et al.*, 2008; Grant Museum, sp. Z910 |
| Primates | Cebidae | Aotus | *Aotus trivirgatus* | NO | NO/YES | Nojima, 1990b; Horovitz and McPhee, 1999; Grant Museum, sp. Z414 |
| Primates | Cebidae | Callicebus | *Callicebus moloch* | NO | NO/YES | Nojima, 1990b; Horovitz and McPhee, 1999 |
| Primates | Cebidae | Pithecia | *Pithecia  monachus* | NO | NO/YES | Nojima, 1990b; Horovitz and McPhee, 1999 |
| Primates | Cebidae | Chiropotes | *Chiropotes satanas* | NO | NO/YES | Nojima, 1990b; Horovitz and McPhee, 1999 |
| Primates | Cebidae | Alouatta | *Alouatta caraya / A. seniculus* | NO | NO/YES | Nojima, 1990b; Horovitz and McPhee, 1999 |
| Primates | Cebidae | Lagothrix | *Lagothrix  lagothricha* | NO | NO/YES | Nojima, 1990b; Horovitz and McPhee, 1999 |

| SUPERORDER/ORDER/INFRAORDER | FAMILY | GENUS | SPECIES | OSSIF. FALX | OSSIF. TENTORIUM | REFERENCES |
|---|---|---|---|---|---|---|
| Primates | Cebidae/Atelidae | Ateles | *Ateles geoffroyi* | NO | YES | Jeffery *et al.*, 2008; Nojima, 1990a |
| Primates | Cebidae | Ateles | *Ateles paniscus* | NO | YES | Nojima, 1990a |
| Primates | Cebidae | Ateles | *Brachyteles* | | YES | Horovitz and McPhee, 1999 |
| Primates | Pitheciidae | Cacajao | *Cacajao sp* | | YES | Horovitz and McPhee, 1999 |
| Carnivora | Felidae | Panthera | *Panthera tigris* | NO | YES | Nojima, 1988; Nojima, 1990c |
| Carnivora | Felidae | Panthera | *Panthera  leo* | NO | YES | Nojima, 1988; Nojima, 1990c |
| Carnivora | Felidae | Panthera | *Panthera pardus* | NO | YES | Nojima, 1988; Nojima, 1990c |
| Carnivora | Felidae | Panthera | *Panthera uncia* | NO | YES | Nojima, 1988; Nojima, 1990c |
| Carnivora | Felidae | Panthera | *Panthera onca* | NO | YES | Nojima, 1990c |
| Carnivora | Felidae | Felis | *Felis catus* | NO | YES | Nojima, 1988; Nojima, 1990c |
| Carnivora | Felidae | Felis | *Felis iriomotensis* | NO | YES | Nojima, 1990c |
| Carnivora | Felidae | Felis | *Felis lynx* | NO | YES | Nojima, 1990c |
| Carnivora | Felidae | Felis | *Felis chaus* | NO | YES | Nojima, 1990c |
| Carnivora | Felidae | Felis | *Felis bengalensis* | NO | YES | Nojima, 1990c |
| Carnivora | Felidae | Felis | *Felis serval* | NO | YES | Nojima, 1990c |
| Carnivora | Viverridae | Paguma | *Paguma larvata* | NO | YES | Nojima, 1988; Nojima, 1990c |
| Carnivora | Herpestidae | Herpestes sp | *Herpestes sp* | NO | YES | Grant Museum, sp. Z366 |
| Carnivora | Hyaenidae | Crocuta | *Crocuta crocuta* | NO | YES | Nojima, 1988; Nojima, 1990c |
| Carnivora | Canidae | Canis | *Canis lupus* | NO | YES | Nojima, 1988; Nojima, 1990c |
| Carnivora | Canidae | Canis | *Canis familiaris* | NO | YES | Klintworth, 1968; Nojima, 1988; Nojima, 1990c |
| Carnivora | Canidae | Lycaon | *Lycaon pictus* | NO | YES | Nojima, 1988; Nojima, 1990c |
| Carnivora | Canidae | Canis | *Canis latrans* | NO | YES | Nojima, 1988 |
| Carnivora | Canidae | Canis | *Canis aureus* | NO | YES | Nojima, 1988; Nojima, 1990c |
| Carnivora | Canidae | Canis | *Canis mesomelas or adustus* | NO | YES | Nojima, 1988 |
| Carnivora | Canidae | Vulpes | *Vulpes vulpes* | NO | YES | Nojima, 1988 |
| Carnivora | Canidae | Chrysocyon | *Chrysocyon brachyurus* | NO | YES | Nojima, 1988; Nojima, 1990c |
| Carnivora | Canidae | Nyctereutes | *Nyctereutes* | NO | YES | Nojima, 1988; Nojima, 1990c |

| SUPERORDER/ORDER/ INFRAORDER | FAMILY | GENUS | SPECIES | OSSIF. FALX | OSSIF. TENTORIUM | REFERENCES |
|---|---|---|---|---|---|---|
| Carnivora | Canidae | Speothos | *Speothos venaticus* | NO | YES | Nojima, 1988; Nojima, 1990c |
| Carnivora | Mephitidae | Conepatus | *Conepatus chinga* | NO | NO | Bryant *et al.*, 1993; Grant Museum, sp. Z376 |
| Carnivora | Mephitidae | Conepatus | *Conepatus humboldtii* | | NO | Bryant *et al.*, 1993 |
| Carnivora | Mephitidae | Conepatus | *Conepatus mesoleucus/leuconotus* | | NO | Bryant *et al.*, 1993 |
| Carnivora | Mephitidae | Mephitis | *Mephitis mephitis* | NO | NO | Nojima, 1990c; Bryant *et al.*, 1993; Grant Museum, sp. Z375 |
| Carnivora | Mephitidae | Mephitis | *Mephitis macroura* | NO | NO | Bryant *et al.*, 1993; Grant Museum, sp. Z375 |
| Carnivora | Mephitidae | Mydaus | *Mydaus javanensis* | | NO | Bryant *et al.*, 1993 |
| Carnivora | Mephitidae | Mydaus | *Mydaus marchei* | | NO | Bryant *et al.*, 1993 |
| Carnivora | Mephitidae | Spilogale | *Spilogale putorius* | | NO | Bryant *et al.*, 1993 |
| Carnivora | Ursidae | Thalarctos | *Thalarctos maritimus* | YES | YES | Nojima, 1988; Nojima, 1990c; Dong, 2008 |
| Carnivora | Ursidae | Ursus | *Ursus arctos* | YES | YES | Nojima, 1988; Nojima, 1990c |
| Carnivora | Ursidae | Ursus | *Ursus arctos middendorffi* | YES | YES | Nojima, 1988; Nojima, 1990c |
| Carnivora | Ursidae | Melursus | *Melursus ursinus* | | YES | Nojima, 1988; Nojima, 1990c |
| Carnivora | Ursidae | Ursus | *Ursus thibetanus* | | YES | Nojima, 1988; Nojima, 1990c |
| Carnivora | Ursidae | Ailuropoda | *Ailuropoda melanoleuca* | | YES | Dong, 2008 |
| Carnivora | Otariidae | Callorhinus | *Callorhinus ursinus* | YES | YES | Nojima, 1988; Nojima, 1990c |
| Carnivora | Otariidae | Arctocephalus | *Arctocephalus australis* | YES | YES | Nojima, 1988; Nojima, 1990c |
| Carnivora | Otariidae | Otaria | *Otaria byronia* | YES | YES | Nojima, 1988; Nojima, 1990c |
| Carnivora | Otariidae | Eumetopias | *Eumetopias jubatus* | YES | YES | Nojima, 1988; Nojima, 1990c |
| Carnivora | Otariidae | Zalophus | *Zalophus californianus* | YES | YES | Nojima, 1988; Nojima, 1990c |
| Carnivora | Phocidae | Hydrurga | *Hydrurga leptonyx* | YES | YES | Nojima, 1988; Nojima, 1990c |
| Carnivora | Phocidae | Erignathus | *Erignathus* | YES | YES | Nojima, 1988 |
| Carnivora | Phocidae | Cystophora | *Cystophora cristata* | YES | YES | Nojima, 1988; Nojima, 1990c |
| Carnivora | Phocidae | Phoca | *Phoca vitulina* | YES | YES | Nojima, 1988; Nojima, 1990c |
| Carnivora | Phocidae | Pusa | *Pusa hispida* | YES | YES | Nojima, 1988; Nojima, 1990c |
| Carnivora | Phocidae | Pagophilus | *Pagophilus groenlandicus* | YES | YES | Nojima, 1988; Nojima, 1990c |

229

| SUPERORDER/ORDER/ INFRAORDER | FAMILY | GENUS | SPECIES | OSSIF. FALX | OSSIF. TENTORIUM | REFERENCES |
|---|---|---|---|---|---|---|
| Carnivora | Phocidae | Histriophoca | *Histriophoca fasciata* | YES | YES | Nojima, 1988; Nojima, 1990c |
| Carnivora | Phocidae | Halichoerus | *Halichoerus grypus* | YES | YES | Nojima, 1988; Nojima, 1990c |
| Carnivora | Odobenidae | Odobenus | *Odobenus rosmarus* | YES | YES | Nojima, 1990c |
| Carnivora | Mustelidae | Eira | *Eira barbara* | | YES | Bryant *et al.*, 1993 |
| Carnivora | Mustelidae | Galictis | *Galictis vittala* | | YES | Bryant *et al.*, 1993 |
| Carnivora | Mustelidae | Galictis | *Galictis cuja* | | YES | Bryant *et al.*, 1993 |
| Carnivora | Mustelidae | Gulo | *Gulo gulo* | | YES | Bryant *et al.*, 1993 |
| Carnivora | Mustelidae | Ictonyx | *Ictonyx striatus* | | YES | Bryant *et al.*, 1993 |
| Carnivora | Mustelidae | Lyncodon | *Lyncodon patagonicus* | | YES | Bryant *et al.*, 1993 |
| Carnivora | Mustelidae | Martes | *Martes martes* | | YES | Bryant *et al.*, 1993 |
| Carnivora | Mustelidae | Martes | *Martes foina* | | YES | Bryant *et al.*, 1993 |
| Carnivora | Mustelidae | Martes | *Martes pennanti / Pekania pennanti* | | YES | Bryant *et al.*, 1993 |
| Carnivora | Mustelidae | Martes | *Martes flavigula* | | YES | Bryant *et al.*, 1993 |
| Carnivora | Mustelidae | Martes | *Martes melampus* | NO | YES | Nojima, 1988; Nojima, 1990c |
| Carnivora | Mustelidae | Mustela | *Mustela erminea* | NO | YES | Bryant et al., 1993; Nojima, 1988; Nojima, 1990c |
| Carnivora | Mustelidae | Mustela | *Mustela frenata* | | YES | Bryant *et al.*, 1993 |
| Carnivora | Mustelidae | Mustela | *Mustela nigripes* | | YES | Bryant *et al.*, 1993 |
| Carnivora | Mustelidae | Mustela | *Mustela putorius* | NO | YES | Bryant et al., 1993; Nojima, 1988; Nojima, 1990c; He *et al.*, 2002 |
| Carnivora | Mustelidae | Mustela | *Mustela sibirica* | | YES | Bryant *et al.*, 1993 |
| Carnivora | Mustelidae | Mustela | *Mustela vison / Neovison vison* | | YES | Bryant *et al.*, 1993 |
| Carnivora | Mustelidae | Poecilictis | *Poecilitis libyca / Ictonyx libyca* | | YES | Bryant *et al.*, 1993 |
| Carnivora | Mustelidae | Poecilogale | *Poecilogale albinucha* | | YES | Bryant *et al.*, 1993 |
| Carnivora | Mustelidae | Vormela | *Vormela peregusna* | | YES | Bryant *et al.*, 1993 |
| Carnivora | Mustelidae | Mellivora | *Mellivora capensis* | | YES | Bryant *et al.*, 1993 |
| Carnivora | Mustelidae | Arctonyx | *Arctonyx sp* | | YES | Bryant *et al.*, 1993 |
| Carnivora | Mustelidae | Meles | *Meles meles* | | YES | Bryant *et al.*, 1993 |

| SUPERORDER/ORDER/ INFRAORDER | FAMILY | GENUS | SPECIES | OSSIF. FALX | OSSIF. TENTORIUM | REFERENCES |
|---|---|---|---|---|---|---|
| Carnivora | Mustelidae | Melogale | *Melogale personata* | | YES | Bryant *et al.*, 1993 |
| Carnivora | Mustelidae | Taxidea | *Taxidea taxus* | | YES | Bryant *et al.*, 1993 |
| Carnivora | Mustelidae | Aonyx | *Aonyx capensis* | | YES | Bryant *et al.*, 1993 |
| Carnivora | Mustelidae | Aonyx | *Aonyx cinerea* | | YES | Bryant *et al.*, 1993 |
| Carnivora | Mustelidae | Enhydra | *Enhydra lutris* | NO | YES | Bryant et al., 1993; Nojima, 1988; Nojima, 1990c |
| Carnivora | Mustelidae | Lutra | *Lutra lutra* | NO | YES | Bryant et al., 1993; Nojima, 1988; Nojima, 1990c |
| Carnivora | Mustelidae | Lontra | *Lontra canadensis* | | YES | Bryant *et al.*, 1993 |
| Carnivora | Mustelidae | Pteronura | *Pteronura brasiliensis* | | YES | Bryant *et al.*, 1993 |
| Carnivora | Procyonidae | Ailurus | *Ailurus fulgens* | NO | YES | Nojima, 1988; Nojima, 1990c |
| Cetacea | Balaenopteridae | Balaenoptera | *Balaenoptera borealis* | NO | NO | Nojima, 1990b |
| Cetacea | Balaenopteridae | Balaenoptera | *Balaenoptera edeni* | NO | NO | Nojima, 1990b |
| Cetacea | Balaenopteridae | Balaenoptera | *Balaenoptera acutorostrata* | NO | NO | Nojima, 1990b |
| Cetacea | Balaenopteridae | Megaptera | *Megaptera novaeangliae* | NO | NO | Nojima, 1990b |
| Cetacea | Eschrichtiidae | Eschrichtius | *Eschrichtius robustus* | NO | NO | Nojima, 1990b |
| Cetacea | Balaenidae | Balaena | *Balaena glacialis* | NO | NO | Nojima, 1990b |
| Cetacea | Physeteridae | Physeter | *Physeter macrocephalus / catodon* | YES | NO | Nojima, 1988 (after Owen, 1866); Nojima, 1990b |
| Cetacea | Physeteridae/Kogiidae | Kogia | *Kogia breviceps* | NO | NO | Nojima, 1990b |
| Cetacea | Physeteridae/Kogiidae | Kogia | *Kogia simus / sima* | NO | NO | Nojima, 1990b |
| Cetacea | Ziphiidae | Berardius | *Berardius bairdii* | YES | YES | Nojima, 1990b |
| Cetacea | Ziphiidae | Ziphius | *Ziphius cavirostris* | YES | YES | Nojima, 1990b |
| Cetacea | Ziphiidae | Mesoplodon | *Mesoplodon ginkgodens* | YES | YES | Nojima, 1990b |
| Cetacea | Ziphiidae | Mesoplodon | *Mesoplodon stejnegeri* | YES | YES | Nojima, 1990b |
| Cetacea | Ziphiidae | Mesoplodon | *Mesoplodon densirostris* | YES | YES | Nojima, 1990b |
| Cetacea | Ziphiidae | Hyperoodon | *Hyperoodon ampullatus* | YES | YES | Nojima, 1990b |
| Cetacea | Platanistidae | Pontoporia | *Pontoporia blainvillei* | NO | NO | Nojima, 1990b |
| Cetacea | Platanistidae | Inia | *Inia geoffrensis* | NO | NO | Nojima, 1990b |
| Cetacea | Platanistidae | Platanista | *Platanista gangetica* | NO | NO | Nojima, 1990b |

| SUPERORDER/ORDER/ INFRAORDER | FAMILY | GENUS | SPECIES | OSSIF. FALX | OSSIF. TENTORIUM | REFERENCES |
|---|---|---|---|---|---|---|
| Cetacea | Delphinidae | Feresa | *Feresa attenuata* | YES | YES | Nojima, 1990b |
| Cetacea | Delphinidae | Grampus | *Grampus griseus* | YES | YES | Nojima, 1990b |
| Cetacea | Delphinidae | Orcinus | *Orcinus orca* | YES | YES | Nojima, 1990b |
| Cetacea | Delphinidae | Pseudorca | *Pseudorca crassidens* | YES | YES | Nojima, 1990b |
| Cetacea | Delphinidae | Peponocephala | *Peponocephala electra* | YES | YES | Nojima, 1990b |
| Cetacea | Delphinidae | Lagenodelphis | *Lagenodelphis hosei* | YES | YES | Nojima, 1990b |
| Cetacea | Delphinidae | Lagenorhynchus | *Lagenorhynchus obscurus* | YES | YES | Nojima, 1990b |
| Cetacea | Delphinidae | Lagenorhynchus | *Lagenorhynchus albirostris* | YES | YES | Nojima, 1990b |
| Cetacea | Delphinidae | Lagenorhynchus | *Lagenorhynchus obliquidens* | YES | YES | Nojima, 1990b |
| Cetacea | Delphinidae | Lissodelphis | *Lissodelphis borealis* | YES | YES | Nojima, 1990b |
| Cetacea | Delphinidae | Tursiops | *Tursiops truncatus* | YES | YES | Nojima, 1988; Colbert *et al.*, 2005 |
| Cetacea | Delphinidae | Tursiops | *Tursiops gilli* | | YES | Klintworth, 1968 |
| Cetacea | Delphinidae | Delphinus | *Delphinus bairdi* | | YES | Klintworth, 1968 |
| Cetacea | Delphinidae | Delphinus | *Delphinus delphis* | YES | YES | Nojima, 1988 |
| Cetacea | Delphinidae | Stenella | *Stenella attenuata* | YES | YES | Nojima, 1988 |
| Cetacea | Delphinidae | Stenella | *Stenella coeruleoalba* | YES | YES | Nojima, 1988 (after Hosokawa and Kamiya, 1965) |
| Cetacea | Delphinidae | Stenella | *Stenella longirostris* | YES | YES | Nojima, 1990b |
| Cetacea | Delphinidae | Steno | *Steno bredanensis* | YES | YES | Nojima, 1990b |
| Cetacea | Delphinidae | Sousa | *Sousa teuszii* | YES | YES | Nojima, 1990b |
| Cetacea | Delphinidae | Globicephala | *Globicephala macrorhynchus* | YES | YES | Nojima, 1988 |
| Cetacea | Monodontidae | Monodon | *Monodon monoceros* | YES | YES | Nojima, 1990b |
| Cetacea | Phocoenidae | Phocoena / phocoenoides | *Phocoenoides dalli* | YES | YES | Nojima, 1988 |
| Cetacea | Phocoenidae | Phocoena | *Phocoena dioptrica* | YES | YES | Racicot and Colbert, 2013 |
| Cetacea | Phocoenidae | Phocoena | *Phocoena phocoena* | YES | YES | Nojima, 1990b; Racicot and Colbert, 2013 |
| Cetacea | Phocoenidae | Phocoena | *Phocoena sinus* | YES | YES | Racicot and Colbert, 2013 |
| Cetacea | Phocoenidae | Phocoena | *Phocoena spinipinnis* | YES | YES | Racicot and Colbert, 2013 |

| SUPERORDER/ORDER/ INFRAORDER | FAMILY | GENUS | SPECIES | OSSIF. FALX | OSSIF. TENTORIUM | REFERENCES |
|---|---|---|---|---|---|---|
| Cetacea | Phocoenidae | Neophocaena | *Neophocaena phocaenoides* | YES | YES | Nojima, 1990b |
| Sirenia | Dugongidae | Dugong | *Dugong dugon* | YES | NO | Nojima, 1988 |
| Sirenia | Trichechidae | Trichetus | *Trichetus manatus* | YES | NO | Nojima, 1988 |
| Perissodactyla | Equidae | Equus | *Equus caballus* | NO | YES | Nojima, 1988; Solano and Brawer, 2004 |
| Perissodactyla | Equidae | Equus | *Equus burchelli* | NO | YES | Nojima, 1988 |
| Perissodactyla | Equidae | Equus | *Equus zebra* | NO | YES | Nojima, 1988 |
| Perissodactyla | Equidae | Equus | *Equus hemionus* | NO | YES | Nojima, 1988 |
| Perissodactyla | Tapiridae | Tapirus | *Tapirus indicus* | NO | NO | Grant Museum, sp. Z163 |
| Hyracoidea | Procaviidae | Procavia | *Procavia capensis* | NO | NO | Grant Museum, sp. Z1743 |
| Tubulidentata | Orycteropodidae | Orycteropus | *Orycteropus afer* | | YES | Shoshani and McKenna, 1998 |
| Artiodactyla | Suidae | Babyrousa | *Babyrousa babyrussa* | NO | NO | Grant Museum, sp. Z111 |
| Artiodactyla | Suidae | Sus | *Sus scrofa domesticus* | NO | NO | Klintworth, 1968; Schmidt, 2015 |
| Artiodactyla | Camelidae | Camelus | *Camelus dromedarius* | | YES | Al-Sagair *et al.*, 2002, El Allali *et al.*, 2017 |
| Artiodactyla | Giraffidae | Giraffa | *Giraffa camelopardalis* | NO | NO | Grant Museum, sp. Z116 |
| Artiodactyla | Cervidae | Odocoileus | *Odocoileus virginianus* | NO | NO | Klintworth, 1968; Grant Museum, sp. Z224 |
| Artiodactyla | Bovidae | Madoqua | *Madoqua phillipsi* | NO | YES | Poggesi *et al.*, 1982; Grant Museum, sp. Z2251 |
| Artiodactyla | Bovidae | | *Capra hircus* | | NO | Klintworth, 1968 |
| Artiodactyla | Bovidae | | *Ovis aries* | | NO | Klintworth, 1968 |
| Pholidota | Manidae | Manis | *Manis crassicaudata* | | YES | Gaudin and Wible, 1999 |
| Pholidota | Manidae | Manis | *Manis gigantea* | | YES | Gaudin and Wible, 1999 |
| Pholidota | Manidae | Manis | *Manis javanica* | | YES | Gaudin and Wible, 1999 |
| Pholidota | Manidae | Manis | *Manis pentadactyla* | | YES | Gaudin and Wible, 1999 |
| Pholidota | Manidae | Manis | *Manis temminckii* | | YES | Gaudin and Wible, 1999 |
| Pholidota | Manidae | Manis | *Manis tetradactyla* | | YES | Gaudin and Wible, 1999 |
| Pholidota | Manidae | Manis | *Manis tricuspis* | | YES | Gaudin and Wible, 1999 |
| Pholidota | Manidae | Manis sp | *Manis sp* | NO | YES | Grant Museum, sp. Z556 (consisting of two skulls) |

| SUPERORDER/ORDER/ INFRAORDER | FAMILY | GENUS | SPECIES | OSSIF. FALX | OSSIF. TENTORIUM | REFERENCES |
|---|---|---|---|---|---|---|
| Pholidota | Manidae | Manis sp | *Manis sp* | NO | YES | Grant Museum, sp. Z556 (consisting of two skulls) |
| Rodentia | Heteromyidae | Dipodomys | *Dipodomys* | | YES | Nikolai, 1983 |
| Rodentia | Heteromyidae | Microdipodops | *Microdipodops* | | YES | Nikolai, 1983 |
| Rodentia | Heteromyidae | Perognathus | *Perognathus* | | YES | Nikolai, 1983 |
| Rodentia | Dipodidae | Dipus sp | *Dipus sp* | NO | UNCERTAIN | Grant Museum, sp. Z209 |
| Rodentia | Hystricidae | Hystrix | *Hystrix indica* | NO | UNCERTAIN | Grant Museum, sp. Z1219b |
| Rodentia | Caviidae | Hydrochoerus | *Hydrochoerus hydrochaeris* | NO | UNCERTAIN | Grant Museum, sp. Z188 |
| Rodentia | Caviidae | | *Cavia porcellus* | | NO | Klintworth, 1968 |
| Rodentia | Dasyproctidae | Dasyprocta sp | *Dasyprocta sp* | NO | UNCERTAIN | Grant Museum, sp. Z3044 |
| Rodentia | Muridae | | *Gerbillus paeba* | | NO | Klintworth, 1968 |
| Rodentia | Muridae | | *Mus musculus* | | NO | Klintworth, 1968 |
| Rodentia | Muridae | | *Rattus norvegicus* | | NO | Klintworth, 1968 |
| Rodentia | Muroidea | | *Mesocricetus auratus* | | NO | Klintworth, 1968 |
| Lagomorpha | Leporidae | Oryctolagus | *Oryctolagus cuniculus* | NO | NO | Klintworth, 1968 |
| Macroscelidea | Macroscelididae | Rhynchocyon | *Rhynchocyon cirnei* | NO | UNCERTAIN | Grant Museum, sp. Z609 |

**Appendix 2: ANSYS code for the muscle wrapping method**

The following code is an example of the creation of one of the muscle strands used to simulate the muscle wrapping described in Chapter 4 for the *Felis silvestris catus* finite element model. The coordinates of the muscle origin node are first established, as well as the coordinates of the first mid-node which are stored in the temporal variable "mynode" from which the "hair" will grow with another node at the end (see Figure 4.8). Then the same instructions are repeated for any subsequent mid-node established in the muscle strand, which is then connected to the previous one via an element. The corresponding muscle force is finally applied to the last node of the strand.

The coordinates of each one of the nodes used in this code example have been approximated to three decimal points to ease the format of the document and allow enough space for the comments.

```
/PREP7
  ET,3,180
  TYPE,3
  nINC=1000000                              ! node number offset
  Height=1                                  ! height of 'hairs'
    originnode = node (73.085, 52.540, 55.518)    ! define muscle origin
    mynode = node (72.544, 49.211, 54.633)        ! skull via point 1
    NSEL,S, , , mynode                        ! select via point
    NGEN,2,nINC,mynode,,,,,Height,1           ! generate node at top of hair
    E,mynode,mynode+nINC                      ! generate hair element
    CP,,ALL,mynode,mynode+nINC                ! define degrees of freedom
    midnode1 = mynode+nINC                    ! define an intermediate node and assign it to variable "midnode1"
    E,originnode,midnode1                     ! create a strand segment element between origin node and "midnode1".
```

```
ALLSEL,ALL                                    ! reselect all
mynode = node(7.17e+001,4.52e+001,5.37e+001)  ! define next node in the strand in variable "mynode"
NSEL,S, , , mynode
NGEN,2,nINC,mynode,,,,,Height,1
E,mynode,mynode+nINC
CP,,ALL,mynode,mynode+nINC
midnode2 = mynode+nINC                         ! define another intermediate node and assign it to variable "midnode2"
E,midnode1,midnode2                            ! create a strand segment element between the first midnode and the second midnode
ALLSEL,ALL
mynode = node(7.05e+001,4.22e+001,5.21e+001)  ! define next node in the strand in variable "mynode"
NSEL,S, , , mynode
NGEN,2,nINC,mynode,,,,,Height,1
E,mynode,mynode+nINC
CP,,ALL,mynode,mynode+nINC
midnode3 = mynode+nINC                          ! define another intermediate node and assign it to var "midnode3"
E,midnode2,midnode3                             ! create a strand segment element between the second midnode and the third midnode
ALLSEL,ALL
mynode = node(6.93e+001,4.02e+001,5.02e+001)  ! define next node in the strand in var "mynode"
NSEL,S, , , mynode
NGEN,2,nINC,mynode,,,,,Height,1
E,mynode,mynode+nINC
CP,,ALL,mynode,mynode+nINC
endnode = mynode+nINC                           ! define the last node of the strand and assign it to var "endnode"
```

```
E,midnode3,endnode                    ! create the last strand segment element between the third midnode and the endnode
F,endnode,FX,-2.89683802339543        ! assign the X component of the muscle force to "endnode"
F,endnode,FY,-3.65971085171068        ! assign the Y component of the muscle force to "endnode"
F,endnode,FZ,-3.567978552077          ! assign the Z component of the muscle force to "endnode"
```

**Appendix 3. Additional contour plots for *Felis silvestris catus***
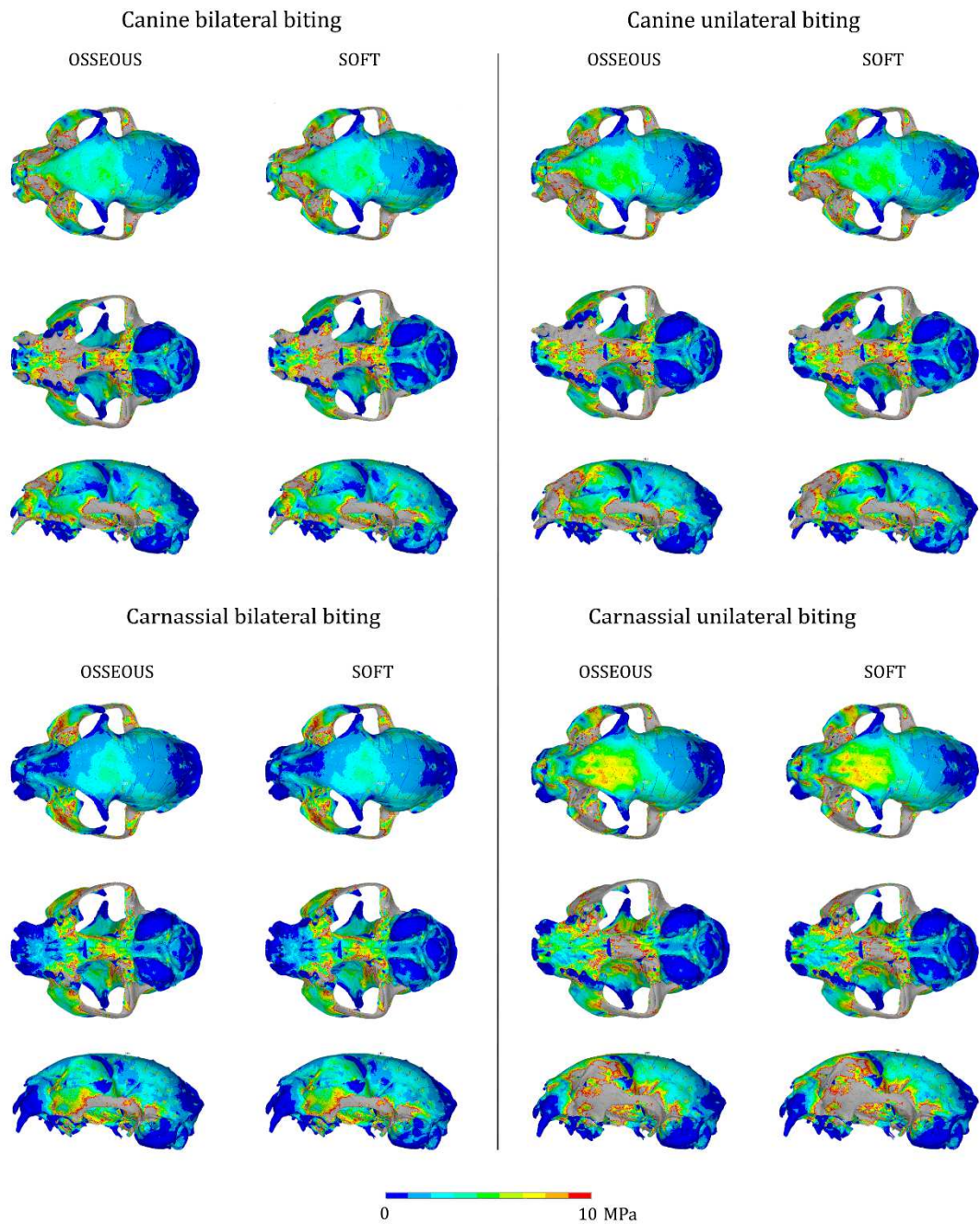


**Figure A1. von Mises stress distributions for different (intrinsic) biting analyses for osseous and soft tentorium models. Canine and carnassial bites, both bilateral and unilateral.**
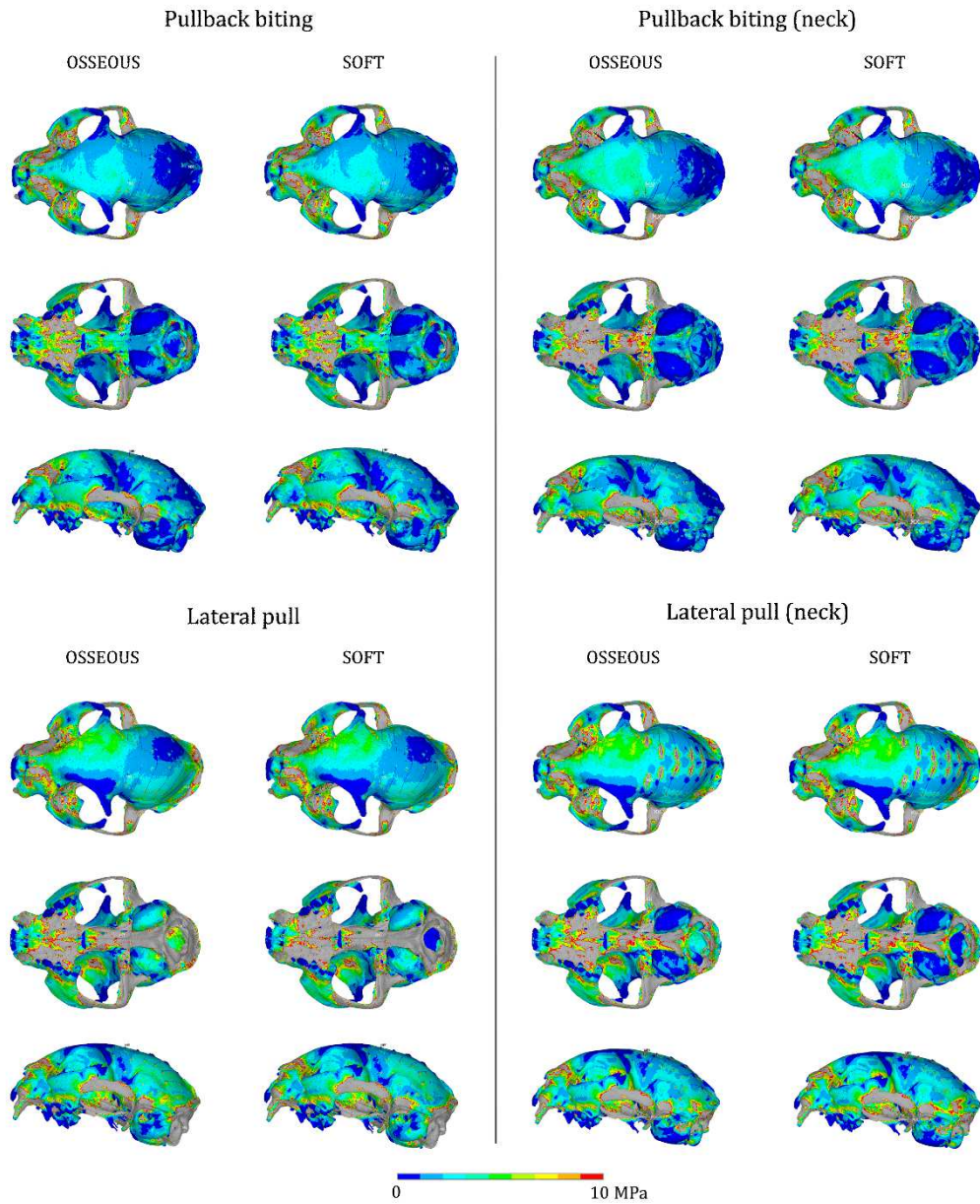
Pullback biting

OSSEOUS    SOFT

Pullback biting (neck)

OSSEOUS    SOFT

Lateral pull

OSSEOUS    SOFT

Lateral pull (neck)

OSSEOUS    SOFT

0    10 MPa

**Figure A2. von Mises stress distributions for extrinsic analyses for osseous and soft tentorium models. Pullback and lateral pull biting with and without neck muscles.**
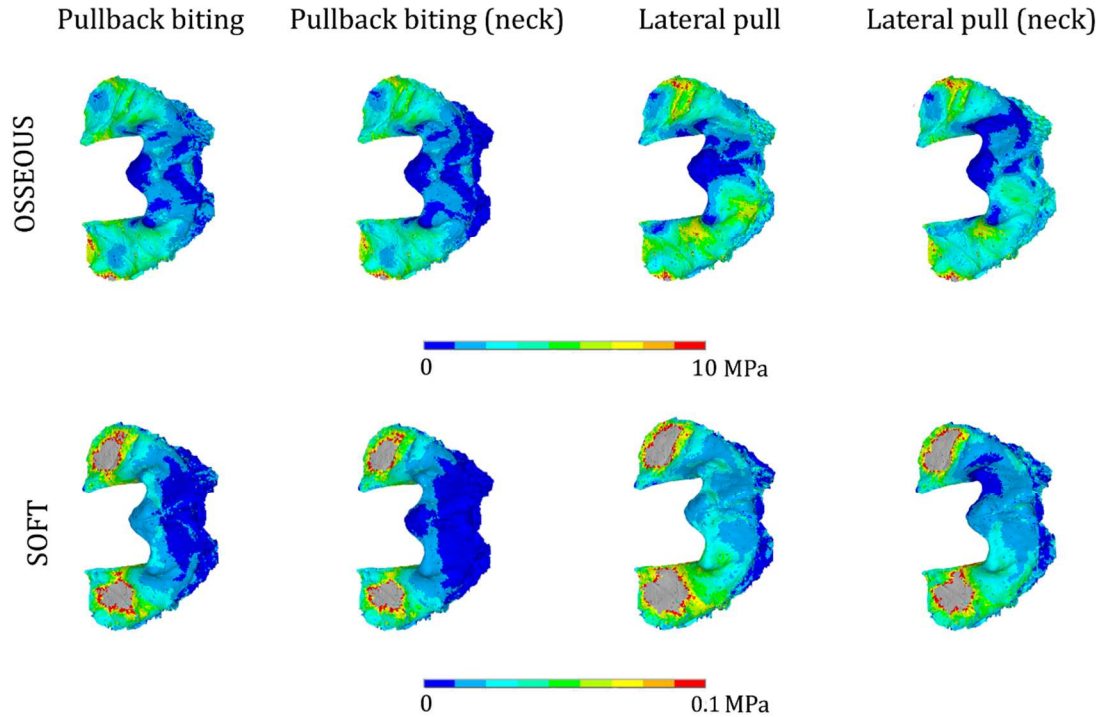
**Figure A3. von Mises stress plots for the tentorium. Top row: Osseous and soft tentorium in dorsal view for all extrinsic regimes. Bottom row: Soft tentorium for the same loading regimes as the top row, but with adjusted contour levels to reveal the stress patterns.**
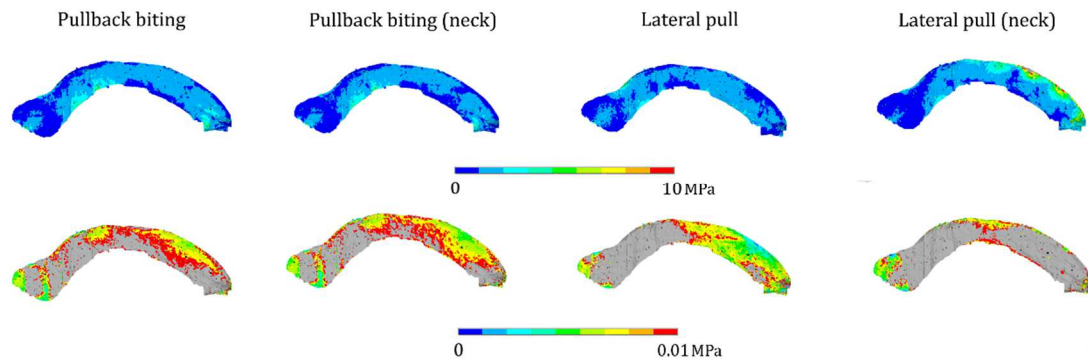


**Figure A4. von Mises stress plots for the falx. Top row: osseous falx cerebri in medial-lateral view for all extrinsic regimes. Bottom row: soft falx cerebri for the same analyses, but with adjusted contour levels to reveal the stress patterns.**
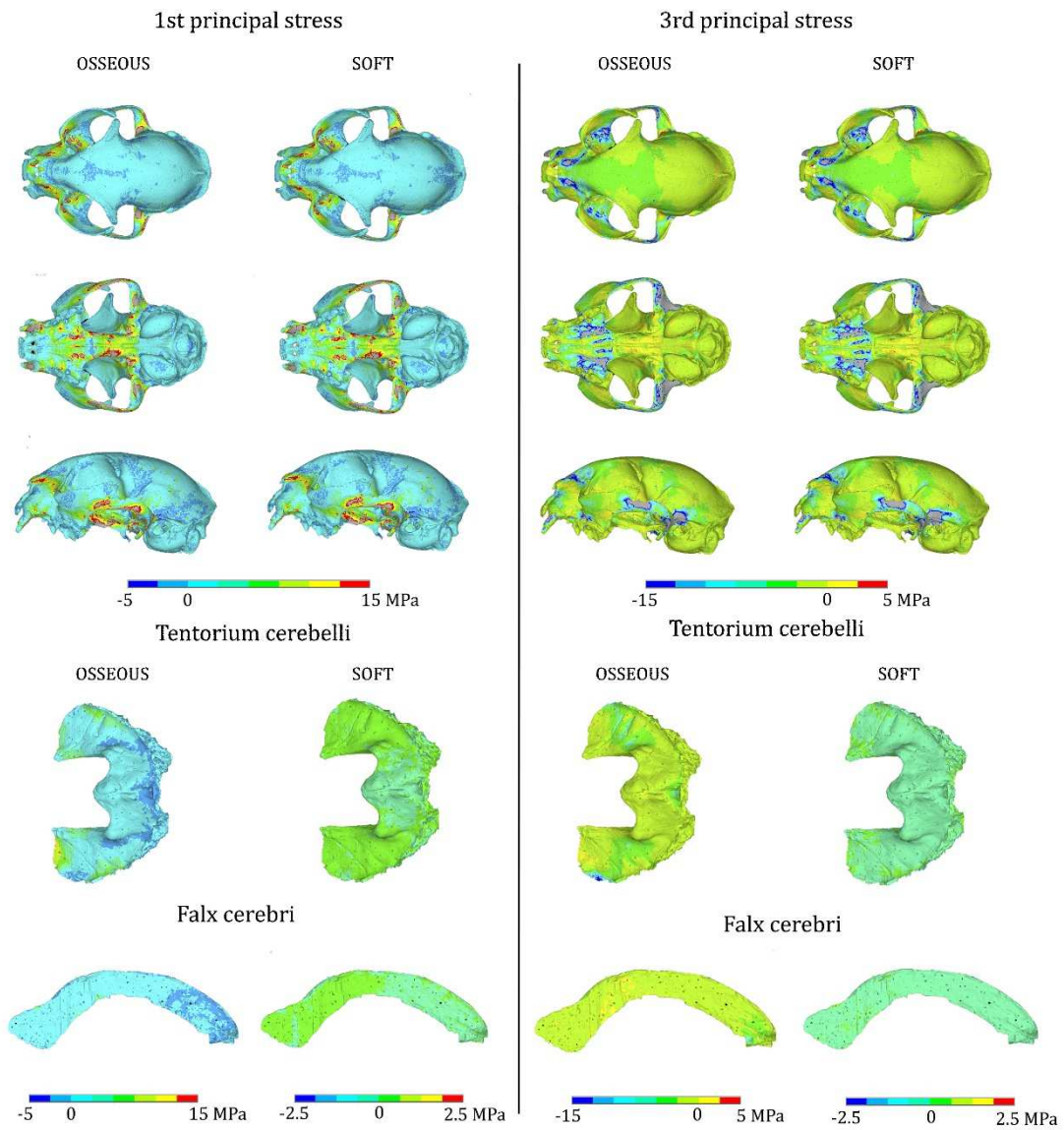
**Figure A5. First and third principal stress for bilateral canine biting. Rows 1-3: Stress distributions in the skull for ossified/non-ossified tentorium. Row 4: Detail of the corresponding ossified/non-ossified tentorium. Row 5: Ossified and non-ossified falx falx cerebri in bilateral canine biting with an osseous tentorium (*Felis silvestris catus* natural condition).**